ALGORITHMS FOR MULTI-MODAL HUMAN MOVEMENT AND BEHAVIOUR MONITORING

JONATHAN TOWNSEND

A thesis submitted in partial fulfilment of the requirements of Nottingham Trent University for the degree of Doctor of Philosophy

June 2011

Abstract

This thesis describes investigations into improvements in the field of automated people tracking using multi-modal infrared (IR) and visible image information. The research question posed is; “To what extent can infrared image information be used to improve visible light based human tracking systems?”

Automated passive tracking of human subjects is an active research area which has been approached in many ways. Typical approaches include the segmentation of the foreground, the location of humans, model initialisation and subject tracking. Sensor reliability evaluation and fusion methods are also key research areas in multi-modal systems.

Shifting illumination and shadows can cause issues with visible images when attempting to extract foreground regions. Images from thermal IR cameras, which use long-wavelength infrared (LWIR) sensors, demonstrate high invariance to illumination.

It is shown that thermal IR images often provide superior foreground masks using pixel level statistical extraction techniques in many scenarios. Experiments are performed to determine if cues are present at the data level that may indicate the quality of the sensor as an input. Modality specific measures are proposed as possible indicators of sensor quality (determined by foreground extraction capability). A sensor and application specific method for scene evaluation is proposed, whereby sensor quality is measured at the pixel level. A neuro-fuzzy inference system is trained using the scene quality measures to assess a series of scenes and make a modality decision. Results show a high degree of accuracy in selecting the optimum modality in a number of separate environmental conditions.

The use of colour to identify subjects post-occlusion is typical in tracking. Effectiveness is reduced as the subject count increases with a consequent increased likelihood of similarity between subjects. Experiments are proposed to determine whether a specific histogram parameter configuration, capable of discriminating between subjects in multiple environmental conditions, can be established. An exhaustive search approach for establishing an improved histogram configuration is undertaken using a novel evaluation metric, which assesses the separation of results from intra-subject and inter-subject histogram comparisons. Multi-modal, multi-dimensional results show that a 2-D Hue and IR configuration provides greater discrimination than either visible or IR configurations.

A tracking system is developed to demonstrate that the methods and configurations can be applied holistically in a real situation. The system is evaluated in a variety of scenarios using challenging subject data aimed at establishing the limits of the system’s capabilities.

Through addressing the research question, contributions to the field have been made consisting of: demonstrating the use of a trained neuro-fuzzy inference system to evaluate modality attributes, and the establishment of a generalised multi-modal histogram-based similarity measure to assist in re-establishing subject identity post-occlusion. The modular nature of these methods has been demonstrated by inclusion in a developed feature-rich tracking system.

Acknowledgements

Thanks to Professor Nasser Sherkat and Dr. Heather Powell for providing their guidance, support and the benefit of their experience throughout the process.

I would like to show my gratitude to all those who gave their time to help with the staged data capture. In particular thanks to Dr Tom Miller, Ian Peatfield, Chia Chaw, Dr Hemin Latif and Carly Farrow. Also thanks to Dr Daniel Rhodes who gave his time to provide guidance on presentation of the results.

I would like to thank the NTU technicians, who are always willing to assist. In particular I would like to thank Tim Randall and Steve Burton for their construction of the camera platform and assistance in positioning it around the university.

Finally I would like to thank my parents, Christopher and Abigail, for their many years of encouragement, and to Carly, for her love and support.

Table of Contents

ABSTRACT .... **I**

ACKNOWLEDGEMENTS .... **II**

TABLE OF CONTENTS .... **III**

LIST OF FIGURES .... **VIII**

LIST OF EQUATIONS .... **XII**

LIST OF ABBREVIATIONS .... **XIII**

1 INTRODUCTION **1**

1.1 AIMS OF THE RESEARCH 3

1.2 THESIS STRUCTURE 5

2 BACKGROUND **9**

2.1 TRACKING DEFINITION 9

2.2 DETECTING HUMANS 10

2.2.1 Reducing the Search Space 10

2.2.2 Contour Based Human Detection 16

2.2.3 Feature Based Detection 17

2.2.4 Distinguishing Between Classes 17

2.3 SPATIOTEMPORAL TRACKING 18

2.3.1 Tracking Methods 19

2.3.2 Occlusion Handling 20

2.4 SUMMARY 22

3 EXPERIMENTAL INFRASTRUCTURE **23**

3.1 EXISTING DATASETS 23

3.2 DATA SPECIFICATION 24

3.2.1 Content 25

3.2.2 Environment Diversity 25

3.2.3 Image Quality 25

3.3 DATA CAPTURE 25
3.3.1 Data capture hardware *26*
3.3.2 Data Capture Software *28*
3.4 DATA PROCESSING 28
3.4.1 Manual Mask Extraction Software *28*
3.4.2 Automated Mask Extraction Software *29*
3.4.3 Data Processing and Comparison *29*
3.4.4 Neuro-fuzzy inference system *29*
3.4.5 Thermal Simulation *29*
3.4.6 Histogram Processing *30*
3.5 SCENARIOS 31
3.5.1 Scenario A *31*
3.5.2 Scenario B *32*
3.5.3 Scenario C *32*
3.5.4 Scenario D *33*
3.5.5 Scenario E *33*
3.5.6 Scenario F *35*
3.5.7 Scenario G *36*
3.6 DATASETS 37
3.6.1 Dataset A *37*
3.6.2 Dataset B *37*
3.6.3 Dataset C *38*
3.6.4 Dataset D *38*
3.6.5 Dataset E *38*
3.6.6 Dataset F *39*
3.6.7 Dataset G *39*
3.7 SUMMARY 39

4 FUZZY CONTRIBUTOR SELECTION FOR MULTI-MODAL SCENE IMAGING 40

4.1 DETERMINING FOREGROUND EXTRACTION CAPABILITY 40
4.1.1 Method *41*
4.1.2 Expected Results *42*

4.1.3 Results and Discussion ... *42*

4.2 THERMAL IR INTRA-REGION SEGMENTATION ... 52

4.2.1 Method ... *53*

4.2.2 Expected Results ... *53*

4.2.3 Results and Discussion ... *53*

4.3 EVALUATING SENSOR RELIABILITY FOR MODALITY SELECTION ... 58

4.3.1 Method ... *58*

4.3.2 Expected Results ... *62*

4.3.3 Results and Discussion ... *63*

4.4 NEURO FUZZY INFERENCE FOR EVALUATING EVIDENCE ... 69

4.4.1 Method ... *69*

4.4.2 Setup ... *71*

4.4.3 Expected Results ... *72*

4.4.4 Results and Discussion ... *73*

4.5 CONCLUSIONS ... 74

5 HISTOGRAM OPTIMISATION ... 75

5.1 EVALUATING THE EFFICACY OF HISTOGRAM CONFIGURATIONS ... 75

5.1.1 Method ... *76*

5.1.2 Expected Results ... *79*

5.1.3 Results and Discussion ... *80*

5.2 MULTI-MODAL PARAMETER OPTIMISATION ... 90

5.2.1 Method ... *90*

5.2.2 Expected Results ... *91*

5.2.3 Results and Discussion ... *91*

5.3 SELF-OCCLUDING REGION NORMALISATION TESTING ... 94

5.3.1 Method ... *94*

5.3.2 Expected Results ... *95*

5.3.3 Results and Discussion ... *95*

5.4 SUMMARY ... 99

6 OCCLUSION HANDLING USING APPEARANCE MODELS ... 102

6.1 TRACKING SYSTEM DESCRIPTION 103

6.1.1 Calibration 103

6.1.2 Foreground Extraction 104

6.1.3 Human Region Identification 105

6.1.4 Tracking 107

6.1.5 Reporting 109

6.2 EVALUATION OF TRAJECTORY RESOLUTION LIMITATIONS 110

6.2.1 Method 111

6.2.2 Expected Results 111

6.2.3 Results and Discussion 112

6.3 MULTI-MODAL HISTOGRAM OCCLUSION RESOLUTION 112

6.3.1 Method 113

6.3.2 Expected Results 113

6.3.3 Results and Discussion 113

6.4 ESTABLISHING LIMITATIONS OF MULTI-MODAL HISTOGRAM OCCLUSION RESOLUTION 118

6.4.1 Method 118

6.4.2 Expected Results 119

6.4.3 Results and Discussion 119

6.5 SUMMARY 125

7 CONCLUSIONS 127

REFERENCES 131

APPENDICES 139

APPENDIX A - THERMAL IR THEORY 140

APPENDIX B 141

VISIBLE RESULTS 141

THERMAL IR RESULTS 143

APPENDIX C - RESOLUTION DEPENDENCE 145

APPENDIX D 147

1-D RESULTS 147

2-D RESULTS 150

List of Figures

FIGURE 1.1 THE ELECTROMAGNETIC SPECTRUM 3

FIGURE 1.2 COMPARISONS BETWEEN A GROUND TRUTH MASK AND A STATISTICALLY EXTRACTED AUTOMATED MASK 6

FIGURE 2.1 MODALITY COMPARISON IN FOGGY CONDITIONS HIGHLIGHTS THE INCREASED CONTRAST OF HUMAN APPEARANCE IN COOLER CONDITIONS. 14

FIGURE 3.1 CAMERA PLATFORM SHOWING BEAM SPLITTER 26

FIGURE 3.2 THERMAL IR CAMERA 26

FIGURE 3.3 VISIBLE LIGHT CAMERA 27

FIGURE 3.4 USE OF A BEAM SPLITTER TO SEPARATE VISIBLE AND THERMAL IR RADIATION TO ACHIEVE REGISTERED IMAGES 27

FIGURE 3.5 (A) SHOWS THE HISTOGRAM REPRESENTATIONS OF A SUBJECT PAIR FROM IMAGES (B) AND (C) 30

FIGURE 3.6 SCENE LAYOUT FOR SCENARIO A 31

FIGURE 3.7 SCENARIO B SCENE LAYOUT 32

FIGURE 3.8 SCENE LAYOUT FOR CANDIDATE CUE EVALUATION EXPERIMENT 33

FIGURE 3.9 SCENARIO E LAYOUT 34

FIGURE 3.10 SCENARIO E - (A) TO (C) SHOWS THE 1ST, 5TH AND LAST IMAGES FROM A SEQUENCE. (D) SHOWS THE MANUAL MASK ASSOCIATED WITH (C). (E) SHOWS THE MASK APPLIED TO (C). 34

FIGURE 3.11 SCENARIO F LAYOUT 35

FIGURE 3.12. SCENARIO F. (A) TO (C) SHOWS THE 1ST, 5TH AND LAST IMAGES FROM A SEQUENCE. (D) SHOWS THE MANUAL MASK ASSOCIATED WITH (C). (E) SHOWS THE MASK APPLIED TO (C). 36

FIGURE 3.13 EXAMPLES OF SCENARIO H SUBJECT IMAGES. SUBJECT 1 IS SHOWN IN (A) AND (B) WHILE SUBJECT 2 IS SHOWN IN (C) AND (D) 37

FIGURE 3.14 THERMAL IR IMAGE OF SUBJECT PAIR (A) WITH MANUALLY SEGMENTED MASKS (B) 38

FIGURE 4.1 VISIBLE TRUE POSITIVE RATE AND FALSE POSITIVE RATE 43

FIGURE 4.2 HISTOGRAM OF VISIBLE TRUE POSITIVE RATE AND FALSE POSITIVE RATE 44

FIGURE 4.3 VISIBLE TRUE NEGATIVE RATE AND FALSE NEGATIVE RATE 45

FIGURE 4.4 HISTOGRAM OF VISIBLE TRUE NEGATIVE RATE AND FALSE NEGATIVE RATE 45

FIGURE 4.5 VISIBLE F-MEASURES ACROSS SAMPLES 46

FIGURE 4.6 THERMAL TRUE POSITIVES / FALSE POSITIVES 48

FIGURE 4.7 HISTOGRAM OF THERMAL TRUE POSITIVES / FALSE POSITIVES 48

FIGURE 4.8 THERMAL TRUE NEGATIVES / FALSE NEGATIVES 49

FIGURE 4.9 HISTOGRAM OF THERMAL IR TRUE NEGATIVES / FALSE NEGATIVES 50

FIGURE 4.10 THERMAL F-MEASURE RESULTS ACROSS SAMPLES 51

FIGURE 4.11 MEAN HISTOGRAM OF ALL SAMPLES SEPARATED INTO SKIN AND CLOTHING DISTRIBUTIONS 54

FIGURE 4.12 MEAN HISTOGRAM OF SKIN PIXEL THERMAL IR READINGS SEPARATED INTO ENTERING AND EXITING DISTRIBUTIONS. 55

FIGURE 4.13 MEAN HISTOGRAM OF CLOTHING PIXEL THERMAL IR READINGS SEPARATED INTO ENTERING AND EXITING DISTRIBUTIONS 55

FIGURE 4.14 MEAN HISTOGRAM OF ENTERING SUBJECT'S SKIN PIXEL THERMAL IR READINGS SEPARATED INTO SKIN AND CLOTHING DISTRIBUTIONS 56

FIGURE 4.15 MEAN HISTOGRAM OF EXITING SUBJECT'S SKIN PIXEL THERMAL IR READINGS SEPARATED INTO SKIN AND CLOTHING DISTRIBUTIONS 57

FIGURE 4.16 BRIGHTNESS AS AN INDICATOR OR FOREGROUND EXTRACTION RELIABILITY 63

FIGURE 4.17 CONTRAST AS AN INDICATOR OR FOREGROUND EXTRACTION RELIABILITY 64

FIGURE 4.18 EDGE INTENSITY AS AN INDICATOR OR FOREGROUND EXTRACTION RELIABILITY 65

FIGURE 4.19 TEMPERATURE AS AN INDICATOR OF FOREGROUND EXTRACTION RELIABILITY 66

FIGURE 4.20 COVARIANCE OF THE BRIGHTNESS CUE WITH F-MEASURE 67

FIGURE 4.21 COVARIANCE OF THE CONTRAST CUE WITH THE F-MEASURE 67

FIGURE 4.22 COVARIANCE OF THE EDGE INTENSITY CUE WITH THE F-MEASURE 68

FIGURE 4.23 COVARIANCE OF THE MEAN TEMPERATURE CUE WITH THE F-MEASURE 68

FIGURE 4.24 DATA FLOW THROUGH THE NEURO-FUZZY INFERENCE SYSTEM 71

FIGURE 4.25 NEURO-FUZZY INFERENCE SYSTEM 71

FIGURE 4.26 MEMBERSHIP FUNCTIONS. (A) MEAN TEMPERATURE, (B) MEAN TEMPERATURE HISTORY,(C) BRIGHTNESS, (D) BRIGHTNESS HISTORY, (E) CONTRAST HISTORY, (F) EDGE INTENSITY HISTORY 72

FIGURE 4.27 TRAINING THE NEURO-FUZZY INFERENCE SYSTEM 73

FIGURE 4.28 MODALITY DECISION EVALUATION RESULTS PRODUCED BY THE TRAINED SYSTEM 73

FIGURE 5.1 PSEUDO-CODE OF DISCRIMINATION ABILITY CALCULATION D_x 78

FIGURE 5.2 TOP 30 1-D VISIBLE HPCTCS SEPARATED BY CHANNEL 83

FIGURE 5.3 TOP 30 1-D VISIBLE HPCTCS SEPARATED BY COMPARISON TECHNIQUE 84

FIGURE 5.4 TOP 30 2-D VISIBLE HPCTCS SEPARATED BY COMPARISON TECHNIQUE 87

FIGURE 5.5 TOP 30 1-D THERMAL HPCTCS SEPARATED BY COMPARISON TECHNIQUE 89

FIGURE 5.6 TOP 30 1-D THERMAL HPCTCS SEPARATED BY COMPARISON TECHNIQUE. DATA POINTS CONNECTED BY BIN SIZE ORDER 89

FIGURE 5.7 TOP 30 2-D MULTI-MODAL HPCTCS SEPARATED BY COMPARISON TECHNIQUE 92

FIGURE 5.8 TOP 30 2-D MULTI-MODAL HPCTCS SEPARATED BY BIN RANGE... 93

FIGURE 5.9 SELF OCCLUDING BODY REGIONS B AND C 95

FIGURE 5.10 TOP 30 MSE SEGMENTED RESULTS DISTRIBUTION BY COMPARISON TECHNIQUE.................. 98

FIGURE 6.1 INFORMATION FLOW THROUGH THE TRACKING SYSTEM WHEN CONFIGURED FOR HISTOGRAM BASED OCCLUSION HANDLING 102

FIGURE 6.2 PERSPECTIVE TRANSFORMATION FOR IMAGE TO GROUND PLANE CONVERSION 104

FIGURE 6.3 HEAD REGION DETECTION USING THE GENERALISED HOUGH TRANSFORM 106

FIGURE 6.4 HEIGHT CALCULATION FOR A SINGLE SUBJECT OVER TIME 106

FIGURE 6.5 UPDATING KNOWN SUBJECTS IN (B) USING CORRESPONDING HUMAN REGIONS KNOWN IN (A) 107

FIGURE 6.6 CREATION OF AN OCCLUSION INSTANCE CONTAINING SUBJECTS FROM THE PREVIOUS FRAME 108

FIGURE 6.7 (A) AND (B) SHOW A PAIR OF FRAMES FROM THE VIDEO REPORTING FUNCTIONALITY. (C) SHOWS THE SUBJECTS' POSITIONS ON A PLAN VIEW OF THE GROUND PLANE... 109

FIGURE 6.8 AN EXAMPLE OF DYNAMIC TRACKING OUTPUT. CIRCLES WITH A NUMBER ABOVE INDICATE PREDICTED POSITION IN *N* FRAMES 110

FIGURE 6.9 POST OCCLUSION COMPARISON RESULTS 115

FIGURE 6.10 HISTOGRAM OF COMPARISON RESULTS 116

FIGURE 6.11 HISTOGRAM OF DIFFERENCE BETWEEN COMPARISON RESULTS 117

FIGURE 6.12 SERIES A AND B DIFFERENCE HISTOGRAMS 117

FIGURE 6.13 CORRECT RESOLUTION OF OCCLUSION INVOLVING SUBJECT NUMBER 5 120

FIGURE 6.14 SUBJECT IDENTIFICATION RESULTS FOR SCENARIOS A-C 121

FIGURE 6.15 BHATTACHARYYA DISTANCE MATCH SCORES. SCENARIO A-C CORRECTLY CLASSIFIED SUBJECTS 122

FIGURE 6.16 SUBJECT IDENTIFICATION RESULTS FOR SCENARIO D... 123

FIGURE 6.17 SCENARIO D RANKED RESULTS 124

FIGURE 6.18 BHATTACHARYYA DISTANCE MATCH SCORES. SCENARIO D CORRECTLY CLASSIFIED SUBJECTS 124

FIGURE C1 IMAGE DIMENSIONS PLOTTED AGAINST D98 RESULT 145

FIGURE C2 MEAN PIXELS PER SUBJECT PLOTTED AGAINST D98 RESULT 146

List of Equations

EQUATION 1 RECALL/SENSITIVITY DEFINITION 7

EQUATION 2 SPECIFICITY DEFINITION 7

EQUATION 3 PRECISION DEFINITION 7

EQUATION 4 F-MEASURE DEFINITION 8

EQUATION 5 PROBABILITY THAT A PIXEL HAS THE CURRENT VALUE AT TIME *N* 41

EQUATION 6 NORMAL DISTRIBUTION OF THE KTH COMPONENT 41

EQUATION 7 MEAN F-MEASURE DEFINITION 59

EQUATION 8 TEMPORAL CALCULATION DEFINITION 59

EQUATION 9 BRIGHTNESS DEFINITION 60

EQUATION 10 CONTRAST DEFINITION 60

EQUATION 11 EDGE STRENGTH DEFINITION 61

EQUATION 12 MEAN TEMPERATURE DEFINITION 61

EQUATION 13 CORRELATION DEFINITION 78

EQUATION 14 CHI-SQUARE DEFINITION 78

EQUATION 15 INTERSECTION DEFINITION 79

EQUATION 16 BHATTACHARYYA DISTANCE DEFINITION 79

EQUATION 17 MEAN SQUARED ERROR DEFINITION 82

List of Abbreviations

CCTV	Closed-Circuit Television
EKF	Extended Kalman Filter
EMD	Earth Movers Distance
FIR	Far-Infrared
FLIR	Forward Looking Infrared
FN	False Negatives
FP	False Positives
HOG	Histogram of Oriented Gradients
HPCTC	Histogram Parameter and Comparison Technique Combination
IR	Infrared
JPDAF	joint probabilistic data association filter
LWIR	Long Wavelength Infrared
MHT	Multiple Hypothesis Tracking
MoG	Mixture of Gaussians
MWIR	Medium Wavelength Infrared
SD	Standard Deviation
SVM	Support Vector Machine
SWIR	Short Wavelength Infrared
TN	True Negatives
TP	True Positives
VGS	Visible Greyscale

1 Introduction

Extracting accurate human movement and behaviour from images is a challenge with wide ranging existing and potential applications, from surveillance to robotics and vehicle safety. Techniques and approaches for translating 2-D value arrays from a camera into an understanding of the scene, its contents, the subjects present and their activities, are under steady development and advancement.

High accuracy human tracking is used in motion capture systems for generating animation in film and 3D games. Such systems typically utilise multiple camera views with highly reflective markers attached with the participation of subjects. Such systems, known as active tracking systems, typically track a single or a small number of subjects concurrently.

In existing closed-circuit television (CCTV) systems in the UK, only a small percentage of video feeds are typically monitored by a human operator. This is due to both the large number of cameras and the consequent high cost of manual monitoring. Such systems are typically used to record a scene, with the resulting footage being reviewed only when an event is known to have occurred. Automating the detection and tracking of human subjects with a high degree of accuracy would enable the replacement of a range of systems reliant on human monitoring and could replace systems in which footage is recorded and reviewed when needed. The addition of methods to translate movements into a description of behaviour would also allow for proactive flagging of events to human operators.

Passive tracking systems, in which subject participation is not required, use marker-less techniques to find humans in images. Such systems are suited to much broader general safety and security applications. Passive tracking is typically used for security or safety purposes. It is not focused upon the minutiae of human pose or body-part position, but on the broader picture of subject location, movement and interaction. As such, passive systems are usually designed to be capable of tracking multiple concurrent subjects in real-time.

The requirements for such systems depend on a number of factors including: the accuracy required; the maximum number of people to track; and the environmental conditions of the scene. Cost and resource requirements are also key considerations.

Applications for accurate tracking systems are wide ranging. Security applications for an accurate system would include tracking subjects between CCTV feeds, locating subjects in unauthorised areas, recognising and flagging behaviours, along with subject identification. Safety applications may include: monitoring occupancy in buildings/licensed premised for fire safety purposes; monitoring the elderly to detect falls or accidents; observing swimmers for signs of drowning; and vehicle-based systems which detect humans in the road. Other areas of use involving multiple subjects include determining footfall (the number of people entering a shop or public place) and measuring subjects' paths through an environment to determine its utilisation. Furthermore, an autonomous and highly accurate passive system capable of detecting small movements of individual subjects would enable many applications. These include: passive motion capture; gesture recognition for use in applications such as sign language analysis; and would allow for quantitative assessment of techniques utilised by human experts for analysis of human body language. The extent of potential applications of human tracking technology in numerous application areas justify investigations into improving the capabilities of tracking systems.

1.1 Aims of the Research

The question is posed; "To what extent can thermal IR image information be used to improve visible light based human tracking systems?"

Forward looking infrared (FLIR) cameras capable of producing thermograms (images of long wavelength infrared radiation (LWIR)) are utilised in a number of fields: astronomy, fire fighting, medical and military applications, locating electrical faults, production line monitoring, insulation analysis, etc. Thermograms are useful as FLIR cameras are sensitive to electromagnetic radiation at ~7-14µmeters. Radiation at these wavelengths is emitted from objects at temperatures in which humans live and work. In order for humans to directly observe the temperature of an object, the temperature must be at least 470C, at which point it appears to glow to a human observer. This means that in order to view a scene, reflected radiations from an external source, such as the sun, or from artificial lighting is required. Figure 1.1 shows the electromagnetic spectrum with the Visible and Infrared regions highlighted. Thermal IR theory is discussed in more detail in Appendix A.

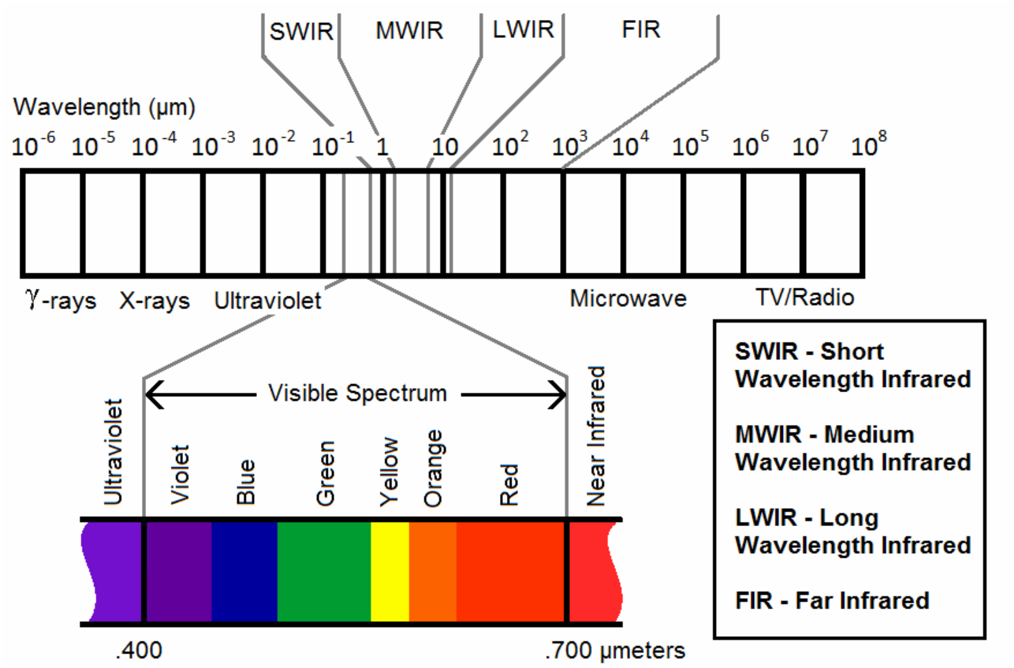

Figure 1.1 The Electromagnetic Spectrum

Usage of thermal IR cameras for commercial surveillance is limited due to the relatively high cost and low spatial resolution in comparison to visible light cameras. Due to the fact that FLIR cameras detect radiation emitted from the scene, the quality of the resulting images does not directly depend on an external illumination source unless the materials are highly reflective. An illumination source would have to heat the surface of materials or objects within the scene before a change in the thermal IR images occurred. This property makes the thermal IR images highly illumination invariant in many typical scenes while also giving other advantages: shadows present in visible light images do not appear in thermograms and the infrared radiation can penetrate fog and smoke. One other differentiating property is that radiation at these wavelengths is partially reflected and partially absorbed by glass. Complementary properties of visible and infrared cameras have been exploited in multi-modal systems (systems utilising information from more than one type of source) using both visible and infrared information as inputs. These systems are discussed in section 2.2.1.1.

Recent advances in the capabilities of LWIR cameras have led to more accessible cameras using semiconductors capable of operating at room temperature as an alternative to cameras with cryogenic cooling requirements. Ferroelectric based cameras are capable of producing higher quality images free of the ‘halo effect’ (in which high contrast boundaries exhibit a strong contrasting border) (Goubet, Katz and Porikli 2006).

In 1 2 investigations into techniques used in typical tracking systems are detailed with detailed investigations into the use of registered thermal IR and visible images described in 2.2.1.1. Two key areas of human tracking are focussed upon as potential avenues of research. Initial investigations focus upon automated extraction of human subject foreground regions from the multi-modal image sequences. Subsequent investigations consider methods for augmenting appearance models (models describing a subjects appearance) in order to improve the resolution of occlusion events (events where subjects occlude each other in the image plane causing partial or total occlusion).

It is proposed that a tracking system is implemented as a framework to demonstrate the capabilities of any developed methods in a complete system, undertaking all stages from capture to path and position reporting.

1.2 Thesis Structure

In the following literature survey chapter, an investigation into the state of the art human tracking systems and approaches is described with a focus on combining information from multi-modal sources. It is noted that certain stages are typical to many tracking systems and investigations probe the different techniques and method used in these stages as well as the variety of input devices and datasets available. Methods for locating human subjects in both visible and thermal IR are investigated along with methods for evaluating the sensor capabilities in multi-modal systems. Approaches for combining multi-modal sources are investigated, along with techniques for describing humans using appearance models to enable spatio-temporal tracking through occlusion events.

Following the literature survey, Chapter 1 describes work to evaluate sensor reliability in multi-modal thermal and visible systems with a focus on improving their foreground extraction capability. A number of cues for measuring scene quality are proposed and experiments are conducted to determine their efficacy in relation to foreground extraction capability using statistical methods. Methods shown to hold a strong indication of the sensor reliability are used as inputs to a neural fuzzy inference system. Measurement of reliability is undertaken by calculating the f-measure (Van Rijsbergen

1979). The F-measure provides an assessment score describing the systems capability in classifying pixels into foreground and background sets. The f-measure provides a balance between the precision and recall in classification analysis. The true positives (TP), true negatives (TN), false positives (FP) (or type I errors) and false negatives (FN) (or type II errors) are shown in Figure 1.2.

Figure 1.2 (a) shows an example of a ground truth foreground mask from a visible image sequence while (b) shows the statistically extracted foreground. Figure 1.2 (c) to (f) show, in blue, pixels classified as true positives, true negatives, false positives and false negatives respectively.

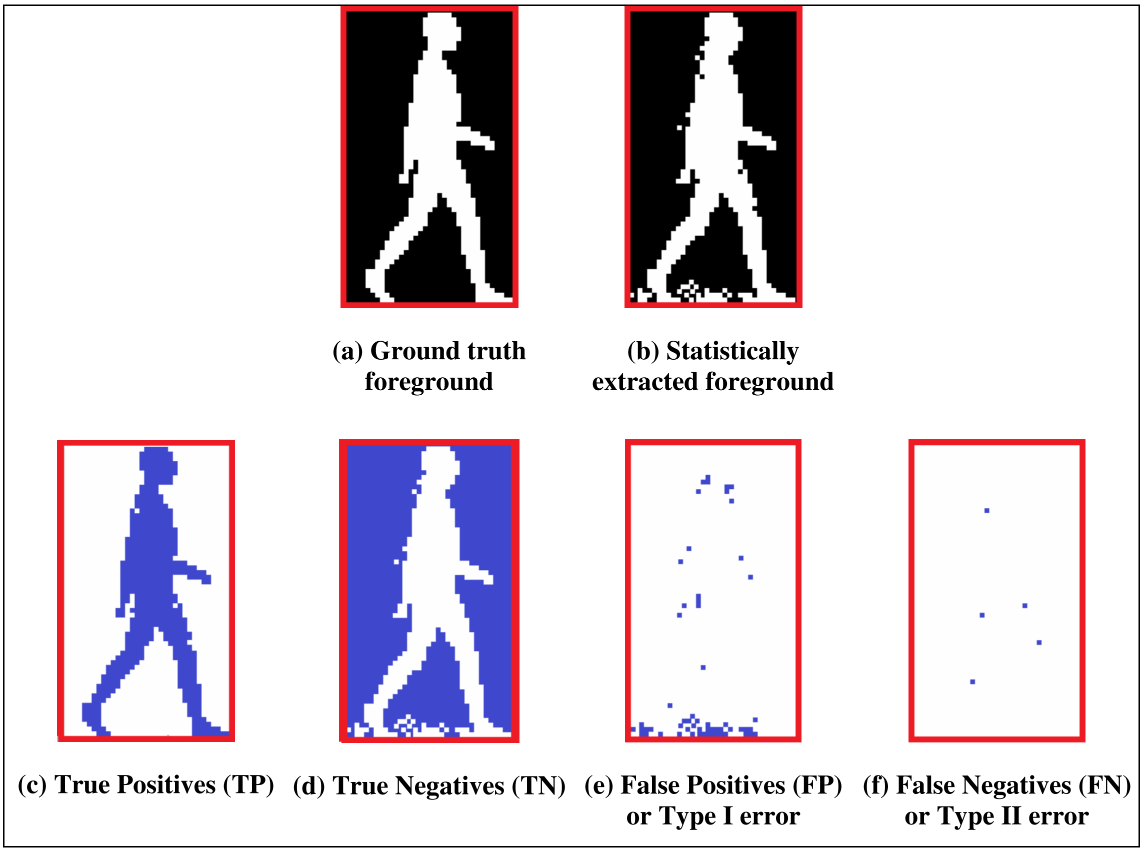

(a) Ground truth foreground **(b) Statistically extracted foreground**

(c) True Positives (TP) **(d) True Negatives (TN)** **(e) False Positives (FP) or Type I error** **(f) False Negatives (FN) or Type II error**

Figure 1.2 Comparisons between a ground truth mask and a statistically extracted automated mask

The true positive rate is the proportion of foreground in the ground truth mask which has been correctly classified as foreground in the statistically extracted mask as shown in Equation 1. This is also known as recall or sensitivity.

$$R = \left(\frac{TP}{TP + FN} \right)$$

Equation 1 Recall/sensitivity definition

The false negative rate is the proportion of foreground in the ground truth masks incorrectly classified as background in the statistically extracted mask. It can be calculated by subtracting Recall from 1.

The true negative rate is the proportion of background in the ground truth mask which has been correctly classified as background in the statistically extracted mask as shown in Equation 2. This is also known as Specificity.

$$Specificty = \frac{TN}{TN + FP}$$

Equation 2 Specificity definition

The false positive rate is the proportion of foreground in the ground truth masks incorrectly classified as background in the statistically extracted mask. It can be calculated by subtracting Specificity from 1.

Precision can be viewed as a measure of the exactness of the positive results and is also known as Positively Predicted Values (PPV). The definition is shown in Equation 3.

$$P = \left(\frac{TP}{TP + FP} \right)$$

Equation 3 Precision definition

Using the precision and recall measurements, which share an inverse relationship, calculation of the F-measure is performed. The F-measure utilises these measures to give an evenly weighted measure of performance as shown in Equation 4 in which precision is P and recall is R.

$$F = 2\left(\frac{P \bullet R}{P + R}\right)$$

Equation 4 F-measure definition

In Chapter 5 , experiments are performed to determine the efficacy of histogram based appearance models for tracking after an occlusion. A metric is established to evaluate the effectiveness of histogram configurations and an exhaustive search approach is used to establish a histogram configuration and histogram comparison technique combination which most satisfies the evaluation metric. It was found that the optimal thermal IR 1-D histogram provides superior performance across environments compared with the best 1-D or 2-D configurations using visible channel representations. It was also shown that a multi-modal configuration consisting of thermal IR combined with Hue channels provided much improved results over single modality configurations.

In Chapter 6 , a tracking framework constructed to test the holistic capabilities of the developed techniques as a whole is described. Experiments to determine the limitations of prior trajectory based occlusion resolution techniques are detailed. This work is furthered by successfully utilising histogram based occlusion resolution to overcome issues identified with trajectory based techniques in scenarios of changing subject trajectory. The concluding experimental work consists of evaluating the limitations of the system in a number of scenarios with poor or highly dynamic lighting conditions and with subjects in similar clothing.

2 Background

This section contains a survey of the current thinking regarding passive human tracking, with a focus on techniques and methods related to the work described in this thesis. In order to establish the scope of the work, the problem is defined as follows: *"To obtain information regarding the properties of position and movement of humans in complex scenarios to a high degree of accuracy using a passive sensing approach which requires no subject co-operation."*

An overview of the typical tracking stages is given with a focus on methods of background modelling for foreground object extraction. The use of multi-modal systems to increase robustness is discussed with a focus on the considerations of using thermal imaging in tracking systems. The use of appearance models for resolving ambiguity is discussed along with a review of approaches for tackling multi-person tracking.

2.1 Tracking Definition

The names of techniques and methods used in person tracking systems often overlap in their scope and usage. The term 'tracking' is used to describe a range of processes in the literature, from an overall description of complete systems, to the specific step of finding spatiotemporal correspondences between frames. In their survey of advances in computer vision Moeslund et al. (Moeslund, Hilton and Krüger 2006) use the functional taxonomy described in the earlier review (Moeslund and Bajers 2001) to categorise the stages of person tracking systems as follows:

Initialisation: Ensuring that the system has enough information to set up its models correctly.

Tracking: Finding spatiotemporal correspondence between objects or subjects in sequences in order to extract the trajectory of the subjects as they traverse the scene.

Pose Estimation: Estimation of a person's physical location and orientation in two or three dimensions using cues from the image or sequence.

Recognition: Determining the identity of a person from known information, or, determining the action being performed through translation of the pose in the frame or movement over a number of frames into a description of behaviour.

In this work the word 'tracking' will be used to describe the overall process of human tracking covering all stages of the process. The term 'spatiotemporal tracking' will cover the specific stage of finding correspondence between segmented foreground objects (categorised as human) in a sequence.

2.2 Detecting Humans

Large image sizes along with the range of possible configurations and poses of subjects in images result in a large search space in which to locate human subjects. In order to achieve realistic search times for real-world applications, this search space must be reduced. Looking for many possible poses in all areas of an image at all possible dimensions is computationally expensive. Sliding window techniques (Dalal and Triggs 2005) (Dalal, Triggs and Schmid 2006) which take this approach cannot be used in current real-time systems without compromises in spatial or temporal resolution.

2.2.1 Reducing the Search Space

The search space for a scene can be reduced by making various assumptions about the scene. Often it is assumed that the scene is on a flat plane (Leibe, et al. 2007), (Enzweiler, Kanter and Gavrila 2008), (Zhao and Nevatia 2004) or by assuming the height and dimensions of subjects are within threshold limits (Gavrila and Munder 2007) (Leibe, et al. 2007).

Often, systems look for new large objects at boundaries of the scene (Haritaoglu, Harwood and Davis 2000), (McKenna, et al. 2000a), (Roth, Doubek and Van Gool 2005), (McKenna, et al. 2000b) or where an object in a scene is not accounted for by the location of any known subjects (Capellades, et al. 2003). An alternative method which also tackles objects merging and splitting is though analysis of a correspondence matrix (Yang, et al. 2005) in which new columns indicate new subjects in the current frame.

The use of domain specific information such as skin detection has been used to detect humans (Vezhnevets, Sazonov and Andreeva 2003), (Martinkauppi, Soriano and Pietikainen 2003). Issues with changing illumination and variation in skin tone have been tackled by removing colour space components aligned with illumination. However, in unconstrained tracking environments a subject's skin may not be visible.

One useful approach taken is to utilise stereo images of a scene to produce a disparity map (Muñoz-Salinas, García-Silvente and Carnicer 2008), (Bertozzi, et al. 2007), (Muñoz-Salinas, Aguirre and García-Silvente 2007), (Hilario, et al. 2005), (Plankers and Fua 2003), (Starck and Hilton 2003) or to utilise temporal differences between images with the assumption that the subject is moving. Temporal techniques typically model the scene by individual pixel; whereby the current image is compared to a model of the background. These contrasts with early methods which an image of the background would be captured in a training phase and subsequent frames would be compared on a pixel by pixel basis. This would produce a mask of pixels based on a threshold value or measures such as co-variance or the Mahalanobis distance (Wren, et al. 1997). Such an approach is prone to incorrect classifications in environments without fixed lighting due to illumination changes and the influence of shadows.

Wren, et al. suggested using a single Gaussian to model a pixel's intensity over time (Wren, et al. 1997). Grimson et al. (1998) suggested that modelling each pixel's value over time as a Mixture of Gaussians (MoG) using a model updating function would allow for an adaptive background model. In this widely used (Velastin, et al. 2005), (Zhao, Nevatia and Wu 2008) and influential work, segmentation of the foreground is performed through comparison of the current pixel value with the Gaussian model using a threshold on the standard deviation of the Gaussian, under assumptions that the background is visible on average for more of the time than foreground objects. See also (Stauffer and Grimson 1999), (Stauffer and Grimson 2000).

This work is further improved by KaewTraKulPong and Bowden (2001). Using multiple Gaussians enables a pixel to represent more than one background such as in the case where a pixel may simultaneously represent the sky or a leaf on a tree in windy weather or to represent other dynamic changes such as the cyclic changes in the surface of water.

These systems allow for gradual changes in illumination, while the Wallflower system (Toyama, et al. 1999) uses a frame-level model to overcome the 'light switch issue' in which sudden illumination affects the whole scene.

An alternative to the MoG approach is presented by Kim et al. in (2004) and in (2005). This approach models each pixel as a codebook consisting of cells which are learned and trimmed over time. This method is further enhanced by Wen et al. (2008) through the use of different ranges for the codebook cells. Javed et al. (2002) add gradient distributions to the MoG model to reduce incorrect classification, while spatial features are used to detect camouflaged objects and shadows.

Each of the above methods generates binary foreground masks. Each mask is created on a pixel by pixel basis. There are typically some false positives and negatives present due to noise and the camouflaging effect. Techniques such as the watershed algorithm are used to join up incomplete shapes (KaewTraKulPong and Bowden 2001) (KaewTraKulPong and Bowden 2003) and morphological operations can be used to clean up the image and produce consequential regions or "Blobs".

Different colour-space representations and combinations can be used for these techniques. A key issue with such techniques is the effect of illumination changes on accuracy. This issue has been tackled using colour-spaces aligned with an axis of illumination (Vezhnevets, Sazonov and Andreeva 2003) such as YUV or HSV.

In tracking systems, issues such as shadows and changing illumination have been tackled through attempting to extract additional information from the colour images (KaewTraKulPong and Bowden 2001), (KaewTraKulPong and Bowden 2003), (Javed, Shafique and Shah 2002) though specific results regarding this aspect are not presented.

2.2.1.1. Multi-Modal Approaches

The use of multiple modalities to capture images has been used extensively in the fields of satellite imagery and astronomy where complementary information can be gathered from multiple sources. In human tracking systems, additional modalities, including laser range data, (Arras, et al. 2008), audio (Zotkin, et al. 2001) and thermal IR images (O'Conaire, et al. 2006), (Colantonio, et al. 2007), (Han and Bhanu 2007), (Davis and Sharma 2007), have been used to complement visible images. Laser range data provides a depth map of the scene and enables retrieval of objects in the image in 3D space. A similar depth map may be obtained using corresponding points in calibrated stereo images (Scharstein and Szeliski 2002).

The use of thermal IR images is extensive in military, security and medical fields. The use of thermal images in people tracking systems is typically justified by the robustness of the image to lighting changes, the lack of shadows in the images and the fact that obtaining clear images in darkness is possible. The lack of shadows in the images has been shown to be helpful in background subtraction (KaewTraKulPong and Bowden 2001), (KaewTraKulPong and Bowden 2003), (Goubet, Katz and Porikli 2006), (Leykin and Hammoud 2006). These properties help thermal imaging support robustness in tracking systems. One distinguishing aspect is that glass reflects or absorbs LWIR radiation. This has been exploited by the use of glass as a beam splitter to enable registered image in multi-modal thermal and visible systems (O'Conaire, et al. 2006). An example of a scene viewed through a visible camera and the matching registered thermal IR image is shown in Figure 2.1.

Figure 2.1 Modality comparison in foggy conditions highlights the increased contrast of human appearance in cooler conditions.

In some constrained situations a simple threshold can be applied to extract humans from the background due to the temperature difference (Yasuda, Naemura and Harashima 2004). However in real world scenarios objects such as heating vents, car exhausts, lights, hot drinks, etc. cause problems with this approach.

2.2.1.2. Modality Selection Techniques

Multi-modal systems are often utilised because they can provide additional detail regarding the content or layout of the scene. When a thermal/visible source combination is used, the robustness of the image when faced with shifting illumination provides a useful addition to the content provided by the visible camera. The nature of the capture devices means that images captured from each modality do not provide equivalent information. For example, reflections may exist in the thermal image that are not present in the visible, lack of illumination may render the visible images inadequate or background temperature or colour may result in the camouflaging of subjects (in which a pixel on the foreground is incorrectly classified as background when the pixel values are similar). These differences extend to the generated foreground masks. Owing to this, a method for combining or evaluating the quality of each mask must be undertaken to optimise extraction. In order to be able to assess the quality of a source, knowledge of how the processes influencing each source can affect reliability is vital. In Rogova and Nimier (2004) and Guo et al. (2006), sensor reliability is divided into sensor-level, data-level and symbol-level reliability approaches. A number of methods are reviewed for evaluation of sensor reliability i.e. Bayesian methods, evidential methods (which explicitly use reliability coefficients) and possibility/fuzzy methods. At the data-level, Snidaro et al. (2004) look at fusion methods for separately calculated target positions from thermal and visible data sources using the strength of the segmented regions as a measure of quality. At the symbol-level, Guo et al. (2006) use information content from each target to assess the reliability of the source. This is performed using an enhanced version of Elouedi's technique using the transferable belief model and utilises the discounting factor as an inverse measure of sensor reliability. This was introduced by Schafer (1976) and justified by work undertaken by Smets (1993).

2.2.2 Contour Based Human Detection

Contour based techniques are used to classify contours, or segments of contours, based upon their shape. Discrete techniques use fixed example models to determine human presence in a contour. The contours extracted from a foreground mask are typically analysed for human silhouette shapes such as head/shoulder regions (Haritaoglu, Harwood and Davis 2000), (Treptow, Cielniak and Duckett 2007), (Wen, Ho and Huang 2008) or full body regions (Pham, et al. 2007). Mori and Malik (2002) look at outlines of individuals for key poses which set up pre-defined model configurations. In work by Rodriguez and Shah (2007) and Beleznai and Bischof (2009), shape context descriptors (Belongie, Mori and Malik 2006) are used in which individual body parts are detected.

Work by Leibe et al. (2005) is based upon the assumption that humans are unique in images and use a number of shape templates to find human regions. As people can wear different colour clothes and have differing appearances, pixel value or gradient levels cannot be used alone. Work by Mori et al. (2004) looks at the contrast between people and the background by performing edge detection, followed by using pose templates to find the outline of a person in the resulting edge image. The detection and use of the human outline is widespread in the literature (Chen, et al. 2005), distance from templates are used by Kervrann and Heitz (1998) , hierarchical template matching is utilised by Gavrila (2000) while Stenger, et al. (2006) use linear classifiers and distance transforms to classify templates.

Continuous shape models utilise class conditional density functions to discriminate between trained sets of object poses. With highly dimensional objects such as humans, multiple sets representing typical poses need are required (Munder, Schnorr and Gavrila 2008) (Jones and Poggio 1998).

2.2.3 Feature Based Detection

A common approach to detecting humans is the use of Haar-like wavelets (Oren, et al. 1997), (Papageorgiou and Poggio 2000), (Heisele, et al. 2001). Viola et al. (2001) and (2005) use AdaBoost (Freund and Schapire 1996), (Freund and Schapire 1997) , (Friedman, Hastie and Tibshirani 2000) to train region rejection rules based on training data. An expanded version using rotated features is presented by Lienhart and Maydt in (Lienhart and Maydt 2002). In Wu and Nevatia's work (2005), the authors introduce edgelet features and demonstrate their usage in a boosted part detector.

Dalal et al. (2005) and (2006) use a Histograms of Oriented Gradients (HOG) on edge detected silhouettes to find human shape features, building on work by Freeman and Roth (1995) and further extended by Zhu et al. (2006).

Regional feature based detection has been used to find distinctive sub-regions of the human body. Modelling the spatial relationship of these regions has allowed for the building of human class description (Leibe, et al. 2007), (Leibe, Seemann and Schiele 2005).

2.2.4 Distinguishing Between Classes

When attempting to determine an object's membership within a class, a method for establishing a discrimination boundary must be used. Single and multi-layer neural networks have been used to discriminate the human class in feature space (Fukushima 1980), (Szarvas, et al. 2005).

Along with being used for feature selection, AdaBoost (Freund and Schapire 1996) has been used to combine weak classifiers for improved classification (Viola, Jones and Snow 2005), (Papageorgiou and Poggio 2000).

The use of support vector machines (SVMs) (Burges 1998) is also commonly utilised for classification tasks. A feature space is built using extracted cues from training examples, and a SVM solution maximises hyperplane boundaries between classes (Shimizu and Poggio 2004), (Zhang, Wu and Nevatia 2007).

2.3 Spatiotemporal Tracking

Obtaining trajectory information for a subject requires the association of detected human subjects between frames. The occurrence of occlusion events must be resolved in order to correctly re-establish the location of the subjects involved.

Under controlled conditions, spatiotemporal tracking can be a fairly simple process. Static backgrounds, even lighting, lack of reflective surfaces, lack of occlusion and a sufficient frame rate permit the use of straightforward background subtraction and spatiotemporal tracking techniques. In real-world conditions, however, tracking is typically undertaken by constructing appearance models to represent the subject, though this is not always the case (Gavrila and Munder 2007). The use of appearance models is intended to capture information that is unique to a subject. Shape, colour and gait are key indicators utilised. Certain aspects of appearance may be shared among subjects, but cues can be combined to give increasingly discriminatory indications using methods such as particle filters (Isard and Blake 1998), (Munder, Schnorr and Gavrila 2008), (Khan, Balch and Dellaert 2004).

Humans do not always travel in a fixed trajectory through a scene; they may stop, change direction or even reverse direction when moving through a scene. This makes modelling a person as a linear progression invalid in many situations. Luber et al. (2009) use a learning system to map a scene's probability of a person changing direction in particular places, such as at the entrance to a corridor. In some tracking systems, the detection and tracking stages have been integrated in a Bayesian framework (Philomin, Duraiswami and Davis 2000), (Sidenbladh and Black 2003).

2.3.1 Tracking Methods

Using scene calibration information, it is possible to translate image co-ordinates to Euclidian space if the flat-plane assumption is used (Estepar, Brun and Westin 2004), (Enzweiler, Kanter and Gavrila 2008), (Zhao and Nevatia 2004). Using Euclidean co-ordinates, statistical techniques such as Alpha Beta trackers, Kalman Filters or particle filters (Han and Bhanu 2007), which are also known as bootstrap filters (Gordon, Salmond and Smith 1993) used in the condensation algorithm (Isard and Blake 1998), (Philomin, Duraiswami and Davis 2000) can be utilised to track subject observations.

A number of Bayesian methods exist for target tracking. The Kalman filter (Reid 1978) (Welch and Bishop 1995) approach has been heavily utilised in the target tracking community (Terzopoulos and Szeliski 1992),(Wachter and Nagel 1997), (Comaniciu, Ramesh and Meer 2003), (Treptow, Cielniak and Duckett 2007), (Lee, et al. 2007), (Jia, Balasuriya and Challa 2008), (Arras, et al. 2008), (Ma, Yao and Yang 2009), (Xu, Cao and Li 2009), (Navarro-Serment, Mertz and Hebert 2010) in which noise in the measurement process is modelled as a Gaussian distribution with a mean of zero.

The method proposed by Reid et al. (Reid 1978) allows for multi-hypothesis tracking. An implementation of this work with a vision-based tracking system is presented by Cox and Hingorani (1996). This technique is widely used as it does not simplify the data association techniques as is required for earlier techniques. Methods such as these are effective at tracking targets where variables of movement and change are fairly constant and can be modelled. However in human tracking scenarios these techniques do not allow for the apparent randomness and direction change which can occur in human movement. Luber et al. (2009) observed that human activity is highly place dependent. In their work, they present an extension to the MHT system in which a spatial affordance map can be used to make position based predictions of human movements based upon the learned history of scenes. Early approaches to multi-hypothesis tracking used variants of the nearest neighbour filter. Schulz et al. (2003) described the joint probabilistic data association filter (JPDAF) in which each candidates for track association are combined into the most probable update using the modelled distributions of track errors and clutter.

In cases where the underlying movements are fairly linear, Kalman filters can be used. Human tracking systems however are generally non linear due to the changes in direction and speed a person may make whilst navigating a scene. A method for estimating non-linear systems with Gaussian noise is the Extended Kalman Filter (EKF) (Welch and Bishop 1995).

2.3.2 Occlusion Handling

During tracking, occlusion of the participant subjects may occur due to obscuration by foreground scenery or interaction within the image plane of other subjects or moving objects. In populated scenes, occlusions with other subjects become likely and occlusion resolution (correctly re-establishing the location of subjects) is required.

In (Senior, et al. 2006), an RGB based appearance model is utilised to represent the subjects tested using the PETS (2001) data.

Jepson et al. (2003) and Dockstader and Tekalp (2001) describe methods for using multiple cameras in order to tackle occlusion. Toet and Franken (2003) utilise motion detection to track subjects participating in partial occlusions. A popular method for representing subjects is to use histograms of pixel intensities (Zhou and Hoang 2005), (Domke 2006), (Schreiber 2008). This technique removes positional information for the member pixels. This has two key effects; firstly objects which have highly active articulation but retain similar colour distributions, such as human subjects, can be effectively modelled. The loss of positional information, which may provide additional information in cases of uncertainty, is a downside. Segmentation of the subject into regional histograms has been used to overcome this issue Khan and Shah (Khan and Shah 2000). However, this approach requires subjects to maintain their upright stance to ensure correct segmentation.

Toyama, et al. (1999) utilise trajectory information to resolve occlusions using the Extended Kalman Filter (EKF) to predict positions. The use of a dynamic 2-D template to represent subjects and resolve occlusion has been demonstrated (Zhu, et al. 2006), (Roh and Lee 2000) and (Senior, et al. 2006).

Occlusions may be handled by two popular approaches. Firstly, detecting the occlusion has occurred and attempting to resolve the occlusion post event. The alternative is to attempt to track the object through occlusion. Some systems described resolve occlusion post-event by evaluation of the appearance models against post occlusion regions. An issue which occurs with occlusions is that it is not possible to update appearance models during the occlusion; this can cause issues as the appearance of the object being tracked may have changed significantly during occlusion.

An approach proposed by McKenna et al. (2000a) is to perform a classification of each foreground pixel in the occlusion area using the appearance models of the subjects involved followed by depth ordering stage using scene knowledge. The final stage involves clearing up any misclassified pixels in the first stage. Projection transformations have been used to determine the distance from the camera by Javed et al. (2002) and Xu et al. (2005), from which the depth ordering of the subjects is inferred.

In work by Rodriguez and Shah (2007) and Beleznai and Bischof (2009), shape context descriptors (Belongie, Mori and Malik 2006) which detect individual body parts, are used to locate partially visible humans in occlusions. Such techniques are useful when groups of subjects enter the scene.

2.4 Summary

A survey of previous foundation work and the current thinking and methods for approaches to human tracking has been undertaken. A focus on multi-modal systems and modality selection along with methods for detection of human regions and model initialisation has been described. Descriptions of tracking methods for known humans and methods for resolving identity and tracking through occlusion instances have been reviewed.

3 Experimental Infrastructure

This chapter details and critiques existing datasets and goes on to provide a data specification for experimental purposes. The specification leads to the acquisition of capture hardware and the design and implementation of a physical capture platform. Software for the capture of image sequences and the processing and analysis of the data is also specified. Data capture scenarios meeting the specification and datasets utilising the images are specified within this chapter.

3.1 Existing Datasets

In order to be able to establish the requirements for human tracking, it is important to determine the level of detail required to undertake tracking. Table 3.1 shows a comparison of datasets contain human subjects traversing a scene with respect to the image modalities, compression, spatial resolution and temporal resolution.

	Name	Frequency	Spatial Resolution	Lossless Compression	Modalities
1	CAVIAR (CAVIAR Test Case Scenarios2007)	25Hz	384x288	N	Visible
2	PETS 2001 (PETS2001 datasets2001)	25Hz	768x576	N	Visible
3	PETS 2006 (PETS2006 datasets2006b)	25Hz	720x576	N	Visible
4	IEEE OTCBVS WS Series Bench (IEEE OTCBVS WS Series Bench2007b)	Non-uniform <30Hz	Visible: 320x240 Infrared: 360x240	Y (thermal 8-bit)	Visible/Thermal IR
5	i-Lids bag and vehicle detection challenge (i-Lids bag and vehicle detection challenge datasets2007c)	25Hz	720 x 576	N	Visible
6	A Framework for Evaluating Stereo-Based Pedestrian Detection Techniques - Pedestrian Detection Data-set (A Framework for Evaluating Stereo-Based Pedestrian Detection Techniques - Pedestrian Detection Data2007a)	6.5Hz	320x240	N	Visible
7	Thermo-Visual Feature Fusion for Object Tracking Using Multiple Spatiogram Trackers - Thermo-Visual	25Hz	Visible: 570x480 Infrared:	N	Visible/Thermal IR

	Datasets (Thermo-Visual Feature Fusion for Object Tracking Using Multiple Spatiogram Trackers - Thermo-Visual Datasets2007d)		160x120		
8	The AIC thermal and visible night-time dataset (AIC Thermal2006a)	25Hz	Visible: 570x480 Infrared: 160x120	N	Visible/Thermal IR

Table 3.1 Human Tracking Dataset Comparison

It is expected that pixel level analysis of human subjects will be undertaken at various stages of the research as a requirement of the scope of the research. In reviewing currently available datasets, it was found that all datasets were compromised by compression, spatial or temporal resolution or the number of subjects/pixel count per subject. For these reasons; high quality uncompressed data will be captured. High quality images will also allow analysis of quality requirement for any developed methods to determine the optimum quality/cost to performance ratio.

While datasets seven and eight show good image resolution, images are stored in a lossy format and are very noisy. Another issue with datasets seven and eight is that the participant subjects display the halo effect in infrared.

3.2 Data specification

In determining the data requirements, any properties shown or expected to influence the capability of any developed system were considered. Properties such as the frequency of subject appearance, subject density, the pixel count per subject, temporal resolution, the illumination: influence of interior, exterior lighting, the time of day and variation of illumination within the scene and temperature conditions. Constraints on data capture and staged/simulated data capture are all considered where appropriate.

3.2.1 Content

Subjects with sufficient pixels per subject per image are required to allow pixel level analysis. It is required that scenes are captured with registered thermal IR and visible image pairs to be able to compare and combine information. Scenes of sparse subject density are required to analyse a subject's appearance as they navigate the scene. Scenes in which subjects interact in the image plane through occlusion of one another are also required.

3.2.2 Environment Diversity

Locations for scenes are determined by the criteria and availability for recording. Scenes with static internal and dynamic, natural lighting are required to be able to address the influence of illumination on the background/subjects. Scenes filmed at different times of the day are also required for this purpose.

Scenes with changes in background temperature are required for analysing thermal background influence on background subtraction.

3.2.3 Image Quality

In order to be able to determine the level of detail required for any developed techniques, high resolution images are necessary. Spatial resolution, temporal resolution and bits per pixel can all be varied to determine the appropriate balance between quality and performance.

3.3 Data Capture

A custom data capture platform has been created in order that image sequences meeting the data specification can be captured.

3.3.1 Data capture hardware

A multi-modal platform consisting of a thermal infrared camera and a visible light camera utilising a thermally reflective beam-splitter has been constructed by the Technicians at the Nottingham Trent University to meet the data requirements. The platform is shown in Figure 3.1.

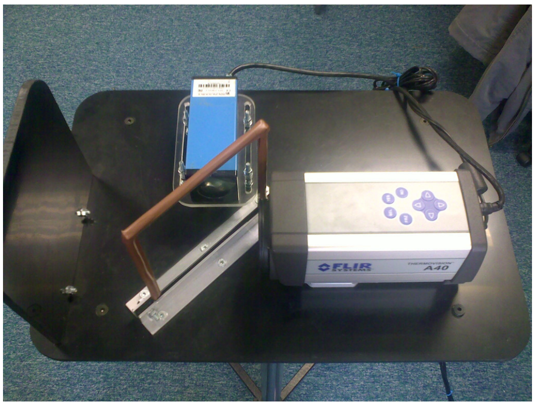

Figure 3.1 Camera platform showing beam splitter

The thermal camera is shown in Figure 3.2. The model is the Flir A40M 16bit Thermal Camera with a 320x240 spatial resolution capable of 50fps capture via FireWire. The camera is sensitive at wavelengths of 7-14µm.

Figure 3.2 Thermal IR camera

The second camera is a colour Visible Camera with a spatial resolution of 1024x768, which uses fixed parameters during data capture. The visible camera is shown in Figure 3.3.

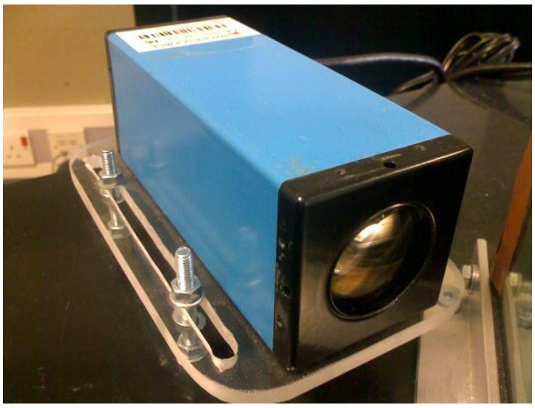

Figure 3.3 Visible light camera

In order to achieve image registration, a thermally reflective beam splitter is positioned at a 45 degree angle between the cameras. Use of the beam splitter allows registration of the images without any disparity between the images by reflecting the thermal IR radiation into the thermal camera while allowing visible light to pass through to the visible camera as shown in Figure 3.4.

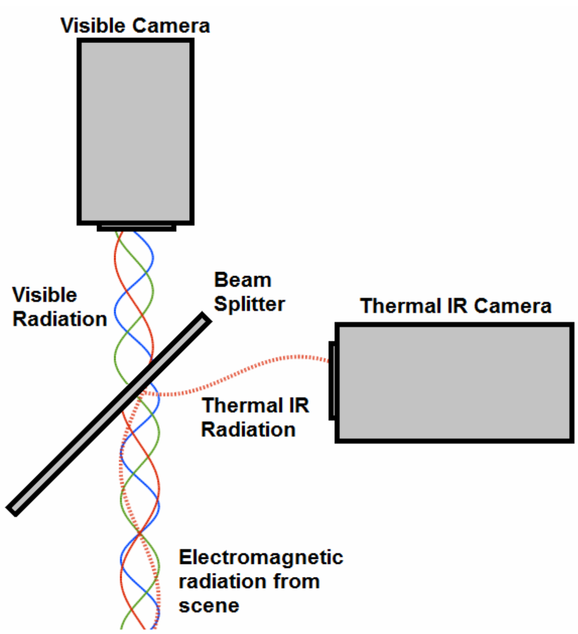

Figure 3.4 Use of a beam splitter to separate visible and thermal IR radiation to achieve registered images

Cameras are positioned at equal distances from a common point on the glass surface to achieve registration. A black surface, shown on the left of Figure 3.1, is used to remove reflection from the scene into the visible light camera.

Image registration is achieved through alignment of camera hardware and configuration of the visible camera parameters to match the thermal IR camera's fixed parameters. Registration accuracy of less than a single pixel in the thermal image was achieved without having to undertake correction for intrinsic camera parameters.

3.3.2 Data Capture Software

Data capture software is produced using C++ to run on the Windows 9x platform. Restrictions on a dual modality capture application due to control compatibility issues result in a client-server capture approach using windows sockets to transmit data from individual camera clients to a server application. This approach also allows for distributed capture; however such method was not required in this case. Images are stored uncompressed. Visible images have a spatial resolution of 1024 by 768 pixels at 24 bits per pixel while thermal images have a spatial resolution of 320x240 at 16 bits per pixel. Data capture is undertaken at 22 frames per second.

3.4 Data Processing

A number of data processing applications are developed for the various stages of data capture. Except where noted, all applications are developed in C++ using the OpenCV image processing library.

3.4.1 Manual Mask Extraction Software

An application is developed which allowed navigation of image sequences, manual region segmentation and mask saving to allow for ground truth foreground/salient region extraction. Extractions of masks in multi-modal images were mapped to allow for dual image extraction regardless of image utilised by the user. The application is controlled using a mouse interacting with the GUI.

3.4.2 Automated Mask Extraction Software

An application was created in C++ for the utilisation of image sequences from the multi-modal source using the OpenCV library or from previously captured sequences stored on disk. Functionality was required to produce the automated masks using KaewTraKulPong and Bowden's statistical background subtraction technique. An application meeting these requirements was implemented while a further application was created to enable a human user to create ground truth optimum masks.

3.4.3 Data Processing and Comparison

An application is developed to automate the comparisons of the statistically produced masks from the visible and thermal IR sources against the ground truth masks at pixel level and calculate the comparison statistics. The application also calculates the static and temporal environmental measures.

3.4.4 Neuro-fuzzy inference system

The fuzzy logic toolbox available for MatLab was utilised for the development of a neuro-fuzzy inference system for evaluation of input data. The system is trained using ground truth data to decide on the optimum modality for given scenarios.

3.4.5 Thermal Simulation

An application is developed which utilises thermal sequences and corresponding foreground masks to alter the background temperature reported in the images by a parameter amount provided.

3.4.6 Histogram Processing

An application is developed which utilises numerous sequences of individual subjects and corresponding masks to calculate and compare histograms. The system allows for combination of various parameters to be compared to provide an optimised histogram and comparison technique for discerning between subjects. The parameters are: bin size, channel type (representation of colour, illumination, etc), number of channels/dimensions and comparison technique.

Comparison of human region histograms against one another is calculated using the following techniques: Intersection, Correlation, Chi-Square, Bhattacharyya distance and the Earth Mover's Distance.

In Figure 3.5, the 2-D IR/Hue histogram of two subjects P_0 and P_1 are shown. In this example, bin sizes in the Hue dimension are 60 degrees of arc while in the thermal IR the bin sizes are 1.66°C. Histograms are normalised before comparison to account for variation in pixel count.

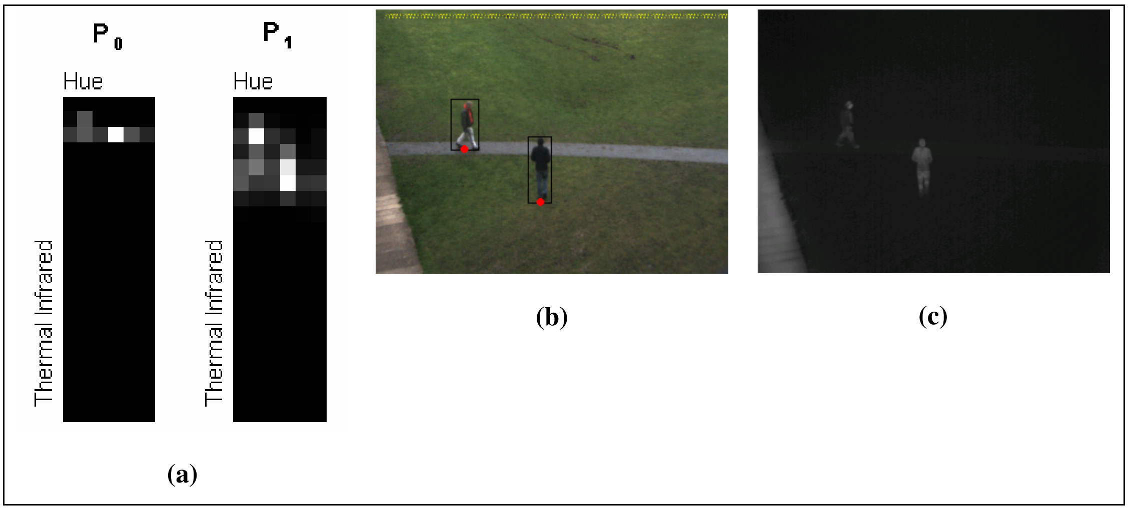

Figure 3.5 (a) shows the histogram representations of a subject pair from images (b) and (c)

3.5 Scenarios

A number of scenarios are described which have been selected in order to meet the data specification requirements. Variations in content and environmental conditions are represented within the scenarios.

3.5.1 Scenario A

Assessments of current scene characteristics are undertaken using a real-world scene. The scene consists of a room illuminated partially by natural lighting partially by artificial indoor fluorescent lighting. The scene location is the entrance to the Computing and Informatics building on the Nottingham Trent University Clifton campus. The location was selected due to the high footfall in the line of sight of the camera at that particular time of day. The location also has lighting influence from the external lighting conditions as is found in many typical scenes. The height of the camera platform is 1330mm with 0° tilt. The camera location is shown in Figure 3.6.

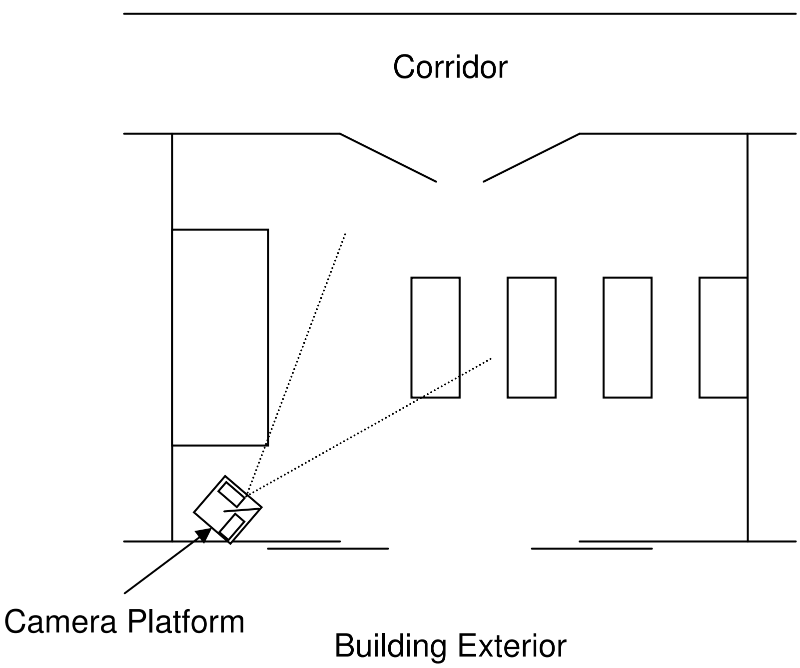

Figure 3.6 Scene layout for Scenario A

3.5.2 Scenario B

The scene used for capture of human regions was chosen to be the entrance to the Computing and Informatics Building on the Nottingham Trent University Clifton campus. Data capture was performed in winter which allowed for thermal IR images of humans exposed to colder outdoor temperatures for variable amounts of time and also human subjects exiting from the warmer indoor environment. The location is also subject to natural lighting from the building exterior. The camera location can be seen in Figure 3.7. The height of the camera platform is 1330mm and angled in line with horizontal.

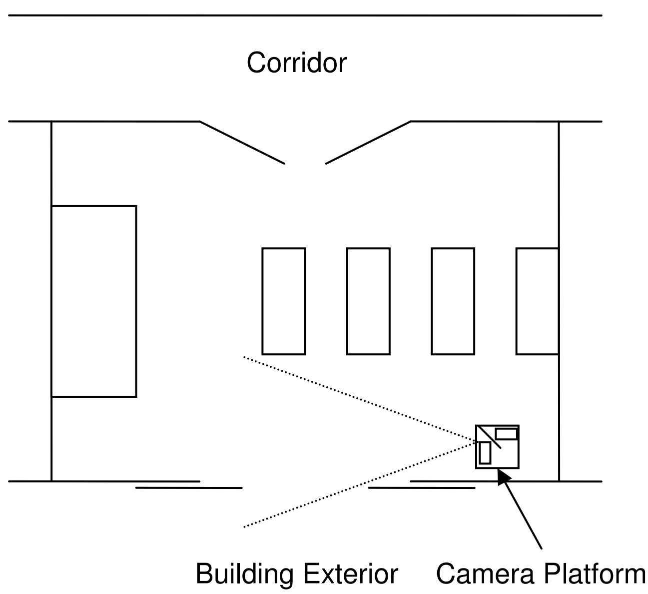

Figure 3.7 Scenario B scene layout

3.5.3 Scenario C

The scene consists of a room illuminated by outside natural lighting from an east facing window on the Nottingham Trent University Clifton campus. The timing of the capture coincides with the declining daylight. The human actor passes in front of the camera twice for each sample as illustrated in Figure 3.8 producing a sequence of images for each sample.

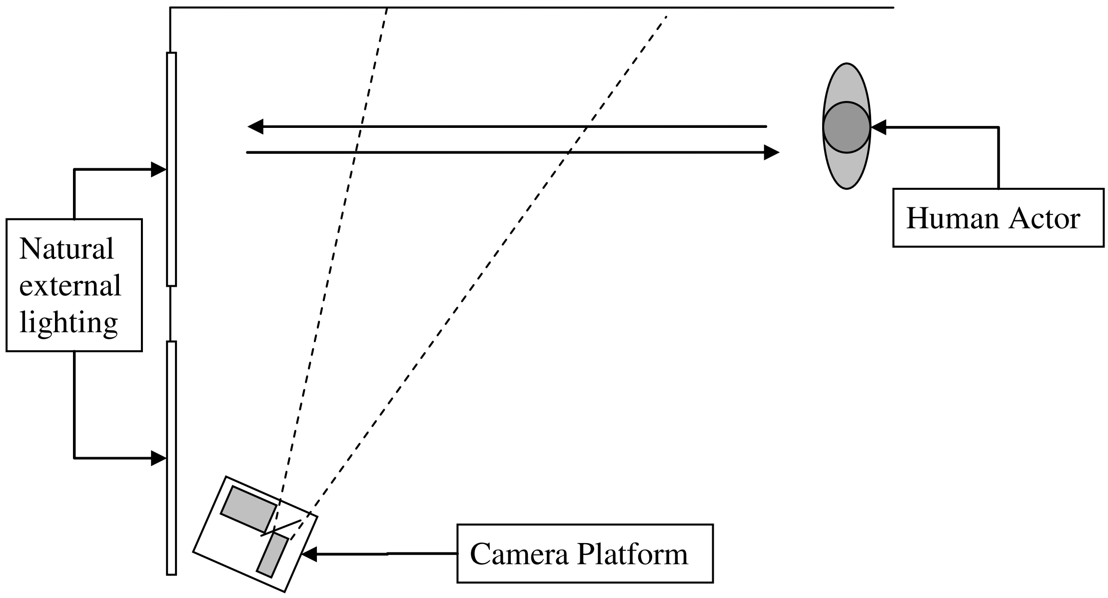

Figure 3.8 Scene layout for candidate cue evaluation experiment

3.5.4 Scenario D

Scene is imaged from an elevated indoor position of an outdoor scene. Capture is performed at different times of the day will be taken using the multi-modal camera platform on the Nottingham Trent University Clifton campus. Data capture is taken during the day, at dusk and at night to allow a range of illumination conditions including changes in brightness due to moving partial cloud cover.

3.5.5 Scenario E

Figure 3.9 shows Scenario E; the Nottingham Trent University Computing and Informatics Building 3rd floor internal corridor. Camera positions were chosen to give elevated views of scenes in order to reduce total occlusion of imaged individuals and to provide a representation of real world camera positioning.

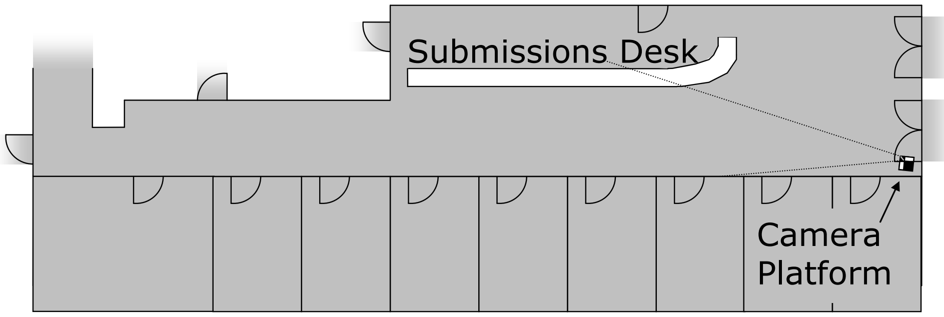

Figure 3.9 Scenario E layout

This scene is artificially lit with little influence from natural light and exhibits low colour contrast as a consequence. Participant subjects tend to travel towards and away from the camera due to the layout of the scene. An example of data captured is shown in Figure 3.10.

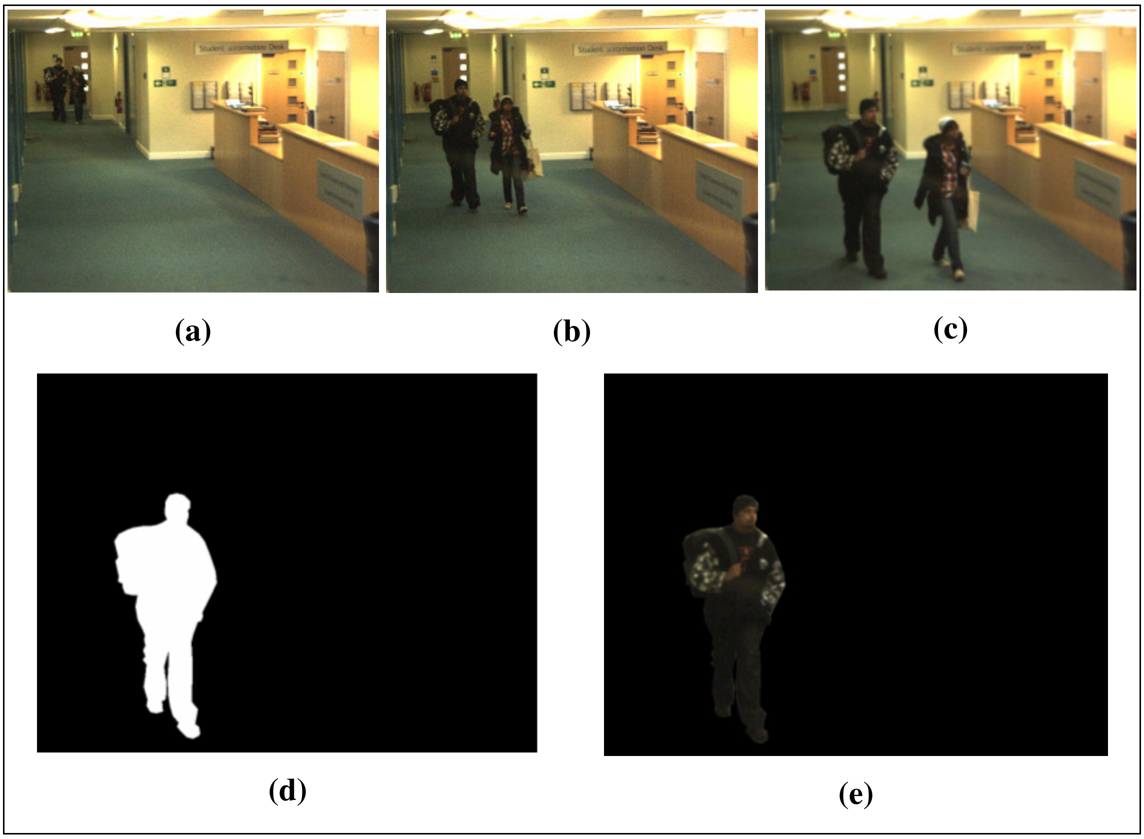

Figure 3.10 Scenario E - (a) to (c) shows the 1st, 5th and last images from a sequence. (d) Shows the manual mask associated with (c). (e) Shows the mask applied to (c).

3.5.6 Scenario F

The environment is the George Elliott Café in the Nottingham Trent University George Elliott building. The environment is lit by natural and artificial lighting and heavily influenced by sunlight on the day of filming. All filming took place during daylight hours. Participant subjects tend to travel from left to right in the scene. Data capture is not staged in either environment. The Scenario is shown in Figure 3.11.

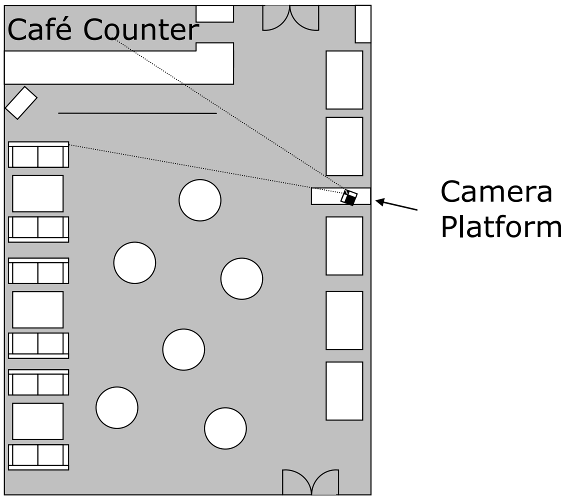

Figure 3.11 Scenario F layout

An example of data capture in Scenario F is show in Figure 3.12.

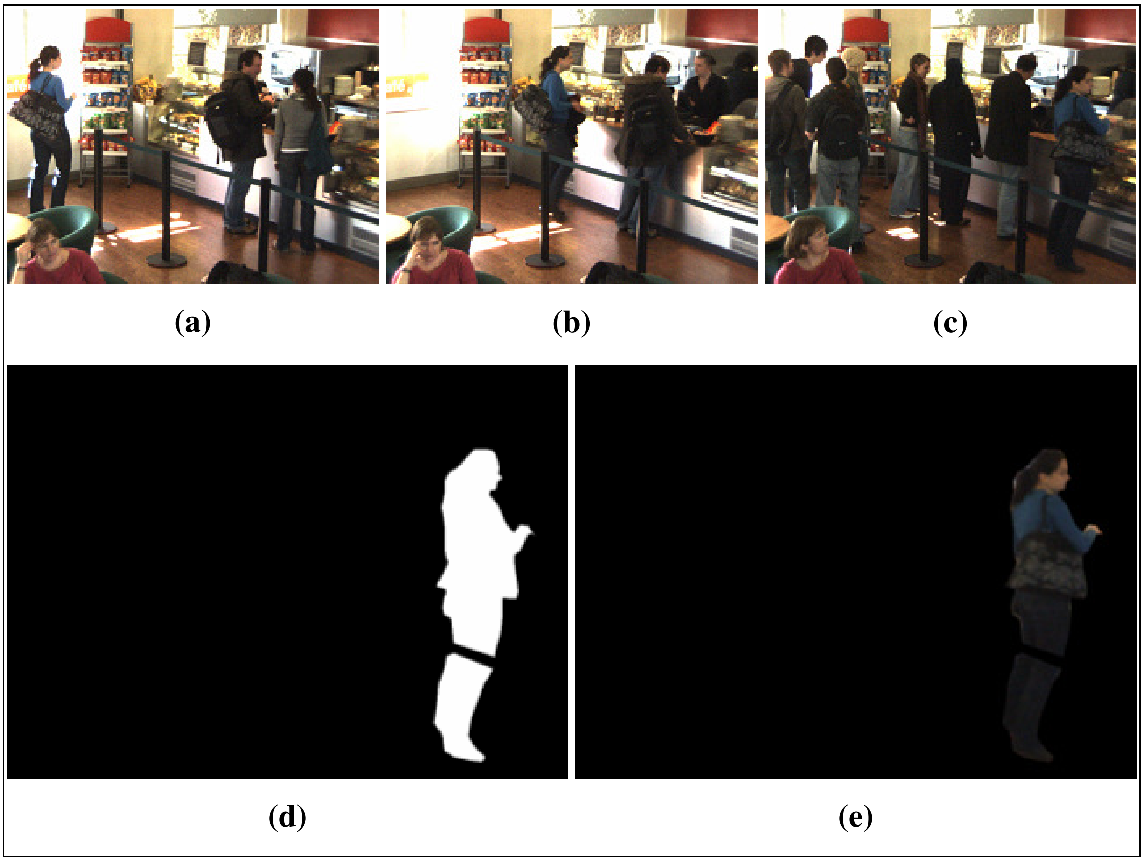

Figure 3.12. Scenario F. (a) to (c) shows the 1st, 5th and last images from a sequence. (d) Shows the manual mask associated with (c). (e) Shows the mask applied to (c).

3.5.7 Scenario G

The scene for the experiments described in this chapter is an outdoor scene filmed from a distance of 31m with a camera elevation of –25° from horizontal and a 22° field of view. The scene sequences were captured during daylight hours with overcast weather giving high consistency in the visible illumination properties. Further sequences were captured under poor lighting conditions.

An alternative outdoor scenario, Scenario H, is presented which consists of subjects in matching uniforms. Examples of images from Scenario H are shown in Figure 3.13.

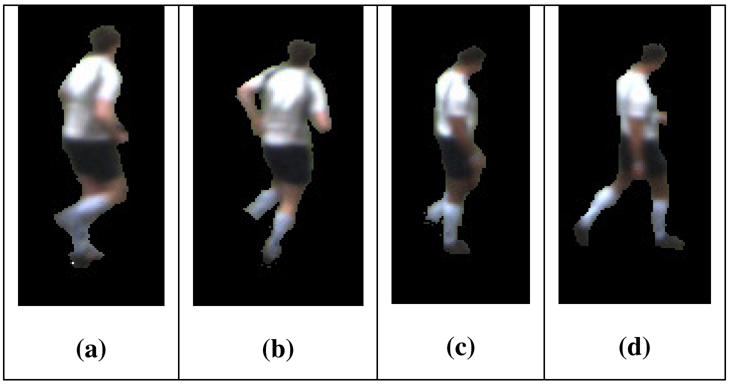

Figure 3.13 Examples of scenario H subject images. Subject 1 is shown in (a) and (b) while Subject 2 is shown in (c) and (d)

3.6 Datasets

Dataset utilised for experiments contain images or sequences from one or more of the scenarios described in 3.5.

3.6.1 Dataset A

Dataset A contains 50 multi-modal image pairs of subjects randomly selected from those images containing human presence in Scenario A. The proximity of the capture and unconstrained nature of the scene allows for sufficient variation and samples for confidence in the results. Human regions are manually segmented to provide human region masks for each image pair.

3.6.2 Dataset B

Dataset B contains 45 images of subjects randomly selected from those containing human presence in Scenario B to allow for a high level of confidence in the results. Only thermal information is utilised in Dataset B.

Human regions are manually segmented to provide human region masks for each image pair. An example of a thermal IR image is shown in Figure 3.14 (a) while the manually masked skin regions of the same image are shown in Figure 3.14 (b).

(a) **(b)**

Figure 3.14 Thermal IR image of subject pair (a) with manually segmented masks (b)

3.6.3 Dataset C

Dataset C consists of 6 multi-modal sequences, taken at 5 minute intervals, of a human subject passing the camera's field of view as the natural light decreases. Each sequence contains 14 to 17 images of the subject Human regions are manually segmented to provide human region masks for each image pair.

In the thermal IR modality the background in all frames with human presence is manually segmented and the background temperature is altered by increments of 1°C to simulate environments with differing temperatures.

3.6.4 Dataset D

A total of 48 images with human presence were available of daylight conditions with 42 late evening and night images. Human regions are manually segmented to provide human region masks for each image pair.

3.6.5 Dataset E

Dataset E consists of data from scenario's E and F. From each scenario, a series of 10 images per subject, in which 11 subjects pass through each scene are captured as they cross a series of boundaries. This gives a total of 110 images per scenario. Human regions are manually segmented to provide human region masks for each image pair.

3.6.6 Dataset F

Dataset E consists of data from Scenario G. A series of 60 full sequences consisting of 30 seconds of background video, followed by two subjects entering into the scene, occluding one another mid-scene and re-emerging from the occlusion. In half of the sequences the subjects continue on in their original direction after the occlusion, these sequences are referred to as Series A. In the remaining sequences, the member subjects change direction during the occlusion event. These sequences are referred to as Series B. A total of 60 sequences were captured consisting of an equal number of sequences in Series A and Series B.

3.6.7 Dataset G

Dataset E consists of data from scenarios E, F G and H. In each scenario, two multi-modal image pairs are taken of 33 individual subjects at different points as they traverse the scene. Separation of images are taken at random distances between 1 and 3 metres to simulate a person’s appearance prior to and post occlusion event. The data set contains 33 pairs of subjects from scenarios E F and G and 11 subjects from scenario H.

3.7 Summary

This chapter provides a data specification for experimental purposes. Analysis of existing datasets found those considered insufficient in meeting the data requirement. Resulting from this, the acquisition of capture hardware and the design and implementation of a physical capture platform is described. Software for the capture of image sequences and the processing and analysis of the data are described. Data capture scenarios meeting the specification and datasets utilising the images have been specified within this chapter.

4 Fuzzy Contributor Selection for Multi-Modal Scene Imaging

This chapter contains the description of investigations into the extraction of foreground objects from the background; a stage typical in tracking systems. Work is undertaken to address the question proposed in 1.1 by:

- Determining the ability of statistically based foreground extraction capabilities using the multimodal image sources;
- Investigating an alternative temperature based approach to extracting humans in thermal IR images;
- Investigating scene properties which may indicate the quality of the scene for foreground extraction.

The work concludes with the implementation of a Neuro-fuzzy inference system for assessing scene properties and determining optimum modality selection.

4.1 Determining foreground extraction capability

Approaching multi-modal scene imaging, investigations began by establishing the precise capabilities of foreground extraction using the multi-modal image sources and a highly capable statistical technique widely utilised in the literature. The purpose of this experiment was to compare the results from each modality to determine each modality's capability for foreground extraction in a real-world high density scenario.

Experimentation commenced with the aim to determine whether using the thermal IR source alone will provide a closer to ground truth estimation of foreground than using the visible spectrum alone. It is theorised that due to high invariance to illumination change and the lack of shadows, thermal IR image sequences will provide superior masks than visible sequences. A standard and established statistical technique for foreground extraction is utilised to assess modality capability,

4.1.1 Method

The samples in Dataset A are used for this experiment. The manually segmented foreground masks are compared with those produced using KaewTraKulPong and Bowden's technique (2001) on a pixel level basis. KaewTraKulPong and Bowden's technique models each pixel as a mixture of *K* Gaussians over time. Each Gaussian has a weight parameter.

To determine if a pixel is foreground, the probability that the pixel has the current value is calculated as shown in Equation 5 where *w* is the weight and $\eta(x;\theta_k)$ is the normal distribution of the kth Gaussian component.

$$p(X_N) = \sum_{j=1}^{K} w_j \eta(X_N;\theta_j)$$

Equation 5 Probability that a pixel has the current value at time *N*

The normal distribution of the kth component is shown in Equation 6 where μ_k is the component's mean and $\Sigma_k = \sigma_k^2 I$ is the covariance.

$$\eta(x;\theta_k) = \eta(x;\mu_k,\Sigma_k) = \frac{1}{(2\pi)^{\frac{b}{2}}\left|\Sigma_k\right|^{\frac{1}{2}}} e^{-\frac{1}{2}(x-\mu_k)^T \Sigma_k^{-1}(x-\mu_k)}$$

Equation 6 Normal distribution of the kth component

Expectation maximisation is used to estimate the Gaussian components. For full details of Gaussian updating and trimming equations please refer to KaewTraKulPong and Bowden (2001).

The F-measure, detailed in 1.2, is utilised to assess modality capability and the results are compared with results published in the literature.

4.1.2 Expected Results

It is expected that the thermal results will provide greater foreground extraction capability due to the lack of shadows and smaller influence from changes in illumination. The thermal source, however, has a poorer spatial resolution and so is expected to produce a lower resolution mask.

4.1.3 Results and Discussion

Initially the visible results are presented to provide a view of the capabilities of typical tracking systems which use visible image sources. Thermal IR results are then presented to contrast with the visible results. The full results for both modalities across the 50 samples are located in Appendix B.

4.1.3.1. Visible Results

Pixel values for the visible images are modelled using the red green and blue components as a vector. A summary of the results from background subtraction undertaken on the visible image sequence is shown in Table 4.1.

Visible Data	True Positive	False Positive	True Negative	False Negative
Mean	0.289	0.083	0.917	0.183
Standard Error	0.027	0.009	0.009	0.013
Standard Deviation	0.194	0.067	0.067	0.092
Sample Variance	0.037	0.004	0.004	0.009
Kurtosis	0.350	4.256	4.256	-0.300
Skewness	0.918	1.987	-1.987	0.467
Range	0.772	0.305	0.305	0.422
Minimum	0.029	0.014	0.681	0.014
Maximum	0.801	0.319	0.986	0.436

Table 4.1 Summary of visible pixel classification results

Figure 4.1 shows the true and false positive rates using the visible image sequence, as defined in 4.1.1. Samples are ordered chronologically, however intervals between samples are not evenly distributed. This makes any changes in the capability over time apparent but the rate of change cannot be derived.

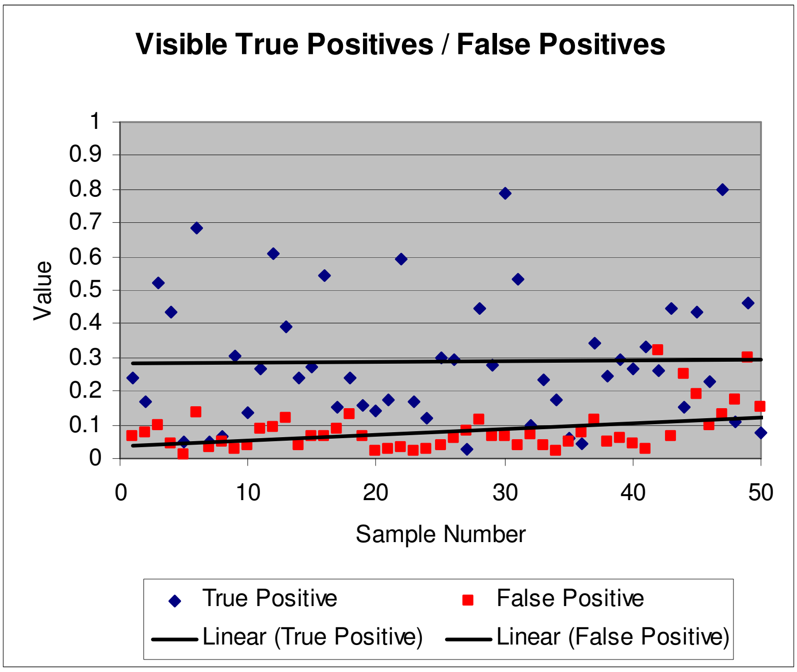

Figure 4.1 Visible true positive rate and false positive rate

Figure 4.2 shows the above data as a histogram of the distribution of true and false positive rates. The range of the bin size for the true positive and false positive rates is 0.05.

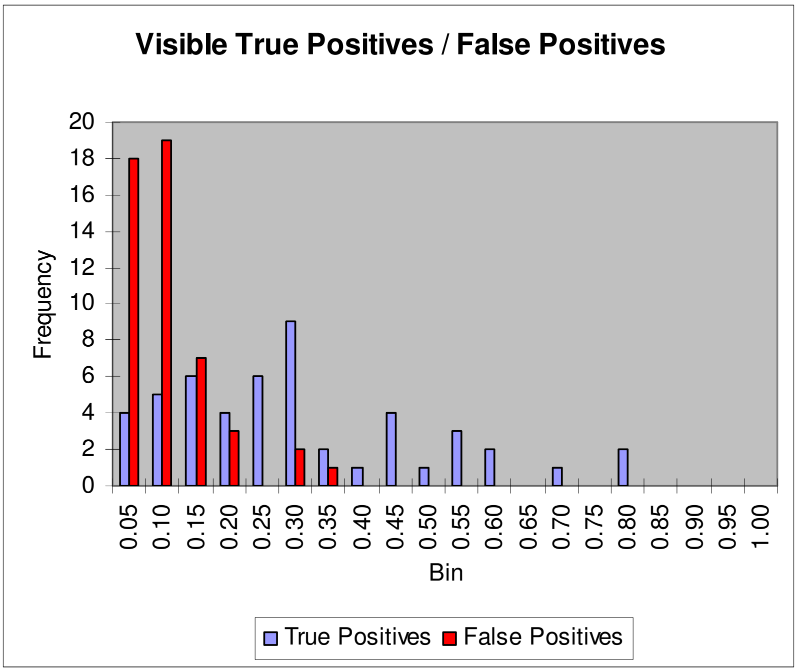

Figure 4.2 Histogram of visible true positive rate and false positive rate

It is observed that at the end of the sequence an increase in the false positives rate occurs, reasons for this are discussed at the end of this section. The true positives remain widely distributed but there is little change in the mean through the sequence.

Figure 4.3 shows the true and false negative rates calculated from the visible image sequence. The distribution of true and false negatives for the visible image sequence is shown in Figure 4.4.

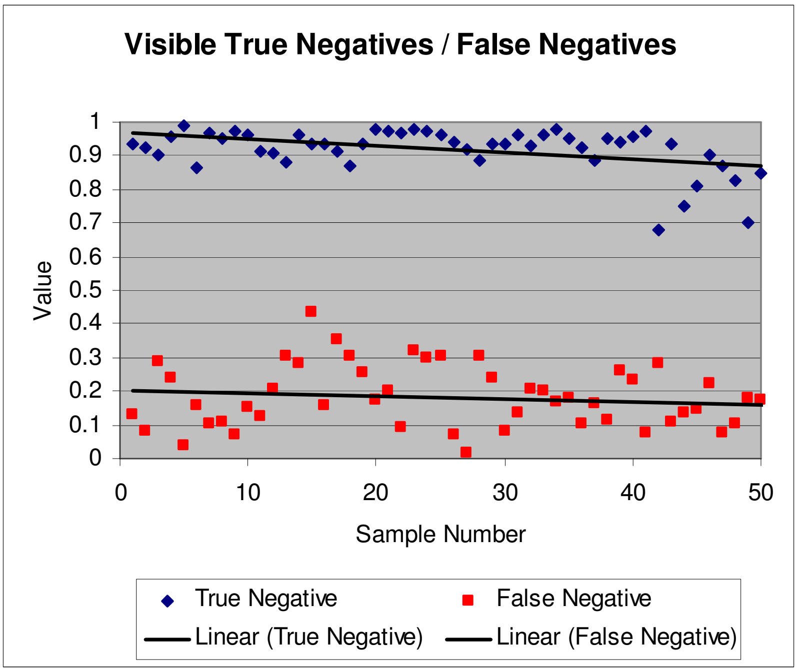

Figure 4.3 Visible true negative rate and false negative rate

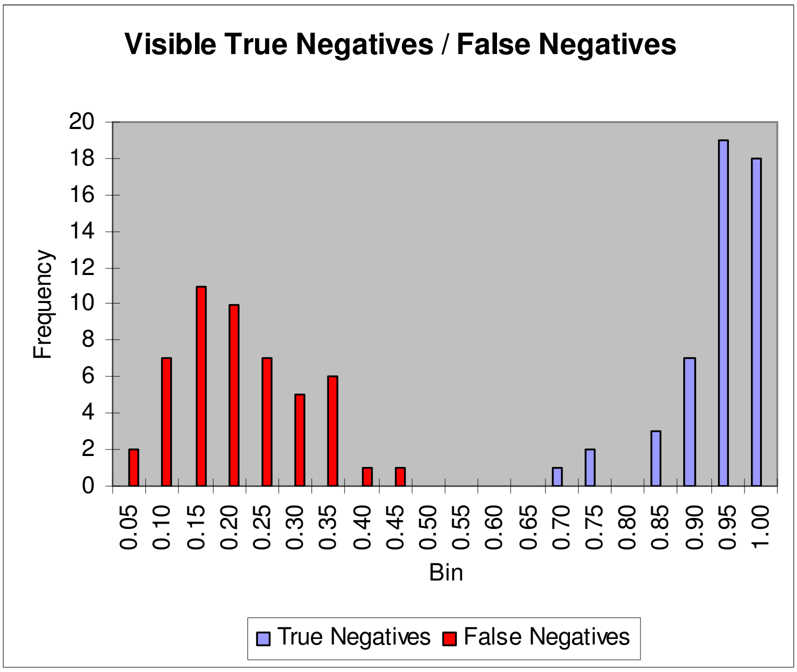

Figure 4.4 Histogram of visible true negative rate and false negative rate

It is noted from the chronological representation of the results that classification of pixels in the visible results fare worse towards the end of the sample set than at the beginning. A decrease in the true negative rate is observed, reflecting the change in the false positive rate over the same period. Upon investigation, it was observed that the lighting conditions change more frequently towards the end of the sequence than at the start. This observation provides a theory accounts for the results: that background pixel values are changing at a greater rate than can be accounted for using the background updating algorithm. If this theory is correct however, tackling the issue by increasing the rate of change of the background decreases the amount of time a pixel value must be visible before it is classified as foreground. This however led to problems with subjects who pause momentarily, as their constituent pixels in the image would be incorporated into the background at an increased rate.

In order to combine the binary classification measures to provide a balanced measure of the capability of the modality, the F-measure (described in Equation 4) is calculated for the visible sequence. The results are shown in Figure 4.5.

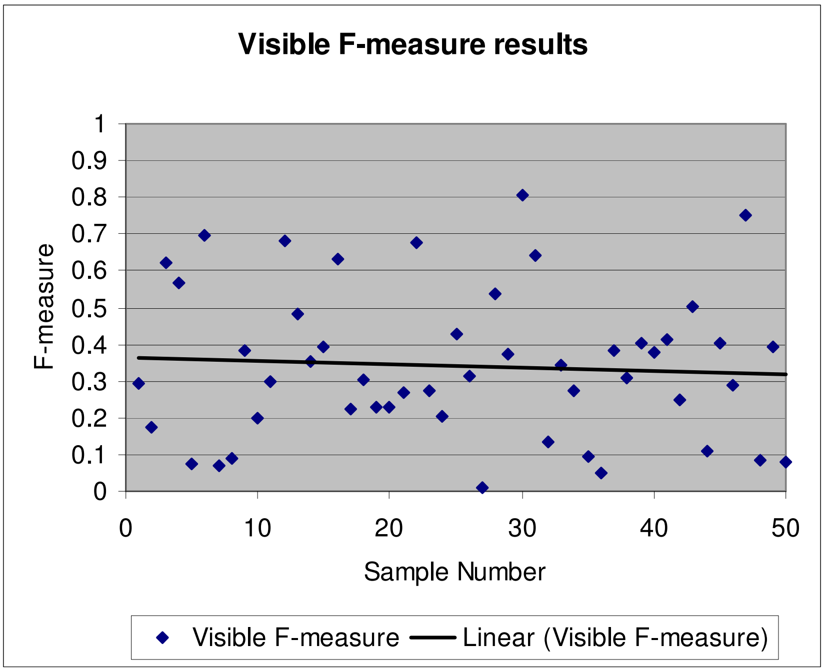

Figure 4.5 Visible F-measures across samples

The mean F-measure for the visible modality is 0.343 with a SD of 0.202. Davies et al. (2005) achieved a mean F-measure across a series of scenarios of 0.584. Comparison of the F-measure results shows a poorer performance than has been demonstrated in the literature. It is expected that this is due to the influence of reflections and changes in illumination towards the end of the sequence. Changes in illumination have been shown in 2.2 to be a key issue with background subtraction in the visible spectrum.

In order to compare the modalities, the results must be compared with those calculated using the thermal IR image source.

4.1.3.2. Thermal IR Results

The thermal IR readings are modelled as scalar values, as the sensor provides a single value per pixel. A summary of the results from background subtraction undertaken on the thermal IR image sequence is shown in Table 4.2.

Thermal Data	**True Positive Rate**	**False Positive Rate**	**True Negative Rate**	**False Negative Rate**
Mean	0.573	0.083	0.917	0.114
Standard Error	0.015	0.007	0.007	0.009
Standard Deviation	0.104	0.048	0.048	0.061
Sample Variance	0.011	0.002	0.002	0.004
Kurtosis	0.639	-0.301	-0.301	-0.212
Skewness	-0.136	0.665	-0.665	0.509
Range	0.519	0.185	0.185	0.254
Minimum	0.334	0.013	0.802	0.009
Maximum	0.853	0.198	0.987	0.262

Table 4.2 Summary of thermal IR pixel classification results

Figure 4.6 shows the true and false positives pixel totals for thermal IR images across the sample set. This makes any changes in the capability over time apparent. However, the rate of change cannot be derived. The samples are ordered chronologically but time intervals between samples are not evenly distributed. Figure 4.7 shows the data as a histogram of the distribution of true and false positives rates.

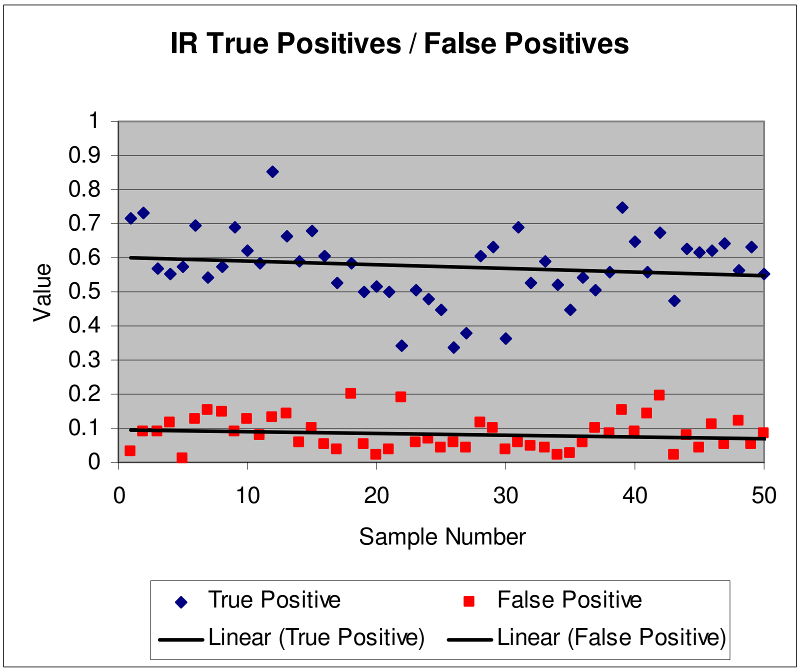

Figure 4.6 Thermal True Positives / False Positives

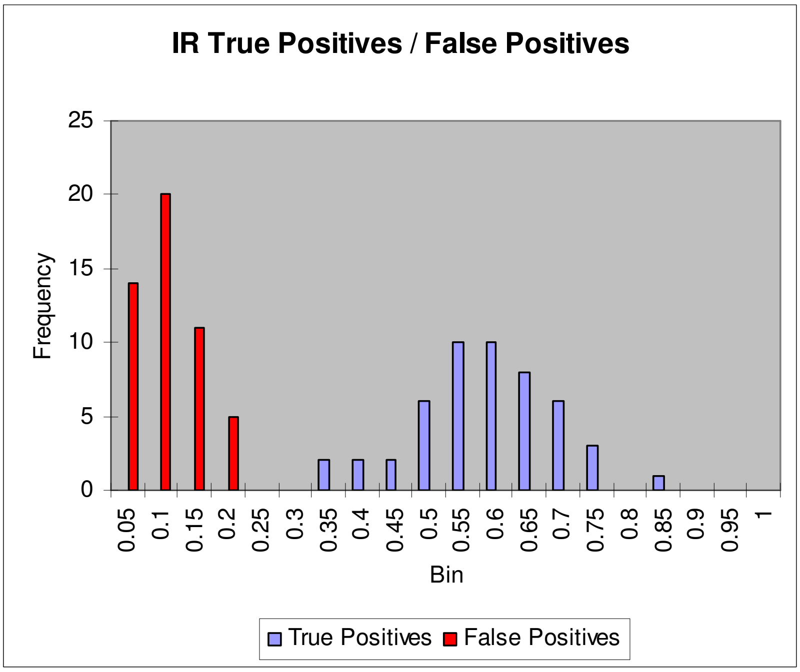

Figure 4.7 Histogram of Thermal True Positives / False Positives

The mean true positive rate achieved across the 50 samples when comparing the ground truth masks with the automated masks from the thermal IR images is 0.573 with a standard deviation of 0.103. The distribution shows clear normal distribution properties. However, the broad range of values shows that some of the samples achieve a high true positive rate with others performing poorly.

The false positives have a mean of 0.083 with a few samples exhibiting more than double the mean. Investigation into the source images for these samples showed that reflections in dense scenes due to the presence of glass and polished wood surfaces were highly influential in producing the false positive rate. Pixels typically classified as background contained reflected incident radiation; consequently the values were outside the SD threshold. In addition to this, a door in the images was classified as foreground when moving.

Figure 4.8 shows the true and false negative rates calculated from the visible image sequence. The distribution of true and false negatives for the visible image sequence is shown in Figure 4.9.

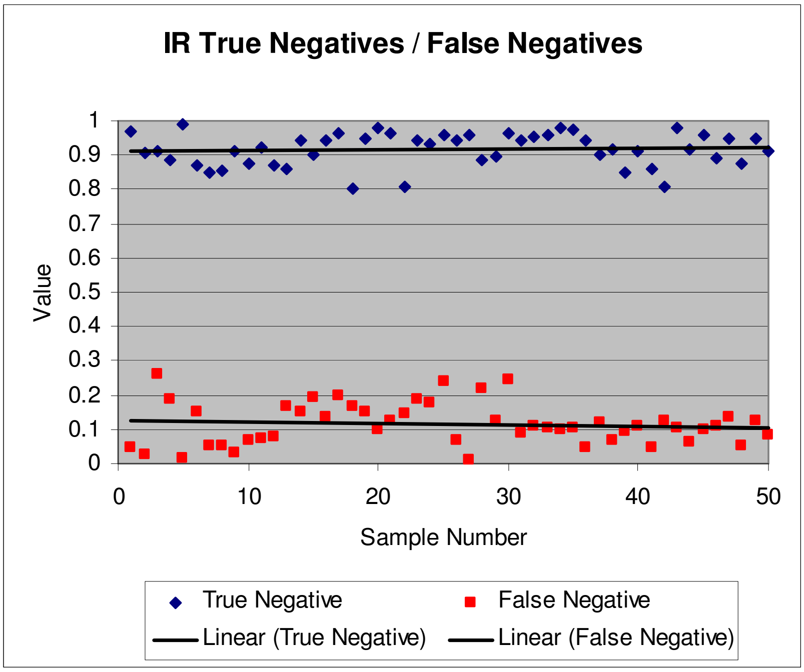

Figure 4.8 Thermal True Negatives / False Negatives

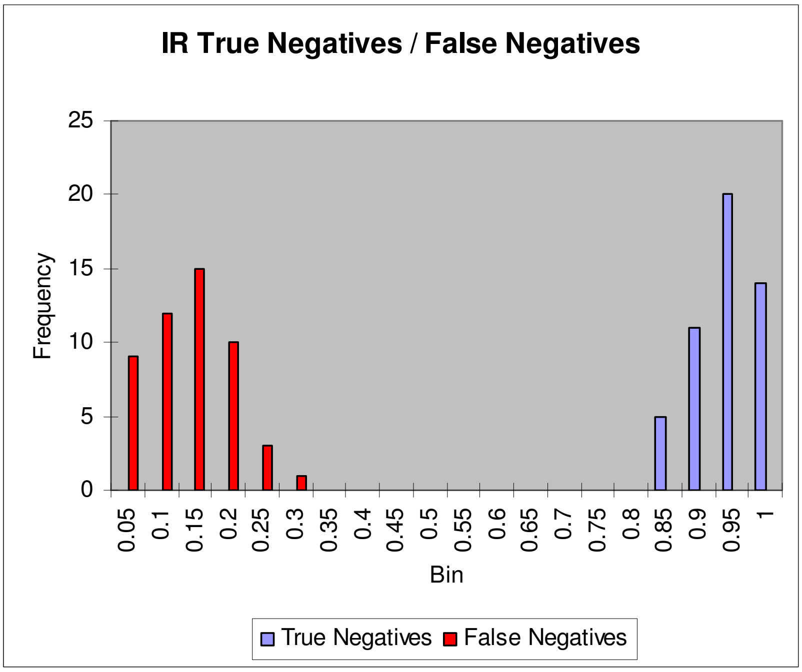

Figure 4.9 Histogram of thermal IR true negatives / false negatives

The histogram of true negatives shows a single distribution with a mean value of 0.916. When observing the chronological order of the true negatives in the thermal case, little change in the ability of the algorithm to pick out the true negatives over time is found.

In comparison to the visible results, the foreground results derived from the thermal IR sequence shows greater discrimination ability across the samples, and has a smaller deviation of results across the sample set.

In order to combine the binary classification measures to provide a balanced measure of the capability of the modality, the F-measure (described in Equation 4) is calculated for the thermal IR sequence. The results are shown in Figure 4.10.

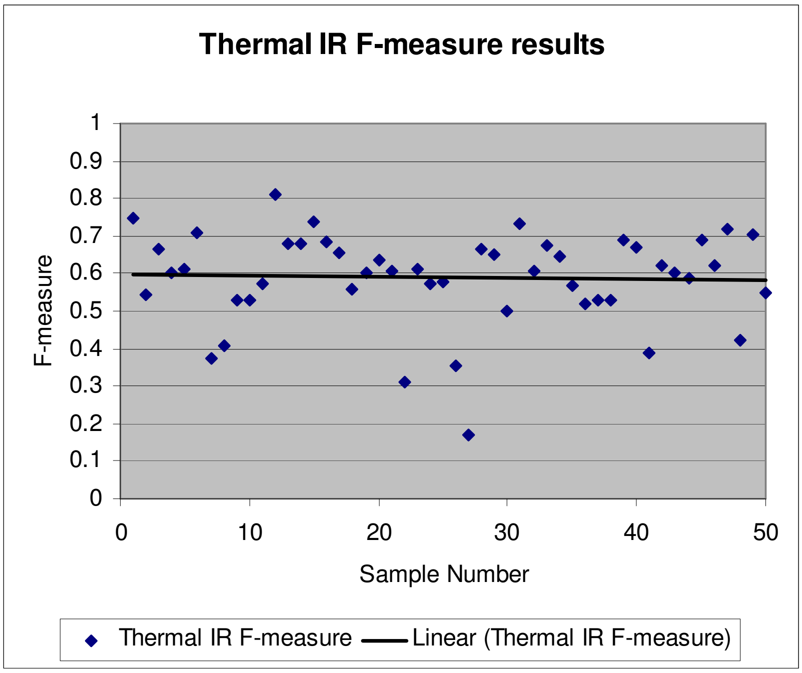

Figure 4.10 Thermal F-measure results across samples

The mean F-measure for the thermal modality is 0.589 with a SD of 0.123. Davies et al. (2005) achieved a mean F-measure across a series of scenarios of 0.7915.

4.1.3.3. Comparison of Visible and Thermal IR Results

The mean F-measure results and SD for each modality are shown in Table 4.3.

Modality	Mean F-measure	Standard Deviation
Visible	0.343	0.202
Thermal IR	0.589	0.123

Table 4.3 Thermal IR and visible mean F-measure results

Utilising KaewTraKulPong and Bowden's algorithm, a strong and more consistent background subtraction capability is observed using the thermal IR images than using the algorithm with the visible images. Observations suggested that the visible background subtraction capability of the algorithm was degraded under changing illumination. Changes in illumination do not affect the IR images directly. If radiation is strong enough to heat the surface of an object, a change will be observed. In most situations this will be a slow change, and within the thresholds of background updating algorithms. A consistent trend across the thermal IR results reflects this observation.

The results are inferior to those demonstrated by Davies et al. (2005). The authors demonstrate a contour saliency based method to exploit features specific to ferroelectric barium strontium titanate ($Ba_XSr_{1-X}TiO_3$) based thermal IR sensors. Artefacts of such sensors include a halo effect around human subjects who contrast sharply with the background scene. This effect is exploited by the authors to segment subjects from the image. This difference means that the results are not directly comparable.

One matter highlighted through evaluation of the results is the classification of subjects behind glass. In the ground truth data has subjects behind glass are classified as foreground. However, due to the absorption and reflection by the glass of wavelengths detected by the thermal IR camera, these areas appear opaque in the IR images.

Results in both modalities were found to have suffered due to false classification of reflections as foreground regions. The scene used for experimentation was highly dynamic with many moving background components such as glass doors and security gates and had a high content of reflective surfaces. The results demonstrate that thermal IR data for background subtractions shows stronger candidature for independent subtraction of human foreground regions than does data sourced from a visible camera.

4.2 Thermal IR Intra-Region Segmentation

Observations made on the results of the previous experiment prompted investigations into a method for extracting regions of interest from candidate foreground regions using thermal properties. The purpose of the experiment is to establish whether a statistically produced foreground mask from the thermal IR source can be combined with a temperature range mask in order to identify skin and clothing regions. These regions would be useful for building appearance models and as inputs to advanced footfall or surveillance systems. Skin detection using thermal images would be useful in pose estimation and as an automated candidate producer for visible camera based facial feature algorithms.

4.2.1 Method

The samples in Dataset B are used for this experiment. In order to evaluate temperature distributions between the clothing and skin component areas of human subjects in thermal IR images, data capture has been undertaken in an environment in which subjects are exposed to a wide range of temperatures. Histograms of the infrared values in manually subtracted regions within each image are compared to determine if the differences in temperature between these regions are sufficient to allow reliable segmentation of subject's component areas.

4.2.2 Expected Results

It is expected that the distribution means for skin, clothing and background scenes will display significant separation on an individual sample basis. The extent to which the values will be distributed and the extent to which they will overlap across the sample set is unknown. There is expected to be significant difference in the mean clothing temperature distribution between the subsets of humans entering and those exiting the buildings.

4.2.3 Results and Discussion

Figure 4.11 shows the normalised distributions of the skin and clothing across the sample set. The temperature measurements are configured to be accurate for the properties of human skin and the environment at the time of capture. The range of emissive, absorption and reflective properties of the clothing's constituent materials means that incident radiation detected from these regions cannot be relied on to provide accurate temperature readings. For this reason, values detected by the camera in the clothing region cannot be seen as temperature accurate and must be viewed as a scalar reading of incident radiation.

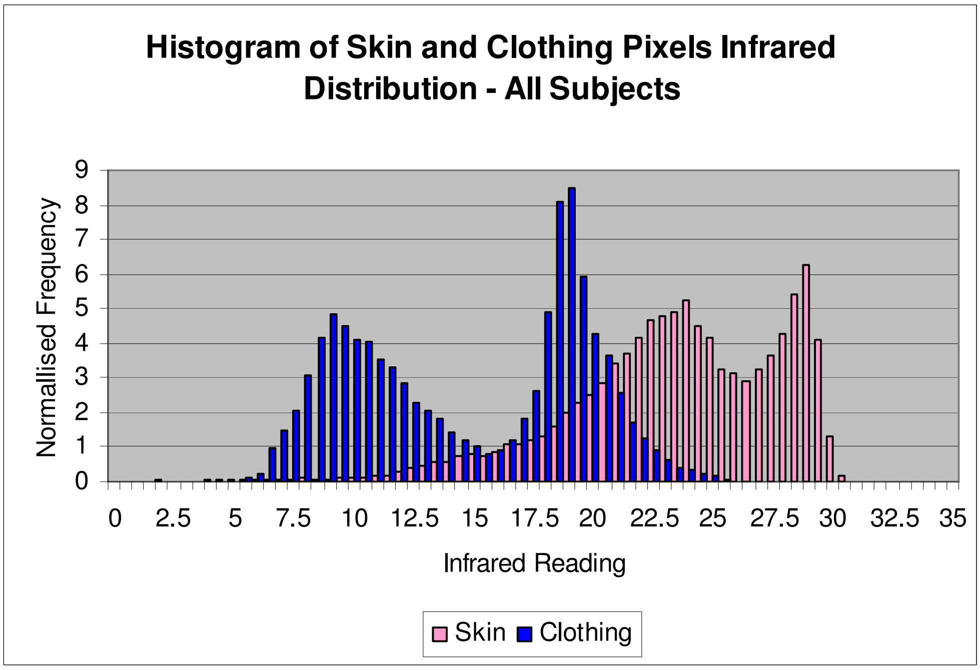

Figure 4.11 Mean histogram of all samples separated into skin and clothing distributions

It can be seen from the histogram that the skin and clothing distributions have a large range and overlap to a considerable extent. Whilst the overall distributions are not Gaussian, they seem to be the result of the summation of constituent distributions that have a more Gaussian shape, indicating that they are made up of discrete subsets. It is theorised that such a mixture of Gaussians may be accounted for by separation of the data into two sets of people, one entering and the other exiting the building. In Figure 4.12, temperatures for pixels representing skin regions across the dataset separated into entering and exiting sets and normalised are shown.

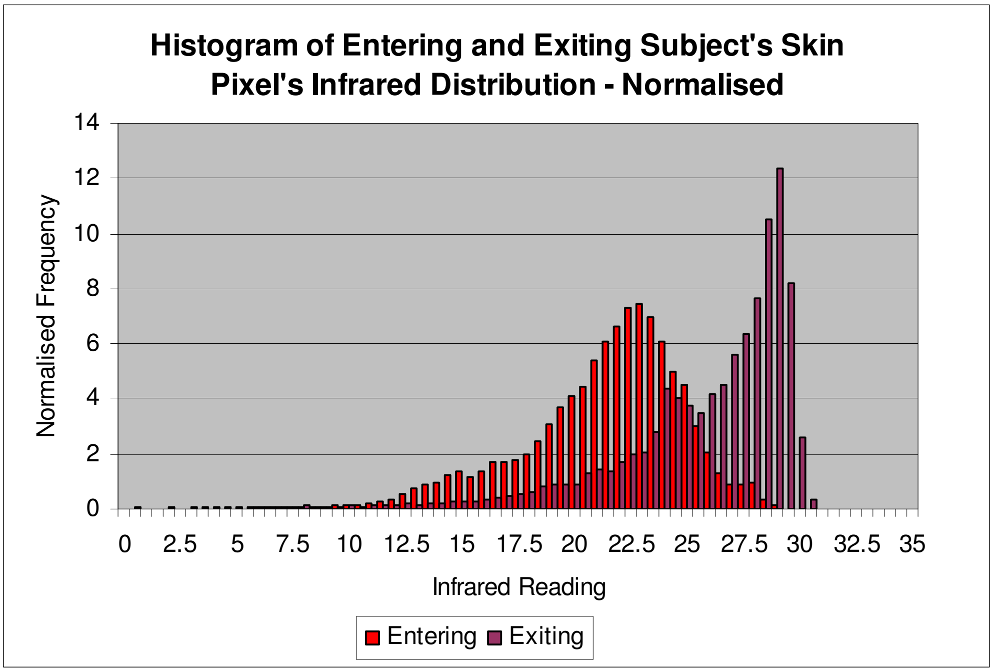

Figure 4.12 Mean histogram of skin pixel thermal IR readings separated into entering and exiting distributions.

Figure 4.13 shows the incident radiation detected at pixels representing clothing regions segmented by subjects entering and exiting the building. The sample subsets are normalised.

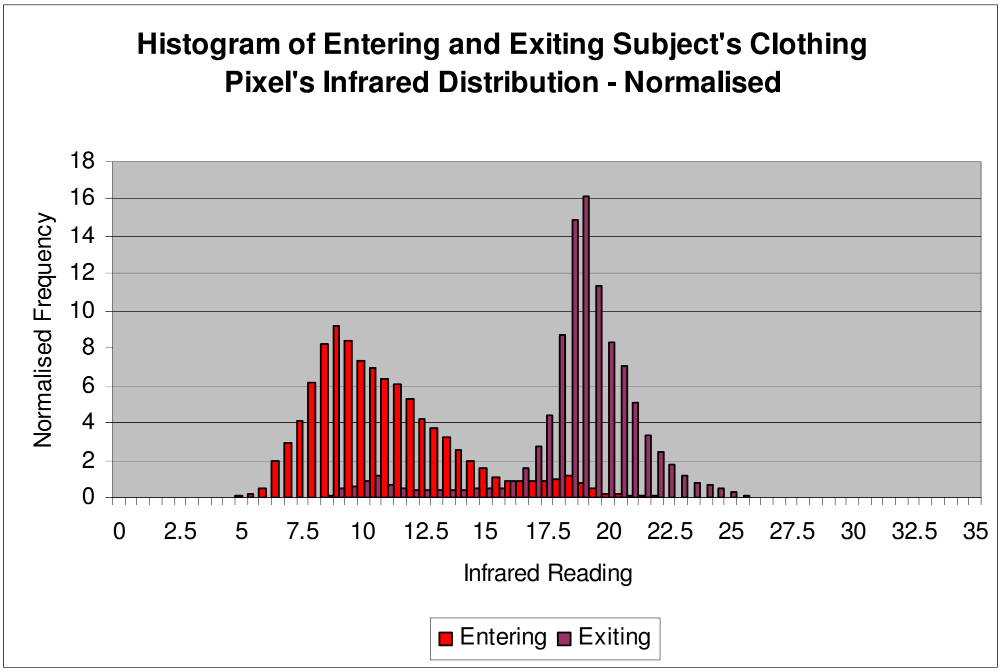

Figure 4.13 Mean histogram of clothing pixel thermal IR readings separated into entering and exiting distributions

It is evident from these results that segmenting the data into entering and exiting subsets, the hypothesis that the observations are caused by multiple Gaussians representing these subsets is confirmed.

The results suggest that in scenes where the human targets are subject to environments with a range of temperatures, a single threshold cannot be used to reliably segment the clothing and skin temperatures across the sample set. Based upon these findings it is hypothesised that the use of higher level context information for altering the threshold may give a higher segmentation capability. By splitting the image set into entering and exit groups, the separation of the data in situations where the human foreground has been segmented can be considered. Figure 4.14 shows the normalised distributions of pixel values for skin and clothing regions on the set of people entering the building.

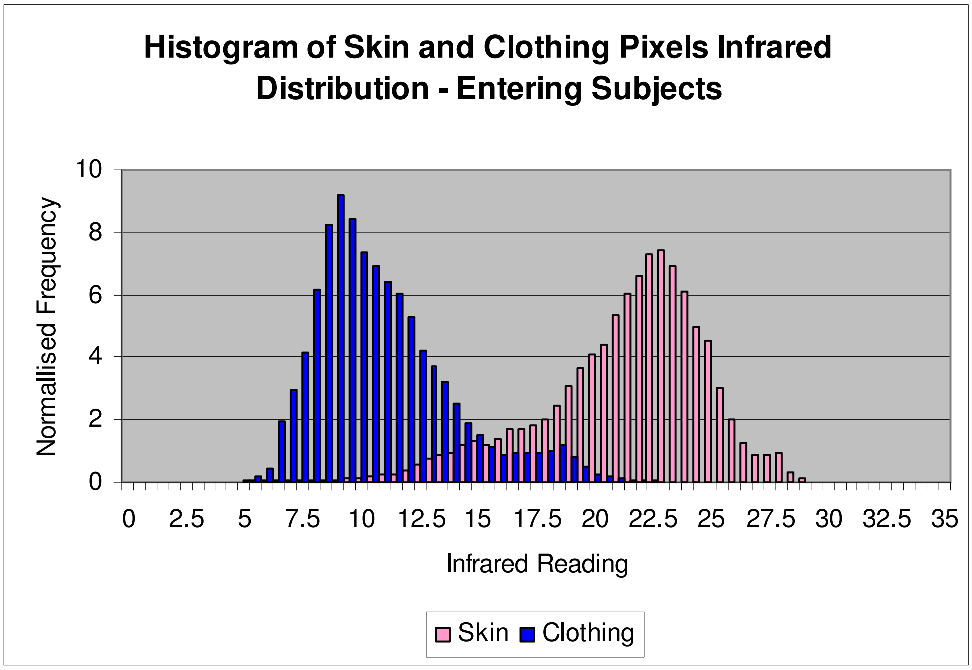

Figure 4.14 Mean histogram of entering subject's skin pixel thermal IR readings separated into skin and clothing distributions

It can be observed that to correctly classify 95% of skin pixels, 87% of clothing pixels would be falsely classified as foreground. Optimal segmentation by thresholding occurs at 15°C allowing 93.63% of skin and 90.88% of clothing to be correctly segmented.

Figure 4.15 shows normalised distributions of pixel values on the set of people exiting the building.

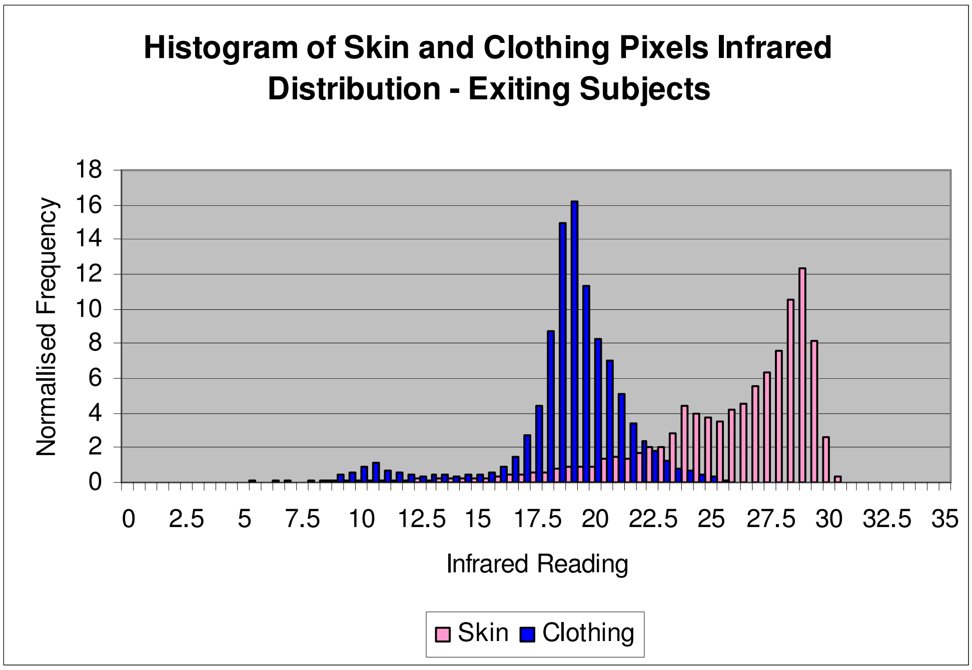

Figure 4.15 Mean histogram of exiting subject's skin pixel thermal IR readings separated into skin and clothing distributions

In this case it can be observed that to correctly classify 95% of skin pixels, 17% of clothing pixels would be falsely classified as foreground. Optimal segmentation by thresholding occurs at 22.5°C allowing 84.89% of skin and 96.56% of clothing to be correctly classified.

Clothing and skin pixels occur in different ratios across the samples so finding the optimum segmentation point cannot be obtained using this low level information alone. Determining a threshold point dynamically in an image could be undertaken after an additional classification step based upon learned scenario data. Alternatively a Gaussian fitting algorithm such as expectation maximisation or Markov chain Monte Carlo methods could be used to fit Gaussian models to the data. However the overlap between skin and clothing values would not allow for highly accurate segmentation on this basis.

4.3 Evaluating Sensor Reliability for Modality Selection

It has been shown in the literature that in situations where a foreground region reflects or emits radiation of the same intensity as the modelled background, pixel level statistical techniques will not be able to correctly classify the foreground regions due to this camouflaging effect. It is clear that to overcome issues in this area, techniques that take further regional or scene information into account are needed. It is therefore reasonable to hypothesise that holistic analysis of the environment may be able to indicate the background subtraction capability of a modality using statistical techniques.

The temperature of the environment surrounding a scene varies throughout the day and the year. It has been noted that in hot weather, human regions can appear cooler than the environment in thermal IR images due to evaporation based cooling; while camouflage and illumination issues affect the quality of background subtraction in the visible modality. It is hypothesised that information present in the full images of the scene may give cues as to the quality of the scene for the stage of statistical background subtraction. In this section, experiments are described which assess a number of proposed measures of cues that may indicate scene quality. The cue measures evaluate properties of the current scene images (static) or changes in a measurement over time (temporal). Cue measures which indicate the quality of the input are used as an input to a Neuro-Fuzzy inference system. The system is trained using results from binary classification of pixel level comparisons between manually segmented foreground masks and the statistically produced foreground masks.

4.3.1 Method

The samples in Dataset C are used for this experiment. Candidate cues are calculated for each sample image and compared to the capability of background subtraction at that point (defined by the F-measure) using covarience. The quality results for each sequence are calculated using the mean F-measure across all images in the sequence as shown in Equation 7 in which n is the number of images constituting the sequence, P is the precision and R is the recall of the image.

$$MF = \frac{\sum_{i=0}^{n}\left(2\left(\frac{P \bullet R}{P+R}\right)\right)}{n}$$

Equation 7 Mean F-measure definition

The F-measure results are used as an indicator of the quality of the information received from the sensor. Using the results from calculation of the candidate cues detailed below, the co-variance of the F-measure with the candidate cue measurement is used to determine the capability of the cue in assessing modality quality.

In order to assess temporal cues, the mean difference between a cue's measurement in the current image and from an image x seconds preceding the current image is calculated. The extent to which these measures co-vary with the F-measure is calculated as described in Equation 8 (where T is the calculated temporal difference n is the number of images, M is the measure and n is the number of images).

$$T = \frac{\sum_{i=0}^{n}\left(M_i - M_{i-x}\right)}{n}$$

Equation 8 Temporal calculation definition

4.3.1.1. Static Visible Candidate Cues

Cue measures are proposed based upon observations of scene dynamics, knowledge of the capture methods and the theory of the nature of visible and infrared electromagnetic radiation along with understanding statistical background subtraction.

In the visible modality, it is known that saturated or unlit visible images will be inadequate for background subtraction. Investigations are undertaken to determine the specifics of the relationship between the brightness values of the background of a visible scene and the background subtraction capability. The scene brightness measure is the mean pixel value of the scene using fixed camera parameters. The calculation is shown in Equation 9 where *B* is the brightness, *n* is the number of images, *X* and *Y* are the dimensions of the image and *r*, *g* and *b* are the red , green and blue pixel intensities.

$$B = \frac{\sum_{i=0}^{n}\left(\frac{\sum_{x=0}^{X}\left(\sum_{y=0}^{Y}\left(\frac{r_{ixy} + g_{ixy} + b_{ixy}}{3}\right)\right)}{XY}\right)}{n}$$

Equation 9 Brightness definition

In addition, it is theorised that the contrast in the visible image may also be an indicator of the background subtraction capability. In images with poor illumination, the contrast between the background and foreground regions is often not sufficient for segmentation of foreground pixels from the background model using statistical techniques, as the current value of a pixel may fall within the SD threshold limits of any Gaussian representing the pixel. Contrast is therefore proposed as another possible cue for background subtraction capability. The contrast calculation is defined in Equation 10.

$$C = \frac{\sum_{i=0}^{n}\left(\sqrt{\frac{\sum_{x=0}^{X}\left(\sum_{y=0}^{Y}\left(M - P_{xy}\right)\right)}{X \bullet Y}}\right)}{n} \quad \text{where } M = \frac{\sum_{i=0}^{n}\left(\frac{\sum_{x=0}^{X}\left(\sum_{y=0}^{Y}\left(P_{xy}\right)\right)}{X \bullet Y}\right)}{n}$$

Equation 10 Contrast definition

A further candidate cue proposed is that of the strength of edges present in the image. This measure, related to contrast, may provide additional information regarding the distinction between objects in the scene. The measure utilises the Sobel operator and is defined in Equation 11.

$$E = \frac{\sum_{i=0}^{n} \left(\frac{\sum_{x=0}^{X} \left(\sum_{y=0}^{Y} \left(|G_X| + |G_X| \right) \right)}{X \bullet Y} \right)}{n}$$

where

$$G_x = \begin{bmatrix} -1 & 0 & +1 \\ -2 & 0 & +2 \\ -1 & 0 & +1 \end{bmatrix} \quad G_y = \begin{bmatrix} -1 & -2 & -1 \\ 0 & 0 & 0 \\ +1 & +2 & +1 \end{bmatrix}$$

Equation 11 Edge strength definition

4.3.1.2. Static Thermal IR Candidate Cues

In the thermal IR modality, it is hypothesised that the temperature of the scene background may indicate the quality of background subtraction using the statistical technique. Using the captured thermal images, the background in all frames is manually segmented and the background temperature is altered by increments of 1°C.

In the thermal modality, the mean temperature of the environment background is proposed as a candidate cue. The measure of this cue is shown in Equation 12.

$$T = \frac{\sum_{i=0}^{n} \left(\frac{\sum_{x=0}^{X} \left(\sum_{y=0}^{Y} \left(P_{xy} \right) \right)}{X \bullet Y} \right)}{n}$$

Equation 12 Mean temperature definition

4.3.1.3. Temporal Candidate Cues

In addition to absolute measures of the proposed cues, it is hypothesised in situations where the brightness and temperature of the scene change; false positives will increase and foreground extraction capability will be reduced due to the background pixel levels shifting outside the threshold on the Gaussian description of the pixel. For this reason analysis of how changes in the measurement of the cues over time can influence the foreground extraction capability will be undertaken. Changes will be calculated over lengths of time from five to sixty seconds by comparing cue measurements between the current and historical frames. Co-variance of the cue measurements and the foreground extraction capability is calculated to determine the capability of the cue measurement.

4.3.2 Expected Results

In the thermal image sequences, it is expected that the incident radiation detected from the scene background will affect the statistical background subtraction capability as camouflaging occurs due to background incident radiation approaching that detected from the human body. It is unknown as to whether the background temperature will change at a rate which cannot be compensated for by the background model's updating algorithm.

It is expected that changes in the brightness of a scene over time will influence the background subtraction capability of the visible source. Changes in brightness over a short period of time are expected to be most influential in reducing the segmentation capability of the background while the extremes of the brightness are expected to show poor capability due to lack of information on scene content.

For all temporal results, changes must be significant enough to cause the pixel scalar or vector to exceed the standard deviation threshold of the background model Gaussian. It is expected that as changes in contrast and the mean temperature will be small over the sample set and these temporal measures will not change significantly within a sequence.

4.3.3 Results and Discussion

Results are separated into modality type and static/temporal sections. Evaluation of the results is undertaken to determine if the proposed measures of scene quality indicate the foreground extraction capability of the statistical technique in the scene.

4.3.3.1. Static Visible Results

Figure 4.16 shows the visible F-measure results calculated from the automated and manually segmented masks comparisons for the visible images plotted alongside the normalised measure of the brightness of the scene. Each measurement is the mean F-measure across the images constituting the sequence. The number of images in a sequence ranges from 14-17 images. It is observed that the decline in the measurements over time has linear characteristics.

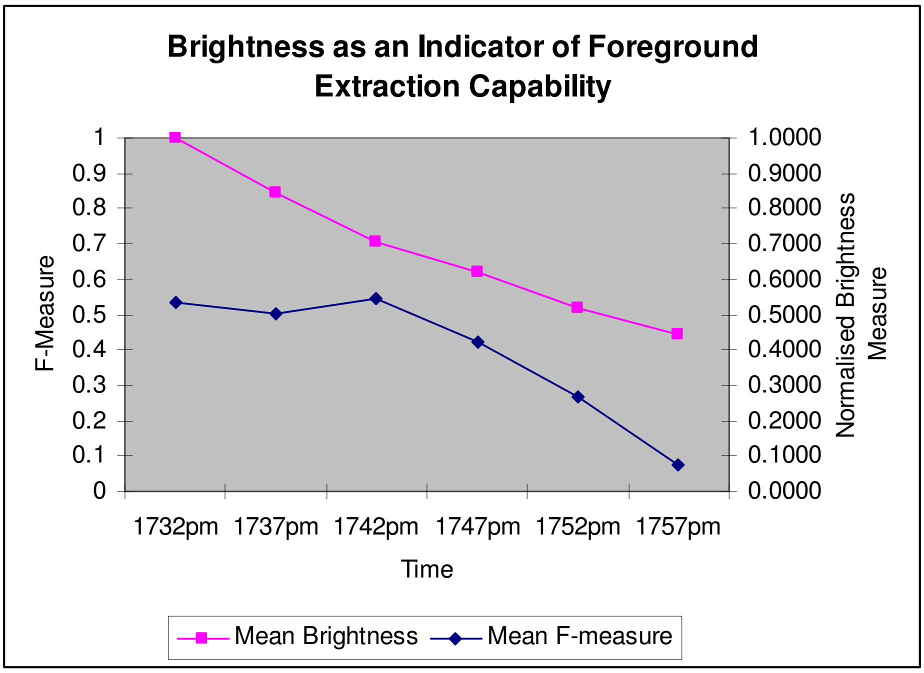

Figure 4.16 Brightness as an indicator or foreground extraction reliability

It can be seen from the results in Figure 4.16 that the mean F-measure results from the foreground extraction algorithm declines with the brightness in the visible sequences. For this reason, brightness is selected as an indicator of visible scene quality.

Figure 4.17 shows the visible F-measure results plotted alongside the normalised measure of the contrast of the scene.

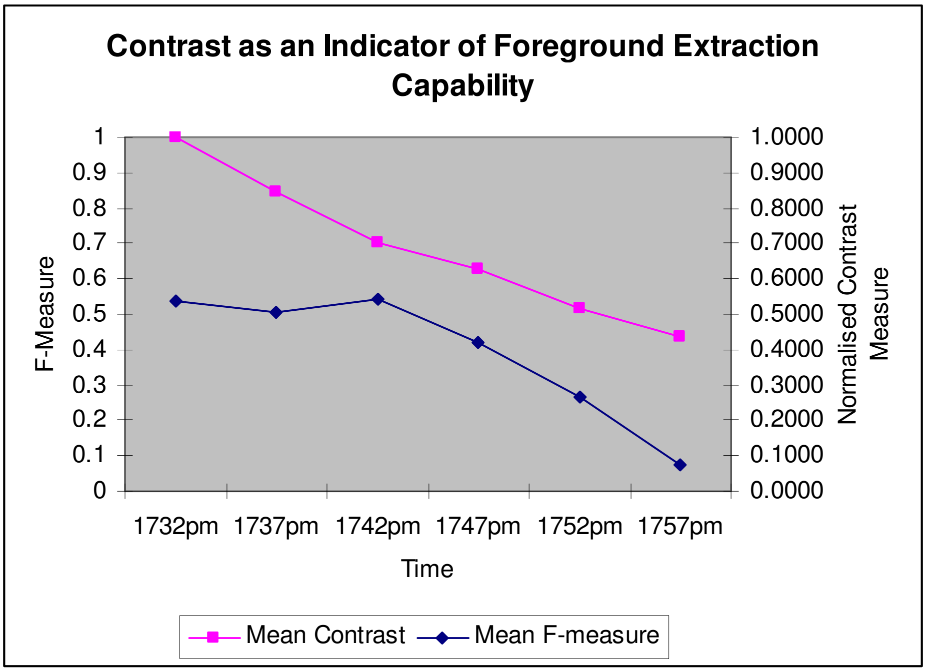

Figure 4.17 Contrast as an indicator or foreground extraction reliability

It is clear that contrast is virtually identical to brightness. It was found that this was due to the presence of pixels in each image at or very close to the minimum value (black pixels). The very high likelihood of a black pixel in any scene means that in many situations contrast will be virtually identical to the brightness measure.

Figure 4.18 shows the visible F-measure results plotted alongside the normalised measure of the edge intensity of the scene.

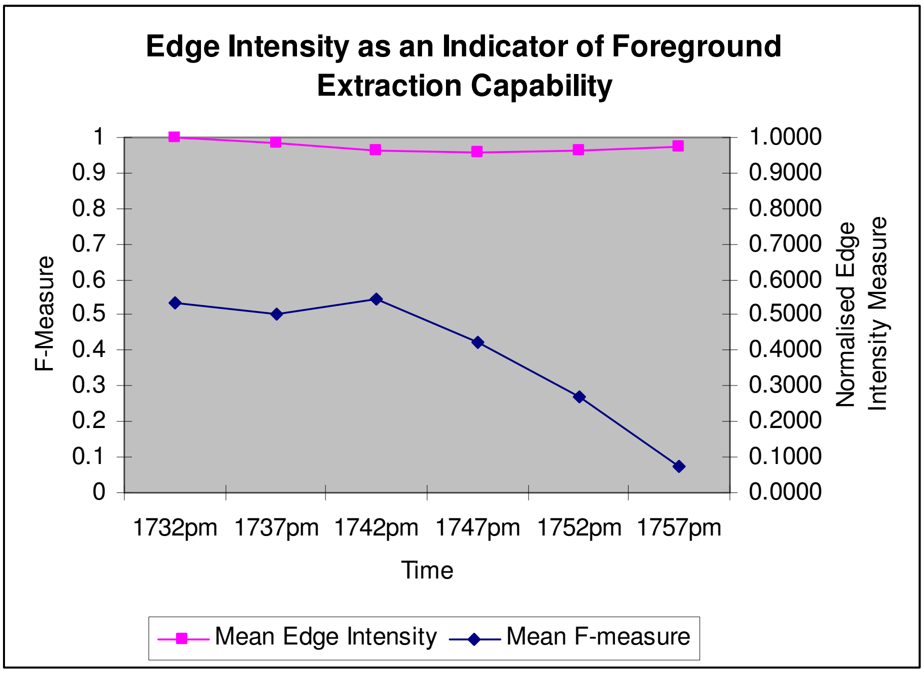

Figure 4.18 Edge Intensity as an indicator or foreground extraction reliability

It is found that measure of edge intensity does not significantly vary with the F-measure over time.

4.3.3.2. Static Thermal IR Results

Figure 4.19 shows the change in mean temperature of the scene and the resulting effect on the on the F-measure. In each scene the background temperature has been artificially increased in 1°C increments. Each point represents the mean F-measure from a number of images from all of the sequences.

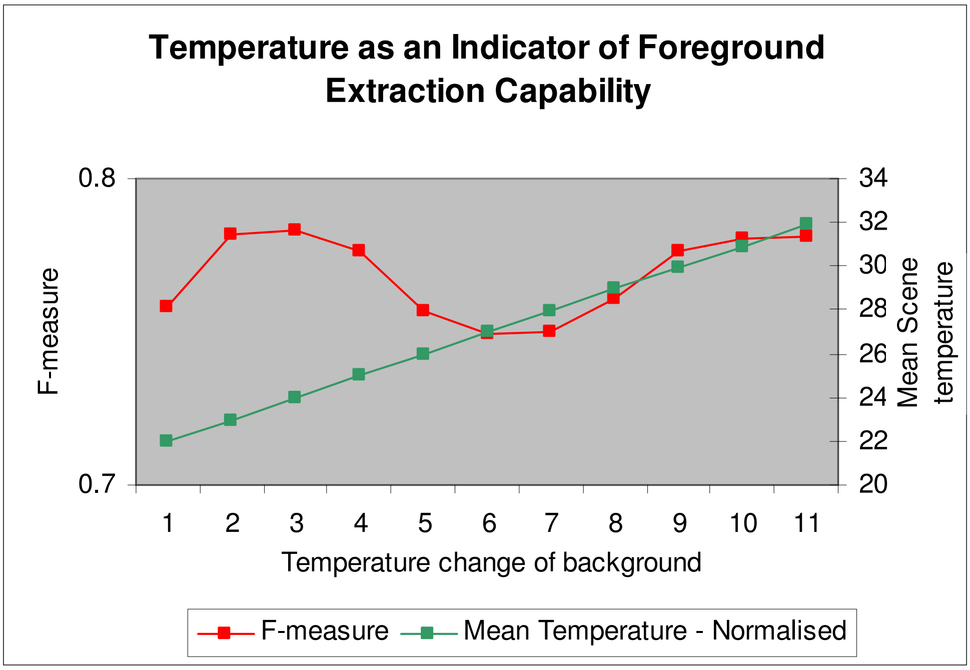

Figure 4.19 Temperature as an indicator of foreground extraction reliability

It is observed from the results that the mean F-measure results are reduced as the temperature of the background reaches that of the surface human temperature. A trough can be seen in the results around the point at which the scene background emits radiation at the equivalent of 28°C from a human subject. It can be derived from these results that the mean temperature of the scene gives an indication of the background subtraction capability using the thermal camera. For this reason the mean scene temperature is selected as an indicator of the foreground extraction capability of the thermal source.

4.3.3.3. Visible Temporal Results

The results of the temporal covariance experiments on the visible source are shown below. Figure 4.20 shows the covariance of the F-measure with the difference in brightness over periods of five to sixty seconds at five second intervals.

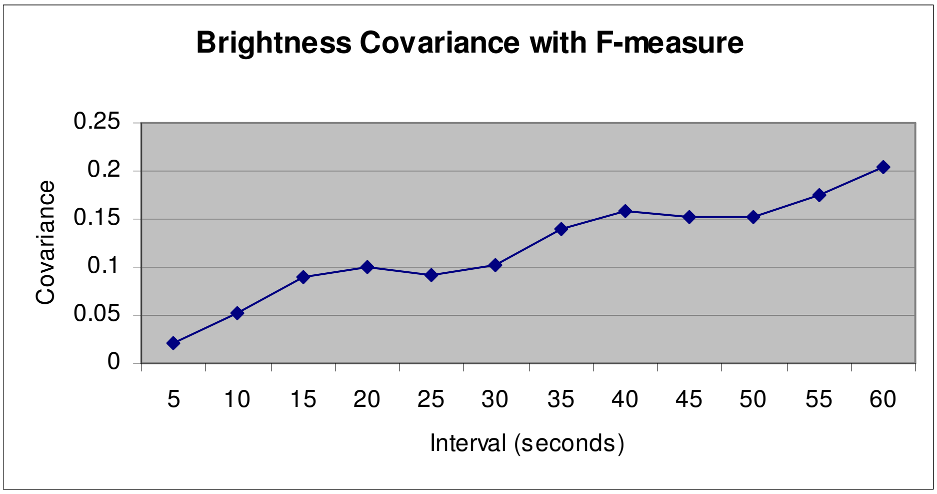

Figure 4.20 Covariance of the Brightness cue with F-measure

It can be observed that the change in brightness over longer periods of time is a strong indicator of the quality of the visible modality. It is expected that this measure will be a key indicator for typical scenes such as those represented where visible foreground extraction capability is strongly influenced by changes in brightness.

Figure 4.21 shows the covariance of change in contrast with the F-measure.

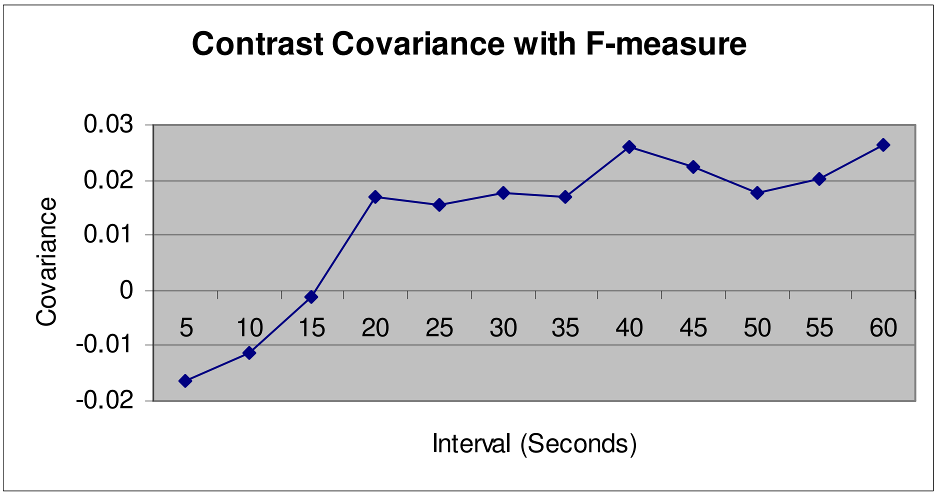

Figure 4.21 Covariance of the Contrast cue with the F-measure

The results show an increasing level of covariance over long periods of time; however the extent of change was minimal. Further work would be required using scenes with higher dynamic contrast to establish the reliability of this cue.

Figure 4.22 shows the covariance of the change in edge intensity with the F-measure.

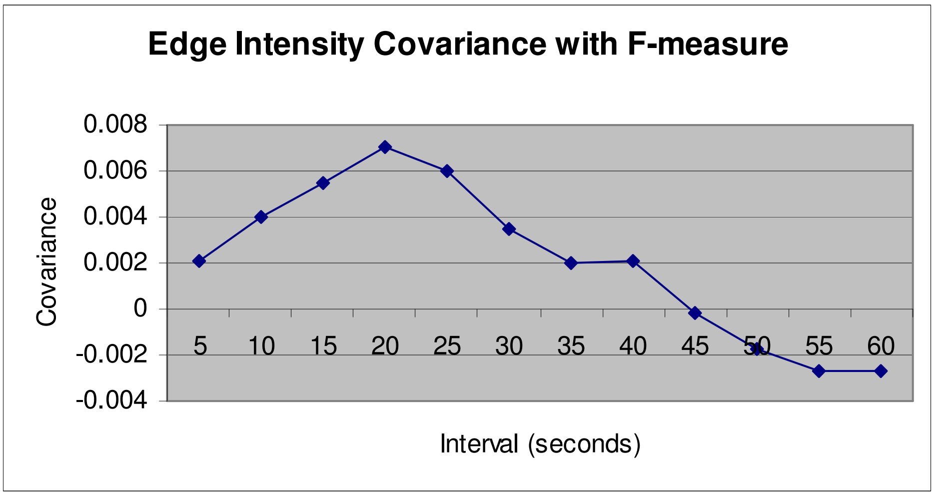

Figure 4.22 Covariance of the Edge Intensity cue with the F-measure

The results show very little co-variance of edge intensity with the F-measure. It is expected that this is due to little change in contrast in the sample sets.

4.3.3.4. Thermal Temporal Results

Figure 4.23 shows the covariance of the F-measure with the change in mean temperature.

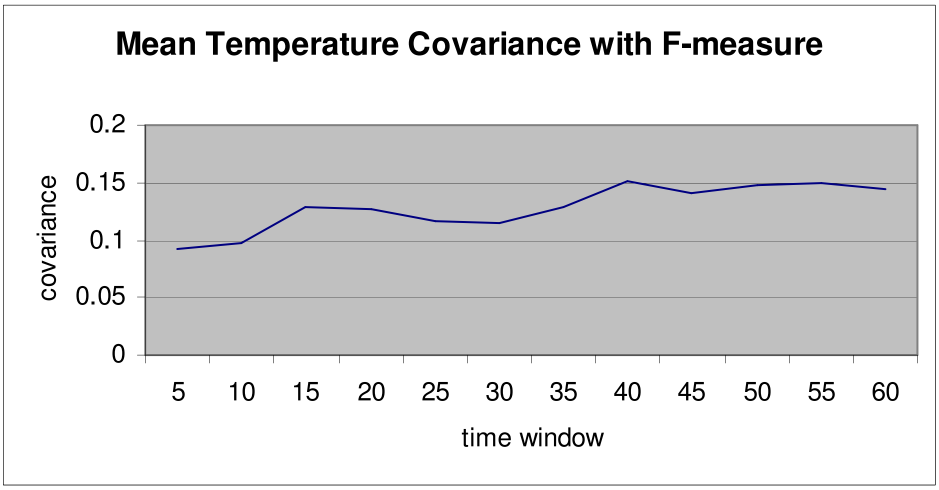

Figure 4.23 Covariance of the Mean Temperature cue with the F-measure

A small covariance is observed which increases as the interval increases. The co-variance levels after an interval of 40 seconds. This result however shows a low covariance, as expected. It is likely that this is due to the samples captured having little representation of events which led to a high rate of temperature change such as rainfall. Such events are typically much rarer than those affecting visible images, such as shifting cloud cover and the switching on and off of lights.

Using covariance with the F-measure, these results indicate that the brightness and temperature are the strongest cues for foreground extraction capability the visible and thermal modalities respectively. It has also been found that a change in brightness over time contains strong indications of the foreground extraction capability of the visible modality. These measures are presented as primary measures of scene quality. While temporal measures of contrast did not show a high quality indication capability, it is expected that the measures will provide useful information in conditions of extreme change not represented in the training set.

4.4 Neuro Fuzzy Inference for Evaluating Evidence

Utilising the cue measures described in the previous section, evaluation of scenes in order to determine the optimum modality is proposed. Neuro-fuzzy inference is selected to evaluate the scenes and determine optimum modality. A neuro-fuzzy inference system uses neural network methods in order to produce a fuzzy reasoning system based upon trained examples. This takes the form of a multi-dimensional decision surface. The decision surface is used to evaluate the cue evidence and make a modality choice.

4.4.1 Method

The samples in Dataset D are used for this experiment. Calculation of the cue measurements is undertaken for each of the samples. For temporal measurements this involves calculations of the quality measures, for periods preceding the sample over intervals determined in the previous experiment.

Manual segmentation of humans region in the image sequences is undertaken. Statistical background subtraction is also undertaken and the results are compared to give background subtraction accuracy measure for each sample and a modality decision for each sample based upon the F-measure results for each modality. This process provides a decision for the optimum modality. This decision is used in conjunction with scene measurements to provide training examples of cues and the corresponding modality decision.

A Sugeno type (Takagi and Sugeno 1985) Neuro-fuzzy inference system is implemented using the MatLab Fuzzy Logic Toolbox and used to make decisions on the optimum modality using the scene evaluation calculations. A training stage is undertaken in which 30 samples containing the cue measurements and the target modality decisions are used to train the system. A second smaller set is used as a testing set to determine how well the system performs on data it has not been tested upon. A checking set is used to ensure over fitting of the model does not occur. Results show the assessment capability of the trained Neuro-fuzzy inference system applied to a set of 48 evaluation samples. Figure 4.24 shows the topography of the system.

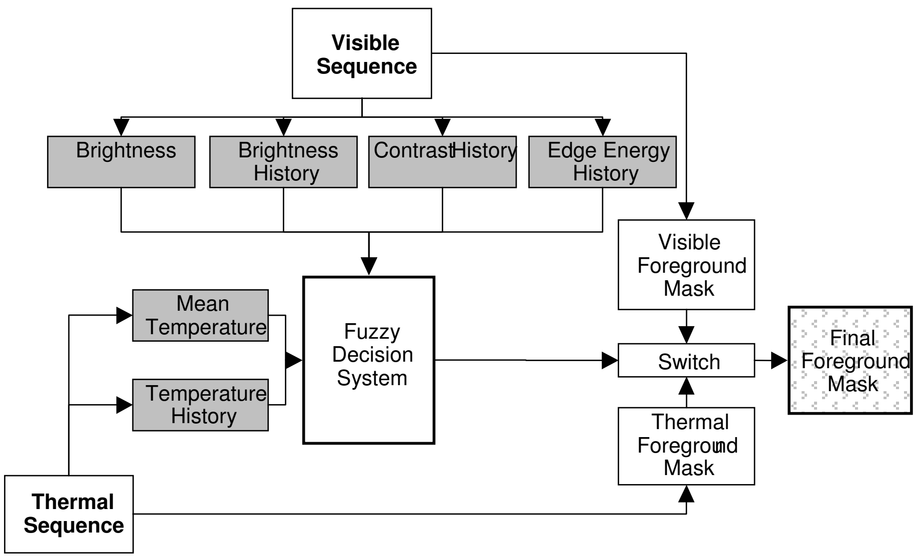

Figure 4.24 Data flow through the neuro-fuzzy inference system

4.4.2 Setup

A Sugeno type neuro-fuzzy inference system (Takagi and Sugeno 1985) with weighted average defuzzification has been selected for use in modality selection. It is favoured for its linear output capabilities, which are ideal for the binary decision requirements. An overview of the system inputs and output function is shown in Figure 4.25.

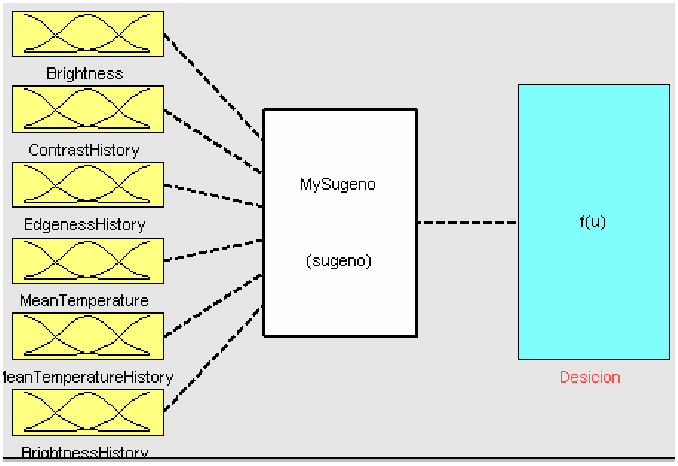

Figure 4.25 Neuro-fuzzy Inference System

Graphical representations of the manually implemented membership functions for each cue measure are shown in Figure 4.26.

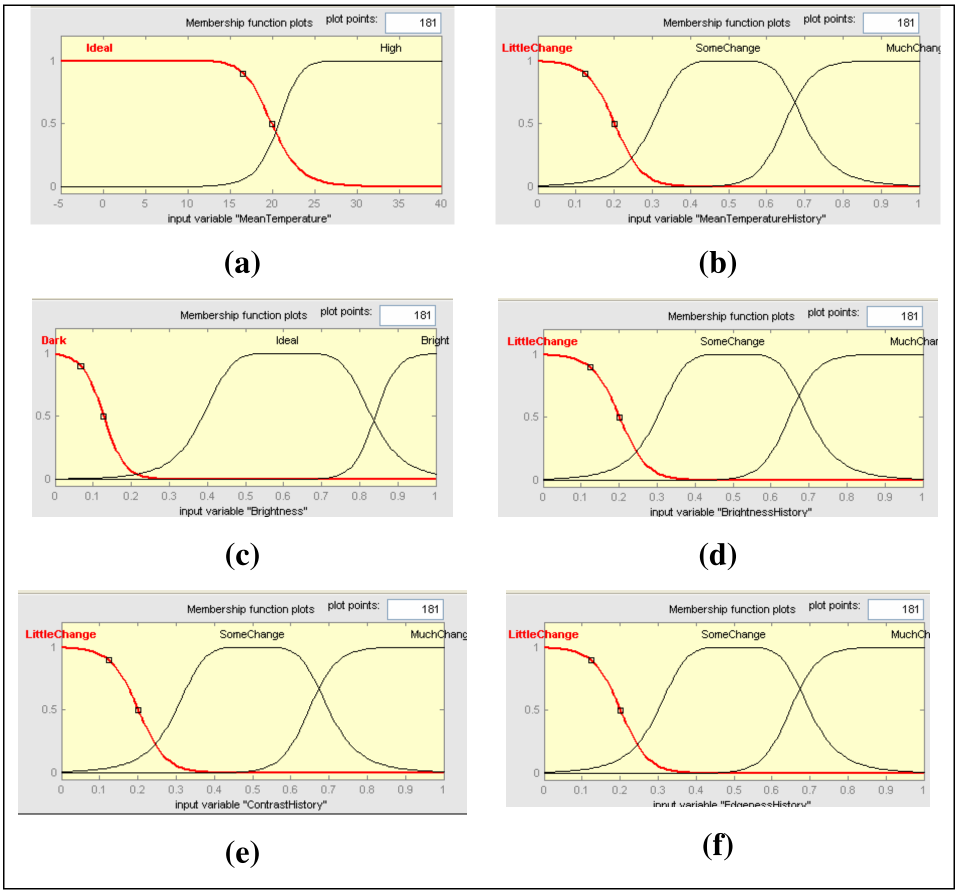

Figure 4.26 Membership functions. (a) Mean temperature, (b) Mean temperature history,(c) Brightness, (d) Brightness history, (e) Contrast history, (f) Edge intensity history

The mean temperature membership function plot has an ‘ideal’ function which reduces as the temperature of the scene approaches the temperature of humans in the scenes. The brightness plot has a range of ideal brightness where the scene is not in darkness and is not saturated. The temporal measures have membership functions representing the degree of change over the established period.

4.4.3 Expected Results

It is expected that the system will be able to choose the optimum modality, defined by the highest F-measure in an image pair at a rate greater than chance using the cues established in 4.3. The extent to which the system will perform above this level however is unknown.

4.4.4 Results and Discussion

Figure 4.27 shows the training iterations of a 40 epoch cycle plotted against the checking data. It is observed that after 9 epochs, the decreasing error rate attained its lowest value, after which little change is observed.

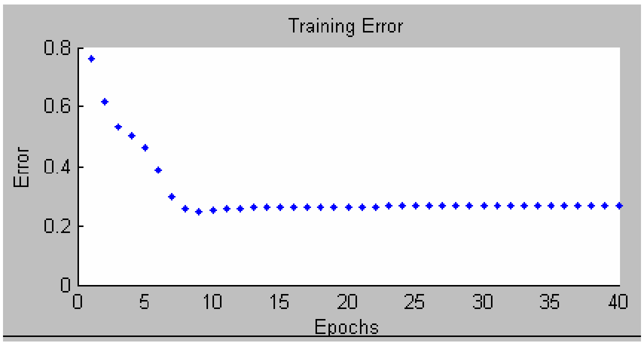

Figure 4.27 Training the neuro-fuzzy inference system

After training the system using a 9 epoch training cycle, the trained system is applied to the evaluation set. The results of the modality predictions for the evaluation set are shown in Figure 4.28 where the predictions are thresholded to provide a binary modality decision.

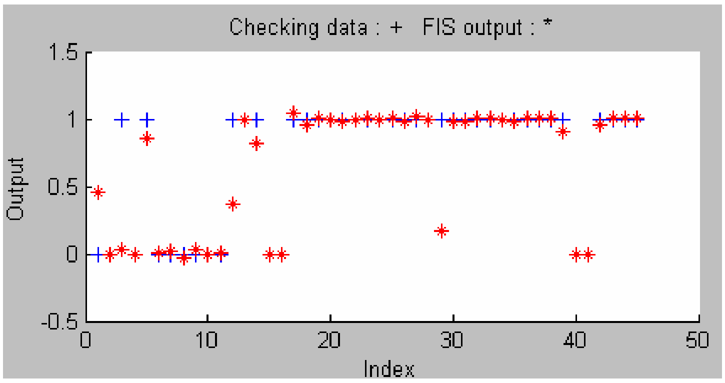

Figure 4.28 Modality decision evaluation results produced by the trained system

Evaluation of the trained system on the 48 sample evaluation set yielded a capability measure of the system to assess the scene at 91.3% with a 95% confidence interval of 8.1%. The resulting trained system shows an effective ability to assess the individual modalities based on current and historical information, achieving an effective modality decision capability.

Further work would involve expanding the sample set to include a greater range of environmental conditions. These might include high temperature backgrounds and scenes of heavy fog. An increased number of samples would also decrease the confidence interval to allow for greater reliability in assessing the system's capabilities.

The system currently runs using the MatLab fuzzy logic toolbox. In order to implement a real-time system integrated in a complete tracking system; a software implementation of the structure, training and assessment functionality would have to be undertaken.

4.5 Conclusions

Work has been undertaken to evaluate a series of proposed cues which it was theorised may indicate the quality of a modality. Assessment of these cues has resulted in a series of cue measures of single frames and measures of temporal changes across an interval. An effective method has been utilised for assessing these measures and providing an optimum modality decision in a number of environmental scenarios. The assessment of the measures of scene cues was achieved utilising a Neuro-fuzzy inference system trained and assessed on comparisons between manually segmented ground truth human regions and automatically extracted regions. The resulting systems show a good decision capability in thermal IR and visible modality decisions. Possible future work would centre on extension of the dataset to include an even greater variety of environmental scenarios and assessment of alternative scene measures which may indicate the quality of the scene for foreground extraction.

5 Histogram Optimisation

The use of colour as a component of a subject's appearance model is widely used due to the large number of possible combinations of skin, hair and clothing permutations. The range of clothing, skin and hair colours makes a large number of combinations available increasing the chances of histogram uniqueness in a multi-subject scenario. Subject identification is typically required after events such as occlusion or for tracking between cameras. Colour is typically represented using histograms or a Mixture-of-Gaussians (MoG) approach.

In this section the capabilities of current histogram utilisation techniques for discriminating between human subjects is investigated and methods for evaluating the effectiveness of techniques is proposed. A hypothesis for augmenting visible histograms to provide additional information using multimodal data is proposed and evaluation against existing techniques is undertaken using an exhaustive search approach. Discrepancies in performance between environments are investigated.

5.1 Evaluating the Efficacy of Histogram Configurations

It is noted by Moeslund and Granum (Moeslund, Hilton and Krüger 2006) that a histogram representation provides greater robustness in environments without high colour contrast levels of a MoG representation. In order to maintain reliability in less well illuminated environments, histogram representation is selected for re-locating subjects after an event such as occlusion or when the subject has left the scene.

Histogram configuration is a parametric problem. Optimising the histogram channels, the numbers of dimensions, the bin sizes along with selecting a method for comparing histograms are all considerations when attempting to achieve optimal discrimination capability, and all impact on the efficacy of histogram usage. In order to optimise the histogram parameter and comparison technique combination, referred to from this point as HPCTC, a method for evaluating HPCTCs is proposed. This performance metric evaluates the separation of inter-person (comparisons between histograms of different subjects) and intra-person (comparisons between histograms of the same subject in different images) results for multiple HPCTCs. It is proposed that the greater the segmentation of these results, the greater the discrimination capability using the HPCTC. Evaluation of the capabilities of the HPCTCs will be undertaken using histograms derived from human regions in visible and thermal images.

In order to verify the capabilities of the metric, comparisons with observations in the literature regarding optimal visible configurations is undertaken. Identification of human regions using histograms representation is typically undertaken by analysis of colour histograms in which channels are aligned with the brightness of the scene. This is to counter illumination variation in typical scenes. The metric is established by comparing the results with these observations in the literature, before moving to multi-modal HPCTCs.

5.1.1 Method

The samples in Dataset E are used for this experiment. A comparison method for evaluation of a HPCTC's discrimination ability is proposed. This method utilises results from inter-person and intra-person comparisons of HPCTCs. HPCTCs tested contain all combinations of bin size, channel type (representation of colour, illumination, etc), number of channels/dimensions and comparison techniques. In Table 5.1 parameters for 1-D visible HPCTCs are listed. The total number of possible combinations gives 120 HPCTCs.

Parameter	Selections
Bin Size	3,6,9,12,15,18,21,24
Channel	Hue, Saturation, Visible Greyscale (VGS)
Histogram Comparison Technique	Correlation, Chi-Square, Intersection, Bhattacharyya distance and the Earth Mover's Distance

Table 5.1 1-D HPCTC parameter options for a 1-D

The use of visible 2-D HPCTCs with dimension independent bin sizes give a total 2880 HPCTCs.

The metric evaluates the separation of results from intra-person comparison and inter-person results. An ideal HPCTC will provide a strong match for different images of the same subject and a weak match for images of different subjects.

Intra-person results are calculated by comparing images of a subject taken at different points in a sequence. This is performed on a number of subjects. Inter-person results are calculated by comparing each of a subject's images with images of different subjects.

The metric determines the best match achieved when comparing results of different subjects. This match score is used as a threshold, above which, comparisons of images of the same subject should give a better match in an ideal HPCTC. The metric evaluates the proportion of intra-person results above this threshold. An optional parameter x allows the threshold to be lowered to reduce any influence of outliers where a large number of intra-person results are used. x is the percentage of inter-person results, once ordered, above which the threshold is set. The pseudo-code calculation of D_x is shown in Figure 5.1.

```
Calculate_D(x)

    ResultList R_inter
    FOR i = 0 TO numPeople-1 BY 1
        FOR j = i + 1 TO numPeople BY 1
            FOR a = 0 TO numHists BY 1
                FOR b = 0 TO numHists BY 1
                    result = compareHistograms(person[i][a],person[j][b],HPCTC)
                    R_inter.add(result)
                NEXT b
            NEXT a
        NEXT j
    NEXT i

    sortlist(R_inter)

    thresholdIndex = R.size/100 * x
    threshold = R_inter[thresholdIndex]

    counter = 0
    FOR i = 0 TO numPeople BY 1
        FOR a = 0 TO numHists-1 BY 1
            FOR b = a TO numHists BY 1
                result = compareHistograms(person[i][a], person[j][b], HPCTC)
                IF result > threshold
                    counter = counter + 1
            NEXT b
        NEXT a
    NEXT i

    possibleResults = (numPeople*numPeople-1)/2 //Reed's law

    D = 100/possibleResults * counter

return D
```

Figure 5.1 Pseudo-code of discrimination ability calculation D_x

Evaluation of visible spectrum HPCTCs is undertaken using single and multi-dimensional histogram representations. HPCTCs using a range of equally sized bins from 3 to 24, independent of dimensions are used. Histogram comparison techniques shown in Equation 13 to Equation 16 are applied for the respective techniques (Bradski and Kaehler 2008). The techniques are Correlation, Chi-Square, Intersection, Bhattacharyya distance (Bhattacharyya 1943) and the Earth Mover's Distance.

$$d_{correl}(H_1, H_2) = \frac{\sum_i H_1'(i) \cdot H_2'(i)}{\sqrt{\sum_i H_1'^2(i) \cdot H_2'^2(i)}}$$

Equation 13 Correlation definition

$$d_{chi-square}(H_1, H_2) = \sum_i \frac{(H_1(i) - H_2(i))^2}{H_1(i) + H_2(i)}$$

Equation 14 Chi-square definition

$$d_{\text{intersection}}(H_1, H_2) = \sum_i \min(H_1(i), H_2(i))$$

Equation 15 Intersection definition

$$d_{\text{Bhattacharyya}}(H_1, H_2) = \sqrt{1 - \sum_i \frac{\sqrt{H_1(i) \cdot H_2(i)}}{\sum_i H_1(i) \cdot \sum_i H_2(i)}}$$

Equation 16 Bhattacharyya Distance definition

The earth mover's distance poses the comparison of histograms as the transportation problem, as the domain is discrete. The distance measure can be viewed as the amount of earth that needs to be moved multiplied by the distance moved in order to turn the first histogram into the second. The problem can be tackled using solutions to the distance transportation problem. The solution used is described by Hillier and Lieberman (1990).

Histograms are calculated for each scenario in Dataset E. Intra-person comparisons yield 605 results for each parameter configuration. Inter-person comparisons yield 5,995 results for each parameter configuration.

The histogram comparison software has been augmented to allow segmentation, normalisation and re-combination of regional histograms utilised in HPCTCs.

5.1.2 Expected Results

Evaluation of the configuration evaluation technique will be undertaken through comparison with results found in the literature. With regard to channel selection, in Scenario E, it is expected that the relative consistency of the artificial lighting will allow representations which include illumination information to be more robust than in more dynamic illumination conditions. It is expected that in Scenario F, the results will reflect those in the literature with techniques utilising channels which show little change under illumination, producing better results.

Results in the literature favour the use of the Bhattacharyya Distance as the preferred histogram comparison measure (Morioka, et al. 2007), (Morioka, et al. 2007, Guo, et al. 2007), with the more recent Earth Mover's Distance gaining favour as a comparison method (Guo, et al. 2007), (Morioka, et al. 2007), (Guo, et al. 2007). It is expected that these measures will be present in the optimum parameter configurations. It is expected that bin sizes for the optimum segmentation techniques will tend toward the fine end of the range.

5.1.3 Results and Discussion

Results are evaluated progressively, starting with 1-D then progressing to 2-D visible HPCTC results evaluation. Result evaluation concludes by comparing the visible results with HPCTCs using Thermal IR and multi-modal channels.

5.1.3.1. Single Channel Visible Results (1-D Histograms)

Using one dimensional histogram representation of the visible HPCTCs, the proposed evaluation metric D, described in 5.1.1, is used to evaluate the samples from Scenario E. The top 10 discrimination capability results are shown in Table 5.2 where the scale ranges from 0 to 100. Full results are available in Appendix D.

	HPCTC			
Rank	**Channel**	**Bin Size**	**Comparison Technique**	**D_{100} Result**
1	VGS	12	Correlation	2.22222
2	VGS	12	Intersection	1.41414
3	VGS	18	Earth Movers Distance	1.41414
4	VGS	15	Intersection	1.21212
5	Hue	24	Earth Movers Distance	1.21212
6	Hue	21	Earth Movers Distance	1.21212
7	VGS	6	Earth Movers Distance	1.0101
8	Hue	15	Earth Movers Distance	1.0101
9	VGS	18	Chi-Square	0.808081
10	VGS	6	Intersection	0.808081

Table 5.2 Scenario E Top 10 ranked by D_{100}

It is noted that the highest ranking HPCTCs show a poor evaluation result. It is hypothesised that due to the nature of the evaluation and the large number of intra-person comparisons, the influence of a single or minority of outliers can skew the results considerably. In order to counter this and obtain a more accurate representation of the capabilities of each HPCTC, evaluation of D_{98} is calculated. The results are shown in Table 5.3.

	HPCTC			
Rank	**Channel**	**Bin Size**	**Comparison Technique**	**D_{98} Result**
1	VGS	12	Chi-Square	22.0202
2	VGS	24	Intersection	21.0101
3	VGS	18	Bhattacharyya	21.0101
4	VGS	6	Chi-Square	20.8081
5	VGS	12	Bhattacharyya	20.404
6	VGS	18	Chi-Square	20.202
7	VGS	24	Chi-Square	19.596
8	VGS	12	Earth Movers Distance	19.596
9	VGS	6	Bhattacharyya	19.3939
10	VGS	21	Chi-Square	19.3939

Table 5.3 Scenario E 1-D Visible Top 10 ranked by D_{98}

From the results shown in Table 5.3, it is observed that a 1 dimensional VGS histogram with a bin size ranging from 6 to 24 gives the best results, with all of the top 10 results providing a discrimination capability within a small range. All tested histogram comparison techniques were present in the top 10 results with the exception of correlation. The best performing HPCTC using correlation had a discrimination capability of 19.1919 while utilising 21 bins and was the first result utilising the Hue channel. The best performing HPCTC utilising Saturation used the earth movers distance to compare histograms, had a bin size of 15 and a discrimination capability of 15.7576. The results show that the VGS image provides superior results than Hue or Saturation in Scenario E, though not by a great margin. The placing of VGS results above Hue in 1-D visible representation are contrary to those described in much of the literature. It is expected that this may be due to the relative consistency of lighting conditions in Scenario E. In order to test this, the results from Scenario F, which is influenced by more dynamic illumination, must be considered. The results are shown in Table 5.4.

	HPCTC			
Rank	**Channel**	**Bin Size**	**Comparison Technique**	**D_{98} Result**
1	Hue	24	Correlation	33.5354
2	Hue	21	Correlation	33.1313
3	Hue	12	Correlation	32.5253
4	Hue	18	Correlation	30.101
5	Hue	12	Bhattacharyya	28.4848
6	Hue	12	Chi-Square	28.4848
7	Hue	24	Bhattacharyya	28.2828
8	Hue	24	Chi-Square	28.2828
9	Hue	21	Bhattacharyya	27.4747
10	Hue	21	Chi-Square	27.4747

Table 5.4 Scenario F 1-D Visible Top 10 ranked by D_{98}

From Scenario F results it is observed that a greater discrimination capability can be achieved using the Hue of the image. The difference between Hue and the closest alternative is much greater in Scenario F. The best non-Hue 1-D visible HPCTC gives a discrimination ability of 17.7778: close to half that using Hue. It is expected that this is due to the comparative consistency of Hue over other channels which contain illumination information. These findings agree with results observed in the literature. The higher discrimination ability observed in Scenario F is thought to be a result of the lower colour contrast in Scenario E.

In order to give a more generalised combined result, assessment of HPCTCs is undertaken to determine the greatest discrimination capability across both environments. The problem is assessed as a minimisation of the mean square error (MSE), where the mean of the square distance from optimal performance across an environment describes the error as shown in Equation 17.

$$MSE = \frac{(100 - D_A)^2 + (100 - D_B)^2}{2}$$

Equation 17 Mean Squared Error definition

The resulting combined result for the 1-D Visible HPCTCs is shown in Figure 3.12.

	HPCTC					
Rank	**Channel**	**Bin Size**	**Comparison Technique**	**Scenario E D_{98} Result**	**Scenario F D_{98} Result**	**MSE**
1	Hue	21	Correlation	19.192	33.131	5500.686
2	Hue	24	Correlation	17.778	33.535	5589.017
3	Hue	18	Correlation	18.384	30.101	5773.537
4	Hue	12	Correlation	15.758	32.525	5824.809
5	Hue	15	Correlation	16.566	26.465	6184.369
6	Hue	9	Correlation	18.586	23.030	6276.295
7	VGS	18	Bhattacharyya	21.010	17.778	6499.947
8	VGS	24	Intersection	21.010	17.172	6549.966
9	VGS	12	Chi-Square	22.020	15.960	6571.819
10	VGS	18	Chi-Square	20.202	17.374	6597.413

Table 5.5 Top 10 1-D Visible HPCTCs ranked by inverse MSE

The top 6 highest ranking techniques using this method utilise the Hue channel and correlation as the comparison technique to optimally discriminate subjects. To further probe the results, the top 30 HPCTC results, ranked inversely by MSE of discrimination ability, are shown in Figure 5.2. The axes constitute the D_{98} result for the HPCTC in environments A and B. The data is segmented into constituent channel sets and clusters evident in the results have been highlighted.

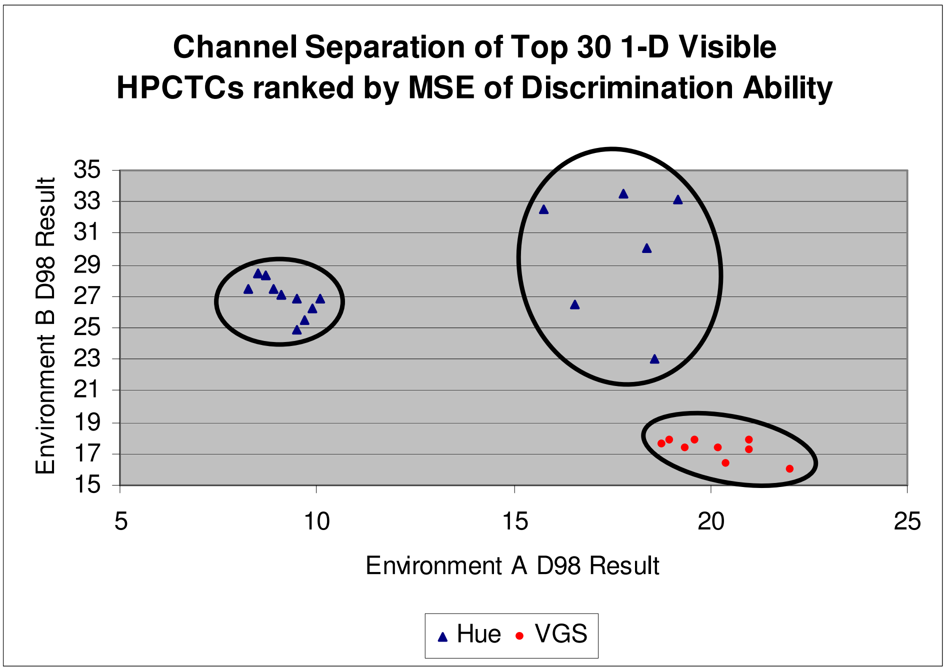

Figure 5.2 Top 30 1-D Visible HPCTCs separated by Channel

Three distinct clusters are identified in the results. Separation of the results into HPCTC constituent channels accounts for a VGS cluster. Both remaining clusters of HPCTCs utilise Hue as their constituent channel. In Figure 5.3, the same HPCTCs results are displayed, however, segmentation of the results is undertaken by comparison technique (delineated by shape) along with channel (delineated by colour).

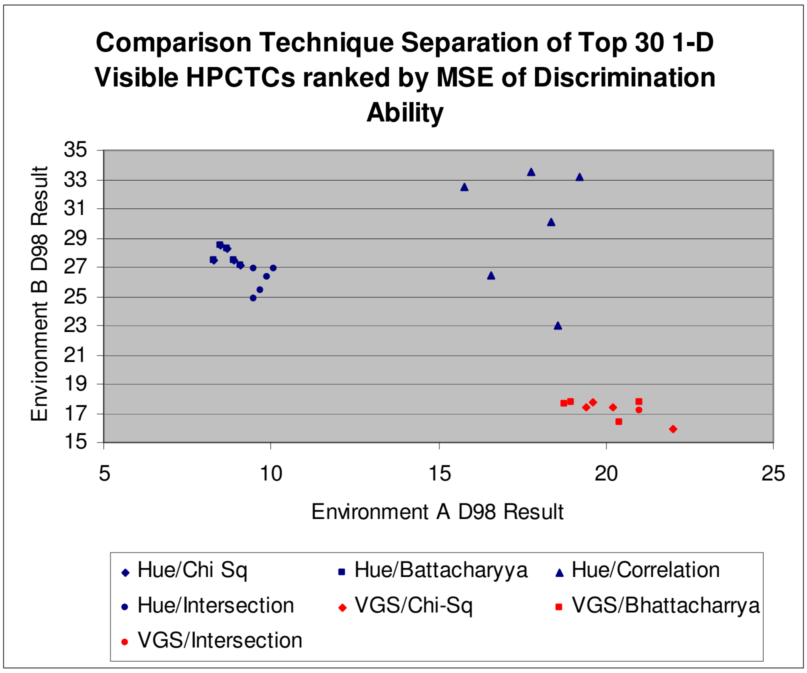

Figure 5.3 Top 30 1-D Visible HPCTCs separated by Comparison Technique

Using comparison technique segmentation, one of the two clusters of HPCTCs utilising Hue is accounted for as utilising correlation to compare histograms. It is observed from these results that the correlation comparison technique cluster evident in the graph provides the optimum balance between environmental conditions represented in Scenario E and Scenario F using a 1-D visible histogram. Results in the other clusters show a mix of capabilities with the notable absence of the Earth Movers Distance.

It is evident from the results that the optimum HPCTC for 1-D visible data utilises Hue and the correlation histogram comparison method. The use of Hue above alternative channel representations corresponds with results described in the literature.

5.1.3.2. Dual Channel Visible Comparisons (2-D Histograms)

The use of multi-dimensional histograms for appearance models enables the combination of histogram distribution information from distinct sources or channels. Initially focussing attention on the channel representations from the widely utilised visible spectrum, a range of HPCTCs representing all possible 2-D channel, bin size and comparison technique combinations are been ranked using the D_{98} evaluation. Table 5.6 shows the results from Scenario E.

	HPCTC			
Rank	**Channel**	**Bin Size**	**Comparison Technique**	**Scenario E D_{98} Result**
1	Hue/VGS	9-21	Chi-Square	29.293
2	Hue/VGS	18-21	Chi-Square	29.293
3	Hue/VGS	24-21	Chi-Square	29.091
4	Hue/VGS	21-21	Chi-Square	28.889
5	Hue/VGS	9-24	Chi-Square	28.889
6	Hue/VGS	15-21	Chi-Square	28.283
7	Hue/VGS	12-24	Chi-Square	28.081
8	Hue/VGS	21-24	Chi-Square	27.879
9	Hue/VGS	12-24	Bhattacharyya	27.879
10	Hue/VGS	9-12	Chi-Square	27.677

Table 5.6 Scenario E 2-D Visible Top 10 ranked by D_{98}

Table 5.7 shows the results from Scenario F.

	HPCTC			
Rank	**Channel**	**Bin Size**	**Comparison Technique**	**Scenario F D_{98} Result**
1	Hue/VGS	12-6	Bhattacharyya	37.576
2	Hue/VGS	15-6	Bhattacharyya	37.576
3	Hue/VGS	24-6	Bhattacharyya	36.970
4	Hue/VGS	18-12	Bhattacharyya	36.970
5	Hue/VGS	21-12	Bhattacharyya	36.970
6	Hue/VGS	18-6	Bhattacharyya	36.970
7	Hue/VGS	21-6	Bhattacharyya	36.768
8	Hue/VGS	15-12	Bhattacharyya	36.768
9	Hue/VGS	24-12	Bhattacharyya	36.768
10	Hue/VGS	9-12	Bhattacharyya	36.768

Table 5.7 Scenario F 2-D Visible Top 10 ranked by D_{98}

It is observed that in both environments, the combination of Hue and VGS in a 2-D histogram has provided increased capability. In the top D_{98} results for Scenario E, the Chi-square technique is strongly placed while in Scenario F the Bhattacharyya Distance gives the best results. Utilising the Mean Squared Error of the D_{98} results, the optimum HPCTCs across the environments are calculated as shown in Table 5.8, ranked inversely by MSE.

	HPCTC					
Rank	**Channel**	**Bin Size**	**Comparison Technique**	**Scenario E D_{98} Result**	**Scenario F D_{98} Result**	**MSE**
1	Hue/VGS	18-21	Chi-Square	29.293	35.960	4550.333
2	Hue/VGS	24-21	Chi-Square	29.091	35.758	4577.593
3	Hue/VGS	21-21	Chi-Square	28.889	35.960	4578.981
4	Hue/VGS	21-12	Bhattacharyya	27.677	36.970	4601.732
5	Hue/VGS	9-21	Chi-Square	29.293	35.152	4602.411
6	Hue/VGS	15-21	Chi-Square	28.283	36.162	4609.349
7	Hue/VGS	18-12	Bhattacharyya	27.273	36.970	4631.039
8	Hue/VGS	12-12	Bhattacharyya	27.273	36.768	4643.792
9	Hue/VGS	24-12	Bhattacharyya	27.273	36.768	4643.792
10	Hue/VGS	9-12	Chi-Square	27.677	36.162	4652.993

Table 5.8 Top 10 2-D Visible HPCTCs ranked by inverse MSE

Comparing the results with Table 5.5, it can be seen that there is a marked improvement using 2-D visible histograms over results utilising only a single dimensional visible histogram. It is notable that all of the top 10 HPCTCs ranked by MSE utilise the Hue and VGS channels. There are a total of 108 combinations of Hue and VGS that provide superior results to the nearest alternative 2-D visible result.

Figure 5.4 shows the distribution of the top 30 results when ranked inversely by MSE segmented into comparison type sets. All of the top 30 HPCTCs utilise either Chi-Square or the Bhattacharyya Distance to compare histograms.

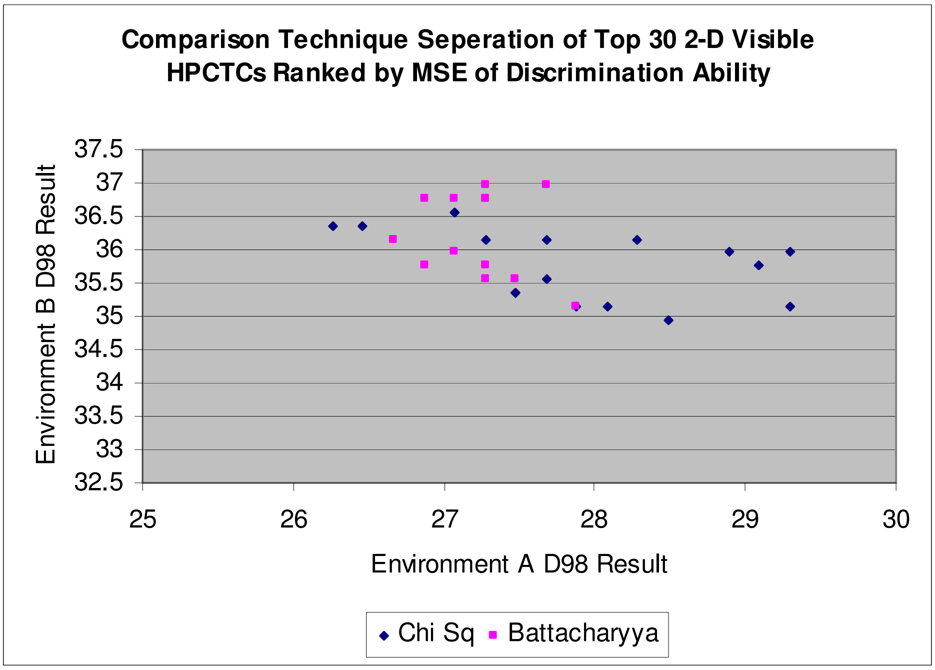

Figure 5.4 Top 30 2-D Visible HPCTCs separated by Comparison Technique

While a strong overlap in the results is evident, the top HPCTCs utilising Chi-Square to compare histograms show a greater discrimination capability in Scenario E while HPCTCs utilising the Bhattacharyya Distance show a greater discrimination capability in Scenario F.

Across the top 30 ranked samples, little consistency was found in the distribution of bin sizes. It was notable however that the number of bins for the Hue channel was never below 9 and never below 12 for the Grey level channel.

These results show that for visible images, HPCTCs utilising a 2-D channel combination of Hue and VGS with bin sizes above 9 and 12 respectively provide the greatest capability for discriminating between humans in environments of consistent and dynamic illumination. The optimal 2-D visible HPCTC between environments when ranked by MSE utilised a Hue/VGS histogram with 18 and 21 bins per respective channel and compares histograms using the Chi-Square method.

5.1.3.3. Thermal IR Comparisons

It has been established in 4.1.3.3 that thermal IR images can often be used in environments where changes in illumination strongly affect the scene. Analysis of the results from HPCTCS utilising 1-D histograms of incident radiation from human regions sourced from a thermal IR camera is detailed below. Table 5.9 shows the top 10 HPCTCS across both environments ranked inversely by MSE.

	HPCTC					
Rank	Channel	Bin Size	Comparison Technique	Scenario E D_{98} Result	Scenario F D_{98} Result	MSE
1	Thermal	24	Chi-Square	76.970	37.172	2238.895
2	Thermal	21	Chi-Square	76.364	36.364	2304.135
3	Thermal	24	Bhattacharyya	78.182	35.152	2340.681
4	Thermal	21	Bhattacharyya	75.354	34.343	2459.120
5	Thermal	24	Intersection	70.505	36.162	2472.645
6	Thermal	21	Intersection	70.707	35.152	2531.701
7	Thermal	24	Correlation	65.253	36.566	2615.650
8	Thermal	18	Chi-Square	68.687	33.737	2685.621
9	Thermal	18	Bhattacharyya	68.889	32.525	2760.368
10	Thermal	24	Earth Movers Distance	74.950	28.283	2885.442

Table 5.9 Top 10 1-D Thermal HPCTCs ranked by inverse MSE

Compared with Table 5.8, it is evident that HPCTCs utilising a 1-D Thermal IR histogram provide a much increased capability over the best 2-D HPCTCs which use visible channel representation. In addition, the results from Scenario F show a similar level of capability to the best 2-D visible configuration while for Scenario E, the best performing HPCTC is more than double that of the best 2-D visible HPCTC.

Bin sizes for the top 10 HPCTCs range between 18 and 24 while a mix of histogram comparison techniques is used. The graph in Figure 5.5 shows the distribution of the top 30 results separated by comparison technique.

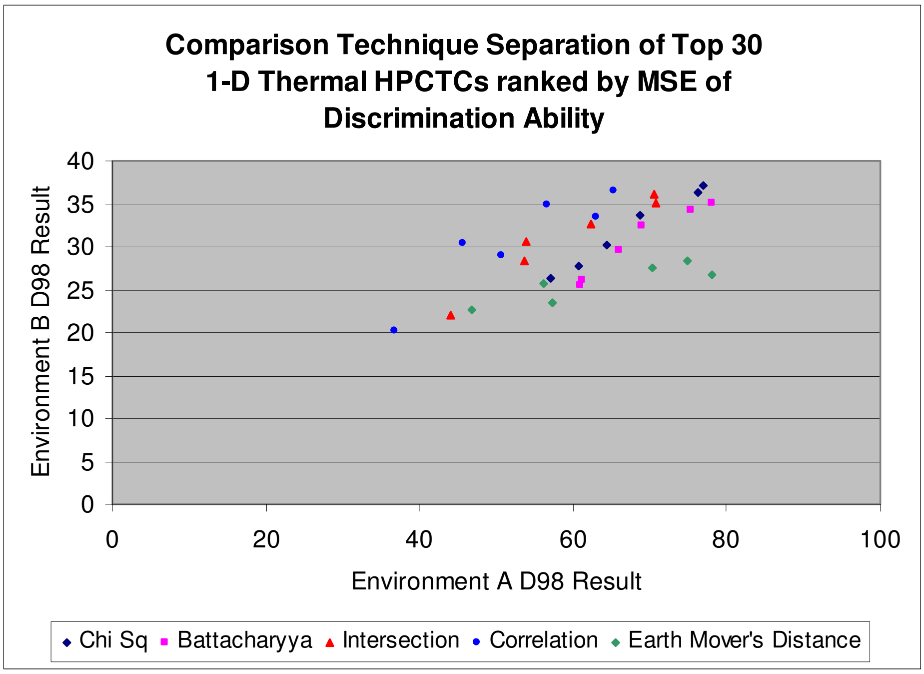

Figure 5.5 Top 30 1-D Thermal HPCTCs separated by Comparison Technique

In almost all of the cases the increase in capability of a comparison technique is related to the increase in bin size. This trend is clear in Figure 5.6 where the data points for each comparison technique are connected in sequential order of bin size from 9 to 24.

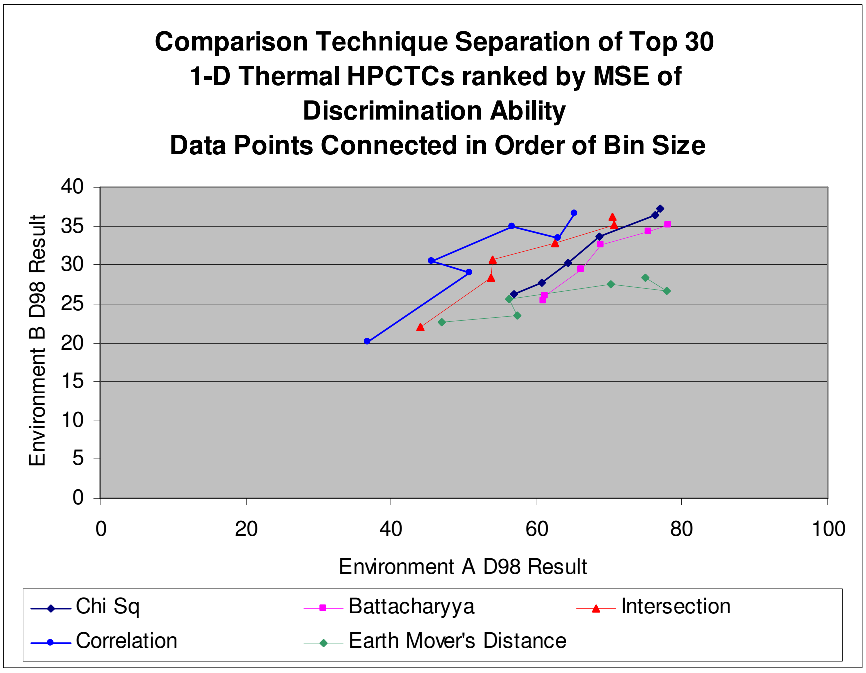

Figure 5.6 Top 30 1-D Thermal HPCTCs separated by Comparison Technique. Data points connected by bin size order

It can be seen from these results that the most effective 1-D thermal IR based HPCTCs configurations utilise Chi-Square as the comparison technique, using a high number of bins to provide optimum discrimination capability. The optimal 1-D thermal IR HPCTC between environments when ranked by MSE 24 bins and compares histograms using the Chi-Square method.

It is concluded that an optimised HPCTC, described in Table 5.9, utilising a single thermal IR channel out-performs the best performing 1-D or 2-D visible HPCTCs.

It is proposed that subsequent investigations will consider whether the use of multi-modal histograms can improve discrimination performance using the D_{98} HPCTC evaluation measure. It is theorised that in situations where thermal information may be similar between subjects, the use of colour may provide further information enabling more accurate discrimination.

5.2 Multi-modal Parameter Optimisation

This section describes experiments undertaken to determine if a multi-modal HPCTC, utilising thermal IR and visible channels can provide improved discriminating capability over uni-modal HPCTCs.

5.2.1 Method

The samples in Dataset E are used for this experiment. It has been shown in 4.1.3.2 that Thermal IR images provide more robust information for differentiating between human subjects than different representations of colour from visible image sources. It is likely that this is due to the invariance in the detected radiation emitted from a subject due to reduced influence of reflective radiation and the prominence of radiation emitted from the subject imaged. It is hypothesised that combinations of thermal and visible information will further increase the ability to discriminate between human subjects by providing additional descriptive information in situations of similar thermal IR histograms.

5.2.2 Expected Results

It is expected that an increase in discrimination capability will be found when thermal IR information is combined with an illumination aligned visible channel such as Hue. Hue has been shown to display the most consistent information in 1-D visible HPCTCs. This consistent information between images of a subject allows a greater discriminating capability utilising Hue.

5.2.3 Results and Discussion

Table 5.10 shows the top 10 2-D Multi-modal HPCTCs ranked inversely by MSE.

	HPCTC					
Rank	Channel	Bin Size	Comparison Technique	Scenario E D_{98} Result	Scenario F D_{98} Result	MSE
1	Thermal/Hue	6-21	Bhattacharyya	80.404	56.566	1135.271
2	Thermal/Hue	12-21	Bhattacharyya	76.970	58.182	1139.578
3	Thermal/Hue	15-21	Bhattacharyya	77.778	57.576	1146.819
4	Thermal/Hue	9-21	Bhattacharyya	78.182	57.172	1155.149
5	Thermal/Hue	18-21	Bhattacharyya	76.970	57.374	1173.698
6	Thermal/Hue	21-21	Bhattacharyya	76.970	57.374	1173.698
7	Thermal/Hue	15-21	Chi-Square	79.192	55.960	1186.267
8	Thermal/Hue	6-18	Chi-Square	81.414	54.950	1187.492
9	Thermal/Hue	6-21	Chi-Square	81.818	54.748	1189.183
10	Thermal/Hue	15-18	Chi-Square	78.182	56.162	1198.920

Table 5.10 Top 10 2-D Multi-modal HPCTCs ranked by inverse MSE

The results show that HPCTCs utilising Hue and thermal channels can provide a much increased capability over uni-modal data sources. Significant gains with the top HPCTCs were observed in both environments with a large gain in capability of assessing Scenario F. The top 176 parameter configurations ranked inversely by MSE use Thermal and Hue as channel inputs use of both the Bhattacharyya Distance and Chi-Square provide high segmentation results.

Figure 5.4 shows the distribution of the top 30 results when ranked by MMSE.

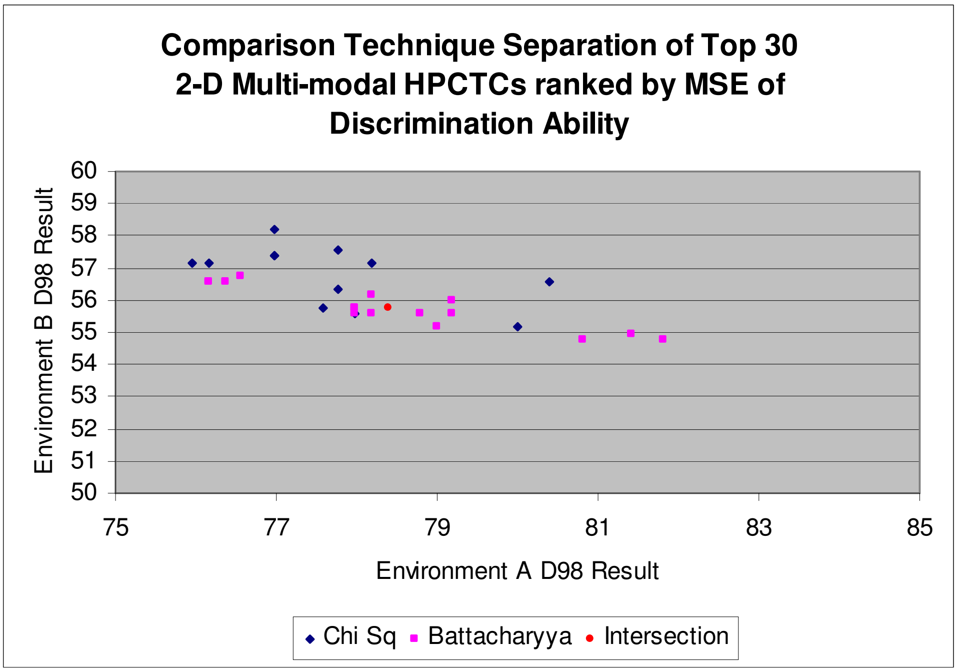

Figure 5.7 Top 30 2-D Multi-modal HPCTCs separated by Comparison Technique

The majority of the top 30 HPCTCs utilise the Bhattacharyya Distances or Chi-Square as the comparison technique, with the 6 best HPCTCs utilising the Bhattacharyya Distance. No clear separation between the techniques can be observed when graphing the top 30 HPCTCs.

It has been noted from the results that all top ranking HPCTCs favour small bin sizes for the thermal information at around 18-21 bins. The Hue however has a wide range of bin sizes in the top rankings configurations. The top 1-D Hue results bin sizes range from 12 to 24 bins. In these multi-modal HPCTCs, Hue bin sizes range from 6 to 15 bins. In Figure 5.8 the segmentation of coarse and fine bins is shown across the top 30 results ranked my MMSE. The range of bin sizes in ‘Coarse’ is 3-9 and in ‘Fine’, 12-24.

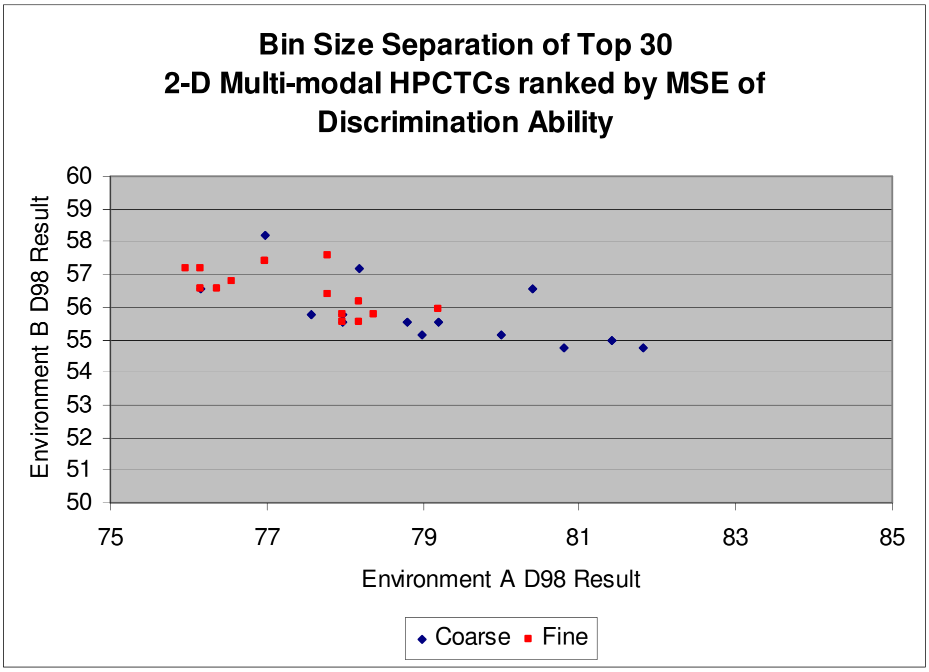

Figure 5.8 Top 30 2-D Multi-modal HPCTCs separated by Bin Range

It can be seen from the resulting graph in Figure 5.8 that there are two overlapping distributions for the coarse and fine bin sizes with HPCTCs utilising coarser bin sizes generally giving better results in Scenario E and finer bin sizes generally giving better results in Scenario F. The extent of the separation however is small.

Is has been established that the optimum configuration for generalised human identification based upon the evidence derived from D_{98} analysis of HPCTCS from Scenario E and Scenario F utilising multi-modal visible and thermal information, is a 2-D Hue and thermal IR histogram consisting of 6 bins for the Hue channel and 21 bins for thermal information. The technique for comparing histograms in this optimum HPCTC is the Bhattacharyya Distance. This HPCTC gives a MSE score of 1135.271.

Differences between Scenario E and Scenario F include the illumination and the direction of movement of the subjects. It is proposed that investigations continue into establishing if the poorer performing HPCTCs in Scenario F, is the result of self occlusion (parts of the subject which obscure other parts during the gait cycle). Such occlusions do not appear so much in Scenario E as participant subjects move towards and away from the camera rather than moving orthogonally.

5.3 Self-Occluding Region Normalisation Testing

This section describes investigations into the effects of self-occlusion of subject body regions on the results. Regions of self occlusion present in Scenario F are normalised to remove the influence of the changing area in the image plane, which may manipulate the subject region balance across the histogram.

5.3.1 Method

The samples in Dataset E are used for this experiment. It is theorised that self occlusion of regions of the body at points in a walking sequence may alter body region weightings in the histogram representations. This may be particularly prominent in scenes in which subjects walk past the camera. The orientation of the subject in these environments obscures arms, legs and portions of the torso at points in the gait cycle. This reduces the area of the body regions in the image plane. The effect of this is the reduction of the region's representation in the resulting body histogram. Occlusion of the rear leg and its visibility mid stride also influence the representation of this region in the resulting histogram.

In order to evaluate the influence of self occlusion the manually segmented body regions utilised in Section 5.1 and 5.2 are automatically segmented into regions in which self occlusion is expected to occur as show in Figure 5.9 using ratios of body height.

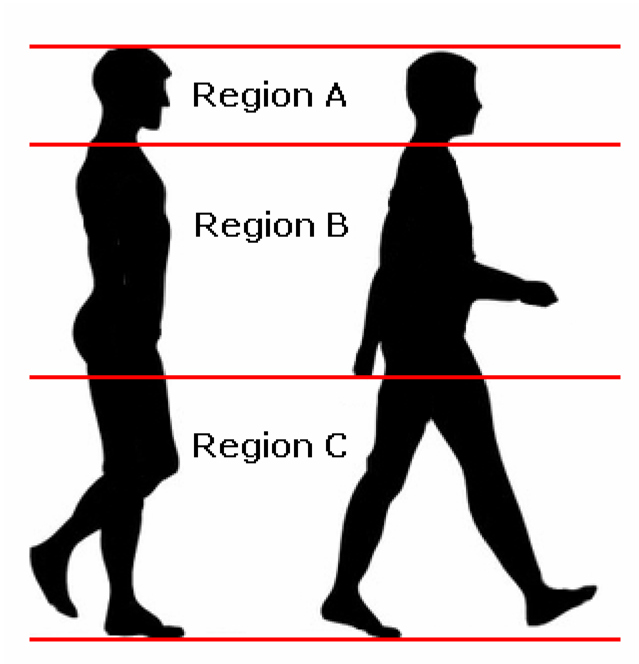

Figure 5.9 Self occluding body regions B and C

Normalisation of regions B and C is undertaken to ensure equal representation of these regions in the resulting histograms across the sequence.

Evaluation is undertaken upon the results through D_{98} evaluation of all possible 1-D and 2-D, single and multi-modal HPCTCs. The D_{98} results are compared with results using histograms without region based normalisation.

5.3.2 Expected Results

It is anticipated that the results will show an increase in the capability of the system to discriminate between Scenario F's subjects when the self occluding regions are normalised. The extent to which self-occlusion may contribute to the lower D_{98} performance of the optimum HPCTCs in Scenario F is unknown.

5.3.3 Results and Discussion

Using normalised regions to tackle self-occlusion, an increase in the capability to discriminate between subjects in Scenario E was observed. The top 10 HPCTCs utilising 1-D and 2-D single and multi-modal channel representations ranked by the result of D_{98} evaluation are shown in Table 5.11.

	HPCTC			
Rank	Channel	Bin Size	Comparison Technique	Scenario E D_{98} Result
1	Thermal/Hue	6-18	Earth Mover's Distance	87.68
2	Thermal/Hue	6-21	Earth Mover's Distance	87.27
3	Thermal/Hue	6-24	Earth Mover's Distance	87.07
4	Thermal/Hue	9-24	Earth Mover's Distance	86.87
5	Thermal/Hue	9-21	Earth Mover's Distance	86.67
6	Thermal/Hue	6-15	Earth Mover's Distance	86.26
7	Thermal/Hue	12-24	Earth Mover's Distance	85.86
8	Thermal/Hue	3-9	Earth Mover's Distance	85.66
9	Thermal/Hue	9-18	Correlation'	85.45
10	VGS/Thermal	6-21	Earth Mover's Distance	85.25

Table 5.11 Top 10 1-D and 2-D, Single and Multi-modal segmented HPCTCs in Scenario E ranked by inverse MSE

Alongside the notable increase in capability of the top HPCTCs is the strong presence of the Earth Mover's Distance as the most successful histogram comparison technique used. Contrary to the hypothesis however, a decrease in discriminating capability was observed in Scenario F. These results, ordered by D_{98} evaluation score, are shown in Table 5.12.

	HPCTC			
Rank	Channel	Bin Size	Comparison Technique	Scenario F D_{98} Result
1	Thermal/Hue	21-6	Bhattacharyya	56.77
2	Thermal/Hue	24-6	Chi-Square	56.77
3	Thermal/Hue	24-6	Bhattacharyya	56.77
4	Thermal/Hue	12-6	Chi-Square	56.57
5	Thermal/Hue	15-6	Chi-Square	56.57
6	Thermal/Hue	18-6	Chi-Square	56.57
7	Thermal/Hue	18-6	Bhattacharyya	56.57
8	Thermal/Hue	21-6	Chi-Square	56.57
9	Thermal/Hue	12-6	Bhattacharyya	55.76
10	Thermal/Hue	15-6	Bhattacharyya	55.76

Table 5.12 Top 10 1-D and 2-D, Single and Multi-modal segmented HPCTCs in Scenario F ranked by inverse MSE

D98 evaluation of the top HPCTCs has shown that tackling instances of self occlusions through region normalisation has not increased the capability to distinguish between subjects in Scenario F. From these results it can be inferred that the reduced capability in Scenario F is not due to changes in body region image area only.

Across both results sets, a HPCTC using a combination of the Hue and Thermal IR information provides the best results. Table 5.13 shows the results when using the segmentation technique ordered inversely by MSE.

	HPCTC					
Rank	**Channel**	**Bin Size**	**Comparison Technique**	**Scenario E D_{98} Result**	**Scenario F D_{98} Result**	**MSE**
1	Thermal/Hue	6-18	Chi-Square	83.8384	53.9394	1191.39
2	Thermal/Hue	9-18	Chi-Square	81.6162	53.9394	1229.77
3	Thermal/Hue	3-18	Chi-Square	84.4444	52.5253	1247.91
4	Thermal/Hue	15-18	Chi-Square	78.7879	54.7475	1248.87
5	Thermal/Hue	15-18	Intersection	81.0101	53.7374	1250.42
6	Thermal/Hue	6-24	Chi-Square	82.8283	52.9293	1255.26
7	Thermal/Hue	24-18	Chi-Square	78.1818	54.7475	1261.91
8	Thermal/Hue	6-21	Chi-Square	84.0404	52.3232	1263.89
9	Thermal/Hue	21-18	Chi-Square	77.9798	54.7475	1266.34
10	Thermal/Hue	18-18	Chi-Square	78.3838	54.5455	1266.69

Table 5.13 Scenario E vs. Scenario F MSE segmented HPCTC ranking results

It can be seen that there is a small decrease in the capability to generalise using the normalised histogram regions when compared to Table 5.10. It is also noted that the majority of the top ranking results use the Chi-Square measure. Of the top 30 results 20 use Chi-Square to compare histograms while he remainder utilise Intersection.

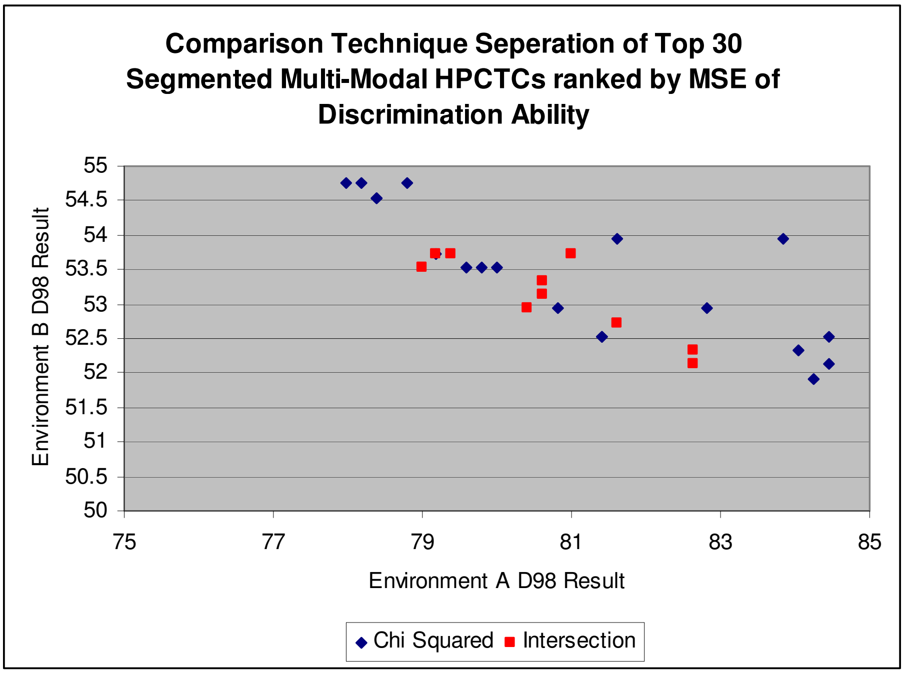

Figure 5.10 Top 30 MSE segmented results distribution by Comparison Technique

The peak configuration across all three tables is shown in row 1 of Table 5.13. It has been determined that region normalisation does not resolve the disparity between the environment's results as demonstrated by the decreased discrimination capability of the top HPCTCs in Scenario F using region normalisation. There must be an alternative cause.

Region normalisation assumes that a similar histogram occurs in regions of self occlusion throughout the gait cycle, and attempts to ensure that increased pixel counts do not influence the region's proportion of the full body histogram. Due to the results of the region normalisation experiment, it is subsequently suggested that each region of self-occlusion may have a significantly different pixel value distribution through its cycle, which region normalisation cannot resolve.

Considering this hypothesis with respect to Scenario E, minimal self occlusion occurs and consistency in lighting mean that little difference in pixel intensities occur during the gait cycle.

5.4 Summary

In this chapter, experiments to optimise both histogram representations of human subjects, and the techniques to compare these histograms were described. The purpose of the experiments was to find techniques for optimum discrimination between human subjects in a tracking environment.

In section 5.1.1, a metric, $D_{x,}$ was proposed for evaluating HPCTCs using results from comparisons of multiple histograms of single subjects and results from comparisons between different subjects. The metric allowed for assessment of the discrimination ability of the HPCTC in question.

Using the metric to assess HPCTCs, an exhaustive search approach was taken to assessing HPCTCs which utilised single channel histograms using visible image data. It was found that the use of the Hue channel gave the best results. This observation concurs with observations in the literature. In order to find the optimum HPCTC across environments, the minimum mean square error, where the error was defined as the distance from optimal performance in each environment was used as the error for combining the scores.

Experimentation continued through assessment of visible data using 2-D histograms, utilising all possible channel combinations. It was found that an increased discrimination capability was observed in a HPCTC where a 2-D combination of Hue and VGS were used.

Further experiments, investigating the usage of thermal IR as an alternative, showed that the best performing HPCTCs utilising a 1-D thermal IR histogram gave improved discrimination ability over the best visible 1-D or 2-D HPCTC.

Histogram optimisation extended into experiments in which evaluation of multi-modal HPCTCs was undertaken. All available channels, bin sizes and comparison technique combinations were assessed. The results of this experiment showed that the optimum HPCTCs utilised a combination of Hue and Thermal IR channels with 6 bins for the Hue channel and 21 bins for thermal information. The technique for comparing histograms in this optimum HPCTC is the Bhattacharyya Distance. This HPCTC provides an increased discrimination capability over the optimum HPCTCs in the previous experiments.

It was noted that across all results, the optimum HPCTCs always provided a greater discriminating capability in Scenario E over Scenario F. It was hypothesised that the differences in performance of configurations between the environments may be attributed to self occlusion in scenes in which subjects move orthogonal to the camera across the image plane. In order to test the hypothesis, the body region in the image plane is split into three segments. Two of the segments containing self occlusion regions; arms/torso and legs. Each region's histogram was normalised before re-combination. Region normalisation provided better results in Scenario E, but failed to improve either Scenario F's results or the combined generalised results.

It was noted that use of the Earth Movers Distance only provided strong results when body region histograms were normalised by area in environments with little self occlusion and consistent lighting. It was found that in environments with self occlusion, changing the area and pixel values across the body region, EMD showed poorer performance than the Bhattacharyya Distance. It is found that for real world human tracking environments in which self-occlusion occurs, the optimum configuration for generalised tracking is that described in Table 5.10.

It is suggested that further work should include the use of different environments, incorporating various illumination or thermal conditions to allow further understanding of the optimum histogram representation. Investigations into the use of non-uniform histogram bins, regional histograms or an increased number of dimensions would improve the understanding of the optimum histogram representation for accurate discrimination between subjects.

6 Occlusion Handling using Appearance Models

This chapter describes work to develop a tracking system capable of detecting and tracking humans in multi-modal thermal IR and visible image sequences. The system is designed to undertake multiple stages of tracking including modality selection, extraction of foreground objects, human region identification, and assessment of temporal correspondences, occlusion handling and reporting. A calibration stage allows for tracking in a Euclidean coordinate system through utilisation of perspective geometry. Figure 6.1 shows an overview of the flow and use of information in the tracking system.

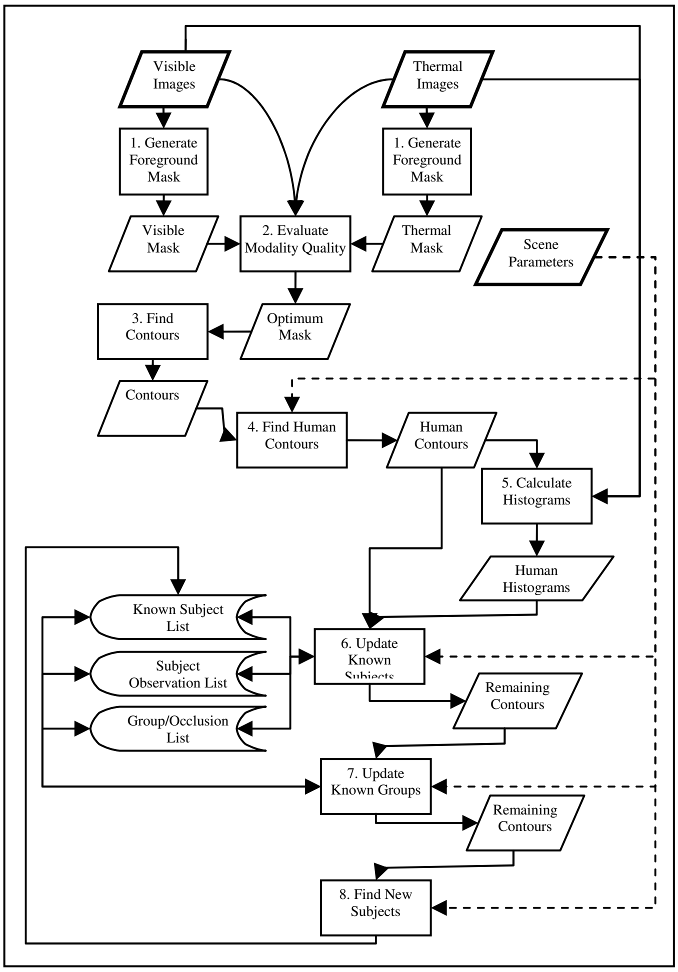

Figure 6.1 Information flow through the tracking system when configured for histogram based occlusion handling

The system is employed to demonstrate usage of methods established in the preceding chapters holistically in an automated system. Experiments are performed which show the limitations of subject-direction based occlusion resolution methods and how distinguishing subjects in a feature space utilising histogram based methods performs.

The limitations of framework along with its histogram based occlusions solving capabilities are tested through experiments in which harsh environmental and subject appearance conditions are used.

6.1 Tracking System Description

This section describes a tracking system designed and developed to allow detection and spatiotemporal tracking of human subjects in scenes whilst utilising multi-modal visible and thermal IR images sources.

6.1.1 Calibration

Calibration of the scene is performed to allow for tracking in a Euclidean coordinate system and to allow translation between points in the image and ground planes. The method assumes that the surface viewed is approximately flat. A homography containing the coefficients of the perspective transform is calculated using corresponding points between the image plane and ground plane images. This homography is used to transform points in the image plane to the ground plane while the inverse homography performs the inverse operation.

The calibration stage utilises distance between points on the ground plane to allow for translation of distance measurement between points in the image plane to real world distances in the ground plane as well as allowing for inverse operations. Figure 6.2 shows the image plane and projected ground plane in reference to the camera viewpoint.

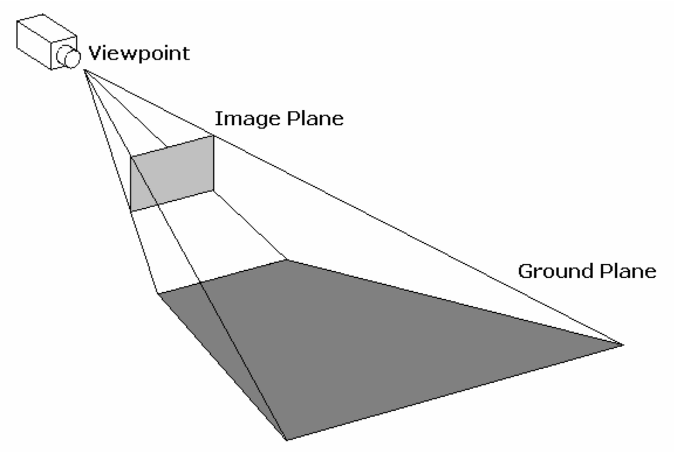

Figure 6.2 Perspective transformation for image to ground plane conversion

The calibration stage allows for establishing entrances to the scene. This will allow for distinguishing between subjects who have left the scene and those who have become occluded by scenery or have remained static. It also reduces the search space for new human subjects.

6.1.2 Foreground Extraction

The system has been developed to allow statistical foreground masks to be calculated from both the thermal and visible modalities using pixel history based statistical methods discussed in 4.1.1. It is also possible to obtain a range mask from the thermal image in which a range of values can be specified to exclude objects above and below those expected from human subjects.

Previous investigations considered evaluation of the scene using measures of modality quality to establish the foreground mask to use. The results showed that in the majority of environments observed, the thermal mask provided a more robust segmentation of human regions. All masks are calculated and available as options in the framework, logical methods for combining the masks such as AND, OR etc. have also been added to the framework. A final step utilises morphological techniques to close small gaps and remove noise from the foreground mask.

6.1.3 Human Region Identification

The framework has a number of methods available for validating humans regions in the foreground masks produced through background subtraction. A contour based search space reduction method has been developed using contextual information to reduce the search space for head shapes in the image. Contours from example images containing generic head shapes of differing orientations are defined. Using the perspective transformation homography on the base point of the contour in the image plane, the size of the object represented by the contour is calculated in Euclidean coordinates.

As humans stand at a normal vector to the ground plane, pixel to real world dimensions ratios remain approximately fixed across the area of a human region. Using this knowledge, the height and width of the person can be calculated. The lack of sub-pixel accuracy in the foreground extraction algorithm, results in noise in the binary masks, which affects the height calculation. The extent of noise influence therefore depends on the dimensions of the subject in the image plane.

A pre-requisite to the head detection algorithm is that the target region has a height within a preset range of typical human height. The expected size of the head in the image plane is calculated using the perspective transform homography. An appropriately sized head contour is then generated and compared to a region at the top of the contour area using the Hough transformation. The maximum value in the returned resulting Hough image is evaluated using a threshold to establish presence. The method was chosen as head shapes are more consistent from different viewpoints while a great number of possible full body poses exist due to the high dimensionality of the human body. Reduction of the search space in the prior stage using scene and subject knowledge reduces the likelihood of false classification significantly.

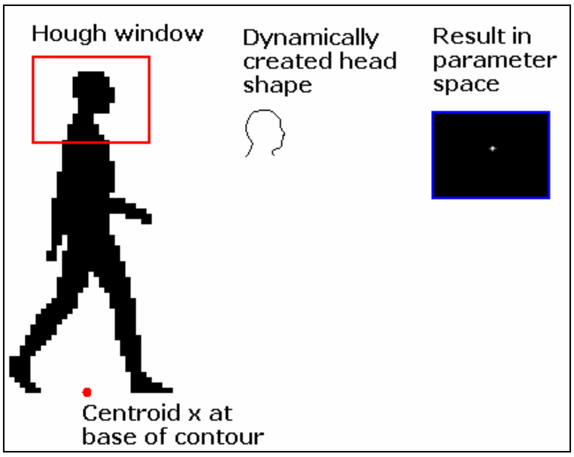

Figure 6.3 Head region detection using the generalised Hough transform

Height calculation for a 100 frames of a sequence in which a human subject walks through the scene is shown in Figure 6.4

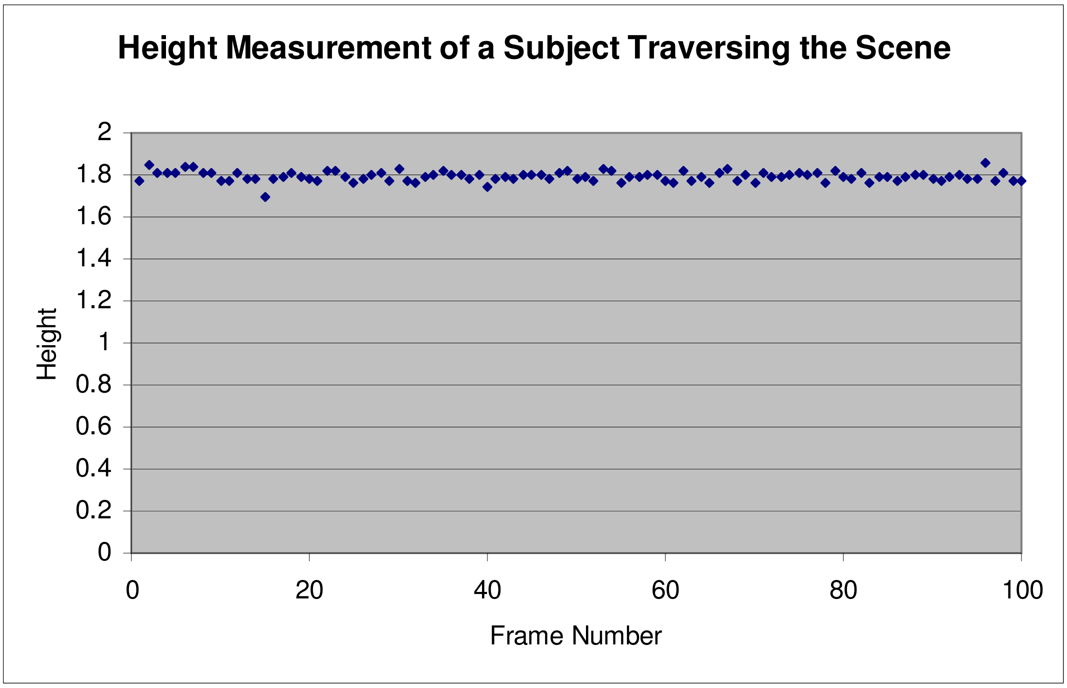

Figure 6.4 Height calculation for a single subject over time

Other methods included for reducing the search space include the evaluation of the ratio between the height and area of the contour with the expectation that groups of people will typically have a greater area to height ratio than individuals. Threshold values were determined through analysis of the extremes of body area in captured sequences.

The sequence for tracking is that known subjects and groups/occlusions are updated before new subjects are searched for. New subjects are searched for on the calibrated boundaries of the scene.

6.1.4 Tracking

Tracking is performed through a contour assessment process. The order of operation is: firstly to find contours exhibiting human features; to update existing known subjects; to updating existing groups and finally to locate new subjects for tracking. A look-up table indicating contour assessment status facilitates this process. The stage of updating individuals involves finding correspondences between known people and current human objects. This process is performed in the image plane.

Updating the location and properties of existing people is undertaken by iterating through contour regions with human features and associating these contours with known human subjects. In Figure 6.5 (a) the current frame with 2 human regions are shown along with the rectangles of 2 known subjects from the previous frame, *t*-1. In (b) the known subjects' positions are updated with the current human region contour positions.

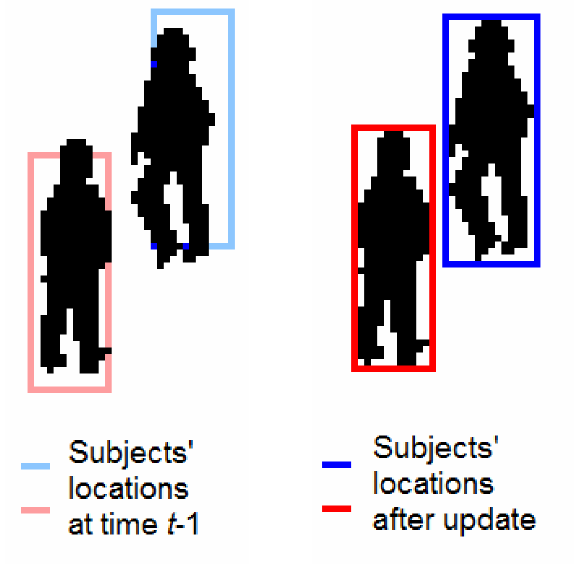

(a) (b)

Figure 6.5 Updating known subjects in (b) using corresponding human regions known in (a)

Occlusion Detection is achieved when attempting to update individuals by iterating through the list of contours. If a detected contour overlaps the location of two previous known people then an occlusion event is flagged. An instance of an occlusion is created with reference to the known subject instances present within the occlusion, as illustrated in Figure 6.6.

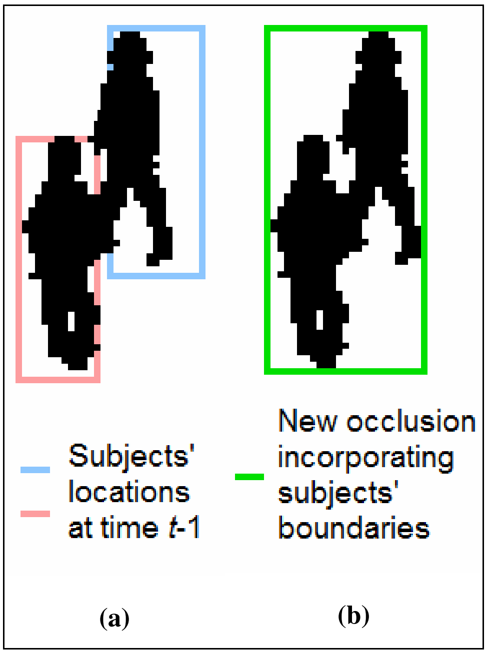

Figure 6.6 Creation of an occlusion instance containing subjects from the previous frame

Tracking and resolving occlusions uses the inverse approach to updating individuals: iteration of known occlusion areas is undertaken and contours with human features in the occlusion area are detected. In the case that the number of human regions matches the number of known members in the occlusion, resolution of the occlusion is attempted using the methods described below. In any other case any contour regions overlapping the occlusion area are used to update the position of the occlusion.

The data structure for the human state and history information consists of a Person List vector, in which each element contains information about the subject's state, position of appearance. For each subject, a vector of observances of the subject is stored. An occlusion list exists which contains references to known subjects in an occlusion state.

In comparison to the system described by Senior, et al. (2006), components are analysed for human shape before tracking. Senior et al. also utilise an RGB colour model with a probability mask, as opposed to a body or regional histogram representation.

6.1.5 Reporting

Reporting in the tracking system consists of a logging system on the subject level to provide a history of subject locations as they traverse the scene. A video output consisting of the multi-modal images and a dynamic map of detected subjects in Euclidean co-ordinates can be generated. A still frame of the output is shown in Figure 6.7.

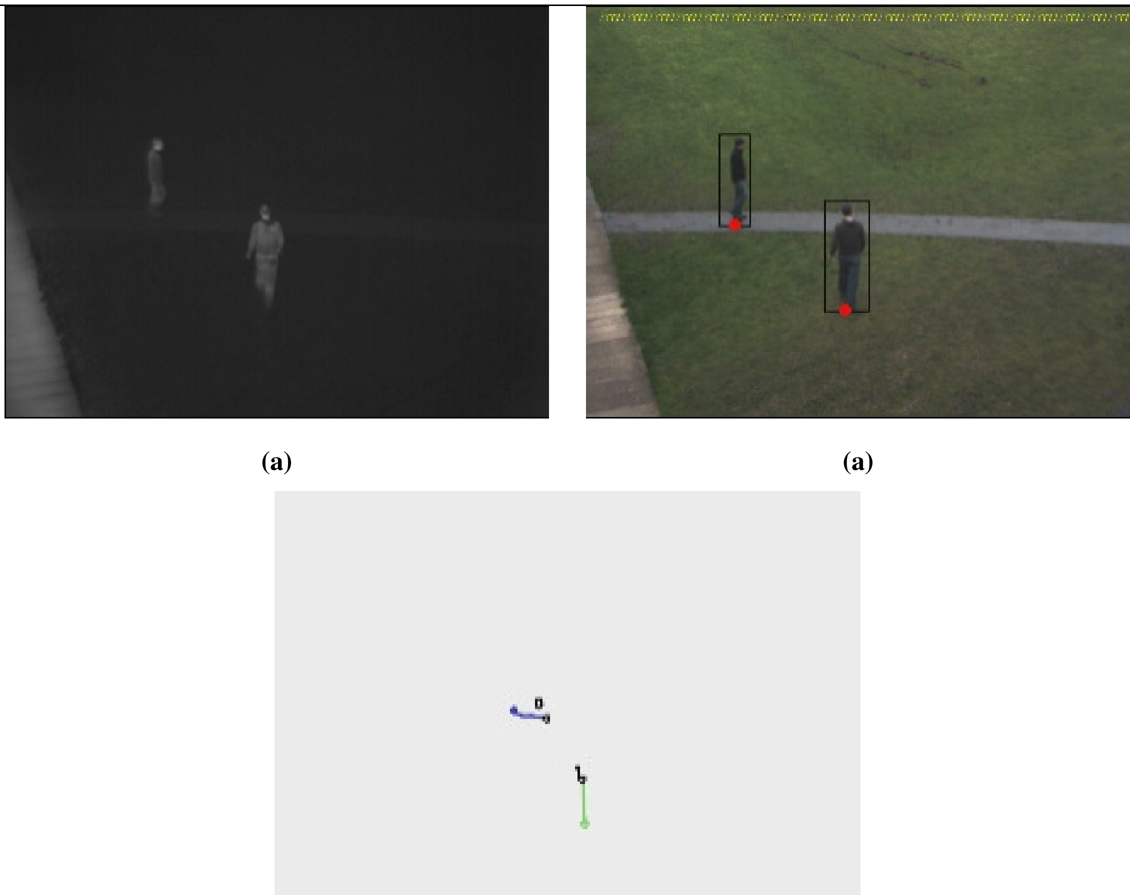

(a) (a)

(c)

Figure 6.7 (a) and (b) show a pair of frames from the video reporting functionality. (c) shows the subjects' positions on a plan view of the ground plane

In Figure 6.8 the tracking window can be seen and in the example shown the predicted positions of the tracked subjects are displayed. In addition, at the termination of tracking activities, a result map is generated detailing subject paths.

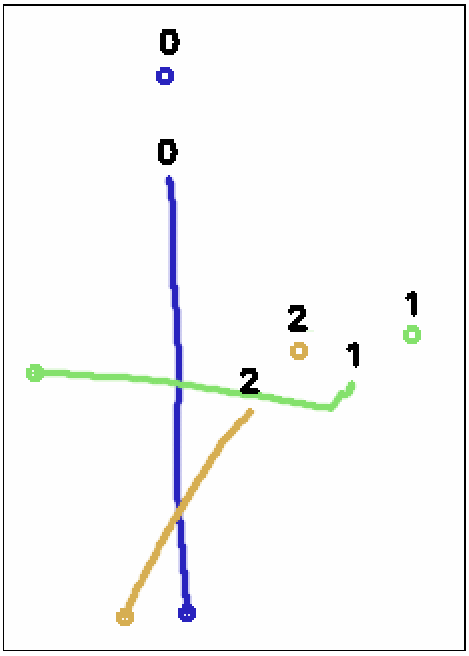

Figure 6.8 An example of dynamic tracking output. Circles with a number above indicate predicted position in *n* frames

6.2 Evaluation of Trajectory Resolution Limitations

Human subjects occlude one another in the image plane due to a number of different circumstances. Subjects may be walking together as they pass the camera, passing each other when walking in different directions, meeting each other to talk or exchange objects, and return in the opposite direction. Under circumstances where subjects do not change direction through the occlusion, it may be possible to re-establish the identity of the subjects after occlusion if the trajectory remains consistent throughout the occlusion, as described by Rosales and Sclaroff (1998).

It is observed that in many circumstances, changes in the subject trajectory in an occlusion can occur due to the proximity of subjects to one another. Subjects may also happen to change direction during an instance of occlusion in the image plane. Such events are common and it is important to resolve them correctly.

This section describes experimentation to evaluate and determine the limitations of using known subject trajectories to re-locate the subjects, post occlusion events.

6.2.1 Method

Series A and B within Dataset F are used for this experiment. Tracking of the individuals is undertaken using location information in the ground plane as described in 6.1.4. This is to allow Euclidean co-ordinate based tracking of the subject movements.

The use of techniques such as alpha beta filters (Hall and McMullen 2004) and Kalman filters (Welch and Bishop 1995) can be employed for path prediction while also modelling noise in the measurement. Path prediction is undertaken in the ground plane using the mean difference in observation over a period prior to the detection of an occlusion event.

The experimental results will answer the question of whether vector information can be used to re-establish identity after an occlusion event, when a change in direction occurs during the occlusion.

6.2.2 Expected Results

It is expected that the results from Series A will show that vector information is sufficient to resolve scenarios in which the movement vector of subjects in the Euclidean co-ordinates successfully. It is expected that the results from Series B will show vector information is insufficient to successfully resolve the occlusion.

6.2.3 Results and Discussion

A summary of the results for utilising movement vector based occlusion resolution is displayed in Table 6.1.

	Series A	Series B
Correctly Resolved	30 (100%)	0 (0%)
Incorrectly Resolved	0 (0%)	30 (100%)

Table 6.1 Vector based occlusion resolution results

It can be seen from these results that all Series A results were correctly resolved using the vector based method. Conversely, all of the sequences in Series B were incorrectly resolved. Using the sample size and the results to calculate a 95% confidence interval for the mean, a confidence interval of ±3.56% is determined. The small confidence limits indicate that vector information alone is not suitable for resolving events where change in direction is significant, such as those in Series B. In order to be able to resolve these scenarios, further information must be considered.

6.3 Multi-Modal Histogram Occlusion Resolution

In 5.2, evaluation of histogram properties was undertaken to establish a HPCTC with an optimum discrimination capability between human subjects. The product of these investigations was an optimised HPCTC which uses Thermal and Hue channels. The histogram utilised 6 bins for the thermal channel while 21 are used for the Hue channel. The comparison technique to distinguish between bins is the Bhattacharyya distance (Bhattacharyya 1943).

In this section an experiment is described in which the histogram configuration is used in the framework described in 6.1.4 to resolve occlusion events. The purpose is to establish if histogram information is sufficient to resolve occlusion events such as those in Series B, while retaining the capability shown through the use of vector information in Series A.

6.3.1 Method

Series A and B within Dataset F are used for this experiment. To determine the capability of the D_x metric, it is evaluated in the context of the tracking framework. The tracking framework updates individual's histograms when they move through the scene. At the point that an occlusion event is detected, a reference to each person and their associated histogram is recorded as an instance of an occlusion object, as shown in Figure 6.1. The histogram configuration used is that established in 5.2.3.

At the point of occlusion resolution, the histograms of subjects recorded as being in the occlusion are compared with the now separate human regions which previously constituted the occlusion. Histograms of objects with the minimum result (best match) are re-established with the updated position of the object. The capability is measured by determining if the subjects were correctly re-established after the occlusion event.

The results from this experiment will answer the question of whether the multi-modal histograms are sufficient to overcome the deficiencies of vector based occlusion resolution.

6.3.2 Expected Results

It is expected that histogram based resolution will provide a much improved capability to discriminate human objects over vector based tracking. As histogram based comparisons do not account for trajectory or motion in the, it not expected that a significant difference in the capability of the method between the series' of sequences will be observed.

6.3.3 Results and Discussion

A summary of the results for utilising histogram based occlusion resolution is displayed in Table 6.2.

	Series A	Series B
Correctly Resolved	30 (100%)	30 (100%)
Incorrectly Resolved	0 (%)	0 (%)

Table 6.2 Histogram based occlusion resolution results

It can be seen from these results that all Series A results were correctly resolved using the histogram based method, these results match the high capability of vector based resolution observed in Series A. In Series B all of the sequences were correctly resolved using histogram based occlusion resolution. These results demonstrate that, for the samples tested, using a 95% confidence interval, histogram information alone is suitable for resolving occlusion events in scenarios where change in direction is as significant as those in Series B with confidence limits of ±3.56%.

Due to the binary nature of the classification, further investigation into the actual comparison results is undertaken. The results of using the Bhattacharyya Distance to compare a subject's histogram to the prior histogram of the same subject (intra-person) and to the histogram of the other subject within the pairing (inter-person) at the point of subject separation in the image plane are displayed in Table 6.3. The sequence initial From A to I indicates the subjects appearing within the sequence.

Sequence	Intra-person result	Inter-person result	Difference
BG Seq A	0.216	0.357	0.141
BG Seq B	0.218	0.290	0.072
CA Seq A	0.147	0.350	0.203
CA Seq B	0.228	0.317	0.088
CB Seq A	0.145	0.469	0.324
CB Seq B	0.253	0.345	0.092
DB Seq A	0.116	0.468	0.352
DB Seq B	0.281	0.343	0.061
EA Seq A	0.173	0.306	0.132
EA Seq B	0.185	0.214	0.030
EB Seq B	0.202	0.366	0.164
EB Seq A	0.090	0.491	0.402
EC Seq A	0.141	0.390	0.249
EC Seq B	0.168	0.449	0.281
ED Seq A	0.146	0.479	0.332
ED Seq B	0.223	0.451	0.228
EF Seq A	0.123	0.300	0.177
EF Seq B	0.255	0.270	0.015
EG Seq A	0.236	0.391	0.155
EG Seq B	0.160	0.511	0.351
FA Seq A	0.131	0.315	0.184
FA Seq B	0.239	0.338	0.099
FB Seq A	0.098	0.405	0.308
FB Seq B	0.327	0.460	0.133
FC Seq A	0.167	0.333	0.166
FC Seq B	0.257	0.310	0.053
GC Seq A	0.166	0.536	0.370
GC Seq B	0.328	0.359	0.031
GD Seq A	0.134	0.496	0.362
GD Seq B	0.190	0.497	0.307
HI Seq A	0.214	0.609	0.396
HI Seq B	0.194	0.607	0.413
BH Seq A	0.216	0.396	0.179
BH Seq B	0.231	0.445	0.214
BI Seq A	0.219	0.545	0.326
BI Seq B	0.218	0.421	0.203
GH Seq A	0.099	0.519	0.420
GH Seq B	0.417	0.549	0.132
GI Seq A	0.135	0.406	0.271
GI Seq B	0.448	0.518	0.070
CH Seq A	0.124	0.521	0.397
CH Seq B	0.337	0.418	0.081
CI Seq A	0.147	0.578	0.430
CI Seq B	0.317	0.606	0.289
AH Seq A	0.091	0.390	0.300
AH Seq B	0.198	0.518	0.320
AI Seq A	0.107	0.565	0.459
AI Seq B	0.212	0.620	0.409
EH Seq A	0.146	0.555	0.409
EH Seq B	0.323	0.437	0.114
EI Seq A	0.140	0.456	0.316
EI Seq B	0.451	0.621	0.170
DH Seq A	0.145	0.273	0.128
DH Seq B	0.247	0.645	0.398
DI Seq A	0.137	0.628	0.491
DI Seq B	0.229	0.458	0.229
FH Seq A	0.315	0.486	0.171
FH Seq B	0.331	0.507	0.177
FI Seq A	0.322	0.639	0.317
FI Seq B	0.338	0.684	0.346

Table 6.3 Histogram based occlusion resolution comparison results

These comparison results are graphed in Figure 6.9.

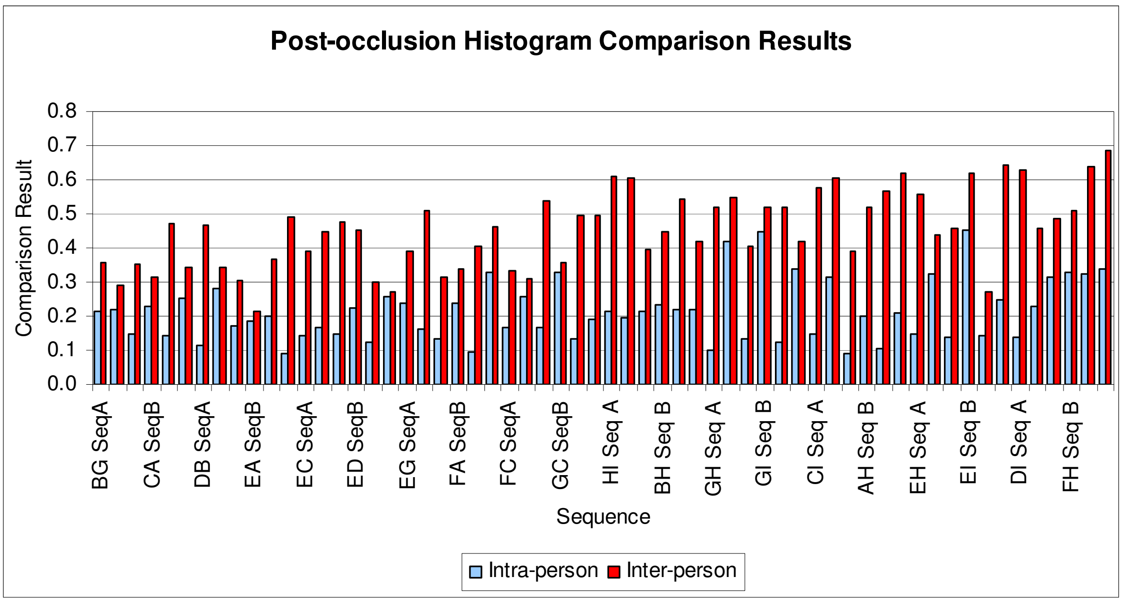

Figure 6.9 Post occlusion comparison results

In all cases the intra-person result has a lower score (better match) than the inter-person result. A histogram displaying the distribution of the Inter-person and Intra-person results is shown in Figure 6.10.

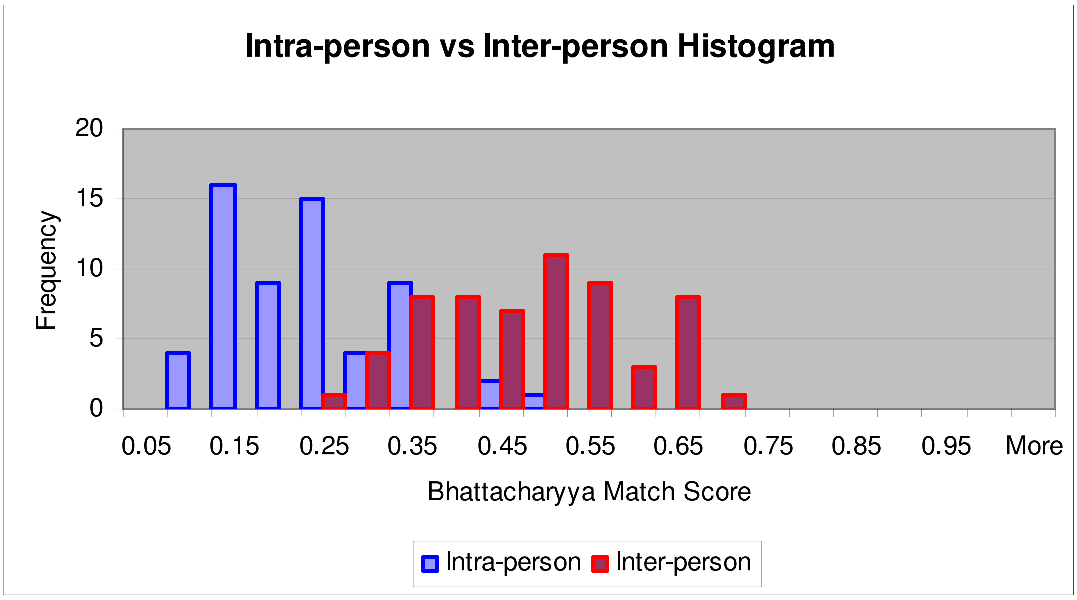

Figure 6.10 Histogram of comparison results

It can be seen that a distinct grouping of the inter-person results around a mean of 0.454 while the intra-person results shows a better match mean at 0.213. This shows that the mean inter-person result is more than twice the mean intra-person result. In Figure 6.11, a histogram of the difference between the intra-person and inter-person results across the range is shown.

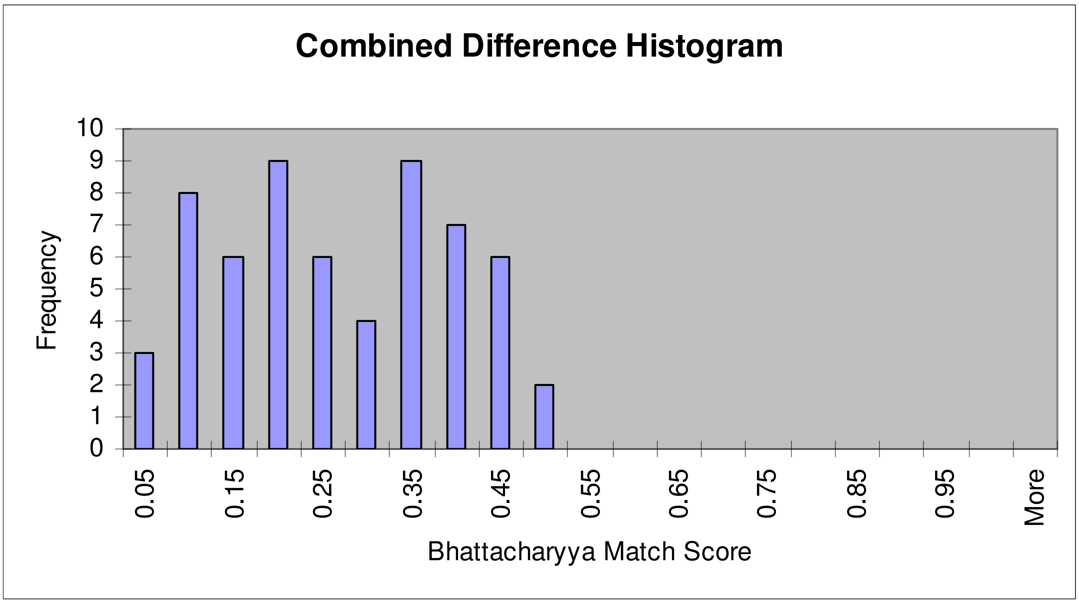

Figure 6.11 Histogram of difference between comparison results

Across the 60 results, there are three occurrences in which the difference between subject comparison results is less than 0.05. It is noted that the results distributions for series A and B are dissimilar. A histogram of these result sets is shown in Figure 6.12.

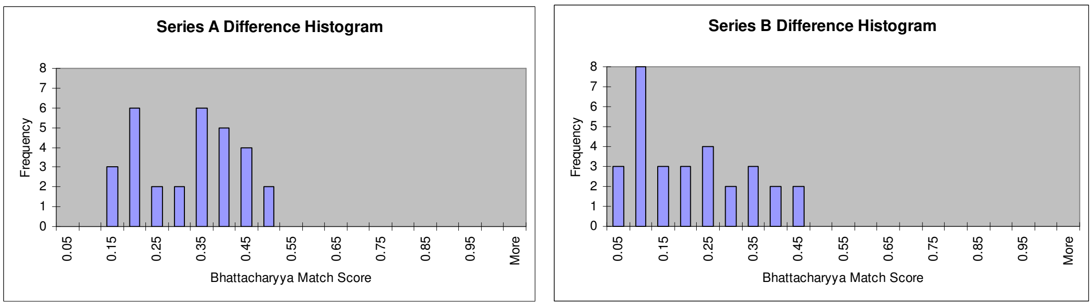

Figure 6.12 Series A and B Difference Histograms

The mean difference between the results for correct and incorrect subject comparisons is 0.296 in series A and 0.186 in series B. It can be seen that all sequences in which the difference between comparison results was less than 0.1 occurred in series B in which the subjects change direction during occlusion. It is expected that this difference in results is due to the significant change in visible surface properties in the images due to the change in direction of the subjects after occlusion.

The results show a strong improvement in individual discrimination capability of over the usage of direction based occlusion resolution. Analysis of the comparison result distribution goes some way to show the capabilities of the method, however, further work is required to establish the limitations of the method. This work is undertaken in the next section.

6.4 Establishing Limitations of Multi-Modal Histogram Occlusion Resolution

This section details work undertaken to establish the limitations of using the multi-modal parameter configuration in difficult environments. This is performed through a series of evaluations of the system's capabilities under environmental conditions of increasing complexity and reducing image quality. Evaluation of the results shows that across the scenarios, the multi-modal approach performs better than the optimal visible and IR alone. A final scenario in which subjects have similar clothing indicates the continuation of this trend; however caution is advised due to the limited number of samples.

6.4.1 Method

The samples in Dataset G are used for this experiment. In scenarios E, F and G; 99 occlusions are simulated. For each subject, their post occlusion histogram will be compared with 10 alternative histograms and the correct histogram from the prior image of the same subject.. If the best matching histogram is of the same subject, the occlusion is correctly resolved. This will happen with three different sets of 10 alternatives subjects for each person providing 3 occlusions per subject and 99 in total with 990 comparisons per scenario. In scenario H however, a total of 11 subjects allows for only 11 results, limiting confidence in the results.

The distance between subjects' sample locations randomly varies from 1-3 meters to remove influence that the gait cycle may have on histogram description. This allows simulation of a number of different occlusions using the same subject histogram to enable inferences to performance in situations of occlusions or groups involving numerous subjects.

Histogram descriptions of the subjects are calculated. Each subject's second histogram is compared with the first histogram of the same subject and the histograms of 10 other subjects from the same scenario. This is to determine the discriminating capability when a high level of uncertainty in the identity of the subject is present. Histogram representations of the optimal 1-D Hue, 1-D IR and 2-D Hue IR will be used. The capability will be judged on the minimum result (best match) across the histograms. The final scenario will consist of subjects in uniformed clothing to test.

6.4.2 Expected Results

The sample size ensures a high level of confidence in results across scenarios A-C. It is expected that the capability of the system will be reduced as the complexity of the scenes increases. It is also expected that the combined 2-D Hue and IR histogram representations will provide superior results across the scenario than the optimal 1-D Hue or 1-D Thermal histogram representations.

6.4.3 Results and Discussion

In Table 6.4, an example of the resolution results for 11 occlusion events is shown. The specific HPCTCs use the 1-D Hue representation of subjects in scenario A. The best match is highlighted in red. The blue boxes indicate intra-person comparisons. A best match inside the blue box indicates a correctly resolved occlusion.

Subject	0	1	2	3	4	5	6	7	8	9	10
0	0.0478	0.1117	0.0689	0.2518	0.0422	0.1351	0.1756	0.1216	0.1027	0.1976	0.2227
1	0.0505	0.0738	0.0384	0.1937	0.0864	0.1098	0.1274	0.0609	0.0446	0.1488	0.1611
2	0.0504	0.0766	0.0164	0.1920	0.0873	0.1043	0.1239	0.0685	0.0401	0.1477	0.1595
3	0.2290	0.1753	0.1966	0.0168	0.2698	0.1717	0.1088	0.1745	0.1658	0.0988	0.0701
4	0.0338	0.0768	0.0719	0.2305	0.0413	0.0896	0.1422	0.1417	0.1050	0.1626	0.2186
5	0.0850	0.0687	0.1048	0.2036	0.0948	0.0511	0.1158	0.1644	0.1250	0.1252	0.2120
6	0.1565	0.0990	0.1316	0.0726	0.1962	0.0895	0.0254	0.1413	0.1114	0.0318	0.0993
7	0.1230	0.1175	0.0862	0.1549	0.1598	0.1439	0.1279	0.0226	0.0536	0.1448	0.1025
8	0.0971	0.1069	0.0652	0.1792	0.1315	0.1379	0.1358	0.0202	0.0436	0.1556	0.1320
9	0.0758	0.0275	0.0618	0.1432	0.1158	0.0554	0.0645	0.0900	0.0526	0.0836	0.1341
10	0.1840	0.1461	0.1479	0.0821	0.2261	0.1619	0.1094	0.1015	0.1098	0.1161	0.0213

Incorectly Resolved Occlusion

Correctly Resolved Occlusion

Table 6.4 Example of a comparison result table for scenario A

In Figure 6.13 an example of results, showing comparisons for subject number 5 from Table 6.4 is shown.

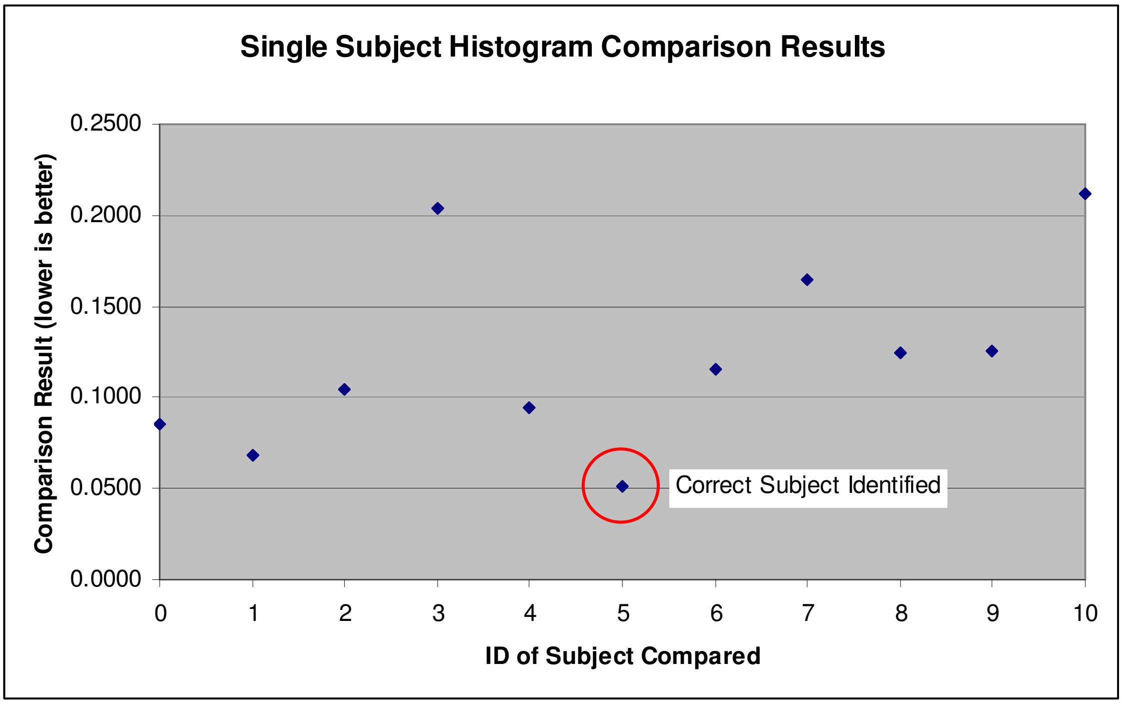

Figure 6.13 Correct resolution of occlusion involving subject number 5

The subject's post occlusion histogram is compared to the pre-occlusion histogram of the same subject and ten alternative subjects. The best match is highlighted, in this case correctly identifying the subject

6.4.3.1. Scenarios A-C Results

The subject identification rate based upon the minimum Bhattacharyya Distance comparison results for scenarios A-C is shown in Table 6.5.

	Scenario A	Scenario B	Scenario C
Hue	60.61%	48.48%	21.21%
Thermal IR	91.92%	63.64%	58.59%
Hue/ Thermal IR	96.97%	71.72%	63.64%

Table 6.5 Identification rates for scenarios A-C

The results for scenarios A-C are graphed in Figure 6.14. The error bars indicate the confidence limits with a 95% confidence interval for the mean.

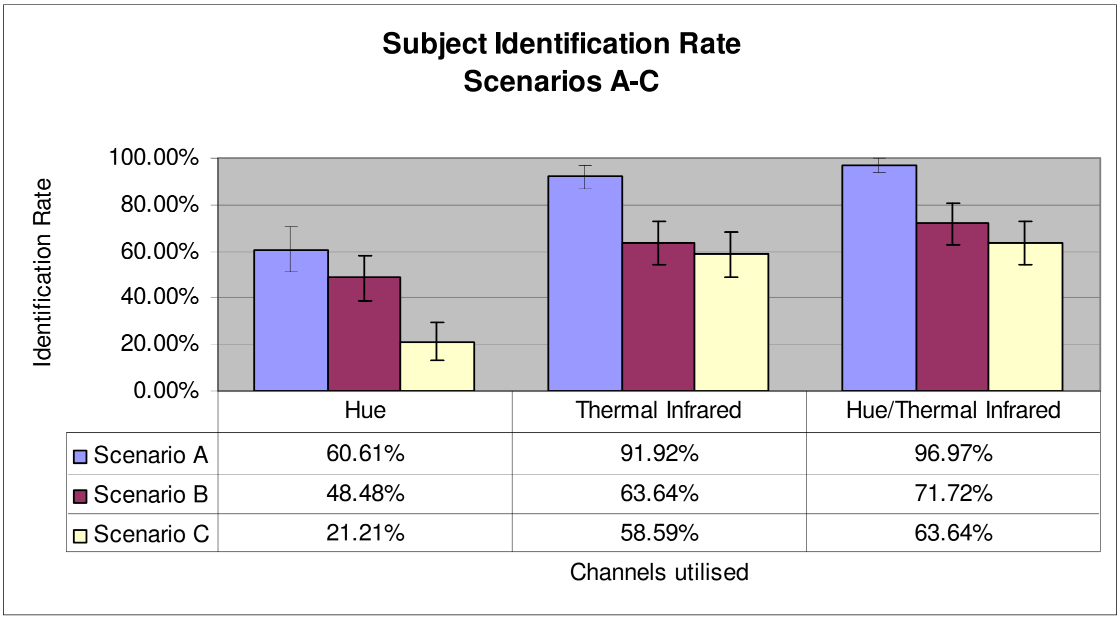

Figure 6.14 Subject identification results for Scenarios A-C

The results from Scenarios A-C show a drop in the capability to discriminate between individuals across all channel representations as the complexity of the scene increases in scenario B and the information available decreases in scenario C. However, across these scenarios, the capability of the 2-D multi-modal histogram provides superior results to the optimum visible and thermal IR histogram HPCTCs.

In Figure 6.15 the mean values of the results in which an occlusion was correctly resolved using the Bhattacharyya Distance is shown for scenarios A-C. The standard deviation of the results is indicated on the graph.

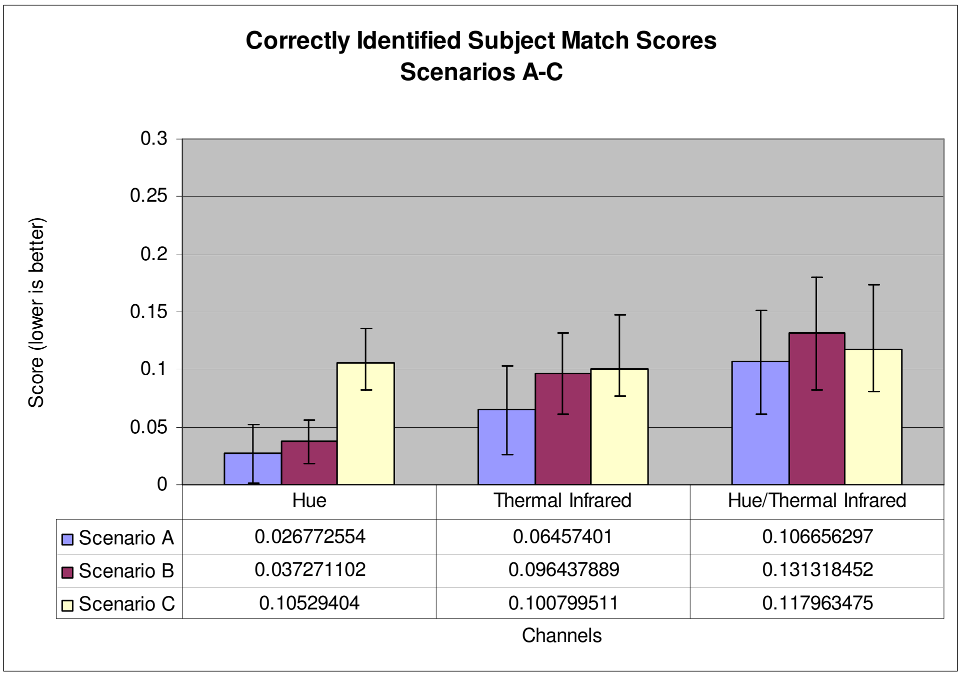

Figure 6.15 Bhattacharyya Distance match scores. Scenario A-C correctly classified subjects

A general trend of an increasing match score (poorer matches) is observed from the best matches with Hue to less certain matches in the 2-D Hue/IR configuration. The exception to this trend is scenario C, in which the mean score for correctly identified subjects is approximately the same across the modality configurations.

6.4.3.2. Scenario D Results

The purpose of scenario D is to give an indication of the capability of the system in resolving subjects who appear very similar due to wearing similar or identical clothing. Scenario D identification rate results are shown in Table 6.6.

	Scenario D
Hue	54.55%
Thermal IR	36.36%
Hue/ Thermal IR	63.64%

Table 6.6 Identification rates for scenario D

These results are graphed in Figure 6.16, with the error bars indicating the confidence limits of a 95% confidence interval.

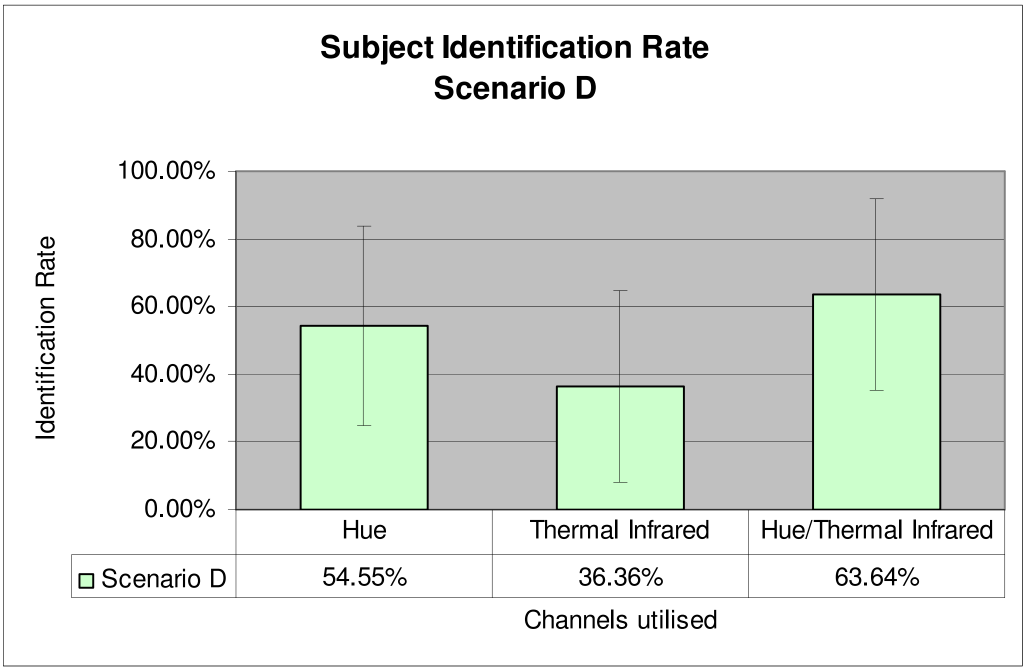

Figure 6.16 Subject identification results for Scenario D

Scenario D results show a higher than expected result for the Hue HPCTC which shows better results than the optimum thermal HPCTC. This is unexpected, as in 5.1.3.3, thermal IR was shown to perform better than any 1-D or 2-D visible HPCTCs. However, caution must be exercised due to the small sample size resulting in wide confidence intervals. Only 2 more subjects were correctly classified by Hue than through the use of IR.

To further explore the results for scenario D, ranking of the comparison results is undertaken. Figure 6.17 shows the position of the correct comparison in the rankings. Thresholding is used, highlighting in green results in which the correct subject was placed in the top three positions.

Rank of correct result			
Subject	**Hue**	**IR**	**2-D Hue/IR**
0	2	1	1
1	4	1	1
2	7	5	4
3	1	2	1
4	2	4	3
5	1	3	4
6	1	8	8
7	1	2	1
8	2	1	1
9	1	1	1
10	1	2	1
Total	9	8	8
	81.82%	72.73%	72.73%

Figure 6.17 Scenario D ranked results

The results show that in this scenario, Hue performed better than thermal or the combined configuration.

Figure 6.18 shows the mean values of the results in which an occlusion was correctly resolved using the Bhattacharyya Distance is shown for scenario D.

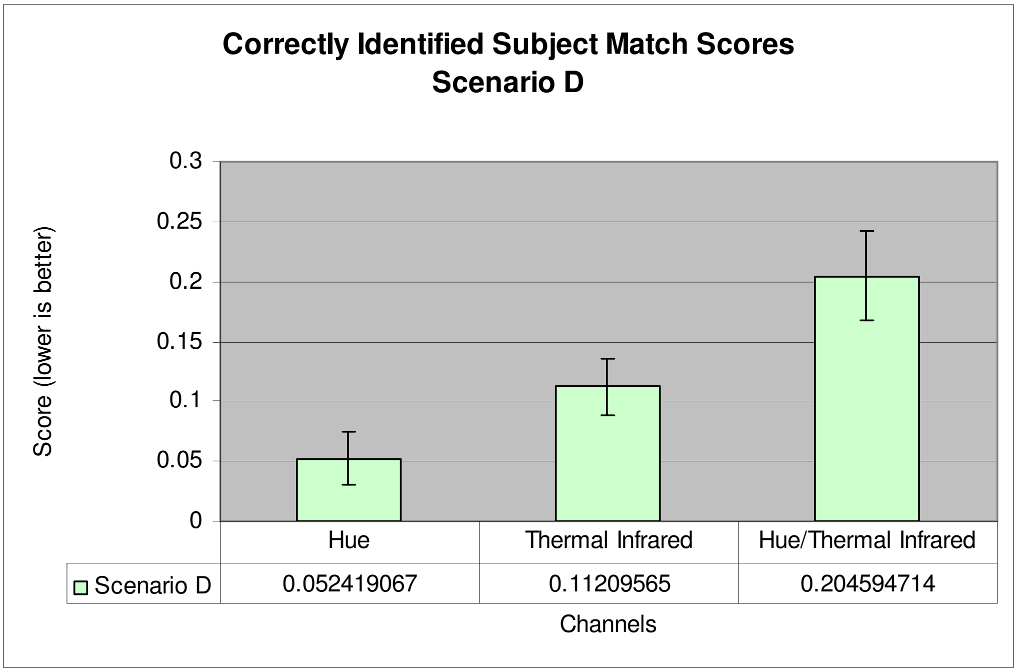

Figure 6.18 Bhattacharyya Distance match scores. Scenario D correctly classified subjects

The Bhattacharyya match score for scenario D follows the trend of an increasing match score observed in Scenario's A-C, however the wider confidence intervals give decreased confidence in the true mean.

6.4.3.3. Discussion

From the results, it can be seen that where subjects have been correctly classified, the Bhattacharyya match scores results are poorer with the multi-modal HPCTC. It is theorised that this is due to the increasing number of bins to represent a subject, as classification results show that the multi-modal HPCTC is better at discriminating between subjects. The number of bins increases at from 21 for the Hue histogram to 24 for the thermal IR histogram to 126 for the multi-modal histogram. The greater number of bins representing a subject means finer quantisation of pixel values. In coarser representations, changes in the appearance of subject between images may not be sufficient for changes in pixel bin placements to occur at a high rate. In finer histogram representations with increased bins, the changes in appearance may cause movement between bins at an increased rate, therefore increasing the comparison distance when comparing histograms.

It can be concluded that regarding scenarios A-C, the established metric maintains its improved capability over optimised single modality configurations in situations of complex or restricted illumination. Regarding scenario D, further samples are required to fully determine the capabilities in discriminating between uniformed subjects.

6.5 Summary

The work outlined in this chapter outlines experiments to determine the holistic capabilities of the methods developed in Chapter 5 . This is achieved by undertaking the design and implementation of a complete tracking system. The chapter commences with the description of the tracking system.

Evaluation of trajectory methods is undertaken using scenarios in which subjects change direction during occlusion. It was found that utilising historical trajectory information was not sufficient to correctly resolve occlusions of this nature.

An alternative method using a feature space representation consisting of histogram representations of the subjects is utilised. Along with the optimal multi-modal HPCTC, the optimal visible and thermal IR 1-D HPCTCs are utilised to show contrast of the multi-modal HPCTC with optimised uni-modal HPCTCs.

Conclusions are drawn that the multi-modal HPCTC established in 5.4 provides a superior occlusion resolution capabilities result than optimised 1-D histograms from either modality. It was found that this was true in a number of scenarios of increasing scene complexity or reduced information availability.

It is suggested that future work would entail increasing the sample size of scenarios with uniformed subjects to more reliably determine the efficacy in discriminating between such subjects. Further extension to the work would entail the integration of the multi-modal histogram into a denser feature space. A feature space utilising other extracted features such as dimensions, gait, etc. and segmented utilising techniques such as SVMs (Burges 1998) or Codebooks (Zhou and Hoang 2005). It is also suggested that establishing the probabilities of subjects changing direction throughout the scene would enable integration of trajectory based occlusion resolution.

7 Conclusions

In section 1.1 the question was posed: “To what extent can thermal IR image information be used to improve visible light based human tracking systems?”

Review of the current knowledge in the field began by investigating the stages typical in tracking systems and the problems encountered at the different stages. The nature and properties of infrared radiation, along with current utilisation of thermal IR images in automated tracking systems were explored. After evaluating existing human tracking datasets, the decision was made to undertake high quality uncompressed multi-modal capture in order to determine the quality requirements for any developed methods, rather than use existing datasets.

Initial investigations focused upon methods for optimising foreground extraction in multi-modal environments. Experimentation showed that the use of thermal information provided a superior foreground mask using statistical extraction techniques than visible information in the majority of scenarios. It was shown that this was due to reductions of problem areas prevalent in visible light images, such as shadows of subjects and variations in external lighting availability and consistency.

A novel system was proposed for evaluating sensor reliability before selecting the optimal foreground mask, using a neuro-fuzzy inference system as a prior stage to classification. This differs in approach to those in the literature, such as that described by Guo et al. (2006), who evaluates sensor reliability for discerning between classes in feature space. The neuro fuzzy inference system was trained using comparisons between manually segmented optimum masks and the automated foreground mask extraction technique. A number of environment descriptors were proposed as indicators of modality quality. Experiments were performed to determine the level of co-variance with each modalities extraction capability. Results from using the trained neuro-fuzzy inference system on a testing dataset showed a high degree of accuracy in selecting the optimum modality in a number of environmental conditions.

Conclusions are drawn that, under the environmental conditions tested, a trained neuro-fuzzy inference system is capable of assessing measures of modality quality to select the optimum modality for foreground extraction with a high degree of success.

It is suggested that future work would focus on increasing the dataset to take into account an increased number of environmental conditions not presented in this work. Further investigation into optimising the membership functions is recommended. It is also suggested that future work investigates alternative multi-modal applications for the developed system where modality specific quality measures can be assessed using application specific evaluation.

Investigations progressed into considering how the properties of thermal IR images could be used in providing a descriptor of the human body for use in tracking systems. It was proposed that thermal IR pixel data could be used to help construct a histogram of subject's appearance. A novel method for evaluating histogram parameter configuration and comparison techniques combinations (HPCTCs), called D_x, was proposed. The method not only attempts to optimise the function parameters, as is the aim of work by Taylor et al. (2006), but also to optimise the method for comparing resulting histograms. The D_x measure was utilised to provide a measure of a HPCTC's discrimination capability. Experiments utilising an exhaustive search approach compared existing visible based methods with a thermal histogram using the measure. An increased discrimination capability was observed over the most superior visible configuration.

The research continued into investigating whether combination of thermal and visible information from the disparate sources could provide an increased capability to discriminate between subjects. Experimental results showed that a specific HPCTC, which used a combined Hue and thermal IR histogram, provided a much increased subject discrimination capability. This was evident even in scenes with changing illumination conditions.

It is concluded that, using the D_x measure, the best thermal IR HPCTCs out performed the best visible 1-D or 2-D HPCTCs by a significant margin. It is also concluded that the most optimal HPCTC evaluated is a multi-modal histogram utilising Hue and thermal IR channels, with 6 bins for the Hue channel and 21 bins for thermal information. The technique for comparing histograms in this optimum HPCTC is the Bhattacharyya Distance. Direct comparisons with the literature are not possible due to the newly developed comparison method and the choice of high quality capture over existing datasets.

This technique's position in the area of parameter optimisation leads to suggestion of future work. As the number of parameters increase, the exhaustive search approach becomes unfeasible due to combinatorial explosion. It is suggested future work investigates the use of heuristic based search methods to traverse parameter space. A limitation of the HPCTC optimisation investigations was the number of environmental conditions represented. It is suggested that future work would focus on increasing the dataset to take into account an increased number of environmental conditions not presented in this work.

The research culminates in the creation of a fully featured tracking system consisting of person detection, Euclidean tracking and occlusion/group handling functionality. Evaluation of trajectory methods was undertaken using scenarios in which subjects change direction during occlusion. Limitations identified with trajectory methods were tackled using a feature space representation consisting of histogram representations of the subjects. Along with the optimal multi-modal HPCTC, the optimal visible and thermal IR 1-D HPCTCs are utilised to show contrast of the multi-modal HPCTC with optimised uni-modal HPCTCs.

It is concluded that histogram representations are capable of resolving occlusions that are the worst-case scenario for trajectory based techniques. Further conclusions are drawn that the multi-modal HPCTC established in 5.4 provides a superior occlusion resolution capabilities result than optimised 1-D histograms from either modality in a number of scenarios of increasing scene complexity or reduced information availability.

It is suggested that future work attempts to increase the feature space representation in the appearance model using additional appearance descriptors to further distinguish between subjects.

The work has tackled the research question proposed at the outset. Novel methods have been proposed, developed and utilised for the evaluation of sensor quality in a multi-modal framework. Novel techniques for optimising histogram representation of subjects in feature space have been described and demonstrated holistically through the development and integration in a fully featured tracking system. Limitations of the capabilities of the system have been evaluated and future work has been proposed to expand on the capabilities achieved.

References

A Framework for Evaluating Stereo-Based Pedestrian Detection Techniques - Pedestrian Detection Data-2007a. [online]. . Available at: http://www.cdvp.dcu.ie/datasets/2007].

*IEEE OTCBVS WS Series Bench*2007b. [online]. . Available at: http://www.cse.ohio-state.edu/otcbvs-bench/2007].

*i-Lids bag and vehicle detection challenge datasets*2007c. [online]. . Available at: http://www.eecs.qmul.ac.uk/~andrea/avss2007_d.html2007].

*Thermo-Visual Feature Fusion for Object Tracking Using Multiple Spatiogram Trackers - Thermo-Visual Datasets*2007d. [online]. . Available at: http://www.cdvp.dcu.ie/datasets/thermo_visual/2007].

*AIC Thermal/Visible Night-time Dataset*2006a. [online]. . Available at: http://www.imagefusion.org/images/oconaire/oconaire.html2007].

*PETS2006 datasets*2006b. [online]. . Available at: http://ftp.cs.rdg.ac.uk/PETS2006/2007].

*PETS2001 datasets*2001. [online]. . Available at: http://www.cvg.cs.rdg.ac.uk/PETS2001/pets2001-dataset.html2007].

ARRAS, K.O., GRZONKA, S., LUBER, M. and BURGARD, W., 2008. Efficient people tracking in laser range data using a multi-hypothesis leg-tracker with adaptive occlusion probabilities. *In: IEEE International Conference on Robotics and Automation, 2008. ICRA 2008, /.* pp. 1710.

BELEZNAI, C., and BISCHOF, H., 2009. Fast human detection in crowded scenes by contour integration and local shape estimation.

BELONGIE, S., MORI, G. and MALIK, J., 2006. Matching with shape contexts. *Statistics and Analysis of Shapes,* , 81-105.

BERTOZZI, M., BROGGI, A., CARAFFI, C., DEL ROSE, M., FELISA, M. and VEZZONI, G., 2007. Pedestrian detection by means of far-infrared stereo vision. *Computer Vision and Image Understanding,* 106 (2-3), 194.

BHATTACHARYYA, A., 1943. On a measure of divergence between two statistical populations defined by their probability distributions. *Bull.Calcutta Math.Soc,* 35 (99-109), 4.

BRADSKI, G.R., and KAEHLER, A., 2008. *Learning OpenCV.* O'Reilly.

BURGES, C.J.C., 1998. A tutorial on support vector machines for pattern recognition. *Data Mining and Knowledge Discovery,* 2 (2), 121-167.

CAPELLADES, M.B., DOERMANN, D., DEMENTHON, D. and CHELLAPPA, R., 2003. An appearance based approach for human and object tracking. *In: Proc. IEEE Int. Conf. on Image Processing,* Citeseer, pp. 85–88.

CHEN, T., HAUSSECKER, H., BOVYRIN, A., BELENOV, R., RODYUSHKIN, K., KURANOV, A. and ERUHIMOV, V., 2005. Computer Vision Workload Analysis: Case Study of Video Surveillance System. *Computer Vision Workload Analysis: Case Study of Video Surveillance System,* Volume 09 Issue 02.

COLANTONIO, S., BENVENUTI, M., DI BONO, M.G., PIERIA, G. and SALVETTIA, O., 2007. Object tracking in a stereo and infrared vision system. *Infrared Physics & Technology,* Volume 49, Issue 3, 266-271.

COMANICIU, D., RAMESH, V. and MEER, P., 2003. Kernel-based object tracking. *IEEE Transactions on Pattern Analysis and Machine Intelligence,* 25 (5), 564.

COX, I.J., and HINGORANI, S.L., 1996. An efficient implementation of Reid's multiple hypothesis tracking algorithm and its evaluation for the purpose of visual tracking. *IEEE Transactions on Pattern Analysis and Machine Intelligence,* 18 (2), 138.

DALAL, N., and TRIGGS, B., 2005. Histograms of oriented gradients for human detection. *In: IEEE Computer Society Conference on Computer Vision and Pattern Recognition,* Citeseer, pp. 886.

DALAL, N., TRIGGS, B. and SCHMID, C., 2006. Human detection using oriented histograms of flow and appearance. *Lecture Notes in Computer Science,* 3952, 428.

DAVIS, J.W., and SHARMA, V., 2007. Background-subtraction using contour-based fusion of thermal and visible imagery. *Computer Vision and Image Understanding,* Volume 106 , Issue 2-3, 162-182.

DAVIS, J.W., and SHARMA, V., 2005. Fusion-Based Background-Subtraction using Contour Saliency. *In: Computer Vision and Pattern Recognition, 2005 IEEE Computer Society Conference on Volume: 3, On page(s): 11- 11, /.*

DOCKSTADER, S.L., and TEKALP, A.M., 2001. Multiple camera fusion for multi-object tracking. *In: Proceedings of the IEEE Workshop on Multi-Object Tracking (WOMOT'01),* IEEE Computer Society, pp. 95.

DOMKE, J.A.A., Y., 2006. Deformation and Viewpoint Invariant Color Histograms. *In: British Machine Vision Conference, /.* pp. 509.

ENZWEILER, M., KANTER, P. and GAVRILA, D.M., 2008. Monocular pedestrian recognition using motion parallax. *In: 2008 IEEE Intelligent Vehicles Symposium,* pp. 792-797.

ESTEPAR, R.S.J., BRUN, A. and WESTIN, C.F., 2004. Robust Generalized Total Least Squares Iterative Closest Point Registration. *LECTURE NOTES IN COMPUTER SCIENCE,* , 234.

FISHER, R., 2007. *CAVIAR Test Case Scenarios* [online]. . Available at: http://homepages.inf.ed.ac.uk/rbf/CAVIARDATA1/2007].

FREEMAN, W.T., and ROTH, M., 1995. Orientation histograms for hand gesture recognition. *In: International Workshop on Automatic Face and Gesture Recognition,* Citeseer, .

FREUND, Y., and SCHAPIRE, R.E., 1997. A decision-theoretic generalization of on-line learning and an application to boosting. *Journal of Computer and System Sciences,* 55 (1), 119-139.

FREUND, Y., and SCHAPIRE, R.E., 1996. Experiments with a new boosting algorithm. *In: MACHINE LEARNING-INTERNATIONAL WORKSHOP THEN CONFERENCE-,* Citeseer, pp. 148-156.

FRIEDMAN, J., HASTIE, T. and TIBSHIRANI, R., 2000. Special invited paper. additive logistic regression: A statistical view of boosting. *The Annals of Statistics,* 28 (2), 337-374.

FUKUSHIMA, K., 1980. Neocognitron: A self-organizing neural network model for a mechanism of pattern recognition unaffected by shift in position. *Biological Cybernetics,* 36 (4), 193-202.

GAVRILA, D., 2000. Pedestrian detection from a moving vehicle. *Lecture Notes in Computer Science,* 1843, 37-49.

GAVRILA, D.M., and MUNDER, S., 2007. Multi-cue pedestrian detection and tracking from a moving vehicle. *International Journal of Computer Vision,* 73 (1), 41-59.

GORDON, N.J., SALMOND, D.J. and SMITH, A.F.M., 1993. Novel approach to nonlinear/non-Gaussian Bayesian state estimation. *In: IEE Proceedings,* pp. 107-113.

GOUBET, E., KATZ, J. and PORIKLI, F., 2006. Pedestrian Tracking Using Thermal Infrared Imaging. *In: SPIE Conference Infrared Technology and Applications XXXII, Vol.797-808,* pp. 797-808.

GRIMSON, W.E.L., STAUFFER, C., ROMANO, R. and LEE, L., 1998. Using adaptive tracking to classify and monitor activities in a site. *In: IEEE Computer Society Conference on Computer Vision and Pattern Recognition,* Institute Of Electrical Engineers Inc (IEEE), pp. 22-31.

GUO, H., SHI, W. and DENG, Y., 2006. Evaluating sensor reliability in classification problems based on evidence theory. *IEEE Transactions on Systems, Man, and Cybernetics, Part B,* 36 (5), 970-981.

GUO, Y., HSU, S., SAWHNEY, H.S., KUMAR, R. and SHAN, Y., 2007. Robust object matching for persistent tracking with heterogeneous features. *IEEE Transactions on Pattern Analysis and Machine Intelligence,* , 824-839.

HALL, D.L., and MCMULLEN, S.A.H., 2004. *Mathematical techniques in multisensor data fusion.* Artech House Publishers.

HAN, J., and BHANU, B., 2007. Fusion of color and infrared video for moving human detection. *Pattern Recognition,* Volume 40 , Issue 6, 1771-1784.

HARITAOGLU, I., HARWOOD, D. and DAVIS, L., 2000. W4: Real-Time Surveillance of People and Their Activities.

HEISELE, B., SERRE, T., PONTIL, M. and POGGIO, T., 2001. Component-based face detection. *In: IEEE Computer Society Conference on Computer Vision and Pattern Recognition,* Citeseer, .

HILARIO, C., COLLADO, J., ARMINGOL, J. and DE LA ESCALERA, A., 2005. *Pedestrian Detection for Intelligent Vehicles Based on Active Contour Models and Stereo Vision.* Springer Berlin / Heidelberg.

HILLIER, F.S., and LIEBERMAN, G.J., 1990. *Introduction to mathematical programming.* McGraw-Hill New York.

ISARD, M., and BLAKE, A., 1998. CONDENSATION - conditional density propagation for visual tracking. *Int.J.Computer Vision,* 29, 1, 5.

JAVED, O., SHAFIQUE, K. and SHAH, M., 2002. A hierarchical approach to robust background subtraction using color and gradient information. *In: Motion and Video Computing, 2002. Proceedings. Workshop on, /.* pp. 22-27.

JEPSON, A.D., FLEET, D.J. and EL-MARAGHI, T.F., 2003. Robust online appearance models for visual tracking. *Pattern Analysis and Machine Intelligence, IEEE Transactions on,* 25 (10), 1296-1311.

JIA, Z., BALASURIYA, A. and CHALLA, S., 2008. Vision based data fusion for autonomous vehicles target tracking using interacting multiple dynamic models. *Computer Vision and Image Understanding,* Volume 109 , Issue 1, 1-21.

JONES, M.J., and POGGIO, T., 1998. Multidimensional morphable models. *In: 6th International Conference on Computer Vision,* Citeseer, pp. 683–688.

KAEWTRAKULPONG, P., and BOWDEN, R., 2003. A real time adaptive visual surveillance system for tracking low-resolution colour targets in dynamically changing scenes. *Image and Vision Computing,* 21 (10), 913-929.

KAEWTRAKULPONG, P., and BOWDEN, R., 2001. An Improved Adaptive Background Mixture Model for Realtime Tracking with Shadow Detection. *In: In Proc. 2nd European Workshop on Advanced Video Based Surveillance Systems, /.*

KERVRANN, C., and HEITZ, F., 1998. A hierarchical Markov modeling approach for the segmentation and tracking of deformable shapes. *Graphical Models and Image Processing,* 60 (3), 173-195.

KHAN, S., and SHAH, M., 2000. Tracking people in presence of occlusion. *In: Asian Conference on Computer Vision,* .

KHAN, Z., BALCH, T. and DELLAERT, F., 2004. An MCMC-based Particle Filter For Tracking Multiple Interacting Targets.

KIM, K., CHALIDABHONGSE, T.H., HARWOOD, D. and DAVIS, L., 2004. Background modelling and subtraction by codebook construction. *In: IEEE International Conference on Image Processing (ICIP),* Citeseer, .

KIRCHHOFF, G., 1860. On the relation between the radiating and absorbing powers of different bodies for light and heat. *Philosophical Magazine Series 4,* 20 (130), 1-21.

KYUNGNAM, K., THANARAT, H., CHALIDABHONGSEB, D. and HARWOODA, L.D., 2005. Real-time foreground–background segmentation using codebook model. *Real-Time Imaging,* Volume 11 Number 3, 172-185.

LEE, S.W., KANG, J., SHIN, J. and PAIK, J., 2007. Hierarchical active shape model with motion prediction for real-time tracking of non-rigid objects. *Computer Vision, IET,* Volume: 1, Issue: 1, 17-24.

LEIBE, B., CORNELIS, N., CORNELIS, K. and VAN GOOL, L., 2007. Dynamic 3d scene analysis from a moving vehicle. *In: IEEE Conference on Computer Vision and Pattern Recognition, 2007. CVPR'07,* pp. 1-8.

LEIBE, B., SEEMANN, E. and SCHIELE, B., 2005. Pedestrian detection in crowded scenes. *In: IEEE Computer Society Conference on Computer Vision and Pattern Recognition,* Citeseer, pp. 878.

LEYKIN, A., and HAMMOUD, R., 2006. Robust Multi-Pedestrian Tracking in Thermal-Visible Surveillance Videos. *In: Computer Vision and Pattern Recognition Workshop, 2006 17-22 June Conference on, /.* pp. 136-136.

LIENHART, R., and MAYDT, J., 2002. An extended set of haar-like features for rapid object detection. *In: IEEE ICIP,* Citeseer, pp. 900–903.

LUBER, M., TIPALDI, G.D. and ARRAS, K.O., 2009. Spatially Grounded Multi-Hypothesis Tracking of People. *In: May 12-17 2009.*

MA, G., YAO, J. and YANG, X., 2009. Prediction of the Position of Pedestrian Crossing Road Section Based on Kalman Predictor. *In: 2009 International Conference on Measuring Technology and Mechatronics Automation,* IEEE, pp. 541-544.

MARTINKAUPPI, B., SORIANO, M. and PIETIKAINEN, M., 2003. Detection of skin color under changing illumination: a comparative study. *Image Analysis and Processing, 2003.Proceedings.12th International Conference on,* , 652-657.

MCKENNA, S.J., JABRI, S., DURIC, Z., ROSENFELD, A. and WECHSLER, H., 2000a. Tracking Groups of People. *Computer Vision and Image Understanding,* 80 (1), 42.

MCKENNA, S.J., JABRI, S., DURIC, Z. and WECHSLER, H., 2000b. Tracking interacting people. *Fg,* , 348.

MOESLUND, T.B., and BAJERS, F., 2001. A survey of computer vision-based human motion capture. *Computer Vision and Image Understanding,* Volume 81 , Issue 3, 231-268.

MOESLUND, T.B., HILTON, A. and KRÜGER, V., 2006. A survey of advances in vision-based human motion capture and analysis. *Computer Vision and Image Understanding,* vol. 104, 90-126.

MORI, G., and MALIK, J., 2002. Estimating human body configurations using shape context matching. *LECTURE NOTES IN COMPUTER SCIENCE,* , 666-680.

MORI, G., REN, X., EFROS, A.A. and MALIK, J., 2004. Recovering human body configurations: Combining segmentation and recognition.

MORIOKA, K., LEE, J.H., KURODA, Y. and HASHIMOTO, H., 2007. Hybrid tracking based on color histogram for intelligent space. *Artificial Life and Robotics,* 11 (2), 204-210.

MUNDER, S., SCHNORR, C. and GAVRILA, D.M., 2008. Pedestrian detection and tracking using a mixture of view-based shape-texture models. *IEEE Transactions on Intelligent Transportation Systems,* 9 (2), 333-343.

MUÑOZ-SALINAS, R., AGUIRRE, E. and GARCÍA-SILVENTE, M., 2007. People detection and tracking using stereo vision and color. *Image and Vision Computing,* Volume 25 , Issue 6, 995-1007.

MUÑOZ-SALINAS, R., GARCÍA-SILVENTE, M. and CARNICER, R.M., 2008. Adaptive multi-modal stereo people tracking without background modelling. *Journal of Visual Communication and Image Representation,* Volume 19 , Issue 2, 75-91.

NAVARRO-SERMENT, L.E., MERTZ, C. and HEBERT, M., 2010. Pedestrian Detection and Tracking Using Three-dimensional LADAR Data. *The International Journal of Robotics Research,* .

O'CONAIRE, C., O'CONNOR, N.E., COOKE, E. and SMEATON, A.F., 2006. Comparison of Fusion Methods for Thermo-Visual Surveillance Tracking. *In: Information Fusion, 2006 9th International Conference on On page(s): 1-7, /.*

OREN, M., PAPAGEORGIOU, C., SINHA, P., OSUNA, E. and POGGIO, T., 1997. Pedestrian detection using wavelet templates. *In: cvpr,* Published by the IEEE Computer Society, pp. 193.

PAPAGEORGIOU, C., and POGGIO, T., 2000. A trainable system for object detection. *International Journal of Computer Vision,* 38 (1), 15-33.

PHAM, Q., GOND, L., BEGARD, J., ALLEZARD, N. and SAYD, P., 2007. Real-Time Posture Analysis in a Crowd using Thermal Imaging. *In: Computer Vision and Pattern Recognition, 2007. CVPR '07. IEEE Conference onOn page(s): 1-8, /.*

PHILOMIN, V., DURAISWAMI, R. and DAVIS, L., 2000. Quasi-random sampling for condensation. *Computer Vision—ECCV 2000,* , 134-149.

PLANCK, M., 1901. On the law of distribution of energy in the normal spectrum. *Annalen Der Physik,* 4 (553), 1.

PLANKERS, R., and FUA, P., 2003. Articulated soft objects for multiview shape and motion capture. *IEEE Transactions on Pattern Analysis and Machine Intelligence,* 25 (9), 1182-1187.

REID, D.B., 1978. An algorithm for tracking multiple targets. *In: 1978 IEEE Conference on Decision and Control including the 17th Symposium on Adaptive Processes, /.*

RODRIGUEZ, M.D., and SHAH, M., 2007. Detecting and segmenting humans in crowded scenes. *In: Proceedings of the 15th international conference on Multimedia,* ACM, pp. 356.

ROGOVA, G.L., and NIMIER, V., 2004. Reliability in information fusion: literature survey. *In: Proceedings of the Seventh International Conference on Information Fusion,* Citeseer, pp. 1158–1165.

ROH, H.K., and LEE, S.W., 2000. Multiple people tracking using an appearance model based on temporal color. *In: Biologically Motivated Computer Vision,* Springer, pp. 429-446.

ROSALES, R., and SCLAROFF, S., 1998. Improved tracking of multiple humans with trajectory prediction and occlusion modeling. *In: IEEE CVPR workshop on the Interpretation of Visual Motion,* Citeseer, .

ROTH, D., DOUBEK, P. and VAN GOOL, L., 2005. Bayesian pixel classification for human tracking. *In: IEEE Workshop on Motion and Video Computing (MOTION'05), Breckenridge, Colorado, .*

SCHARSTEIN, D., and SZELISKI, R., 2002. A taxonomy and evaluation of dense two-frame stereo correspondence algorithms. *International Journal of Computer Vision,* 47 (1), 7-42.

SCHREIBER, D., 2008. Generalizing the Lucas-Kanade algorithm for histogram-based tracking. *Pattern Recognition Letters,* 29 (7), 852-861.

SCHULZ, D., BURGARD, W., FOX, D. and CREMERS, A.B., 2003. People tracking with mobile robots using sample-based joint probabilistic data association filters. *The International Journal of Robotics Research,* 22 (2), 99.

SENIOR, A., HAMPAPUR, A., TIAN, Y.L., BROWN, L., PANKANTI, S. and BOLLE, R., 2006. Appearance models for occlusion handling. *Image and Vision Computing,* 24 (11), 1233.

SHAFER, G., 1976. *A mathematical theory of evidence.* Princeton university press Princeton, NJ.

SHIMIZU, H., and POGGIO, T., 2004. Direction estimation of pedestrian from multiple still images. *In: 2004 IEEE Intelligent Vehicles Symposium,* pp. 596-600.

SIDENBLADH, H., and BLACK, M.J., 2003. Learning the Statistics of People in Images and Video. *International Journal of Computer Vision,* 54, 183–209.

SMETS, P., 1993. Belief functions: the disjunctive rule of combination and the generalized Bayesian theorem. *Classic Works of the Dempster-Shafer Theory of Belief Functions,* , 633-664.

SNIDARO, L., FORESTI, G.L., NIU, R. and VARSHNEY, P.K., 2004. Sensor fusion for video surveillance. *In: 7th Int. Conf. on Information Fusion,* Citeseer, pp. 2049-2074.

STARCK, J., and HILTON, A., 2003. Model-based multiple view reconstruction of people. *In: IEEE International Conference on Computer Vision,* Citeseer, pp. 915–922.

STAUFFER, C., and GRIMSON, W.E.L., 2000. Learning patterns of activity using real-time tracking. *IEEE Transactions on Pattern Analysis and Machine Intelligence,* 22 (8), 747-757.

STAUFFER, C., and GRIMSON, W.E.L., 1999. Adaptive background mixture models for real-time tracking. *In: Computer Vision and Pattern Recognition, 1999. IEEE Computer Society Conference on.Volume: 2, On page(s): -252 Vol. 2, /.*

STENGER, B., THAYANANTHAN, A., TORR, P.H.S. and CIPOLLA, R., 2006. Model-based hand tracking using a hierarchical bayesian filter. *IEEE Transactions on Pattern Analysis and Machine Intelligence,* 28 (9).

SZARVAS, M., YOSHIZAWA, A., YAMAMOTO, M. and OGATA, J., 2005. Pedestrian detection with convolutional neural networks. *In: IEEE Intelligent Vehicles Symposium, 2005. Proceedings,* pp. 224-229.

TAKAGI, T., and SUGENO, M., 1985. Fuzzy identification of systems and its applications to modeling and control. *IEEE Transactions on Systems, Man, and Cybernetics,* SMC-15, 116-132.

TAYLOR, M., ZARAGOZA, H., CRASWELL, N., ROBERTSON, S. and BURGES, C., 2006. Optimisation methods for ranking functions with multiple parameters. *In: Proceedings of the 15th ACM international conference on Information and knowledge management,* ACM, pp. 593.

TERZOPOULOS, D., and SZELISKI, R., 1992. Tracking with Kalman snakes. *Active Vision,* , 3-20.

TOET, A., and FRANKEN, E.M., 2003. Perceptual evaluation of different image fusion schemes. *Displays,* Volume 24, Number 1, 25-37.

TOYAMA, K., KRUMM, J., BRUMITT, B. and MEYERS, B., 1999. Wallflower: Principles and practice of background maintenance. *In: International Conference on Computer Vision,* Kerkyra, Greece, pp. 29.

TREPTOW, A., CIELNIAK, G. and DUCKETT, T., 2007. Real-Time People Tracking for Mobile Robots using Thermal Vision. *In: Mechatronics and Automation, 2007. ICMA 2007. International Conference on Page(s):3565 - 3570,* .

VAN RIJSBERGEN, C.J., 1979. Information Retrieval. *Buttersworth, London,* .

VELASTIN, S.A., BOGHOSSIAN, B.A., LO, B.P.L., JIE, S. and VICENCIO-SILVA, M.A., 2005. PRISMATICA: toward ambient intelligence in public transport environments. *Systems, Man and Cybernetics, Part A, IEEE Transactions on,* Volume: 35, Issue: 1, 164-182.

VEZHNEVETS, V., SAZONOV, V. and ANDREEVA, A., 2003. A survey on pixel-based skin color detection techniques. *In: Proc. Graphicon,* Citeseer, .

VIOLA, P., and JONES, M., 2001. Rapid Object Detection using a Boosted Cascade of Simple Classifiers. *In: Proc. IEEE CVPR 2001,* .

VIOLA, P., JONES, M.J. and SNOW, D., 2005. Detecting Pedestrians Using Patterns of Motion and Appearance. *International Journal of Computer Vision,* 63 (2), 153.

WACHTER, S., and NAGEL, H.-., 1997. Tracking Persons in Monocular Image Sequences. *In: Nonrigid and Articulated Motion Workshop, 1997. Proceedings., IEEE,* .

WELCH, G., and BISHOP, G., 1995. An introduction to the Kalman filter. *University of North Carolina at Chapel Hill, Chapel Hill, NC,* .

WEN, W., HO, M. and HUANG, C., 2008. People tracking and counting for applications in video surveillance system. *Audio, Language and Image Processing, 2008.ICALIP 2008.International Conference on,* , 1677-1682.

WIEN, W., 1898. Ueber die Fragen, welche die translatorische Bewegung des Lichtäthers betreffen.

WREN, C.R., AZARBAYEJANI, A., DARRELL, T. and PENTLAND, A.P., 1997. Pfinder: Real-Time Tracking of the Human Body. *IEEE Transactions on Pattern Analysis and Machine Intelligence,* VOL. 19, NO. 7, 780-785.

WU, B., and NEVATIA, R., 2005. Detection of Multiple, Partially Occluded Humans in a Single Image by Bayesian Combination of Edgelet Part Detectors. *In: Computer Vision, 2005. ICCV 2005. Tenth IEEE International Conference on, /.*

XU, L.Q., PUIG, P., RES, B.T. and VENTURING, B.T., 2005. A hybrid blob-and appearance-based framework for multi-object tracking through complex occlusions. *In: Visual Surveillance and Performance Evaluation of Tracking and Surveillance, 2005. 2nd Joint IEEE International Workshop on,* pp. 73-80.

XU, Y.W., CAO, X.B. and LI, T., 2009. Extended Kalman filter based pedestrian localization for collision avoidance. *In: International Conference on Mechatronics and Automation, 2009. ICMA 2009,* pp. 4366-4370.

YANG, T., LI, S.Z., PAN, Q. and LI, J., 2005. Real-time multiple objects tracking with occlusion handling in dynamic scenes.

YASUDA, K., NAEMURA, T. and HARASHIMA, H., 2004. Thermo-key: human region segmentation from video. *Computer Graphics and Applications, IEEE,* 24 (1), 26-30.

ZHANG, L., WU, B. and NEVATIA, R., 2007. Detection and tracking of multiple humans with extensive pose articulation. *In: Proceedings of the 2007 IEEE Computer Society Conference on Computer Vision and Pattern Recognition,* Citeseer, pp. 1–8.

ZHAO, T., and NEVATIA, R., 2004. Tracking multiple humans in complex situations. *IEEE Transactions on Pattern Analysis and Machine Intelligence,* , 1208-1221.

ZHAO, T., NEVATIA, R. and WU, B., 2008. Segmentation and Tracking of Multiple Humans in Crowded Environments. July.

ZHOU, J., and HOANG, J., 2005. Real Time Robust Human Detection and Tracking System. *Computer Vision and Pattern Recognition - Workshops, 2005.CVPR Workshops.IEEE Computer Society Conference on,* , 149-149.

ZHU, Q., AVIDAN, S., YEH, M.C. and CHENG, K.T., 2006. Fast human detection using a cascade of histograms of oriented gradients. *In: CVPR,* Citeseer, pp. 4.

ZOTKIN, D., DURAISWAMI, R., NANDA, H. and DAVIS, L.S., 2001. Multimodal tracking for smart videoconferencing. *In: Second International Conference on Multimedia and Expo, Tokyo, Japan,* Citeseer, .

Appendices

Appendix A - Thermal IR Theory

The energy emitted from an object is dependent of the temperature of the object and the radiation wavelength. In addition to energy transmission, objects both absorb and reflect energy from the environment. A theoretical object radiation with complete absorption, no reflection and complete emission is known as a perfect blackbody. Kirchoff's Law (Kirchhoff 1860) states that the emissivity of an object equals its absorptivity under thermal equilibrium.

In practice no objects are perfect blackbodies, but the concept allows for calculation of the emission properties of a blackbody object using Planck's Law of Blackbody Radiation (Planck 1901).

Radiation emitted from a blackbody occurs at a range of wavelengths dependent on temperature and is often illustrated by a curve with the intensity of radiation increasing with temperature. Each radiation curve has a distinct peak indicating maximum radiation intensity. The maximum can be calculated using Wien's displacement law (Wien 1898) which states that the shape of an energy distribution at a given temperature is the same shape as at any other temperature, but the wavelength is displaced.

The emissivity of real-world objects is calculated using the ratio between the radiation a theoretical perfect blackbody at this temperature and that of a normal object at this temperature.

Detected radiation detected is also influenced by the absorption and emission of gases in the atmosphere between the object and the detector. This influence is highly dependence on the wavelength of the radiation.

Appendix B

Visible Results

Sample	ID	pixelCount	pixelsForeground		TruePositives		TrueNegatives		False Positives	False Negatives	True Positive	False Positive	False Negative	True Negative	precision	recall/sensitivity	accuracy	f measure
1	ImageID 3832	588081	84873	14%	20268	23%	469236	93%	33972	64605	0.23880386	0.06751085	0.128386274	0.93248915	0.373672566	0.23880386	0.832375132	0.291389015
2	ImageID 4489	588081	51568	8%	8805	17%	494824	92%	41689	42763	0.170745424	0.077703616	0.079705431	0.922296384	0.174377154	0.170745424	0.856393932	0.17254218
3	ImageID 4906	588081	223004	37%	116902	52%	329416	90%	35661	106102	0.524214812	0.097680763	0.2906291	0.902319237	0.766253941	0.524214812	0.75893967	0.622536059
4	ImageID 5015	588081	174679	29%	75583	43%	396072	95%	17330	99096	0.432696546	0.041920455	0.239708565	0.958079545	0.813481429	0.432696546	0.802023871	0.564912254
5	ImageID 5147	588081	23746	4%	1185	4%	556711	98%	7624	22561	0.049903142	0.013509706	0.039978027	0.986490294	0.134521512	0.049903142	0.948672037	0.072799877
6	ImageID 5279	588081	193165	32%	131898	68%	340398	86%	54518	61267	0.682825564	0.138049611	0.155139321	0.861950389	0.707546563	0.682825564	0.803113857	0.694966292
7	ImageID 6089	588081	58030	9%	2706	4%	513630	96%	16421	55324	0.046631053	0.030980038	0.104374862	0.969019962	0.141475401	0.046631053	0.8780015	0.070142696
8	ImageID 6834	588081	62442	10%	4215	6%	499800	95%	25839	58227	0.067502642	0.049157311	0.110773744	0.950842689	0.140247554	0.067502642	0.857050304	0.091139076
9	ImageID 6878	588081	53848	9%	16434	30%	518522	97%	15711	37414	0.305192393	0.029408517	0.070033113	0.970591483	0.511245917	0.305192393	0.909663805	0.382217157
10	ImageID 7097	588081	88205	14%	11763	13%	482167	96%	17709	76442	0.133359787	0.035426786	0.152921925	0.964573214	0.399124593	0.133359787	0.839901306	0.19992012
11	ImageID 7270	588081	85996	14%	23033	26%	457628	91%	44457	62963	0.267838039	0.088544768	0.125403069	0.911455232	0.34128019	0.267838039	0.817338088	0.300131608
12	ImageID 7403	588081	202760	34%	122891	60%	350362	90%	34959	79869	0.606090945	0.090726952	0.207279126	0.909273048	0.77853025	0.606090945	0.804741184	0.68157289
13	ImageID 7761	588081	195610	33%	77022	39%	345537	88%	46934	118588	0.393752876	0.119585906	0.302157357	0.880414094	0.621365646	0.393752876	0.718538773	0.482041268
14	ImageID 8280	588081	159825	27%	37806	23%	411458	96%	16798	122019	0.236546222	0.039224202	0.284920702	0.960775798	0.69236686	0.236546222	0.763949184	0.352620215
15	ImageID 8696	588081	220013	37%	59624	27%	343879	93%	24189	160389	0.271002168	0.065718835	0.435759153	0.934281165	0.711393221	0.271002168	0.686135073	0.392487806
16	ImageID 8792	588081	151544	25%	82529	54%	408964	93%	27573	69015	0.54458771	0.063163031	0.158096565	0.936836969	0.749568582	0.54458771	0.835757319	0.630844729
17	ImageID 8915	588081	172858	29%	26381	15%	378195	91%	37028	146477	0.152616599	0.089176178	0.352767067	0.910823822	0.416045041	0.152616599	0.687959652	0.223315148
18	ImageID 9025	588081	167020	28%	39913	23%	366718	87%	54343	127107	0.238971381	0.12906206	0.301873125	0.87093794	0.423453149	0.238971381	0.691454068	0.305523661
19	ImageID 9156	588081	137536	23%	21605	15%	421986	93%	28559	115931	0.157086145	0.063387675	0.25731281	0.936612325	0.430687346	0.157086145	0.754302554	0.230207778
20	ImageID 10120	588081	99077	16%	14058	14%	479298	98%	9706	85019	0.141889641	0.019848508	0.173861564	0.980151492	0.591567076	0.141889641	0.83892525	0.228881237
21	ImageID 10127	588081	115585	19%	19895	17%	459403	97%	13093	95690	0.172124411	0.027710287	0.202520233	0.972289713	0.603098096	0.172124411	0.81502038	0.267814475
22	ImageID 11755	588081	106217	18%	62708	59%	465475	96%	16389	43509	0.590376305	0.034011671	0.090293112	0.965988329	0.792798716	0.590376305	0.898146684	0.676775635
23	ImageID 12378	588081	162856	27%	27051	16%	416840	98%	8385	135805	0.166103797	0.019718972	0.319372097	0.980281028	0.763376228	0.166103797	0.754812687	0.272840054

24	ImageID 12407	588081	150318	25%	18309	12%	425032	97%	12731	132009	0.12180178	0.029081946	0.30155358	0.970918054	0.589851804	0.12180178	0.753877442	0.201910034
25	ImageID 12421	588081	177781	30%	52744	29%	395513	96%	14787	125037	0.296679623	0.036039483	0.304745308	0.963960517	0.781033896	0.296679623	0.762236835	0.430015654
26	ImageID 12793	588081	53864	9%	15811	29%	502312	94%	31905	38053	0.293535571	0.059722922	0.071231354	0.940277078	0.331356358	0.293535571	0.881040197	0.311301437
27	ImageID 13297	588081	8186	1%	240	2%	533180	91%	46715	7946	0.029318348	0.080557687	0.013702481	0.919442313	0.005111277	0.029318348	0.90705192	0.008704956
28	ImageID 13407	588081	208862	35%	92848	44%	336356	88%	42863	116014	0.444542329	0.113029674	0.305928764	0.886970326	0.684159722	0.444542329	0.729838237	0.538916282
29	ImageID 13451	588081	146996	24%	40585	27%	411595	93%	29490	106411	0.276095948	0.066857862	0.241248285	0.933142138	0.57916518	0.276095948	0.768907684	0.373932953
30	ImageID 14167	588081	165035	28%	129943	78%	395875	93%	27171	35092	0.787366316	0.064227058	0.08295079	0.935772942	0.827061879	0.787366316	0.894125129	0.80672608
31	ImageID 15554	588081	133444	22%	70932	53%	438206	96%	16431	62512	0.531548814	0.036140921	0.137498708	0.963859079	0.811922667	0.531548814	0.865761689	0.642479632
32	ImageID 16277	588081	109076	18%	10488	9%	444752	92%	34253	98588	0.096153141	0.071508648	0.205818311	0.928491352	0.23441586	0.096153141	0.774111049	0.136369842
33	ImageID 16321	588081	121513	20%	28668	23%	449682	96%	16886	92845	0.235925374	0.036191938	0.198995645	0.963808062	0.62931905	0.235925374	0.813408357	0.343191654
34	ImageID 17110	588081	99687	16%	17571	17%	476521	97%	11873	82116	0.176261699	0.02431029	0.168134744	0.97568971	0.596759951	0.176261699	0.840176778	0.272142243
35	ImageID 17219	588081	93249	15%	5775	6%	469549	94%	25283	87474	0.061930959	0.051094109	0.176775148	0.948905891	0.18594243	0.061930959	0.808262807	0.092915121
36	ImageID 17543	588081	56053	9%	2541	4%	491920	92%	40108	53512	0.045332096	0.07538701	0.100581172	0.92461299	0.059579357	0.045332096	0.840804243	0.051488318
37	ImageID 17767	588081	115673	19%	39841	34%	419499	88%	52909	75832	0.344427827	0.111998527	0.16052226	0.888001473	0.429552561	0.344427827	0.781082878	0.382309054
38	ImageID 17789	588081	78005	13%	18873	24%	483989	94%	26087	59132	0.241946029	0.051143359	0.115927823	0.948856641	0.419773132	0.241946029	0.85508969	0.306965397
39	ImageID 18095	588081	159045	27%	46616	29%	402262	93%	26774	112429	0.293099437	0.06240502	0.262050271	0.93759498	0.635181905	0.293099437	0.763292812	0.401109988
40	ImageID 18149	588081	141586	24%	37695	26%	427157	95%	19338	103891	0.26623395	0.043310675	0.232681217	0.956689325	0.660933144	0.26623395	0.790455737	0.379570937
41	ImageID 18862	588081	58078	9%	19109	32%	514404	97%	15599	38969	0.329023038	0.029431909	0.073525999	0.970568091	0.550564711	0.329023038	0.907210061	0.411894036
42	ImageID 20396	588081	163580	27%	42570	26%	289253	68%	135248	121010	0.260239638	0.318604668	0.285064111	0.681395332	0.239402085	0.260239638	0.564247102	0.249386347
43	ImageID 20615	588081	97169	16%	43208	44%	460036	93%	30876	53961	0.444668567	0.062895183	0.109919904	0.937104817	0.583229847	0.444668567	0.85573926	0.504610138
44	ImageID 20900	588081	81471	13%	12359	15%	379465	74%	127145	69112	0.15169815	0.250972148	0.136420521	0.749027852	0.088592442	0.15169815	0.666275564	0.111858808
45	ImageID 21035	588081	122667	20%	53462	43%	377577	81%	87837	69205	0.435830337	0.188728745	0.14869557	0.811271255	0.378360781	0.435830337	0.732958555	0.405067319
46	ImageID 21119	588081	132009	22%	29934	22%	410290	89%	45782	102075	0.226757267	0.100383273	0.223813345	0.899616727	0.395345766	0.226757267	0.748577152	0.288207967
47	ImageID 21151	588081	161916	27%	129705	80%	371685	87%	54480	32211	0.801063514	0.127837809	0.075583401	0.872162191	0.704210441	0.801063514	0.852586633	0.749521094
48	ImageID 21179	588081	60043	10%	6492	10%	436645	82%	91393	53551	0.108122512	0.173080346	0.10141505	0.826919654	0.066322726	0.108122512	0.753530551	0.08221468
49	ImageID 21207	588081	147537	25%	67984	46%	308459	70%	132085	79553	0.460792886	0.299822492	0.180579011	0.700177508	0.339802768	0.460792886	0.640121004	0.391155504
50	ImageID 21468	588081	92114	15%	6798	7%	420866	84%	75101	85316	0.073799857	0.151423381	0.172019509	0.848576619	0.083004676	0.073799857	0.72721955	0.078132094
											TP	FP	FN	TN	precision	recall/sensitivity	accuracy	F-measure
										MEAN	**0.288501129**	**0.082948276**	**0.183412972**	**0.917051724**	**0.479348669**	**0.288501129**	**0.796624105**	**0.343194376**

Thermal IR Results

Sample	ID	pixelCount	pixelsForeground		TruePositives		TrueNegatives		False Positives	False Negatives	True Positive	False Positive	False Negative	True Negative	precision	recall/sensitivity	accuracy	f measure
1	ImageID 3832	76800	11102	14%	7933	71%	63568	96%	2130	3169	0.714555936	0.032421078	0.048235867	0.967578922	0.788333499	0.714555936	0.931002604	0.749633829
2	ImageID 4489	76800	6750	8%	4946	73%	63610	90%	6440	1804	0.732740741	0.091934333	0.025753034	0.908065667	0.434393114	0.732740741	0.89265625	0.545434495
3	ImageID 4906	76800	29043	37%	16512	56%	43526	91%	4231	12531	0.568536308	0.088594342	0.262390854	0.911405658	0.796027576	0.568536308	0.781744792	0.663319005
4	ImageID 5015	76800	22747	29%	12545	55%	47780	88%	6273	10202	0.551501297	0.116052763	0.18874068	0.883947237	0.666648953	0.551501297	0.785481771	0.603632864
5	ImageID 5147	76800	3127	4%	1794	57%	72714	98%	959	1333	0.573712824	0.01301698	0.018093467	0.98698302	0.651652742	0.573712824	0.97015625	0.610204082
6	ImageID 5279	76800	25222	32%	17466	69%	44945	87%	6633	7756	0.692490683	0.128601342	0.150374191	0.871398658	0.724760364	0.692490683	0.812643229	0.708258146
7	ImageID 6089	76800	7576	9%	4126	54%	58723	84%	10501	3450	0.544614572	0.151695944	0.049838206	0.848304056	0.282081083	0.544614572	0.818346354	0.371661487
8	ImageID 6834	76800	8169	10%	4687	57%	58634	85%	9997	3482	0.573754438	0.145663039	0.050735091	0.854336961	0.319190956	0.573754438	0.824492188	0.410186846
9	ImageID 6878	76800	6958	9%	4789	68%	63546	90%	6296	2169	0.688272492	0.09014633	0.031055812	0.90985367	0.432025259	0.688272492	0.889778646	0.530842986
10	ImageID 7097	76800	11513	14%	7124	61%	57060	87%	8227	4389	0.618778772	0.126012836	0.067226247	0.873987164	0.464074002	0.618778772	0.835729167	0.530375223
11	ImageID 7270	76800	11229	14%	6532	58%	60560	92%	5011	4697	0.581708077	0.076420979	0.071632276	0.923579021	0.565884086	0.581708077	0.87359375	0.573686984
12	ImageID 7403	76800	26387	34%	22515	85%	43719	86%	6694	3872	0.853261076	0.132783211	0.076805586	0.867216789	0.770824061	0.853261076	0.862421875	0.809950356
13	ImageID 7761	76800	25498	33%	16844	66%	44137	86%	7165	8654	0.660600831	0.139663171	0.168687381	0.860336829	0.701570244	0.660600831	0.794023438	0.680469429
14	ImageID 8280	76800	20797	27%	12289	59%	52903	94%	3100	8508	0.590902534	0.055354177	0.151920433	0.944645823	0.798557411	0.590902534	0.848854167	0.679212955
15	ImageID 8696	76800	28667	37%	19507	68%	43392	90%	4741	9160	0.680468832	0.098497912	0.190306027	0.901502088	0.80447872	0.680468832	0.818997396	0.737295663
16	ImageID 8792	76800	19739	25%	11926	60%	53936	94%	3125	7813	0.604184609	0.054765952	0.136923643	0.945234048	0.7923726	0.604184609	0.857578125	0.68559931
17	ImageID 8915	76800	22487	29%	11863	52%	52353	96%	1960	10624	0.527549251	0.036087125	0.195606945	0.963912875	0.858207336	0.527549251	0.836145833	0.653428807
18	ImageID 9025	76800	21807	28%	12716	58%	44098	80%	10895	9091	0.583115513	0.198116124	0.165311949	0.801883876	0.538562534	0.583115513	0.739765625	0.559954203
19	ImageID 9156	76800	17898	23%	8975	50%	55942	94%	2960	8923	0.501452676	0.050252963	0.151488914	0.949747037	0.751989946	0.501452676	0.845273438	0.6016827
20	ImageID 10120	76800	12949	16%	6687	51%	62388	97%	1463	6262	0.516410534	0.022912719	0.098072074	0.977087281	0.820490798	0.516410534	0.899414063	0.633868904
21	ImageID 10127	76800	15088	19%	7528	49%	59497	96%	2215	7560	0.498939555	0.035892533	0.122504537	0.964107467	0.772657292	0.498939555	0.872721354	0.606338851
22	ImageID 11755	76800	13877	18%	4753	34%	50879	80%	12044	9124	0.342509188	0.191408547	0.145002622	0.808591453	0.282967197	0.342509188	0.724375	0.309904153
23	ImageID 12378	76800	21206	27%	10744	50%	52476	94%	3118	10462	0.506649062	0.056085189	0.188185775	0.943914811	0.775068533	0.506649062	0.823177083	0.612752367
24	ImageID 12407	76800	19562	25%	9336	47%	53441	93%	3797	10226	0.477251815	0.066337049	0.178657535	0.933662951	0.710880987	0.477251815	0.817408854	0.571096498
25	ImageID 12421	76800	23132	30%	10293	44%	51530	96%	2138	12839	0.44496801	0.03983752	0.239230081	0.96016248	0.828010619	0.44496801	0.804986979	0.578860051
26	ImageID 12793	76800	7042	9%	2355	33%	65837	94%	3921	4687	0.334422039	0.056208607	0.067189426	0.943791393	0.375239006	0.334422039	0.887916667	0.353656705
27	ImageID 13297	76800	1074	1%	407	37%	72467	95%	3259	667	0.378957169	0.043036738	0.008808071	0.956963262	0.111020185	0.378957169	0.948880208	0.171729958

28	ImageID 13407	76800	27221	35%	16434	60%	43840	88%	5739	10787	0.603725065	0.115754654	0.217571956	0.884245346	0.741171695	0.603725065	0.784817708	0.66542495
29	ImageID 13451	76800	19129	24%	12047	62%	51772	89%	5899	7082	0.629776779	0.102287111	0.122800021	0.897712889	0.671291653	0.629776779	0.830976563	0.649871881
30	ImageID 14167	76800	21481	27%	7830	36%	53202	96%	2117	13651	0.36450817	0.038268949	0.246768741	0.961731051	0.787172012	0.36450817	0.7946875	0.498281787
31	ImageID 15554	76800	17373	22%	11978	68%	56013	94%	3414	5395	0.689460657	0.057448634	0.090783651	0.942551366	0.778196466	0.689460657	0.885299479	0.73114604
32	ImageID 16277	76800	14250	18%	7475	52%	59718	95%	2832	6775	0.524561404	0.045275779	0.108313349	0.954724221	0.725235277	0.524561404	0.874908854	0.608787718
33	ImageID 16321	76800	15838	20%	9376	59%	58458	95%	2504	6462	0.591993939	0.041074768	0.106000459	0.958925232	0.789225589	0.591993939	0.883255208	0.676527888
34	ImageID 17110	76800	13012	16%	6790	52%	62534	98%	1254	6222	0.521826007	0.01965887	0.097541857	0.98034113	0.844107409	0.521826007	0.90265625	0.644946809
35	ImageID 17219	76800	12180	15%	5460	44%	63066	97%	1554	6720	0.448275862	0.024048282	0.103992572	0.975951718	0.778443114	0.448275862	0.892265625	0.56892779
36	ImageID 17543	76800	7303	9%	3964	54%	65440	94%	4057	3339	0.542790634	0.058376621	0.048045239	0.941623379	0.494202718	0.542790634	0.903697917	0.517358392
37	ImageID 17767	76800	15099	19%	7662	50%	55580	90%	6121	7437	0.507450825	0.099204227	0.120532892	0.900795773	0.555902198	0.507450825	0.823463542	0.530572675
38	ImageID 17789	76800	10118	13%	5648	55%	61024	91%	5658	4470	0.558213086	0.084850484	0.067034582	0.915149516	0.499557757	0.558213086	0.868125	0.527259149
39	ImageID 18095	76800	20702	26%	15433	74%	47528	84%	8570	5269	0.745483528	0.15276837	0.093924917	0.84723163	0.642961297	0.745483528	0.819804688	0.690437311
40	ImageID 18149	76800	18450	24%	11971	64%	53133	91%	5217	6479	0.648834688	0.08940874	0.111036847	0.91059126	0.696474284	0.648834688	0.847708333	0.671810988
41	ImageID 18862	76800	7503	9%	4178	55%	59486	85%	9811	3325	0.556843929	0.141579001	0.047981875	0.858420999	0.298663235	0.556843929	0.828958333	0.388795831
42	ImageID 20396	76800	21308	27%	14383	67%	44805	80%	10687	6925	0.675004693	0.192586319	0.124792763	0.807413681	0.573713602	0.675004693	0.770677083	0.620250981
43	ImageID 20615	76800	12699	16%	6000	47%	62887	98%	1214	6699	0.472478148	0.018938862	0.10450695	0.981061138	0.831716108	0.472478148	0.896966146	0.602621403
44	ImageID 20900	76800	10648	13%	6649	62%	60790	91%	5362	3999	0.624436514	0.08105575	0.060451687	0.91894425	0.553575889	0.624436514	0.878111979	0.586874972
45	ImageID 21035	76800	15979	20%	9809	61%	58180	95%	2641	6170	0.613868202	0.043422502	0.101445225	0.956577498	0.787871486	0.613868202	0.885273438	0.690069999
46	ImageID 21119	76800	17191	22%	10640	61%	53104	89%	6505	6551	0.618928509	0.109127816	0.109899512	0.890872184	0.620589093	0.618928509	0.83	0.619757689
47	ImageID 21151	76800	21060	27%	13483	64%	52797	94%	2943	7577	0.640218424	0.052798708	0.135934697	0.947201292	0.820832826	0.640218424	0.863020833	0.719361895
48	ImageID 21179	76800	7843	10%	4410	56%	60441	87%	8516	3433	0.56228484	0.123497252	0.049784648	0.876502748	0.34117283	0.56228484	0.844414063	0.424671385
49	ImageID 21207	76800	19231	25%	12109	62%	54550	94%	3019	7122	0.629660444	0.052441418	0.123712415	0.947558582	0.800436277	0.629660444	0.867955729	0.704851713
50	ImageID 21468	76800	12018	15%	6654	55%	59209	91%	5573	5364	0.553669496	0.086026983	0.082800778	0.913973017	0.544205447	0.553669496	0.857591146	0.54889668
											TP	FP	FN	TN	precision	recall/sensitivity	accuracy	F-measure
										MEAN	**0.573332053**	**0.083353992**	**0.114488687**	**0.916646008**	**0.639893747**	**0.573332053**	**0.84864401**	**0.588610856**

Appendix C - Resolution Dependence

In order to determine image dimension requirements, and therefore hardware requirements, high resolution cameras were utilised for capture. After data capture, the capability of the D_{98} measure to distinguish between subjects was tested, with increasing source image dimensions using the optimum multi-modal HPCTC.

Figure C1 shows the mean D98 result for the optimum multi-modal HPCTC described in 5.1.3.3.

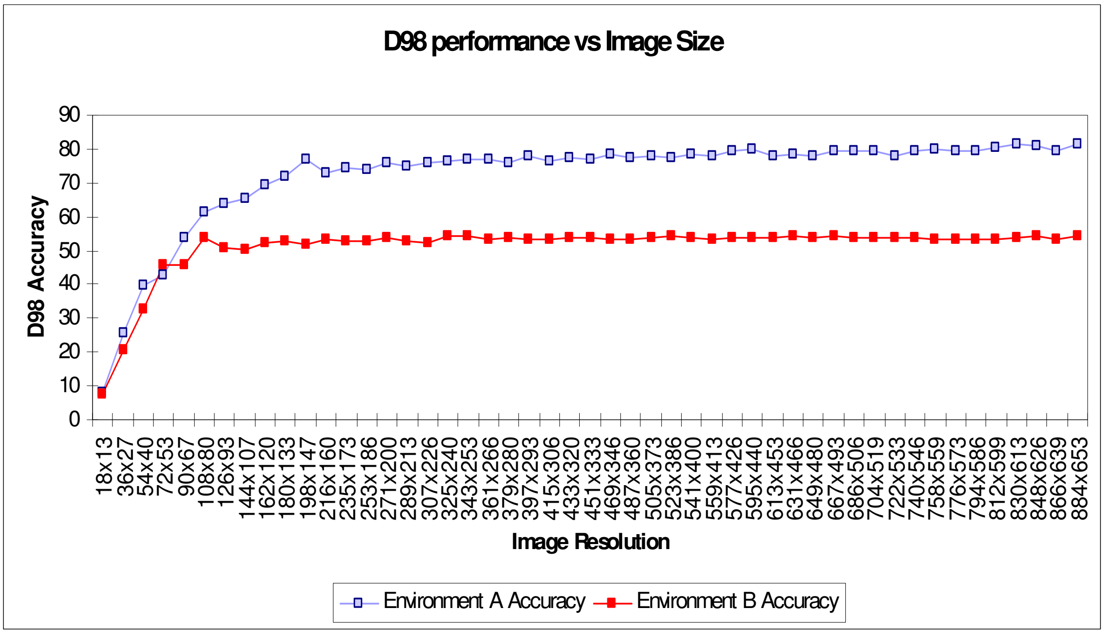

Figure C1 Image Dimensions plotted against D98 result

A clear plateau is observed in both scenarios. The results however depend on the number of pixels which represent a subject. In Figure C2, the mean visible pixel count are shown. Pixels from the thermal source are interpolated to match the visible source dimensions.

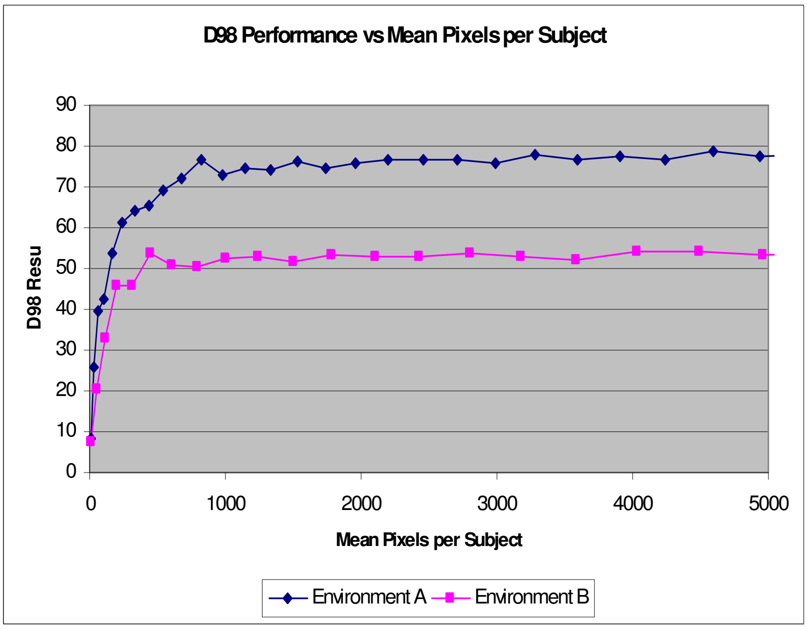

Figure C2 Mean pixels per subject plotted against D98 result

These results show that performance measured using the D_{98} metric plateaus at around 500 to 800 pixels. It is evident that representing subjects with more pixels than this does not increase the discrimination performance to any significant degree.

It is therefore recommended that the minimum number of pixel to represent a subject is 500 pixels.

Appendix D

1-D Results

Results are sorted by MSE of Scenario E and Scenario F D^{98} Results

HPCTC			Env A D98	Env B D98	MSE	MSE Rank
Channel	Bin Size	Comparison Technique				
Thermal IR	24	Chi Squared	76.9697	37.1717	2238.895	1
Thermal IR	21	Chi Squared	76.3636	36.3636	2304.135	2
Thermal IR	24	Bhattacharyya	78.1818	35.1515	2340.681	3
Thermal IR	21	Bhattacharyya	75.3535	34.3434	2459.12	4
Thermal IR	24	Intersection	70.5051	36.1616	2472.645	5
Thermal IR	21	Intersection	70.7071	35.1515	2531.701	6
Thermal IR	24	Correlation	65.2525	36.5657	2615.65	7
Thermal IR	18	Chi Squared	68.6869	33.7374	2685.621	8
Thermal IR	18	Bhattacharyya	68.8889	32.5253	2760.368	9
Thermal IR	24	Earth Mover's Distance	74.9495	28.2828	2885.442	10
Thermal IR	21	Correlation	63.0303	33.5354	2892.151	11
Thermal IR	21	Earth Mover's Distance	77.9798	26.6667	2931.331	12
Thermal IR	18	Intersection	62.4242	32.7273	2968.778	13
Thermal IR	18	Correlation	56.5657	34.9495	3059.053	14
Thermal IR	15	Chi Squared	64.4444	30.303	3060.936	15
Thermal IR	15	Bhattacharyya	66.0606	29.4949	3061.426	16
Thermal IR	18	Earth Mover's Distance	70.303	27.4747	3070.915	17
Thermal IR	12	Chi Squared	60.8081	27.6768	3383.325	18
Thermal IR	15	Intersection	53.9394	30.7071	3461.542	19
Thermal IR	12	Bhattacharyya	61.2121	26.0606	3485.768	20
Thermal IR	9	Bhattacharyya	61.0101	25.4545	3538.622	21
Thermal IR	12	Intersection	53.7374	28.2828	3641.792	22
Thermal IR	9	Chi Squared	56.9697	26.2626	3644.405	23
Thermal IR	15	Earth Mover's Distance	56.1616	25.6566	3724.373	24
Thermal IR	12	Correlation	50.7071	28.8889	3743.289	25
Thermal IR	12	Earth Mover's Distance	57.3737	23.4343	3839.654	26
Thermal IR	15	Correlation	45.6566	30.5051	3891.373	27
Thermal IR	9	Earth Mover's Distance	46.8687	22.6263	4404.812	28
Thermal IR	9	Intersection	44.0404	22.0202	4606.163	29
Thermal IR	9	Correlation	36.7677	20.202	5183.022	30
Thermal IR	6	Bhattacharyya	35.7576	17.9798	5427.2	31
Hue	21	Correlation	19.1919	33.1313	5500.686	32
Thermal IR	6	Chi Squared	34.1414	17.3737	5582.23	33
Hue	24	Correlation	17.7778	33.5354	5589.017	34
Hue	18	Correlation	18.3838	30.101	5773.537	35
Hue	12	Correlation	15.7576	32.5253	5824.809	36
Hue	15	Correlation	16.5657	26.4646	6184.369	37
Hue	9	Correlation	18.5859	23.0303	6276.295	38
Thermal IR	6	Earth Mover's Distance	27.4747	14.5455	6281.195	39
Thermal IR	6	Intersection	28.6869	13.1313	6315.865	40
VGS	18	Bhattacharyya	21.0101	17.7778	6499.947	41

VGS	24	Intersection	21.0101	17.1717	6549.966	42
VGS	12	Chi Squared	22.0202	15.9596	6571.819	43
Thermal IR	6	Correlation	23.2323	14.7475	6580.634	44
VGS	18	Chi Squared	20.202	17.3737	6597.413	45
VGS	24	Chi Squared	19.596	17.7778	6612.647	46
VGS	24	Bhattacharyya	18.9899	17.7778	6661.563	47
VGS	21	Chi Squared	19.3939	17.3737	6662.224	48
VGS	12	Bhattacharyya	20.404	16.3636	6665.285	49
VGS	21	Bhattacharyya	18.7879	17.5758	6694.577	50
Hue	12	Intersection	10.101	26.8687	6715.009	51
Hue	24	Chi Squared	8.68687	28.2828	6740.722	52
Hue	24	Bhattacharyya	8.68687	28.2828	6740.722	53
Hue	12	Chi Squared	8.48485	28.4848	6744.723	54
Hue	12	Bhattacharyya	8.48485	28.4848	6744.723	55
Hue	24	Intersection	9.49495	26.8687	6769.676	56
Hue	21	Intersection	9.89899	26.2626	6777.698	57
Hue	21	Chi Squared	8.88889	27.4747	6780.577	58
Hue	21	Bhattacharyya	8.88889	27.4747	6780.577	59
Hue	18	Chi Squared	9.09091	27.0707	6791.573	60
Hue	18	Bhattacharyya	9.09091	27.0707	6791.573	61
Hue	15	Chi Squared	8.28283	27.4747	6835.979	62
Hue	15	Bhattacharyya	8.28283	27.4747	6835.979	63
Hue	18	Intersection	9.69697	25.4545	6855.834	64
Hue	15	Intersection	9.49495	24.8485	6919.456	65
Hue	9	Bhattacharyya	8.48485	25.4545	6966.027	66
VGS	15	Bhattacharyya	18.5859	14.3434	6982.654	67
Hue	9	Chi Squared	8.48485	25.0505	6996.225	68
VGS	18	Intersection	17.5758	15.1515	6996.508	69
VGS	21	Intersection	16.1616	16.3636	7011.962	70
VGS	6	Chi Squared	20.8081	11.9192	7014.792	71
VGS	15	Chi Squared	18.1818	13.7374	7067.727	72
VGS	6	Bhattacharyya	19.3939	12.1212	7110.013	73
Hue	9	Intersection	9.29293	22.4242	7122.889	74
VGS	18	Correlation	15.3535	15.7576	7130.906	75
VGS	12	Intersection	18.7879	11.7172	7194.629	76
Saturation	9	Chi Squared	15.1515	15.1515	7199.268	77
Saturation	9	Bhattacharyya	15.1515	15.1515	7199.268	78
Saturation	18	Chi Squared	14.9495	14.9495	7233.588	79
VGS	12	Earth Mover's Distance	19.596	10.303	7255.178	80
VGS	9	Bhattacharyya	14.5455	14.9495	7268.03	81
Saturation	18	Bhattacharyya	14.5455	14.7475	7285.23	82
Saturation	21	Chi Squared	14.7475	14.5455	7285.23	83
Saturation	12	Chi Squared	14.1414	15.1515	7285.484	84
VGS	9	Chi Squared	14.1414	14.9495	7302.643	85
Saturation	18	Intersection	13.9394	15.1515	7302.847	86
Saturation	21	Bhattacharyya	14.5455	14.3434	7319.762	87
Saturation	24	Chi Squared	14.5455	14.3434	7319.762	88
Saturation	12	Bhattacharyya	14.1414	14.7475	7319.844	89
Saturation	24	Correlation	14.1414	14.7475	7319.844	90
Saturation	6	Chi Squared	14.9495	13.9394	7320.007	91
Saturation	6	Bhattacharyya	14.9495	13.9394	7320.007	92
Saturation	24	Bhattacharyya	14.3434	14.1414	7354.376	93
VGS	9	Correlation	15.7576	12.5253	7374.303	94

Hue	6	Chi Squared	8.48485	20	7387.511	95
Hue	6	Bhattacharyya	8.48485	20	7387.511	96
Saturation	18	Correlation	13.1313	14.9495	7389.879	97
Hue	6	Intersection	10.7071	17.3737	7400.164	98
Saturation	15	Chi Squared	13.9394	13.9394	7406.427	99
Saturation	15	Bhattacharyya	13.9394	13.9394	7406.427	100
VGS	24	Correlation	13.7374	14.1414	7406.468	101
Saturation	21	Intersection	13.5354	14.3434	7406.59	102
Saturation	15	Correlation	13.1313	14.5455	7424.321	103
Saturation	9	Intersection	12.9293	14.7475	7424.648	104
VGS	15	Intersection	16.9697	10.7071	7433.626	105
Saturation	12	Correlation	12.3232	15.1515	7443.245	106
Saturation	15	Earth Mover's Distance	15.7576	11.7172	7445.317	107
VGS	6	Correlation	18.3838	9.09091	7462.833	108
Saturation	12	Intersection	13.1313	13.9394	7476.299	109
Saturation	21	Correlation	12.5253	14.5455	7477.147	110
VGS	24	Earth Mover's Distance	17.7778	9.29293	7494.131	111
Saturation	24	Intersection	12.5253	14.3434	7494.438	112
Saturation	24	Earth Mover's Distance	14.9495	11.9192	7495.907	113
Saturation	18	Earth Mover's Distance	15.1515	11.7172	7496.56	114
Saturation	15	Intersection	12.3232	14.3434	7512.137	115
VGS	6	Intersection	19.1919	7.67677	7526.764	116
VGS	9	Intersection	13.5354	12.7273	7546.326	117
Saturation	12	Earth Mover's Distance	14.1414	12.1212	7547.191	118
Saturation	21	Earth Mover's Distance	14.9495	11.3131	7549.477	119
VGS	21	Correlation	13.9394	12.1212	7564.555	120
Hue	9	Earth Mover's Distance	10.7071	15.3535	7569.126	121
VGS	21	Earth Mover's Distance	17.1717	8.88889	7580.881	122
VGS	15	Correlation	16.1616	9.69697	7591.757	123
VGS	12	Correlation	16.5657	9.29293	7594.527	124
Saturation	9	Correlation	11.7172	13.9394	7600.14	125
Saturation	6	Earth Mover's Distance	14.1414	11.5152	7600.63	126
Hue	21	Earth Mover's Distance	10.5051	15.1515	7604.303	127
Hue	18	Earth Mover's Distance	10.303	15.3535	7605.291	128
Saturation	9	Earth Mover's Distance	14.1414	11.3131	7618.533	129
Thermal IR	3	Correlation	10.9091	14.3434	7637.121	130
Hue	12	Earth Mover's Distance	9.89899	15.3535	7641.611	131
Thermal IR	3	Earth Mover's Distance	12.7273	12.3232	7651.873	132
Hue	15	Earth Mover's Distance	9.89899	15.1515	7658.73	133
Thermal IR	3	Intersection	12.7273	11.9192	7687.376	134
Hue	6	Correlation	11.3131	13.1313	7705.769	135
Saturation	6	Intersection	13.1313	11.3131	7705.769	136
Hue	24	Earth Mover's Distance	9.09091	15.1515	7731.865	137
Thermal IR	3	Chi Squared	16.3636	7.87879	7740.682	138
Thermal IR	3	Bhattacharyya	16.3636	7.87879	7740.682	139
VGS	6	Earth Mover's Distance	16.7677	7.47475	7744.269	140
VGS	18	Earth Mover's Distance	14.3434	9.49495	7764.109	141
VGS	9	Earth Mover's Distance	13.7374	9.89899	7779.714	142
VGS	15	Earth Mover's Distance	14.7475	8.48485	7821.506	143
Saturation	6	Correlation	10.9091	11.3131	7901.277	144
Hue	6	Earth Mover's Distance	8.48485	12.5253	8013.423	145
Hue	3	Intersection	10.5051	9.89899	8063.765	146
Saturation	3	Chi Squared	13.7374	6.66667	8076.173	147

Saturation	3	Bhattacharyya	13.7374	6.66667	8076.173	148
Hue	3	Chi Squared	9.69697	10.5051	8081.987	149
Hue	3	Bhattacharyya	9.69697	10.5051	8081.987	150
Saturation	3	Intersection	11.7172	6.26263	8290.274	151
Hue	3	Earth Mover's Distance	8.08081	8.88889	8375.186	152
Saturation	3	Earth Mover's Distance	10.9091	5.65657	8418.936	153
VGS	3	Bhattacharyya	6.86869	5.05051	8844.423	154
VGS	3	Chi Squared	6.66667	5.05051	8863.258	155
Saturation	3	Correlation	5.85859	3.83838	9054.831	156
VGS	3	Intersection	3.83838	5.05051	9131.231	157
VGS	3	Earth Mover's Distance	3.83838	5.05051	9131.231	158
Hue	3	Correlation	4.0404	4.44444	9169.555	159
VGS	3	Correlation	4.0404	3.63636	9247.098	160

2-D Results

Results are sorted by MSE of Scenario E and Scenario F D[98] Results

HPCTC			Env A D98	Env B D98	MSE	MSE Rank
Channels	**Bin Size**	**Comparison Technique**				
Hue/Thermal IR	6-21	Bhattacharyya	80.404	56.5657	1135.271	1
Hue/Thermal IR	12-21	Bhattacharyya	76.9697	58.1818	1139.578	2
Hue/Thermal IR	15-21	Bhattacharyya	77.7778	57.5758	1146.819	3
Hue/Thermal IR	9-21	Bhattacharyya	78.1818	57.1717	1155.149	4
Hue/Thermal IR	18-21	Bhattacharyya	76.9697	57.3737	1173.698	5
Hue/Thermal IR	21-21	Bhattacharyya	76.9697	57.3737	1173.698	6
Hue/Thermal IR	15-21	Chi Squared	79.1919	55.9596	1186.267	7
Hue/Thermal IR	6-18	Chi Squared	81.4141	54.9495	1187.492	8
Hue/Thermal IR	6-21	Chi Squared	81.8182	54.7475	1189.183	9
Hue/Thermal IR	15-18	Chi Squared	78.1818	56.1616	1198.92	10
Hue/Thermal IR	15-24	Bhattacharyya	77.7778	56.3636	1198.981	11
Hue/Thermal IR	15-18	Bhattacharyya	76.1616	57.1717	1201.266	12
Hue/Thermal IR	9-24	Chi Squared	79.1919	55.5556	1204.141	13
Hue/Thermal IR	6-18	Bhattacharyya	80	55.1515	1205.694	14
Hue/Thermal IR	24-21	Bhattacharyya	75.9596	57.1717	1206.102	15
Hue/Thermal IR	9-21	Chi Squared	80.8081	54.7475	1208.059	16
Hue/Thermal IR	15-24	Chi Squared	76.5657	56.7677	1209.099	17
Hue/Thermal IR	15-18	Intersection	78.3838	55.7576	1212.325	18
Hue/Thermal IR	6-24	Chi Squared	78.7879	55.5556	1212.629	19
Hue/Thermal IR	12-21	Chi Squared	77.9798	55.7576	1221.14	20
Hue/Thermal IR	24-21	Chi Squared	77.9798	55.7576	1221.14	21
Hue/Thermal IR	15-15	Chi Squared	76.3636	56.5657	1222.609	22
Hue/Thermal IR	18-21	Chi Squared	78.1818	55.5556	1225.669	23
Hue/Thermal IR	9-18	Chi Squared	78.9899	55.1515	1226.406	24
Hue/Thermal IR	18-18	Bhattacharyya	74.7475	57.3737	1227.345	25
Hue/Thermal IR	12-24	Chi Squared	76.1616	56.5657	1227.404	26
Hue/Thermal IR	24-18	Chi Squared	76.1616	56.5657	1227.404	27
Hue/Thermal IR	9-15	Bhattacharyya	77.9798	55.5556	1230.097	28

Hue/Thermal IR	21-21	Chi Squared	77.9798	55.5556	1230.097	29
Hue/Thermal IR	9-18	Bhattacharyya	77.5758	55.7576	1230.117	30
Hue/Thermal IR	9-15	Chi Squared	78.7879	55.1515	1230.671	31
Hue/Thermal IR	3-18	Chi Squared	82.0202	53.7374	1231.751	32
Hue/Thermal IR	12-18	Chi Squared	76.9697	55.9596	1234.976	33
Hue/Thermal IR	3-18	Bhattacharyya	81.2121	53.9394	1237.282	34
Hue/Thermal IR	21-18	Bhattacharyya	74.3434	57.3737	1237.631	35
Hue/Thermal IR	6-15	Bhattacharyya	78.3838	55.1515	1239.324	36
Hue/Thermal IR	21-18	Chi Squared	76.7677	55.9596	1239.648	37
Hue/Thermal IR	21-18	Intersection	76.7677	55.9596	1239.648	38
Hue/Thermal IR	24-15	Bhattacharyya	74.5455	57.1717	1241.097	39
Hue/Thermal IR	3-21	Chi Squared	82.0202	53.5354	1241.116	40
Hue/Thermal IR	12-15	Bhattacharyya	75.5556	56.5657	1242.034	41
Hue/Thermal IR	12-18	Bhattacharyya	75.5556	56.5657	1242.034	42
Hue/Thermal IR	15-15	Bhattacharyya	75.5556	56.5657	1242.034	43
Hue/Thermal IR	18-18	Chi Squared	76.5657	55.9596	1244.362	44
Hue/Thermal IR	24-18	Intersection	76.5657	55.9596	1244.362	45
Hue/Thermal IR	6-24	Bhattacharyya	78.9899	54.7475	1244.607	46
Hue/Thermal IR	12-15	Chi Squared	75.7576	56.3636	1245.915	47
Hue/Thermal IR	21-24	Chi Squared	75.7576	56.3636	1245.915	48
Hue/Thermal IR	9-9	Chi Squared	77.1717	55.5556	1248.218	49
Hue/Thermal IR	24-18	Correlation	80.6061	53.9394	1248.851	50
Hue/Thermal IR	12-9	Chi Squared	73.5354	57.5758	1250.094	51
Hue/Thermal IR	18-24	Chi Squared	75.7576	56.1616	1254.75	52
Hue/Thermal IR	24-15	Chi Squared	74.9495	56.5657	1257.033	53
Hue/Thermal IR	15-9	Chi Squared	72.9293	57.7778	1257.768	54
Hue/Thermal IR	24-18	Bhattacharyya	74.5455	56.7677	1258.482	55
Hue/Thermal IR	9-12	Chi Squared	75.9596	55.9596	1258.749	56
Hue/Thermal IR	21-15	Chi Squared	75.1515	56.3636	1260.792	57
Hue/Thermal IR	24-24	Chi Squared	75.1515	56.3636	1260.792	58
Hue/Thermal IR	3-24	Chi Squared	80.8081	53.5354	1263.644	59
Hue/Thermal IR	18-15	Bhattacharyya	74.3434	56.7677	1263.646	60
Hue/Thermal IR	3-21	Bhattacharyya	82.2222	52.9293	1265.85	61
Hue/Thermal IR	18-18	Intersection	77.1717	55.1515	1266.26	62
Hue/Thermal IR	12-18	Intersection	76.7677	55.3535	1266.525	63
Hue/Thermal IR	15-21	Intersection	78.3838	54.5455	1266.686	64
Hue/Thermal IR	21-24	Bhattacharyya	76.3636	55.5556	1266.992	65
Hue/Thermal IR	21-15	Bhattacharyya	74.5455	56.5657	1267.235	66
Hue/Thermal IR	6-15	Chi Squared	78.7879	54.3434	1267.239	67
Hue/Thermal IR	12-24	Bhattacharyya	75.9596	55.7576	1267.665	68
Hue/Thermal IR	3-15	Bhattacharyya	79.798	53.7374	1274.174	69
Hue/Thermal IR	18-15	Chi Squared	74.9495	56.1616	1274.666	70
Hue/Thermal IR	15-15	Intersection	77.1717	54.9495	1275.339	71
Hue/Thermal IR	18-24	Bhattacharyya	76.3636	55.3535	1275.995	72
Hue/Thermal IR	24-24	Bhattacharyya	75.9596	55.5556	1276.623	73
Hue/Thermal IR	15-24	Intersection	76.5657	55.1515	1280.277	74
Hue/Thermal IR	9-18	Intersection	80.404	53.3333	1280.892	75
Hue/Thermal IR	15-9	Bhattacharyya	72.9293	57.1717	1283.543	76
Hue/Thermal IR	15-12	Bhattacharyya	73.1313	56.9697	1286.767	77
Hue/Thermal IR	18-9	Chi Squared	73.1313	56.9697	1286.767	78
Hue/Thermal IR	24-21	Intersection	77.3737	54.5455	1289.031	79
Hue/Thermal IR	3-12	Chi Squared	78.9899	53.7374	1290.826	80
Hue/Thermal IR	3-15	Chi Squared	79.798	53.3333	1292.951	81

Hue/Thermal IR	12-9	Bhattacharyya	73.5354	56.5657	1293.457	82
Hue/Thermal IR	3-18	Intersection	80.202	53.1313	1294.318	83
Hue/Thermal IR	18-9	Bhattacharyya	72.5253	57.1717	1294.561	84
Hue/Thermal IR	12-12	Chi Squared	73.7374	56.3636	1296.93	85
Hue/Thermal IR	24-12	Bhattacharyya	72.7273	56.9697	1297.703	86
Hue/Thermal IR	21-12	Bhattacharyya	72.9293	56.7677	1300.927	87
Hue/Thermal IR	6-18	Intersection	79.3939	53.3333	1301.196	88
Hue/Thermal IR	24-24	Intersection	75.1515	55.3535	1305.379	89
Hue/Thermal IR	24-9	Chi Squared	72.1212	57.1717	1305.745	90
Hue/Thermal IR	21-21	Intersection	76.5657	54.5455	1307.639	91
Hue/Thermal IR	3-9	Chi Squared	80.404	52.7273	1309.356	92
Hue/Thermal IR	15-12	Chi Squared	73.9394	55.9596	1309.356	93
Hue/Thermal IR	9-21	Intersection	78.9899	53.3333	1309.603	94
Hue/Thermal IR	21-9	Chi Squared	72.5253	56.7677	1311.945	95
Hue/Thermal IR	6-12	Bhattacharyya	76.7677	54.3434	1312.132	96
Hue/Thermal IR	6-9	Bhattacharyya	76.3636	54.5455	1312.395	97
Hue/Thermal IR	21-9	Bhattacharyya	72.1212	56.9697	1314.417	98
Hue/Thermal IR	12-12	Bhattacharyya	72.7273	56.5657	1315.169	99
Hue/Thermal IR	9-24	Bhattacharyya	76.9697	54.1414	1316.703	100
Hue/Thermal IR	9-24	Intersection	78.1818	53.5354	1317.496	101
Hue/Thermal IR	18-24	Intersection	75.7576	54.7475	1317.741	102
Hue/Thermal IR	24-9	Bhattacharyya	71.9192	56.9697	1320.069	103
Hue/Thermal IR	18-21	Intersection	76.3636	54.3434	1321.602	104
Hue/Thermal IR	24-15	Intersection	76.3636	54.3434	1321.602	105
Hue/Thermal IR	24-12	Chi Squared	72.1212	56.7677	1323.13	106
Hue/Thermal IR	18-15	Intersection	77.3737	53.7374	1326.089	107
Hue/Thermal IR	6-12	Chi Squared	76.1616	54.3434	1326.397	108
Hue/Thermal IR	9-12	Bhattacharyya	75.3535	54.7475	1327.619	109
Hue/Thermal IR	24-15	Correlation	75.3535	54.7475	1327.619	110
Hue/Thermal IR	15-9	Intersection	75.9596	54.3434	1331.233	111
Hue/Thermal IR	12-24	Intersection	75.1515	54.7475	1332.618	112
Hue/Thermal IR	9-9	Intersection	78.7879	52.9293	1332.802	113
Hue/Thermal IR	21-12	Chi Squared	73.3333	55.7576	1334.251	114
Hue/Thermal IR	18-12	Bhattacharyya	72.9293	55.9596	1336.19	115
Hue/Thermal IR	9-15	Intersection	80	52.3232	1336.539	116
Hue/Thermal IR	21-24	Intersection	74.9495	54.7475	1337.658	117
Hue/Thermal IR	15-6	Bhattacharyya	68.6869	58.7879	1339.474	118
Hue/Thermal IR	9-9	Bhattacharyya	75.9596	54.1414	1340.476	119
Hue/Thermal IR	21-18	Correlation	80.6061	51.9192	1343.943	120
Hue/Thermal IR	6-9	Chi Squared	76.5657	53.7374	1344.697	121
Hue/Thermal IR	24-24	Correlation	75.7576	54.1414	1345.353	122
Hue/Thermal IR	3-24	Bhattacharyya	79.3939	52.3232	1348.844	123
Hue/Thermal IR	12-15	Intersection	76.5657	53.5354	1354.063	124
Hue/Thermal IR	6-24	Intersection	76.9697	53.3333	1354.088	125
Hue/Thermal IR	15-6	Chi Squared	68.6869	58.3838	1356.209	126
Hue/Thermal IR	15-18	Correlation	82.0202	51.1111	1356.699	127
Hue/Thermal IR	18-12	Chi Squared	73.1313	55.3535	1357.619	128
Hue/Thermal IR	12-21	Intersection	75.9596	53.7374	1359.084	129
Hue/Thermal IR	3-9	Bhattacharyya	79.798	51.9192	1359.942	130
Hue/Thermal IR	18-9	Intersection	75.1515	54.1414	1360.23	131
Hue/Thermal IR	15-12	Intersection	74.3434	54.5455	1362.186	132
Hue/Thermal IR	3-24	Intersection	78.1818	52.5253	1364.94	133
Hue/Thermal IR	24-12	Intersection	72.7273	55.3535	1368.555	134

Hue/Thermal IR	21-15	Intersection	75.5556	53.7374	1368.878	135
Hue/Thermal IR	21-9	Intersection	75.1515	53.9394	1369.513	136
Hue/Thermal IR	6-21	Intersection	78.3838	52.3232	1370.169	137
Hue/Thermal IR	24-9	Intersection	74.3434	54.3434	1371.393	138
Hue/Thermal IR	3-21	Intersection	79.596	51.7172	1373.776	139
Hue/Thermal IR	21-6	Bhattacharyya	68.0808	58.3838	1375.372	140
Hue/Thermal IR	12-12	Intersection	73.7374	54.5455	1377.918	141
Hue/Thermal IR	18-12	Intersection	73.7374	54.5455	1377.918	142
Hue/Thermal IR	3-12	Bhattacharyya	78.3838	52.1212	1379.82	143
Hue/Thermal IR	24-21	Correlation	76.9697	52.7273	1382.551	144
Hue/Thermal IR	24-6	Bhattacharyya	67.4747	58.5859	1386.511	145
Hue/Thermal IR	21-21	Correlation	77.9798	52.1212	1388.634	146
Hue/Thermal IR	9-12	Intersection	75.7576	53.1313	1392.184	147
Hue/Thermal IR	6-15	Intersection	78.5859	51.7172	1394.896	148
Hue/Thermal IR	12-18	Correlation	78.5859	51.7172	1394.896	149
Hue/Thermal IR	12-6	Bhattacharyya	67.8788	57.9798	1398.734	150
Hue/Thermal IR	18-6	Chi Squared	67.6768	57.9798	1405.243	151
Hue/Thermal IR	18-6	Bhattacharyya	66.8687	58.5859	1406.405	152
Hue/Thermal IR	18-18	Correlation	80.8081	50.5051	1409.037	153
Hue/Thermal IR	12-9	Intersection	74.1414	53.5354	1413.813	154
Hue/Thermal IR	21-12	Intersection	72.7273	54.3434	1414.163	155
Hue/Thermal IR	21-6	Chi Squared	67.8788	57.5758	1415.792	156
Hue/Thermal IR	9-6	Bhattacharyya	69.4949	56.3636	1417.348	157
Hue/Thermal IR	21-15	Correlation	74.9495	52.9293	1421.589	158
Hue/Thermal IR	9-6	Chi Squared	69.899	55.9596	1422.814	159
Hue/Thermal IR	15-15	Correlation	77.5758	51.5152	1426.81	160
Hue/Thermal IR	12-15	Correlation	75.3535	52.5253	1430.649	161
Hue/Thermal IR	3-15	Intersection	77.7778	51.3131	1432.12	162
Hue/Thermal IR	3-12	Intersection	74.1414	53.1313	1432.671	163
Hue/Thermal IR	24-9	Correlation	72.7273	53.9394	1432.69	164
Hue/Thermal IR	18-15	Correlation	75.9596	52.1212	1435.16	165
Hue/Thermal IR	21-24	Correlation	76.3636	51.9192	1435.221	166
Hue/Thermal IR	6-6	Chi Squared	71.3131	54.7475	1435.363	167
Hue/Thermal IR	24-6	Chi Squared	66.4646	58.1818	1436.692	168
Hue/Thermal IR	12-6	Chi Squared	67.6768	57.1717	1439.526	169
Hue/Thermal IR	6-6	Bhattacharyya	70.5051	55.1515	1440.669	170
Hue/Thermal IR	15-9	Correlation	75.9596	51.9192	1444.852	171
Hue/Thermal IR	6-12	Intersection	75.5556	52.1212	1444.954	172
Hue/Thermal IR	15-21	Correlation	79.798	50.101	1449.016	173
Hue/Thermal IR	18-21	Correlation	77.7778	50.9091	1451.871	174
Hue/Thermal IR	3-6	Chi Squared	73.3333	53.1313	1453.894	175
Hue/Thermal IR	3-9	Intersection	77.5758	50.9091	1456.381	176
Hue/Thermal IR	12-21	Correlation	75.5556	51.5152	1474.152	177
VGS/Thermal IR	9-21	Chi Squared	74.7475	51.9192	1474.726	178
Hue/Thermal IR	21-9	Correlation	71.9192	53.3333	1483.156	179
Hue/Thermal IR	3-6	Bhattacharyya	74.3434	51.9192	1485.012	180
Hue/Thermal IR	15-24	Correlation	78.3838	49.899	1488.685	181
Hue/Thermal IR	6-9	Intersection	75.5556	51.1111	1493.827	182
Hue/Thermal IR	9-18	Correlation	82.8283	48.0808	1495.235	183
Hue/Thermal IR	18-9	Correlation	73.1313	52.1212	1507.153	184
Hue/Thermal IR	12-24	Correlation	75.1515	50.9091	1513.682	185
Hue/Thermal IR	18-24	Correlation	75.9596	50.5051	1513.843	186
VGS/Thermal IR	9-24	Chi Squared	73.9394	51.5152	1514.965	187

Hue/Thermal IR	24-12	Correlation	68.6869	54.5455	1523.311	188
VGS/Thermal IR	9-18	Intersection	76.7677	49.899	1524.925	189
Hue/Thermal IR	15-6	Intersection	71.1111	52.9293	1525.11	190
Hue/Thermal IR	9-21	Earth Mover's Distance	84.4444	46.8687	1532.456	191
VGS/Thermal IR	9-18	Chi Squared	74.3434	50.9091	1534.089	192
Hue/Thermal IR	12-9	Correlation	70.7071	52.9293	1536.862	193
Hue/Thermal IR	6-15	Earth Mover's Distance	83.4343	47.0707	1537.967	194
VGS/Thermal IR	9-21	Intersection	74.9495	50.5051	1538.636	195
Hue/Thermal IR	18-6	Correlation	70.303	53.1313	1539.293	196
Hue/Thermal IR	18-6	Intersection	70.5051	52.9293	1542.8	197
VGS/Thermal IR	9-24	Intersection	74.7475	50.5051	1543.717	198
Hue/Thermal IR	9-24	Correlation	78.3838	48.6869	1550.147	199
Hue/Thermal IR	9-24	Earth Mover's Distance	86.0606	46.0606	1551.883	200
Hue/Thermal IR	9-15	Correlation	79.1919	48.2828	1553.823	201
Hue/Thermal IR	24-6	Correlation	68.0808	54.1414	1560.923	202
Hue/Thermal IR	9-9	Correlation	76.3636	49.2929	1564.945	203
Hue/Thermal IR	15-12	Correlation	70.303	52.5253	1567.879	204
Hue/Thermal IR	18-12	Correlation	68.6869	53.5354	1569.735	205
Hue/Thermal IR	9-21	Correlation	79.3939	47.8788	1570.615	206
Hue/Thermal IR	24-6	Intersection	68.2828	53.7374	1573.104	207
VGS/Thermal IR	9-9	Intersection	76.3636	48.8889	1585.512	208
Hue/Thermal IR	9-6	Intersection	72.3232	50.9091	1587.961	209
Hue/Thermal IR	21-12	Correlation	68.6869	53.1313	1588.593	210
Hue/Thermal IR	21-6	Intersection	68.8889	52.9293	1591.776	211
Hue/Thermal IR	6-18	Correlation	78.7879	47.6768	1593.835	212
Hue/Thermal IR	21-6	Correlation	69.0909	52.7273	1595.04	213
VGS/Thermal IR	9-15	Chi Squared	73.5354	49.697	1615.383	214
Hue/Thermal IR	12-12	Correlation	67.6768	53.1313	1620.732	215
Hue/Thermal IR	6-12	Earth Mover's Distance	81.6162	46.0606	1623.711	216
Hue/Thermal IR	12-24	Earth Mover's Distance	82.0202	45.8586	1627.282	217
Hue/Thermal IR	6-6	Intersection	71.1111	50.7071	1632.179	218
Hue/Thermal IR	6-24	Correlation	76.5657	47.8788	1632.893	219
Hue/Thermal IR	12-6	Intersection	68.6869	52.1212	1636.445	220
VGS/Thermal IR	9-15	Intersection	74.9495	48.4848	1640.672	221
VGS/Thermal IR	9-21	Bhattacharyya	72.3232	49.697	1648.199	222
VGS/Thermal IR	9-24	Bhattacharyya	72.5253	49.4949	1652.812	223
Hue/Thermal IR	15-6	Correlation	69.697	51.1111	1654.198	224
VGS/Thermal IR	9-15	Bhattacharyya	71.3131	50.101	1656.424	225
VGS/Thermal IR	9-18	Bhattacharyya	71.1111	50.101	1662.239	226
Hue/Thermal IR	6-21	Earth Mover's Distance	85.2525	44.2424	1663.199	227
VGS/Thermal IR	9-9	Chi Squared	72.7273	49.0909	1667.768	228
Hue/Thermal IR	6-18	Earth Mover's Distance	85.6566	44.0404	1668.605	229
Hue/Thermal IR	9-18	Earth Mover's Distance	81.6162	45.0505	1678.706	230
Hue/Thermal IR	3-6	Intersection	71.1111	49.697	1682.48	231
Hue/Thermal IR	6-21	Correlation	76.5657	46.4646	1707.603	232
Hue/Thermal IR	6-24	Earth Mover's Distance	85.4545	43.2323	1717.072	233
Hue/Thermal IR	12-6	Correlation	66.6667	51.7172	1721.169	234
Hue/Thermal IR	9-12	Correlation	69.899	49.4949	1728.418	235
VGS/Thermal IR	12-18	Intersection	69.0909	49.899	1732.741	236
VGS/Thermal IR	24-18	Intersection	66.6667	51.3131	1740.762	237
VGS/Thermal IR	18-18	Intersection	67.4747	50.7071	1743.843	238
VGS/Thermal IR	18-18	Chi Squared	66.8687	51.1111	1743.904	239
VGS/Thermal IR	18-21	Intersection	66.8687	51.1111	1743.904	240

Hue/Thermal IR	3-9	Earth Mover's Distance	83.6364	43.2323	1745.17	241
VGS/Thermal IR	9-12	Intersection	69.899	49.0909	1748.903	242
Hue/Thermal IR	12-21	Earth Mover's Distance	78.9899	44.6465	1752.717	243
VGS/Thermal IR	9-9	Bhattacharyya	69.697	49.0909	1755.004	244
VGS/Thermal IR	9-21	Correlation	78.7879	44.6465	1756.982	245
Hue/Thermal IR	9-6	Correlation	70.303	48.6869	1757.473	246
VGS/Thermal IR	9-12	Chi Squared	70.9091	48.2828	1760.475	247
VGS/Thermal IR	18-24	Intersection	66.2626	51.1111	1764.168	248
Hue/Thermal IR	6-15	Correlation	72.5253	47.2727	1767.514	249
Hue/Thermal IR	9-15	Earth Mover's Distance	78.7879	44.4444	1768.189	250
VGS/Thermal IR	18-21	Chi Squared	66.6667	50.7071	1770.449	251
VGS/Thermal IR	9-24	Correlation	77.9798	44.6465	1774.45	252
VGS/Thermal IR	12-21	Intersection	68.8889	49.0909	1779.819	253
Hue/Thermal IR	15-24	Earth Mover's Distance	79.1919	44.0404	1782.227	254
Hue/Thermal IR	6-9	Correlation	70.101	48.2828	1784.309	255
VGS/Thermal IR	21-21	Chi Squared	66.4646	50.5051	1787.184	256
VGS/Thermal IR	21-18	Intersection	66.6667	50.303	1790.45	257
VGS/Thermal IR	24-21	Intersection	66.0606	50.7071	1790.836	258
VGS/Thermal IR	9-18	Correlation	80.404	43.4343	1791.841	259
VGS/Thermal IR	12-18	Chi Squared	68.0808	49.2929	1795.023	260
VGS/Thermal IR	12-24	Chi Squared	67.0707	49.899	1797.224	261
VGS/Thermal IR	18-15	Chi Squared	66.0606	50.5051	1800.814	262
VGS/Thermal IR	24-24	Intersection	64.8485	51.3131	1803.021	263
VGS/Thermal IR	12-24	Intersection	67.4747	49.4949	1804.33	264
VGS/Thermal IR	9-12	Bhattacharyya	70.101	47.8788	1805.285	265
VGS/Thermal IR	24-18	Chi Squared	64.4444	51.5152	1807.488	266
Hue/Thermal IR	3-12	Earth Mover's Distance	79.596	43.4343	1808.001	267
Hue/Thermal IR	3-18	Correlation	75.5556	45.0505	1808.488	268
VGS/Thermal IR	21-18	Chi Squared	65.4545	50.7071	1811.591	269
VGS/Thermal IR	24-21	Chi Squared	64.8485	51.1111	1812.876	270
VGS/Thermal IR	12-24	Bhattacharyya	66.2626	50.101	1814.061	271
VGS/Thermal IR	18-15	Intersection	67.4747	49.2929	1814.553	272
VGS/Thermal IR	15-18	Intersection	68.6869	48.4848	1817.163	273
VGS/Thermal IR	24-15	Intersection	66.0606	50.101	1820.897	274
VGS/Thermal IR	18-24	Chi Squared	65.6566	50.303	1824.63	275
Hue/Thermal IR	3-24	Correlation	73.5354	45.6566	1826.79	276
VGS/Thermal IR	12-21	Bhattacharyya	67.0707	49.2929	1827.774	277
VGS/Thermal IR	12-21	Chi Squared	67.6768	48.8889	1828.567	278
VGS/Thermal IR	15-21	Chi Squared	67.6768	48.8889	1828.567	279
VGS/Thermal IR	15-21	Intersection	67.6768	48.8889	1828.567	280
VGS/Thermal IR	12-15	Intersection	68.4848	48.2828	1833.938	281
VGS/Thermal IR	18-15	Bhattacharyya	65.2525	50.303	1838.59	282
VGS/Thermal IR	21-21	Intersection	64.8485	50.5051	1842.687	283
Hue/Thermal IR	3-9	Correlation	72.3232	45.8586	1848.648	284
Hue/Thermal IR	12-18	Earth Mover's Distance	77.1717	43.6364	1848.993	285
VGS/Thermal IR	24-18	Correlation	71.5152	46.2626	1849.546	286
VGS/Thermal IR	15-18	Chi Squared	66.6667	49.0909	1851.423	287
VGS/Thermal IR	12-9	Bhattacharyya	67.2727	48.6869	1852.055	288
VGS/Thermal IR	18-9	Bhattacharyya	65.6566	49.697	1854.93	289
VGS/Thermal IR	15-24	Chi Squared	66.8687	48.8889	1855.014	290
VGS/Thermal IR	21-24	Chi Squared	65.0505	50.101	1855.689	291
VGS/Thermal IR	15-15	Intersection	69.0909	47.4747	1857.14	292
VGS/Thermal IR	18-9	Chi Squared	66.6667	48.8889	1861.727	293

VGS/Thermal IR	12-15	Bhattacharyya	66.8687	48.6869	1865.359	294
VGS/Thermal IR	18-12	Chi Squared	65.8586	49.2929	1868.423	295
VGS/Thermal IR	21-9	Chi Squared	67.0707	48.4848	1869.077	296
VGS/Thermal IR	18-21	Bhattacharyya	65.4545	49.4949	1872.078	297
VGS/Thermal IR	12-15	Chi Squared	67.8788	47.8788	1874.195	298
VGS/Thermal IR	12-18	Bhattacharyya	65.0505	49.697	1875.93	299
Saturation/Thermal IR	6-21	Chi Squared	72.9293	45.0505	1876.135	300
VGS/Thermal IR	15-21	Bhattacharyya	65.8586	49.0909	1878.686	301
VGS/Thermal IR	15-24	Intersection	67.0707	48.2828	1879.504	302
VGS/Thermal IR	21-15	Intersection	66.6667	48.4848	1882.462	303
VGS/Thermal IR	12-9	Chi Squared	67.2727	48.0808	1883.34	304
VGS/Thermal IR	24-15	Chi Squared	63.6364	50.5051	1886.028	305
VGS/Thermal IR	24-24	Chi Squared	63.6364	50.5051	1886.028	306
VGS/Thermal IR	18-12	Bhattacharyya	65.0505	49.4949	1886.116	307
VGS/Thermal IR	21-24	Bhattacharyya	64.4444	49.899	1887.155	308
VGS/Thermal IR	21-21	Bhattacharyya	64.6465	49.697	1890.131	309
Saturation/Thermal IR	12-9	Chi Squared	68.6869	47.0707	1891.011	310
VGS/Thermal IR	15-9	Chi Squared	66.0606	48.6869	1892.459	311
Hue/Thermal IR	3-21	Correlation	73.1313	44.6465	1892.969	312
VGS/Thermal IR	21-15	Bhattacharyya	64.8485	49.4949	1893.197	313
VGS/Thermal IR	21-18	Bhattacharyya	63.4343	50.5051	1893.398	314
VGS/Thermal IR	12-9	Intersection	67.4747	47.6768	1897.806	315
VGS/Thermal IR	18-18	Bhattacharyya	63.0303	50.7071	1898.274	316
Saturation/Thermal IR	15-9	Chi Squared	69.0909	46.6667	1899.907	317
VGS/Thermal IR	21-15	Chi Squared	64.6465	49.4949	1900.318	318
VGS/Thermal IR	21-18	Correlation	74.5455	43.8384	1901.028	319
Hue/Thermal IR	6-9	Earth Mover's Distance	78.3838	42.2222	1902.767	320
VGS/Thermal IR	21-9	Bhattacharyya	66.0606	48.4848	1902.849	321
VGS/Thermal IR	15-24	Bhattacharyya	64.8485	49.2929	1903.419	322
VGS/Thermal IR	15-15	Chi Squared	66.2626	48.2828	1906.44	323
VGS/Thermal IR	15-9	Bhattacharyya	66.0606	48.2828	1913.276	324
VGS/Thermal IR	24-9	Bhattacharyya	64.8485	49.0909	1913.682	325
VGS/Thermal IR	15-12	Chi Squared	65.2525	48.6869	1920.211	326
VGS/Thermal IR	9-9	Correlation	79.798	41.4141	1920.214	327
Saturation/Thermal IR	9-18	Chi Squared	72.1212	44.6465	1920.619	328
VGS/Thermal IR	24-24	Bhattacharyya	63.2323	50.101	1920.887	329
Saturation/Thermal IR	6-18	Chi Squared	73.7374	43.8384	1921.925	330
Hue/Thermal IR	15-21	Earth Mover's Distance	76.9697	42.4242	1922.684	331
VGS/Thermal IR	6-21	Bhattacharyya	69.697	45.8586	1924.782	332
VGS/Thermal IR	15-12	Intersection	64.2424	49.2929	1924.908	333
Hue/Thermal IR	9-12	Earth Mover's Distance	76.3636	42.6263	1925.21	334
VGS/Thermal IR	6-24	Bhattacharyya	69.2929	46.0606	1926.192	335
Hue/Thermal IR	3-6	Earth Mover's Distance	72.5253	44.2424	1931.885	336
Saturation/Thermal IR	12-18	Chi Squared	71.7172	44.6465	1931.963	337
VGS/Thermal IR	6-21	Chi Squared	71.3131	44.8485	1932.313	338
VGS/Thermal IR	21-24	Correlation	71.3131	44.8485	1932.313	339
Saturation/Thermal IR	18-9	Chi Squared	69.0909	46.0606	1932.416	340
VGS/Thermal IR	15-9	Intersection	70.101	45.4545	1934.581	341
VGS/Thermal IR	24-9	Chi Squared	64.2424	49.0909	1935.171	342
VGS/Thermal IR	21-24	Intersection	63.6364	49.4949	1936.538	343
VGS/Thermal IR	21-12	Chi Squared	65.0505	48.4848	1937.642	344
Saturation/Thermal IR	6-9	Intersection	70.7071	45.0505	1938.761	345
Saturation/Thermal IR	9-21	Chi Squared	70.7071	45.0505	1938.761	346

VGS/Thermal IR	24-18	Bhattacharyya	62.4242	50.303	1940.866	347
Saturation/Thermal IR	6-18	Intersection	74.7475	43.0303	1941.618	348
VGS/Thermal IR	12-12	Bhattacharyya	67.0707	47.0707	1942.925	349
Saturation/Thermal IR	9-9	Chi Squared	69.0909	45.8586	1943.332	350
VGS/Thermal IR	15-15	Bhattacharyya	65.4545	48.0808	1944.497	351
Saturation/Thermal IR	6-24	Chi Squared	70.5051	45.0505	1944.698	352
VGS/Thermal IR	24-15	Bhattacharyya	63.0303	49.697	1948.575	353
VGS/Thermal IR	24-24	Correlation	67.8788	46.4646	1948.905	354
Saturation/Thermal IR	6-9	Bhattacharyya	71.1111	44.6465	1949.289	355
Saturation/Thermal IR	6-15	Intersection	73.1313	43.6364	1949.391	356
VGS/Thermal IR	18-24	Bhattacharyya	63.8384	49.0909	1949.699	357
VGS/Thermal IR	24-21	Bhattacharyya	63.8384	49.0909	1949.699	358
Saturation/Thermal IR	6-9	Chi Squared	70.7071	44.8485	1949.881	359
Hue/Thermal IR	18-24	Earth Mover's Distance	76.1616	42.2222	1953.272	360
VGS/Thermal IR	24-12	Chi Squared	63.4343	49.2929	1954.13	361
VGS/Thermal IR	21-21	Correlation	71.7172	44.2424	1954.413	362
VGS/Thermal IR	18-9	Intersection	67.6768	46.4646	1955.414	363
Saturation/Thermal IR	15-18	Chi Squared	70.7071	44.6465	1961.042	364
VGS/Thermal IR	9-12	Correlation	73.5354	43.2323	1961.473	365
VGS/Thermal IR	12-12	Chi Squared	65.8586	47.4747	1962.271	366
VGS/Thermal IR	6-21	Intersection	71.7172	44.0404	1965.697	367
Hue/Thermal IR	3-15	Earth Mover's Distance	81.0101	40.202	1968.209	368
Saturation/Thermal IR	9-15	Intersection	71.5152	44.0404	1971.43	369
Saturation/Thermal IR	9-24	Chi Squared	69.899	44.8485	1973.879	370
Saturation/Thermal IR	3-24	Chi Squared	73.9394	42.8283	1973.879	371
VGS/Thermal IR	24-12	Bhattacharyya	63.4343	48.8889	1974.697	372
Saturation/Thermal IR	12-21	Chi Squared	69.4949	45.0505	1975.004	373
VGS/Thermal IR	21-12	Bhattacharyya	64.8485	47.8788	1976.124	374
VGS/Thermal IR	24-9	Intersection	66.0606	47.0707	1976.697	375
Saturation/Thermal IR	6-18	Bhattacharyya	70.9091	44.2424	1977.595	376
Saturation/Thermal IR	18-18	Chi Squared	70.9091	44.2424	1977.595	377
VGS/Thermal IR	6-18	Chi Squared	70.5051	44.4444	1978.187	378
VGS/Thermal IR	15-18	Bhattacharyya	64.0404	48.2828	1983.881	379
VGS/Thermal IR	6-24	Chi Squared	69.4949	44.8485	1986.125	380
Saturation/Thermal IR	12-15	Intersection	71.3131	43.8384	1988.532	381
Saturation/Thermal IR	12-9	Bhattacharyya	68.2828	45.4545	1990.596	382
Saturation/Thermal IR	3-21	Chi Squared	75.9596	41.6162	1993.304	383
VGS/Thermal IR	9-15	Correlation	77.3737	41.0101	1995.879	384
VGS/Thermal IR	18-12	Intersection	62.0202	49.4949	1996.615	385
VGS/Thermal IR	21-9	Intersection	65.4545	47.0707	1997.451	386
VGS/Thermal IR	6-15	Chi Squared	71.7172	43.4343	1999.798	387
VGS/Thermal IR	6-18	Intersection	71.3131	43.6364	1999.897	388
VGS/Thermal IR	12-18	Correlation	70.5051	44.0404	2000.713	389
Saturation/Thermal IR	12-24	Chi Squared	69.697	44.4444	2002.348	390
Saturation/Thermal IR	15-21	Chi Squared	69.2929	44.6465	2003.468	391
VGS/Thermal IR	12-12	Intersection	64.6465	47.4747	2004.389	392
VGS/Thermal IR	24-21	Correlation	67.4747	45.6566	2005.55	393
Saturation/Thermal IR	21-18	Chi Squared	69.899	44.2424	2007.49	394
Saturation/Thermal IR	24-21	Chi Squared	69.4949	44.4444	2008.493	395
Saturation/Thermal IR	6-21	Bhattacharyya	71.7172	43.2323	2011.244	396
Saturation/Thermal IR	6-21	Intersection	72.1212	43.0303	2011.387	397
VGS/Thermal IR	9-6	Intersection	72.5253	42.8283	2011.731	398
Saturation/Thermal IR	9-9	Intersection	70.5051	43.8384	2012.037	399

Saturation/Thermal IR	9-9	Bhattacharyya	67.8788	45.2525	2014.53	400
Saturation/Thermal IR	21-21	Chi Squared	68.8889	44.6465	2015.955	401
Saturation/Thermal IR	6-15	Chi Squared	71.5152	43.2323	2016.978	402
VGS/Thermal IR	18-18	Correlation	71.9192	43.0303	2017.039	403
Saturation/Thermal IR	21-9	Chi Squared	68.0808	45.0505	2019.141	404
Saturation/Thermal IR	15-24	Chi Squared	69.0909	44.4444	2020.899	405
Saturation/Thermal IR	18-21	Chi Squared	69.0909	44.4444	2020.899	406
VGS/Thermal IR	6-21	Earth Mover's Distance	82.0202	38.9899	2022.753	407
Saturation/Thermal IR	21-15	Intersection	69.697	44.0404	2024.874	408
Hue/Thermal IR	3-18	Earth Mover's Distance	81.2121	39.1919	2025.305	409
VGS/Thermal IR	6-18	Bhattacharyya	66.8687	45.6566	2025.444	410
Hue/Thermal IR	3-15	Correlation	69.2929	44.2424	2025.918	411
Saturation/Thermal IR	9-15	Chi Squared	70.303	43.6364	2029.384	412
Saturation/Thermal IR	15-9	Intersection	70.303	43.6364	2029.384	413
Saturation/Thermal IR	6-24	Bhattacharyya	69.899	43.8384	2030.098	414
Saturation/Thermal IR	24-9	Chi Squared	67.2727	45.2525	2034.182	415
VGS/Thermal IR	6-9	Intersection	72.1212	42.6263	2034.484	416
Saturation/Thermal IR	15-15	Intersection	70.101	43.6364	2035.403	417
Saturation/Thermal IR	18-24	Chi Squared	68.8889	44.2424	2038.405	418
Saturation/Thermal IR	3-15	Chi Squared	74.1414	41.6162	2038.668	419
VGS/Thermal IR	15-12	Bhattacharyya	64.8485	46.6667	2040.034	420
Saturation/Thermal IR	3-18	Chi Squared	75.9596	40.8081	2040.811	421
Saturation/Thermal IR	12-15	Chi Squared	69.4949	43.8384	2042.343	422
Hue/Thermal IR	6-12	Correlation	66.6667	45.4545	2043.16	423
VGS/Thermal IR	6-15	Bhattacharyya	68.6869	44.2424	2044.71	424
Saturation/Thermal IR	15-18	Intersection	70.5051	43.2323	2046.26	425
Hue/Thermal IR	12-15	Earth Mover's Distance	73.3333	41.8182	2048.117	426
Saturation/Thermal IR	12-9	Intersection	69.2929	43.8384	2048.526	427
Saturation/Thermal IR	3-18	Intersection	75.5556	40.8081	2050.605	428
Saturation/Thermal IR	6-24	Intersection	71.5152	42.6263	2051.563	429
Saturation/Thermal IR	15-9	Bhattacharyya	67.0707	45.0505	2051.893	430
VGS/Thermal IR	18-21	Correlation	70.303	43.2323	2052.242	431
Saturation/Thermal IR	3-21	Bhattacharyya	74.9495	41.0101	2053.668	432
Saturation/Thermal IR	18-15	Intersection	69.4949	43.6364	2053.708	433
VGS/Thermal IR	6-9	Chi Squared	69.0909	43.8384	2054.749	434
Saturation/Thermal IR	24-18	Chi Squared	69.0909	43.8384	2054.749	435
Saturation/Thermal IR	21-24	Chi Squared	68.6869	44.0404	2055.994	436
Saturation/Thermal IR	18-9	Intersection	69.697	43.4343	2058.975	437
Saturation/Thermal IR	24-15	Intersection	68.8889	43.8384	2061.013	438
VGS/Thermal IR	24-15	Correlation	69.899	43.2323	2064.321	439
VGS/Thermal IR	15-18	Correlation	72.7273	41.8182	2064.461	440
Saturation/Thermal IR	9-21	Bhattacharyya	69.4949	43.4343	2065.12	441
Saturation/Thermal IR	9-18	Intersection	72.5253	41.8182	2069.99	442
VGS/Thermal IR	21-12	Intersection	61.0101	48.6869	2076.623	443
VGS/Thermal IR	6-9	Bhattacharyya	68.6869	43.6364	2078.683	444
Hue/Thermal IR	21-24	Earth Mover's Distance	73.9394	41.0101	2079.482	445
VGS/Thermal IR	6-24	Intersection	70.101	42.8283	2081.277	446
Saturation/Thermal IR	9-21	Intersection	69.697	43.0303	2081.909	447
VGS/Thermal IR	24-12	Intersection	60.6061	48.8889	2082.112	448
Hue/Thermal IR	15-18	Earth Mover's Distance	74.7475	40.6061	2082.662	449
Saturation/Thermal IR	15-15	Chi Squared	69.2929	43.2323	2082.749	450
Saturation/Thermal IR	15-18	Bhattacharyya	68.4848	43.6364	2085.032	451
VGS/Thermal IR	21-15	Correlation	71.1111	42.2222	2086.421	452

Saturation/Thermal IR	12-18	Intersection	71.1111	42.2222	2086.421	453
VGS/Thermal IR	6-15	Intersection	72.3232	41.6162	2087.337	454
Saturation/Thermal IR	3-9	Chi Squared	72.3232	41.6162	2087.337	455
Saturation/Thermal IR	9-18	Bhattacharyya	69.0909	43.2323	2088.972	456
Saturation/Thermal IR	24-18	Intersection	69.0909	43.2323	2088.972	457
Saturation/Thermal IR	3-24	Bhattacharyya	73.1313	41.2121	2088.972	458
Saturation/Thermal IR	12-18	Bhattacharyya	68.8889	43.2323	2095.236	459
Saturation/Thermal IR	12-21	Bhattacharyya	68.8889	43.2323	2095.236	460
Saturation/Thermal IR	15-21	Bhattacharyya	68.4848	43.4343	2096.443	461
VGS/Thermal IR	12-21	Correlation	67.6768	43.8384	2099.457	462
Saturation/Thermal IR	12-21	Intersection	69.4949	42.8283	2099.582	463
Saturation/Thermal IR	21-18	Intersection	69.4949	42.8283	2099.582	464
Saturation/Thermal IR	21-9	Intersection	68.6869	43.2323	2101.541	465
Saturation/Thermal IR	21-21	Intersection	68.6869	43.2323	2101.541	466
Hue/Thermal IR	3-21	Earth Mover's Distance	79.798	38.3838	2102.338	467
Saturation/Thermal IR	24-24	Chi Squared	68.2828	43.4343	2102.83	468
Saturation/Thermal IR	18-15	Chi Squared	68.8889	43.0303	2106.724	469
Hue/Thermal IR	18-21	Earth Mover's Distance	73.7374	40.6061	2108.68	470
VGS/Thermal IR	3-21	Chi Squared	71.5152	41.6162	2110.026	471
Saturation/Thermal IR	9-24	Intersection	69.899	42.4242	2110.521	472
Saturation/Thermal IR	21-18	Bhattacharyya	67.6768	43.6364	2110.822	473
Saturation/Thermal IR	21-9	Bhattacharyya	65.2525	45.0505	2113.418	474
Saturation/Thermal IR	18-9	Bhattacharyya	65.8586	44.6465	2114.823	475
Saturation/Thermal IR	6-15	Bhattacharyya	71.3131	41.6162	2115.803	476
Saturation/Thermal IR	18-18	Intersection	69.697	42.4242	2116.622	477
VGS/Thermal IR	6-18	Earth Mover's Distance	81.6162	37.5758	2117.372	478
Saturation/Thermal IR	24-9	Intersection	68.4848	43.0303	2119.377	479
Saturation/Thermal IR	18-21	Bhattacharyya	68.0808	43.2323	2120.704	480
Saturation/Thermal IR	18-18	Bhattacharyya	67.6768	43.4343	2122.234	481
Saturation/Thermal IR	24-9	Bhattacharyya	65.2525	44.8485	2124.538	482
Saturation/Thermal IR	9-24	Bhattacharyya	68.6869	42.8283	2124.557	483
Saturation/Thermal IR	3-18	Bhattacharyya	73.5354	40.404	2126.029	484
VGS/Thermal IR	6-12	Bhattacharyya	66.4646	44.0404	2128.05	485
VGS/Thermal IR	12-24	Correlation	66.0606	44.2424	2130.396	486
Saturation/Thermal IR	15-21	Intersection	68.4848	42.8283	2130.906	487
Saturation/Thermal IR	21-15	Chi Squared	68.4848	42.8283	2130.906	488
Saturation/Thermal IR	12-24	Bhattacharyya	68.0808	43.0303	2132.191	489
Saturation/Thermal IR	18-21	Intersection	68.2828	42.8283	2137.292	490
Saturation/Thermal IR	15-24	Bhattacharyya	67.8788	43.0303	2138.659	491
Saturation/Thermal IR	24-15	Chi Squared	68.0808	42.8283	2143.719	492
VGS/Thermal IR	6-24	Earth Mover's Distance	82.2222	36.9697	2144.434	493
VGS/Thermal IR	9-24	Earth Mover's Distance	83.6364	36.5657	2145.839	494
Saturation/Thermal IR	3-24	Intersection	72.7273	40.404	2147.742	495
Hue/Thermal IR	3-12	Correlation	64.2424	45.0505	2149.027	496
Saturation/Thermal IR	21-21	Bhattacharyya	67.8788	42.8283	2150.187	497
Saturation/Thermal IR	3-9	Bhattacharyya	73.5354	40	2150.188	498
VGS/Thermal IR	15-24	Correlation	68.8889	42.2222	2153.087	499
VGS/Thermal IR	18-24	Correlation	68.0808	42.6263	2155.288	500
Saturation/Thermal IR	18-24	Bhattacharyya	67.2727	43.0303	2158.311	501
VGS/Thermal IR	9-21	Earth Mover's Distance	83.6364	36.3636	2158.679	502
Saturation/Thermal IR	12-24	Intersection	68.6869	42.2222	2159.392	503
Saturation/Thermal IR	15-24	Intersection	67.8788	42.6263	2161.756	504
Saturation/Thermal IR	24-21	Bhattacharyya	67.8788	42.6263	2161.756	505

Saturation/Thermal IR	18-24	Intersection	67.4747	42.8283	2163.249	506
Saturation/Thermal IR	21-24	Intersection	67.4747	42.8283	2163.249	507
Saturation/Thermal IR	21-24	Bhattacharyya	67.4747	42.8283	2163.249	508
Saturation/Thermal IR	24-24	Bhattacharyya	67.4747	42.8283	2163.249	509
Saturation/Thermal IR	9-15	Bhattacharyya	69.697	41.6162	2163.47	510
VGS/Thermal IR	24-6	Intersection	63.2323	45.4545	2163.538	511
VGS/Thermal IR	6-12	Chi Squared	67.0707	43.0303	2164.943	512
Saturation/Thermal IR	3-15	Intersection	73.3333	39.798	2167.697	513
Saturation/Thermal IR	6-12	Bhattacharyya	69.899	41.4141	2169.189	514
Hue/Thermal IR	3-24	Earth Mover's Distance	80.202	37.1717	2169.678	515
VGS/Thermal IR	18-9	Correlation	72.3232	40.202	2170.903	516
Saturation/Thermal IR	3-12	Bhattacharyya	72.3232	40.202	2170.903	517
Saturation/Thermal IR	24-18	Bhattacharyya	67.4747	42.6263	2174.818	518
VGS/Thermal IR	3-24	Chi Squared	70.101	41.2121	2174.984	519
VGS/Thermal IR	6-12	Intersection	68.0808	42.2222	2178.555	520
VGS/Thermal IR	3-21	Bhattacharyya	70.303	41.0101	2180.86	521
VGS/Thermal IR	9-6	Chi Squared	67.2727	42.6263	2181.409	522
Saturation/Thermal IR	24-21	Intersection	67.2727	42.6263	2181.409	523
VGS/Thermal IR	15-6	Intersection	69.0909	41.6162	2182.02	524
Saturation/Thermal IR	3-12	Chi Squared	70.9091	40.6061	2186.958	525
VGS/Thermal IR	15-21	Correlation	69.697	41.2121	2187.144	526
Saturation/Thermal IR	12-15	Bhattacharyya	69.0909	41.4141	2193.84	527
Saturation/Thermal IR	9-12	Bhattacharyya	67.8788	42.0202	2196.714	528
Saturation/Thermal IR	18-12	Chi Squared	66.0606	43.0303	2198.715	529
VGS/Thermal IR	12-6	Chi Squared	63.4343	44.6465	2200.53	530
VGS/Thermal IR	18-6	Intersection	65.2525	43.4343	2203.534	531
VGS/Thermal IR	24-12	Correlation	63.6364	44.4444	2204.368	532
Saturation/Thermal IR	15-15	Bhattacharyya	68.6869	41.4141	2206.409	533
Saturation/Thermal IR	18-15	Bhattacharyya	67.8788	41.8182	2208.447	534
VGS/Thermal IR	3-24	Bhattacharyya	68.8889	41.2121	2211.959	535
Saturation/Thermal IR	3-21	Intersection	73.9394	38.7879	2213.038	536
Saturation/Thermal IR	15-12	Chi Squared	66.6667	42.4242	2213.041	537
VGS/Thermal IR	12-6	Intersection	64.6465	43.6364	2213.363	538
Saturation/Thermal IR	6-12	Chi Squared	67.6768	41.8182	2214.956	539
VGS/Thermal IR	15-15	Correlation	70.7071	40.202	2216.937	540
Saturation/Thermal IR	24-24	Intersection	66.8687	42.2222	2217.979	541
VGS/Thermal IR	9-6	Correlation	71.9192	39.596	2218.587	542
VGS/Thermal IR	9-6	Bhattacharyya	65.4545	43.0303	2219.469	543
VGS/Thermal IR	12-15	Correlation	66.4646	42.4242	2219.798	544
Saturation/Thermal IR	12-12	Chi Squared	66.4646	42.4242	2219.798	545
Saturation/Thermal IR	21-12	Chi Squared	66.0606	42.6263	2221.812	546
Saturation/Thermal IR	15-12	Bhattacharyya	66.6667	42.2222	2224.692	547
Saturation/Thermal IR	24-15	Bhattacharyya	67.6768	41.6162	2226.729	548
VGS/Thermal IR	21-9	Correlation	69.899	40.404	2228.877	549
VGS/Thermal IR	18-6	Chi Squared	60.6061	46.0606	2230.669	550
Saturation/Thermal IR	21-15	Bhattacharyya	67.8788	41.4141	2232.04	551
VGS/Thermal IR	12-6	Bhattacharyya	62.8283	44.4444	2234.08	552
Saturation/Thermal IR	12-12	Bhattacharyya	67.0707	41.8182	2234.73	553
Saturation/Thermal IR	24-12	Chi Squared	65.2525	42.8283	2237.996	554
VGS/Thermal IR	6-15	Earth Mover's Distance	80.6061	35.9596	2238.648	555
Saturation/Thermal IR	6-18	Correlation	69.4949	40.404	2241.122	556
Saturation/Thermal IR	9-12	Chi Squared	66.0606	42.2222	2245.079	557
Saturation/Thermal IR	3-15	Bhattacharyya	73.1313	38.5859	2246.809	558

Hue/Thermal IR	24-24	Earth Mover's Distance	69.697	40.202	2247.036	559
Saturation/Thermal IR	3-18	Correlation	71.7172	39.1919	2248.771	560
Hue/Thermal IR	9-9	Earth Mover's Distance	74.9495	37.7778	2249.565	561
VGS/Thermal IR	21-12	Correlation	66.2626	42.0202	2249.935	562
VGS/Thermal IR	9-18	Earth Mover's Distance	81.2121	35.5556	2253.033	563
VGS/Thermal IR	21-6	Chi Squared	61.6162	44.8485	2257.502	564
VGS/Thermal IR	21-6	Intersection	63.0303	43.8384	2260.442	565
VGS/Thermal IR	18-15	Correlation	68.0808	40.8081	2261.258	566
VGS/Thermal IR	3-18	Bhattacharyya	66.6667	41.4141	2271.708	567
VGS/Thermal IR	15-6	Chi Squared	63.8384	43.0303	2276.604	568
VGS/Thermal IR	3-18	Chi Squared	68.6869	40.202	2278.156	569
Saturation/Thermal IR	3-9	Intersection	71.5152	38.7879	2279.153	570
VGS/Thermal IR	15-9	Correlation	68.4848	40.202	2284.504	571
Saturation/Thermal IR	18-12	Bhattacharyya	65.2525	42.0202	2284.523	572
VGS/Thermal IR	9-15	Earth Mover's Distance	80.8081	35.1515	2286.828	573
VGS/Thermal IR	6-18	Correlation	74.1414	37.3737	2295.36	574
Saturation/Thermal IR	6-9	Earth Mover's Distance	70.9091	38.7879	2296.601	575
Saturation/Thermal IR	6-24	Correlation	67.2727	40.6061	2299.356	576
VGS/Thermal IR	12-24	Earth Mover's Distance	77.9798	35.7576	2305.988	577
Saturation/Thermal IR	21-12	Bhattacharyya	65.2525	41.6162	2308.028	578
Hue/Thermal IR	18-18	Earth Mover's Distance	68.8889	39.596	2308.272	579
Hue/Thermal IR	21-21	Earth Mover's Distance	68.8889	39.596	2308.272	580
VGS/Thermal IR	3-15	Chi Squared	68.0808	40	2309.418	581
VGS/Thermal IR	18-6	Bhattacharyya	59.596	45.2525	2314.886	582
VGS/Thermal IR	3-9	Chi Squared	65.6566	41.2121	2317.743	583
Hue/Thermal IR	15-15	Earth Mover's Distance	68.8889	39.3939	2320.5	584
VGS/Thermal IR	15-6	Bhattacharyya	62.8283	42.8283	2325.169	585
VGS/Thermal IR	6-6	Intersection	70.7071	38.3838	2327.315	586
Saturation/Thermal IR	15-24	Earth Mover's Distance	71.1111	38.1818	2328.029	587
VGS/Thermal IR	3-24	Intersection	71.3131	37.9798	2334.722	588
VGS/Thermal IR	24-6	Chi Squared	60.202	44.4444	2335.153	589
VGS/Thermal IR	12-21	Earth Mover's Distance	77.1717	35.5556	2337.106	590
Saturation/Thermal IR	6-21	Correlation	68.2828	39.3939	2339.54	591
VGS/Thermal IR	3-21	Intersection	71.9192	37.5758	2342.656	592
VGS/Thermal IR	21-6	Bhattacharyya	59.3939	44.8485	2345.272	593
Hue/Thermal IR	12-12	Earth Mover's Distance	68.4848	39.1919	2345.416	594
VGS/Thermal IR	15-24	Earth Mover's Distance	79.1919	34.7475	2345.433	595
VGS/Thermal IR	15-12	Correlation	63.8384	41.8182	2346.392	596
VGS/Thermal IR	18-12	Correlation	63.8384	41.8182	2346.392	597
VGS/Thermal IR	24-9	Correlation	65.8586	40.6061	2346.635	598
Saturation/Thermal IR	24-12	Bhattacharyya	65.0505	41.0101	2350.638	599
Hue/Thermal IR	6-6	Correlation	57.3737	46.2626	2352.355	600
VGS/Thermal IR	3-15	Bhattacharyya	65.8586	40.404	2358.659	601
VGS/Thermal IR	6-12	Earth Mover's Distance	76.7677	35.3535	2359.455	602
VGS/Thermal IR	3-12	Chi Squared	66.4646	40	2362.312	603
Saturation/Thermal IR	12-18	Correlation	67.4747	39.3939	2365.497	604
Saturation/Thermal IR	24-12	Intersection	64.2424	41.2121	2367.312	605
Saturation/Thermal IR	15-18	Correlation	67.6768	39.1919	2371.207	606
Saturation/Thermal IR	18-18	Correlation	67.2727	39.3939	2372.088	607
Saturation/Thermal IR	21-18	Correlation	67.2727	39.3939	2372.088	608
Saturation/Thermal IR	6-12	Intersection	63.6364	41.4141	2377.31	609
VGS/Thermal IR	3-12	Bhattacharyya	67.0707	39.3939	2378.719	610
VGS/Thermal IR	3-9	Bhattacharyya	63.4343	41.4141	2384.679	611

Saturation/Thermal IR	18-12	Intersection	63.4343	41.4141	2384.679	612
Saturation/Thermal IR	9-18	Correlation	66.8687	39.3939	2385.391	613
Saturation/Thermal IR	15-12	Intersection	63.6364	41.2121	2389.164	614
Saturation/Thermal IR	21-12	Intersection	64.2424	40.8081	2391.143	615
Saturation/Thermal IR	9-21	Earth Mover's Distance	74.5455	35.5556	2400.506	616
Saturation/Thermal IR	9-9	Correlation	63.4343	41.0101	2408.429	617
Saturation/Thermal IR	6-15	Correlation	65.4545	39.798	2408.836	618
Hue/Thermal IR	6-6	Earth Mover's Distance	67.2727	38.7879	2408.999	619
VGS/Thermal IR	24-6	Bhattacharyya	58.3838	44.4444	2409.166	620
Saturation/Thermal IR	24-18	Correlation	66.8687	38.9899	2409.958	621
Saturation/Thermal IR	9-18	Earth Mover's Distance	73.1313	35.9596	2411.55	622
Saturation/Thermal IR	18-9	Correlation	64.4444	40.202	2420.001	623
Saturation/Thermal IR	12-12	Intersection	62.4242	41.4141	2422.124	624
Saturation/Thermal IR	12-24	Earth Mover's Distance	72.7273	35.9596	2422.486	625
VGS/Thermal IR	15-21	Earth Mover's Distance	77.9798	33.9394	2424.446	626
VGS/Thermal IR	6-9	Earth Mover's Distance	77.3737	34.1414	2424.652	627
Saturation/Thermal IR	21-9	Correlation	63.6364	40.6061	2424.973	628
Saturation/Thermal IR	15-9	Correlation	64.2424	40.202	2427.203	629
VGS/Thermal IR	3-18	Intersection	70.7071	36.7677	2428.199	630
Hue/Thermal IR	3-6	Correlation	56.3636	45.6566	2428.67	631
VGS/Thermal IR	3-21	Earth Mover's Distance	77.7778	33.9394	2428.915	632
Saturation/Thermal IR	15-24	Correlation	64.8485	39.798	2429.954	633
Saturation/Thermal IR	6-18	Earth Mover's Distance	78.1818	33.7374	2433.383	634
Saturation/Thermal IR	3-21	Correlation	70.101	36.9697	2433.384	635
Saturation/Thermal IR	9-15	Earth Mover's Distance	70.101	36.9697	2433.384	636
Saturation/Thermal IR	3-9	Earth Mover's Distance	77.5758	33.9394	2433.424	637
VGS/Thermal IR	9-12	Earth Mover's Distance	76.9697	34.1414	2433.875	638
Saturation/Thermal IR	6-6	Bhattacharyya	64.0404	40.202	2434.447	639
VGS/Thermal IR	3-24	Earth Mover's Distance	79.3939	33.3333	2434.53	640
Saturation/Thermal IR	6-12	Earth Mover's Distance	70.9091	36.5657	2435.095	641
Saturation/Thermal IR	6-9	Correlation	63.2323	40.6061	2439.75	642
Saturation/Thermal IR	12-9	Correlation	63.2323	40.6061	2439.75	643
Saturation/Thermal IR	6-6	Chi Squared	62.8283	40.8081	2442.708	644
Saturation/Thermal IR	12-18	Earth Mover's Distance	69.697	36.9697	2445.545	645
Saturation/Thermal IR	12-21	Earth Mover's Distance	70.5051	36.5657	2446.93	646
Saturation/Thermal IR	21-24	Correlation	64.6465	39.596	2449.257	647
Saturation/Thermal IR	12-6	Bhattacharyya	64.2424	39.798	2451.443	648
VGS/Thermal IR	6-6	Bhattacharyya	63.8384	40	2453.831	649
Saturation/Thermal IR	24-9	Correlation	63.8384	40	2453.831	650
Saturation/Thermal IR	3-24	Correlation	68.8889	37.1717	2457.648	651
Saturation/Thermal IR	15-21	Earth Mover's Distance	69.2929	36.9697	2457.872	652
Saturation/Thermal IR	9-6	Chi Squared	63.0303	40.404	2459.221	653
Saturation/Thermal IR	6-21	Earth Mover's Distance	77.3737	33.5354	2464.746	654
VGS/Thermal IR	6-21	Correlation	69.899	36.5657	2464.99	655
Saturation/Thermal IR	18-24	Correlation	63.8384	39.798	2465.971	656
Saturation/Thermal IR	9-24	Correlation	64.8485	39.1919	2466.626	657
Saturation/Thermal IR	12-6	Chi Squared	62.8283	40.404	2466.709	658
VGS/Thermal IR	12-15	Earth Mover's Distance	73.9394	34.7475	2468.522	659
VGS/Thermal IR	18-24	Earth Mover's Distance	77.1717	33.5354	2469.337	660
VGS/Thermal IR	3-9	Intersection	65.4545	38.7879	2470.156	661
VGS/Thermal IR	3-15	Intersection	68.8889	36.9697	2470.36	662
Saturation/Thermal IR	24-24	Correlation	64.2424	39.3939	2475.853	663
Saturation/Thermal IR	6-15	Earth Mover's Distance	74.1414	34.5455	2476.479	664

Saturation/Thermal IR	18-24	Earth Mover's Distance	67.8788	37.3737	2476.912	665
Saturation/Thermal IR	15-18	Earth Mover's Distance	67.4747	37.5758	2477.338	666
Saturation/Thermal IR	9-6	Bhattacharyya	63.8384	39.596	2478.152	667
Saturation/Thermal IR	12-24	Correlation	63.8384	39.596	2478.152	668
VGS/Thermal IR	3-18	Earth Mover's Distance	77.9798	33.1313	2478.156	669
Saturation/Thermal IR	9-12	Intersection	62.8283	40.202	2478.768	670
Saturation/Thermal IR	9-12	Earth Mover's Distance	66.2626	38.1818	2479.851	671
VGS/Thermal IR	12-18	Earth Mover's Distance	75.5556	33.9394	2480.766	672
Saturation/Thermal IR	9-21	Correlation	65.4545	38.5859	2482.542	673
VGS/Thermal IR	6-6	Chi Squared	64.6465	38.9899	2486.051	674
Saturation/Thermal IR	9-24	Earth Mover's Distance	76.3636	33.5354	2488.111	675
Saturation/Thermal IR	9-9	Earth Mover's Distance	64.2424	39.1919	2488.115	676
Saturation/Thermal IR	15-6	Bhattacharyya	64.2424	39.1919	2488.115	677
Saturation/Thermal IR	21-24	Earth Mover's Distance	66.6667	37.7778	2491.356	678
Saturation/Thermal IR	6-24	Earth Mover's Distance	77.9798	32.9293	2491.684	679
Hue/Thermal IR	24-21	Earth Mover's Distance	66.2626	37.9798	2492.359	680
Hue/Thermal IR	21-18	Earth Mover's Distance	65.4545	38.3838	2494.974	681
Saturation/Thermal IR	18-6	Bhattacharyya	63.0303	39.798	2495.52	682
Saturation/Thermal IR	21-6	Chi Squared	63.0303	39.798	2495.52	683
Saturation/Thermal IR	12-15	Earth Mover's Distance	67.2727	37.3737	2496.565	684
Saturation/Thermal IR	15-6	Chi Squared	63.6364	39.3939	2497.705	685
Saturation/Thermal IR	18-21	Earth Mover's Distance	66.0606	37.9798	2499.194	686
VGS/Thermal IR	6-24	Correlation	68.6869	36.5657	2502.21	687
VGS/Thermal IR	18-21	Earth Mover's Distance	75.1515	33.7374	2504.09	688
Saturation/Thermal IR	12-21	Correlation	65.2525	38.1818	2514.439	689
Saturation/Thermal IR	15-21	Correlation	64.8485	38.3838	2516.092	690
Saturation/Thermal IR	9-15	Correlation	64.0404	38.7879	2520.007	691
Saturation/Thermal IR	18-21	Correlation	64.0404	38.7879	2520.007	692
Saturation/Thermal IR	21-21	Correlation	64.0404	38.7879	2520.007	693
Saturation/Thermal IR	18-6	Chi Squared	62.6263	39.596	2522.718	694
VGS/Thermal IR	6-15	Correlation	70.5051	35.3535	2524.56	695
Saturation/Thermal IR	3-6	Bhattacharyya	65.2525	37.9798	2526.947	696
Saturation/Thermal IR	24-21	Correlation	63.8384	38.7879	2527.291	697
Saturation/Thermal IR	21-6	Bhattacharyya	62.8283	39.3939	2527.417	698
VGS/Thermal IR	12-12	Correlation	60.6061	40.8081	2527.78	699
Saturation/Thermal IR	12-15	Correlation	63.4343	38.9899	2529.641	700
Saturation/Thermal IR	3-15	Earth Mover's Distance	76.7677	32.7273	2532.678	701
VGS/Thermal IR	21-24	Earth Mover's Distance	74.5455	33.5354	2532.737	702
Saturation/Thermal IR	24-6	Bhattacharyya	62.0202	39.596	2545.554	703
Saturation/Thermal IR	24-6	Chi Squared	61.8182	39.596	2553.247	704
Saturation/Thermal IR	21-15	Correlation	63.4343	38.5859	2554.371	705
Saturation/Thermal IR	18-15	Correlation	63.0303	38.7879	2556.84	706
Saturation/Thermal IR	24-15	Correlation	63.6364	38.3838	2559.434	707
VGS/Thermal IR	12-9	Correlation	64.6465	37.7778	2560.736	708
Saturation/Thermal IR	3-12	Intersection	65.6566	37.1717	2563.432	709
Saturation/Thermal IR	15-15	Correlation	62.8283	38.7879	2564.328	710
VGS/Thermal IR	3-15	Earth Mover's Distance	74.1414	33.1313	2570.045	711
Saturation/Thermal IR	3-15	Correlation	66.8687	36.3636	2573.637	712
Saturation/Thermal IR	3-18	Earth Mover's Distance	78.3838	31.5152	2578.714	713
VGS/Thermal IR	3-9	Earth Mover's Distance	75.9596	32.3232	2579.045	714
VGS/Thermal IR	15-18	Earth Mover's Distance	75.1515	32.5253	2585.142	715
Saturation/Thermal IR	15-12	Correlation	60.404	39.798	2596.062	716
Saturation/Thermal IR	3-12	Earth Mover's Distance	74.1414	32.7273	2597.142	717

Saturation/Thermal IR	3-21	Earth Mover's Distance	77.9798	31.1111	2615.285	718
VGS/Thermal IR	9-9	Earth Mover's Distance	74.7475	32.1212	2622.61	719
Saturation/Thermal IR	18-12	Correlation	60	39.596	2624.322	720
Hue/Thermal IR	18-15	Earth Mover's Distance	64.2424	36.9697	2625.712	721
VGS/Thermal IR	21-6	Correlation	66.0606	35.9596	2626.528	722
Saturation/Thermal IR	24-24	Earth Mover's Distance	63.8384	37.1717	2627.528	723
VGS/Thermal IR	24-6	Correlation	61.0101	38.7879	2633.567	724
Saturation/Thermal IR	3-6	Chi Squared	63.2323	37.3737	2636.959	725
Saturation/Thermal IR	21-21	Earth Mover's Distance	63.2323	37.3737	2636.959	726
Saturation/Thermal IR	18-18	Earth Mover's Distance	63.4343	37.1717	2642.223	727
Saturation/Thermal IR	15-15	Earth Mover's Distance	62.8283	37.3737	2651.894	728
Saturation/Thermal IR	3-24	Earth Mover's Distance	78.7879	30.303	2653.812	729
VGS/Thermal IR	21-21	Earth Mover's Distance	71.7172	32.7273	2662.766	730
VGS/Thermal IR	15-15	Earth Mover's Distance	70.303	33.3333	2663.18	731
VGS/Thermal IR	6-12	Correlation	63.0303	36.9697	2669.789	732
Saturation/Thermal IR	6-12	Correlation	60.6061	38.3838	2674.218	733
VGS/Thermal IR	3-12	Intersection	64.6465	35.9596	2675.521	734
Saturation/Thermal IR	24-12	Correlation	59.596	38.9899	2677.358	735
Saturation/Thermal IR	12-12	Correlation	59.1919	39.1919	2681.463	736
Hue/Thermal IR	3-3	Chi Squared	54.1414	42.8283	2685.807	737
Hue/Thermal IR	9-3	Chi Squared	46.2626	50.101	2688.809	738
Saturation/Thermal IR	21-12	Correlation	59.798	38.5859	2693.946	739
VGS/Thermal IR	12-12	Earth Mover's Distance	68.6869	33.5354	2699.027	740
Saturation/Thermal IR	9-12	Correlation	59.798	38.3838	2706.378	741
Saturation/Thermal IR	24-6	Intersection	62.0202	36.9697	2707.642	742
Hue/Thermal IR	15-12	Earth Mover's Distance	62.6263	36.5657	2710.352	743
VGS/Thermal IR	18-6	Correlation	60	38.1818	2710.745	744
VGS/Thermal IR	3-18	Correlation	67.8788	33.7374	2711.252	745
VGS/Thermal IR	24-24	Earth Mover's Distance	71.9192	31.9192	2711.763	746
VGS/Thermal IR	3-12	Earth Mover's Distance	72.7273	31.5152	2716.984	747
VGS/Thermal IR	18-18	Earth Mover's Distance	70.7071	32.3232	2719.112	748
VGS/Thermal IR	6-9	Correlation	68.6869	33.1313	2725.967	749
Hue/Thermal IR	12-9	Earth Mover's Distance	64.2424	35.3535	2728.888	750
VGS/Thermal IR	3-24	Correlation	70.303	32.3232	2731.031	751
Saturation/Thermal IR	24-21	Earth Mover's Distance	60.404	37.5758	2732.312	752
VGS/Thermal IR	3-21	Correlation	70.5051	31.9192	2752.472	753
VGS/Thermal IR	3-6	Chi Squared	61.8182	36.3636	2753.721	754
Saturation/Thermal IR	21-6	Intersection	59.798	37.5758	2756.491	755
Saturation/Thermal IR	21-18	Earth Mover's Distance	59.596	37.5758	2764.632	756
Saturation/Thermal IR	3-9	Correlation	63.2323	35.1515	2778.596	757
Saturation/Thermal IR	12-12	Earth Mover's Distance	60	36.9697	2786.409	758
Saturation/Thermal IR	18-15	Earth Mover's Distance	58.9899	37.5758	2789.305	759
Saturation/Thermal IR	12-6	Intersection	57.7778	38.1818	2802.102	760
Hue/Thermal IR	24-18	Earth Mover's Distance	61.2121	35.9596	2802.837	761
Saturation/Thermal IR	18-6	Intersection	58.7879	37.3737	2810.245	762
VGS/Thermal IR	3-6	Bhattacharyya	60.202	36.1616	2829.611	763
VGS/Thermal IR	21-18	Earth Mover's Distance	69.2929	31.3131	2830.408	764
Saturation/Thermal IR	12-9	Earth Mover's Distance	56.5657	38.1818	2854.014	765
Saturation/Thermal IR	3-12	Correlation	59.1919	36.3636	2857.446	766
Hue/Thermal IR	9-3	Bhattacharyya	44.8485	48.2828	2858.178	767
Saturation/Thermal IR	15-6	Intersection	56.9697	37.7778	2861.604	768
VGS/Thermal IR	24-21	Earth Mover's Distance	68.4848	31.1111	2869.444	769
Hue/Thermal IR	21-15	Earth Mover's Distance	60.202	35.3535	2881.525	770

VGS/Thermal IR	18-15	Earth Mover's Distance	67.6768	31.1111	2895.235	771
VGS/Thermal IR	6-6	Earth Mover's Distance	68.0808	30.9091	2896.194	772
Saturation/Thermal IR	9-6	Intersection	54.7475	38.7879	2897.355	773
Hue/Thermal IR	6-3	Chi Squared	46.6667	45.6566	2898.823	774
VGS/Thermal IR	12-9	Earth Mover's Distance	67.2727	30.9091	2922.314	775
Saturation/Thermal IR	15-12	Earth Mover's Distance	55.7576	37.5758	2927.085	776
Hue/Thermal IR	6-3	Bhattacharyya	46.4646	45.2525	2931.664	777
VGS/Thermal IR	24-18	Earth Mover's Distance	67.2727	30.7071	2936.291	778
Hue/Thermal IR	3-3	Bhattacharyya	50.101	41.6162	2949.289	779
VGS/Thermal IR	15-12	Earth Mover's Distance	66.8687	30.7071	2949.595	780
VGS/Thermal IR	12-6	Correlation	59.596	34.5455	2958.387	781
VGS/Thermal IR	21-15	Earth Mover's Distance	65.8586	30.9091	2969.594	782
Hue/Thermal IR	15-3	Chi Squared	39.596	52.1212	2970.511	783
VGS/Thermal IR	3-9	Correlation	66.0606	30.5051	2990.712	784
Hue/Thermal IR	12-3	Bhattacharyya	38.9899	52.3232	2997.655	785
Hue/Thermal IR	21-3	Chi Squared	39.596	51.5152	2999.71	786
Saturation/Thermal IR	24-18	Earth Mover's Distance	55.1515	36.7677	3004.856	787
Hue/Thermal IR	15-9	Earth Mover's Distance	59.3939	33.7374	3019.794	788
Hue/Thermal IR	18-3	Chi Squared	39.3939	51.3131	3021.757	789
Hue/Thermal IR	21-3	Bhattacharyya	38.9899	51.7172	3026.731	790
VGS/Thermal IR	3-15	Correlation	65.6566	30.101	3032.67	791
Saturation/Thermal IR	6-6	Intersection	53.1313	37.7778	3034.139	792
Hue/Thermal IR	12-3	Chi Squared	38.3838	52.3232	3034.817	793
Saturation/Thermal IR	21-15	Earth Mover's Distance	54.7475	36.5657	3035.85	794
VGS/Thermal IR	9-6	Earth Mover's Distance	66.2626	29.697	3040.362	795
Hue/Thermal IR	18-3	Bhattacharyya	39.3939	50.9091	3041.508	796
Hue/Thermal IR	18-12	Earth Mover's Distance	56.9697	34.7475	3054.748	797
VGS/Thermal IR	18-12	Earth Mover's Distance	63.6364	30.7071	3061.909	798
Hue/Thermal IR	15-3	Bhattacharyya	38.1818	51.5152	3086.133	799
Saturation/Thermal IR	3-6	Earth Mover's Distance	58.3838	33.3333	3088.178	800
Hue/Thermal IR	9-6	Earth Mover's Distance	56.7677	34.3434	3089.91	801
VGS/Thermal IR	15-6	Correlation	56.3636	34.5455	3094.213	802
VGS/Thermal IR	24-15	Earth Mover's Distance	63.8384	29.697	3125.087	803
Hue/Thermal IR	24-15	Earth Mover's Distance	56.5657	33.9394	3125.271	804
Hue/Thermal IR	24-3	Chi Squared	37.5758	51.1111	3143.453	805
Saturation/Thermal IR	18-12	Earth Mover's Distance	51.5152	37.1717	3149.086	806
Hue/Thermal IR	24-3	Bhattacharyya	37.1717	51.3131	3158.905	807
VGS/Thermal IR	15-9	Earth Mover's Distance	65.2525	28.2828	3175.373	808
Saturation/Thermal IR	15-9	Earth Mover's Distance	52.3232	35.7576	3200.082	809
Saturation/Thermal IR	24-6	Correlation	52.3232	35.7576	3200.082	810
VGS/Thermal IR	3-6	Earth Mover's Distance	61.8182	29.697	3200.181	811
Saturation/Thermal IR	21-6	Correlation	51.9192	35.7576	3219.425	812
Saturation/Thermal IR	15-6	Correlation	50.9091	36.3636	3229.754	813
Hue/Thermal IR	21-12	Earth Mover's Distance	54.7475	33.5354	3232.666	814
Saturation/Thermal IR	18-6	Correlation	51.1111	35.9596	3245.649	815
VGS/Thermal IR	3-6	Intersection	58.7879	30.7071	3249.972	816
Saturation/Thermal IR	24-15	Earth Mover's Distance	52.3232	34.9495	3252.322	817
VGS/Thermal IR	3-12	Correlation	61.0101	29.0909	3274.156	818
Saturation/Thermal IR	12-6	Correlation	49.4949	36.7677	3274.544	819
Saturation/Thermal IR	6-6	Earth Mover's Distance	53.3333	33.3333	3311.115	820
Saturation/Thermal IR	9-6	Correlation	49.899	35.7576	3318.598	821
Hue/Thermal IR	18-9	Earth Mover's Distance	55.5556	31.7172	3318.923	822
VGS/Thermal IR	21-12	Earth Mover's Distance	61.4141	28.0808	3330.622	823

VGS/Thermal IR	6-6	Correlation	57.5758	30.101	3342.841	824
Hue/Thermal IR	3-3	Intersection	44.6465	39.798	3344.145	825
Saturation/Thermal IR	3-6	Intersection	52.5253	33.3333	3349.148	826
VGS/Thermal IR	18-9	Earth Mover's Distance	60.6061	28.0808	3362.125	827
Saturation/Thermal IR	6-6	Correlation	47.2727	36.9697	3376.493	828
Saturation/Thermal IR	21-12	Earth Mover's Distance	50.5051	34.1414	3393.55	829
Hue/Thermal IR	24-12	Earth Mover's Distance	52.7273	32.3232	3407.429	830
VGS/Thermal IR	24-12	Earth Mover's Distance	59.3939	27.8788	3425.161	831
VGS/Thermal IR	12-6	Earth Mover's Distance	57.9798	28.4848	3440.061	832
Hue/Thermal IR	12-6	Earth Mover's Distance	51.3131	32.1212	3488.973	833
Saturation/Thermal IR	18-9	Earth Mover's Distance	49.4949	33.3333	3497.607	834
VGS/Thermal IR	21-9	Earth Mover's Distance	59.1919	26.4646	3536.378	835
Saturation/Thermal IR	9-6	Earth Mover's Distance	49.899	32.1212	3558.821	836
Saturation/Thermal IR	24-12	Earth Mover's Distance	47.8788	32.7273	3621.118	837
Hue/Thermal IR	21-9	Earth Mover's Distance	51.9192	29.697	3627.138	838
Hue/Thermal IR	15-3	Intersection	31.3131	49.0909	3654.813	839
Saturation/Thermal IR	3-6	Correlation	44.4444	34.9495	3658.996	840
Hue/Thermal IR	9-3	Intersection	33.7374	45.8586	3661.012	841
Hue/Thermal IR	3-3	Correlation	38.7879	40.202	3661.361	842
Saturation/Thermal IR	21-9	Earth Mover's Distance	46.4646	33.1313	3668.731	843
Hue/Thermal IR	6-3	Intersection	34.7475	44.0404	3694.683	844
VGS/Thermal IR	12-3	Chi Squared	41.8182	35.7576	3756.104	845
Hue/Thermal IR	18-3	Intersection	30.101	48.6869	3759.452	846
VGS/Thermal IR	12-3	Bhattacharyya	41.0101	36.3636	3764.7	847
Hue/Thermal IR	21-3	Intersection	29.0909	49.2929	3799.655	848
VGS/Thermal IR	24-9	Earth Mover's Distance	56.1616	24.6465	3799.978	849
Hue/Thermal IR	24-9	Earth Mover's Distance	48.8889	29.2929	3805.919	850
Saturation/Thermal IR	12-6	Earth Mover's Distance	46.4646	30.9091	3819.796	851
Hue/Thermal IR	15-6	Earth Mover's Distance	47.2727	30.101	3833.019	852
Hue/Thermal IR	3-3	Earth Mover's Distance	40.6061	35.1515	3866.482	853
Saturation/Thermal IR	24-9	Earth Mover's Distance	43.6364	32.3232	3878.502	854
VGS/Thermal IR	6-3	Chi Squared	48.6869	28.2828	3888.196	855
Hue/Thermal IR	12-3	Intersection	28.0808	48.8889	3892.358	856
VGS/Thermal IR	15-6	Earth Mover's Distance	54.3434	24.4444	3896.587	857
Hue/Thermal IR	24-3	Intersection	27.4747	49.4949	3905.342	858
Hue/Thermal IR	15-3	Correlation	26.4646	50.101	3948.683	859
Hue/Thermal IR	9-3	Correlation	29.2929	45.8586	3965.393	860
VGS/Thermal IR	6-3	Bhattacharyya	46.4646	28.4848	3990.231	861
VGS/Thermal IR	18-3	Bhattacharyya	36.5657	36.5657	4023.91	862
Saturation/Thermal IR	6-3	Bhattacharyya	42.2222	31.3131	4028.082	863
Saturation/Thermal IR	3-3	Chi Squared	45.6566	28.2828	4048.281	864
Hue/Thermal IR	24-3	Correlation	23.6364	51.9192	4071.581	865
VGS/Thermal IR	21-3	Bhattacharyya	35.3535	36.9697	4075.994	866
Saturation/Thermal IR	15-6	Earth Mover's Distance	43.0303	29.899	4079.848	867
Hue/Thermal IR	12-3	Correlation	23.6364	51.5152	4091.088	868
Saturation/Thermal IR	6-3	Chi Squared	43.0303	29.697	4094.029	869
VGS/Thermal IR	18-6	Earth Mover's Distance	51.1111	23.8384	4095.357	870
Saturation/Thermal IR	9-3	Bhattacharyya	41.2121	31.1111	4100.849	871
Hue/Thermal IR	21-3	Correlation	24.6465	49.697	4104.271	872
VGS/Thermal IR	24-3	Bhattacharyya	35.3535	36.3636	4114.381	873
Hue/Thermal IR	18-6	Earth Mover's Distance	44.4444	28.2828	4114.891	874
VGS/Thermal IR	15-3	Chi Squared	40	31.9192	4117.498	875
Saturation/Thermal IR	3-3	Bhattacharyya	44.8485	27.8788	4121.578	876

VGS/Thermal IR	9-3	Bhattacharyya	38.7879	32.9293	4122.7	877
VGS/Thermal IR	15-3	Bhattacharyya	37.9798	33.5354	4132.024	878
VGS/Thermal IR	18-3	Chi Squared	36.5657	34.5455	4154.101	879
Hue/Thermal IR	18-3	Correlation	24.6465	48.6869	4155.592	880
Hue/Thermal IR	6-3	Correlation	28.0808	43.8384	4163.248	881
VGS/Thermal IR	12-3	Intersection	37.9798	32.7273	4186.061	882
Saturation/Thermal IR	9-3	Chi Squared	41.8182	29.2929	4192.308	883
VGS/Thermal IR	21-3	Chi Squared	35.5556	34.9495	4192.324	884
VGS/Thermal IR	24-3	Chi Squared	35.7576	34.7475	4192.487	885
Saturation/Thermal IR	12-3	Bhattacharyya	40.202	30.303	4216.736	886
VGS/Thermal IR	9-3	Chi Squared	38.5859	31.7172	4217.116	887
Saturation/Thermal IR	18-3	Bhattacharyya	38.9899	30.9091	4247.892	888
Saturation/Thermal IR	15-3	Chi Squared	40.6061	29.0909	4277.868	889
Saturation/Thermal IR	12-3	Chi Squared	40	29.4949	4285.485	890
Saturation/Thermal IR	21-3	Bhattacharyya	38.9899	30.303	4289.952	891
Saturation/Thermal IR	15-3	Bhattacharyya	39.3939	29.899	4293.625	892
Hue/Thermal IR	21-6	Earth Mover's Distance	42.2222	27.4747	4299.097	893
VGS/Thermal IR	3-6	Correlation	44.4444	25.6566	4306.683	894
Saturation/Thermal IR	18-3	Chi Squared	40.404	28.6869	4318.621	895
VGS/Thermal IR	21-6	Earth Mover's Distance	47.2727	23.2323	4336.724	896
Saturation/Thermal IR	18-6	Earth Mover's Distance	39.798	28.8889	4340.535	897
Saturation/Thermal IR	24-3	Bhattacharyya	37.9798	30.303	4352.089	898
Saturation/Thermal IR	21-3	Chi Squared	38.9899	28.8889	4389.51	899
VGS/Thermal IR	24-3	Intersection	32.3232	34.3434	4445.469	900
Saturation/Thermal IR	24-3	Chi Squared	38.3838	28.2828	4469.956	901
VGS/Thermal IR	24-6	Earth Mover's Distance	45.2525	22.2222	4523.337	902
Hue/Thermal IR	24-6	Earth Mover's Distance	39.596	26.4646	4528.049	903
Hue/Grey	18-21	Chi Squared	29.2929	35.9596	4550.333	904
VGS/Thermal IR	6-3	Intersection	40.202	25.4545	4566.416	905
VGS/Thermal IR	15-3	Intersection	36.9697	28.0808	4572.595	906
Hue/Grey	24-21	Chi Squared	29.0909	35.7576	4577.593	907
Hue/Grey	21-21	Chi Squared	28.8889	35.9596	4578.981	908
Saturation/Thermal IR	21-6	Earth Mover's Distance	36.7677	28.0808	4585.348	909
Hue/Grey	21-12	Bhattacharyya	27.6768	36.9697	4601.732	910
Hue/Grey	9-21	Chi Squared	29.2929	35.1515	4602.411	911
Hue/Grey	15-21	Chi Squared	28.2828	36.1616	4609.349	912
Hue/Grey	18-12	Bhattacharyya	27.2727	36.9697	4631.039	913
Hue/Grey	12-12	Bhattacharyya	27.2727	36.7677	4643.792	914
Hue/Grey	24-12	Bhattacharyya	27.2727	36.7677	4643.792	915
Hue/Grey	9-12	Chi Squared	27.6768	36.1616	4652.993	916
Hue/Grey	9-12	Bhattacharyya	27.0707	36.7677	4658.503	917
Hue/Grey	21-12	Chi Squared	27.0707	36.5657	4671.297	918
Hue/Grey	24-12	Chi Squared	27.0707	36.5657	4671.297	919
Hue/Grey	9-24	Chi Squared	28.4848	34.9495	4672.996	920
Hue/Grey	15-12	Bhattacharyya	26.8687	36.7677	4673.255	921
VGS/Thermal IR	21-3	Intersection	28.2828	35.1515	4674.342	922
Hue/Grey	18-12	Chi Squared	27.2727	36.1616	4682.301	923
Hue/Grey	12-24	Chi Squared	28.0808	35.1515	4688.85	924
Hue/Grey	12-21	Chi Squared	27.6768	35.5556	4691.863	925
Hue/Grey	12-24	Bhattacharyya	27.8788	35.1515	4703.398	926
Hue/Grey	21-24	Chi Squared	27.8788	35.1515	4703.398	927
Hue/Grey	21-21	Bhattacharyya	27.4747	35.5556	4706.5	928
Hue/Grey	18-24	Bhattacharyya	27.2727	35.7576	4708.173	929

Hue/Grey	24-24	Bhattacharyya	27.0707	35.9596	4709.928	930
Hue/Grey	15-24	Chi Squared	27.4747	35.3535	4719.545	931
Hue/Grey	18-24	Chi Squared	27.4747	35.3535	4719.545	932
Hue/Grey	21-24	Bhattacharyya	27.2727	35.5556	4721.17	933
Hue/Grey	18-21	Bhattacharyya	26.6667	36.1616	4726.557	934
Hue/Grey	15-12	Chi Squared	26.4646	36.3636	4728.523	935
Hue/Grey	9-21	Bhattacharyya	26.8687	35.7576	4737.636	936
VGS/Thermal IR	3-3	Bhattacharyya	40.404	23.0303	4738.009	937
Hue/Grey	12-12	Chi Squared	26.2626	36.3636	4743.398	938
Hue/Grey	24-21	Bhattacharyya	26.2626	36.3636	4743.398	939
Hue/Grey	15-24	Bhattacharyya	26.8687	35.5556	4750.634	940
Hue/Grey	12-21	Bhattacharyya	26.4646	35.9596	4754.314	941
Hue/Grey	15-21	Bhattacharyya	26.4646	35.9596	4754.314	942
Hue/Grey	24-24	Chi Squared	27.0707	35.1515	4762.005	943
VGS/Thermal IR	18-3	Intersection	28.0808	33.9394	4768.187	944
Hue/Grey	9-24	Bhattacharyya	26.6667	35.3535	4778.471	945
VGS/Thermal IR	3-3	Chi Squared	40.6061	22.2222	4788.511	946
Hue/Grey	9-15	Chi Squared	26.6667	34.9495	4804.67	947
Hue/Grey	9-6	Bhattacharyya	25.2525	36.5657	4805.55	948
Hue/Grey	21-18	Chi Squared	25.6566	35.9596	4814.057	949
Saturation/Thermal IR	24-6	Earth Mover's Distance	34.7475	26.6667	4817.831	950
Hue/Grey	9-18	Bhattacharyya	25.6566	35.7576	4827.014	951
Hue/Grey	21-15	Chi Squared	25.6566	35.7576	4827.014	952
Hue/Grey	12-18	Bhattacharyya	25.4545	35.7576	4842.059	953
Hue/Grey	15-18	Chi Squared	25.4545	35.7576	4842.059	954
Hue/Grey	24-15	Bhattacharyya	24.8485	36.3636	4848.67	955
Hue/Grey	12-6	Bhattacharyya	23.8384	37.5758	4848.685	956
Hue/Grey	18-15	Chi Squared	25.8586	35.1515	4851.138	957
Hue/Grey	24-18	Chi Squared	25.2525	35.5556	4870.135	958
Hue/Grey	24-6	Bhattacharyya	24.0404	36.9697	4871.34	959
Hue/Grey	24-15	Chi Squared	25.0505	35.7576	4872.257	960
Hue/Grey	18-18	Chi Squared	24.8485	35.9596	4874.46	961
Hue/Grey	9-18	Chi Squared	25.2525	35.3535	4883.179	962
Hue/Grey	21-6	Bhattacharyya	24.0404	36.7677	4884.092	963
Hue/Grey	12-15	Chi Squared	25.0505	35.5556	4885.254	964
VGS/Thermal IR	9-3	Intersection	28.8889	31.3131	4887.339	965
Hue/Grey	21-18	Bhattacharyya	24.4444	36.1616	4891.995	966
Hue/Grey	24-18	Bhattacharyya	24.4444	36.1616	4891.995	967
Hue/Grey	12-18	Chi Squared	24.6465	35.7576	4902.618	968
Hue/Grey	15-18	Bhattacharyya	24.2424	36.1616	4907.278	969
Hue/Grey	9-6	Chi Squared	25.2525	34.9495	4909.378	970
Hue/Grey	18-6	Bhattacharyya	23.4343	36.9697	4917.563	971
Hue/Grey	18-18	Bhattacharyya	24.0404	36.1616	4922.601	972
Hue/Grey	15-6	Bhattacharyya	23.0303	37.3737	4923.194	973
Hue/Grey	9-15	Bhattacharyya	24.0404	35.9596	4935.517	974
Saturation/Thermal IR	18-3	Intersection	31.1111	28.2828	4944.519	975
Hue/Thermal IR	6-3	Earth Mover's Distance	30.101	29.0909	4956.985	976
Hue/Grey	18-15	Bhattacharyya	23.4343	36.1616	4968.824	977
VGS/Thermal IR	6-3	Earth Mover's Distance	38.3838	21.6162	4970.288	978
Hue/Grey	15-15	Bhattacharyya	23.2323	36.3636	4971.436	979
Hue/Grey	15-15	Chi Squared	24.2424	35.1515	4972.271	980
Hue/Grey	15-12	Intersection	25.2525	33.9394	4975.596	981
Hue/Grey	12-15	Bhattacharyya	23.8384	35.5556	4976.835	982

Hue/Grey	21-15	Bhattacharyya	23.4343	35.9596	4981.74	983
Hue/Grey	24-6	Chi Squared	24.0404	35.1515	4987.594	984
Saturation/Thermal IR	21-3	Intersection	30.5051	28.0808	5000.956	985
Saturation/Thermal IR	15-3	Intersection	30.7071	27.8788	5001.487	986
Hue/Grey	18-12	Intersection	25.0505	33.7374	5004.08	987
Hue/Grey	9-12	Intersection	25.8586	32.7273	5011.282	988
Hue/Grey	21-6	Chi Squared	24.0404	34.7475	5013.875	989
Hue/Grey	6-24	Chi Squared	25.2525	33.3333	5015.819	990
Hue/Grey	21-9	Chi Squared	23.6364	35.1515	5018.364	991
Hue/Grey	15-6	Chi Squared	23.4343	35.3535	5020.738	992
Hue/Grey	18-21	Intersection	24.2424	34.1414	5038.285	993
Hue/Grey	21-12	Intersection	25.0505	33.1313	5044.425	994
Saturation/Thermal IR	12-3	Intersection	30.7071	27.2727	5045.383	995
Hue/Grey	18-6	Chi Squared	23.4343	34.9495	5046.937	996
Hue/Grey	9-9	Chi Squared	24.2424	33.9394	5051.608	997
Hue/Grey	24-12	Intersection	24.4444	33.5354	5063.096	998
Hue/Grey	6-12	Bhattacharyya	22.8283	35.3535	5067.321	999
Hue/Grey	12-6	Chi Squared	22.8283	35.3535	5067.321	1000
Hue/Grey	15-21	Intersection	23.6364	34.3434	5071.094	1001
Hue/Grey	12-24	Intersection	24.6465	33.1313	5074.787	1002
Hue/Grey	18-9	Bhattacharyya	23.0303	34.9495	5077.951	1003
Hue/Grey	21-21	Intersection	24.0404	33.7374	5080.296	1004
Hue/Grey	15-24	Intersection	24.4444	33.1313	5090.036	1005
Hue/Grey	24-9	Chi Squared	22.4242	35.3535	5098.587	1006
Saturation/Thermal IR	24-3	Intersection	29.2929	27.8788	5100.481	1007
Hue/Grey	24-21	Intersection	23.2323	34.3434	5102.034	1008
Hue/Grey	12-12	Intersection	24.2424	33.1313	5105.318	1009
Hue/Grey	6-18	Chi Squared	22.4242	35.1515	5111.666	1010
Hue/Grey	15-9	Chi Squared	22.6263	34.7475	5122.289	1011
Saturation/Thermal IR	3-3	Earth Mover's Distance	33.7374	23.4343	5126.519	1012
Hue/Grey	21-24	Intersection	24.2424	32.7273	5132.415	1013
Hue/Grey	12-21	Intersection	22.6263	34.5455	5135.491	1014
Hue/Grey	21-9	Bhattacharyya	22.6263	34.5455	5135.491	1015
Hue/Grey	18-9	Chi Squared	22.4242	34.7475	5137.947	1016
Hue/Grey	24-24	Intersection	24.2424	32.5253	5146.025	1017
Hue/Grey	24-9	Bhattacharyya	22.6263	34.3434	5148.739	1018
Hue/Grey	15-9	Bhattacharyya	21.8182	35.1515	5158.861	1019
Saturation/Thermal IR	9-3	Intersection	30.101	26.2626	5161.537	1020
Hue/Grey	6-12	Chi Squared	22.6263	34.1414	5162.022	1021
Saturation/Thermal IR	6-3	Intersection	31.1111	25.2525	5166.435	1022
Hue/Thermal IR	9-3	Earth Mover's Distance	28.0808	28.0808	5172.371	1023
Saturation/Thermal IR	3-3	Intersection	33.9394	22.6263	5175.346	1024
Hue/Grey	6-21	Bhattacharyya	22.6263	33.9394	5175.346	1025
Hue/Grey	9-9	Bhattacharyya	22.6263	33.9394	5175.346	1026
Hue/Grey	18-24	Intersection	23.8384	32.5253	5176.712	1027
Hue/Grey	6-24	Bhattacharyya	23.4343	32.9293	5180.393	1028
Hue/Grey	9-21	Intersection	23.4343	32.9293	5180.393	1029
Hue/Grey	9-24	Intersection	24.8485	31.3131	5182.819	1030
Hue/Grey	12-9	Chi Squared	22.6263	33.7374	5188.711	1031
Hue/Grey	12-9	Bhattacharyya	22.4242	33.9394	5191.004	1032
VGS/Thermal IR	3-3	Intersection	36.3636	20.404	5192.557	1033
Hue/Grey	6-21	Chi Squared	22.2222	34.1414	5193.371	1034
Hue/Sat	21-3	Correlation	22.0202	34.1414	5209.102	1035

Hue/Grey	6-18	Bhattacharyya	21.2121	34.7475	5232.711	1036
Hue/Grey	6-12	Intersection	23.4343	31.7172	5262.424	1037
Hue/Grey	6-15	Chi Squared	21.6162	33.7374	5267.376	1038
VGS/Thermal IR	12-3	Earth Mover's Distance	31.9192	23.0303	5279.665	1039
VGS/Thermal IR	12-3	Correlation	26.2626	28.2828	5290.28	1040
Hue/Sat	21-9	Correlation	20	34.9495	5315.784	1041
Hue/Sat	24-12	Correlation	19.596	35.3535	5321.987	1042
Hue/Sat	24-3	Correlation	20.6061	33.9394	5333.697	1043
Hue/Sat	24-18	Correlation	20.404	34.1414	5336.439	1044
Hue/Sat	24-15	Correlation	20.202	34.3434	5339.255	1045
Hue/Sat	18-3	Correlation	21.0101	33.3333	5341.927	1046
Hue/Sat	21-12	Correlation	20.8081	33.5354	5344.45	1047
Saturation/Thermal IR	6-3	Correlation	23.2323	30.7071	5347.393	1048
Hue/Grey	6-24	Intersection	23.6364	30.101	5358.635	1049
Hue/Sat	21-9	Chi Squared	18.5859	35.9596	5364.714	1050
Hue/Sat	21-6	Chi Squared	18.3838	36.1616	5368.273	1051
Hue/Sat	21-6	Correlation	20	34.1414	5368.678	1052
Saturation/Thermal IR	9-3	Correlation	22.2222	31.5152	5369.777	1053
Saturation/Thermal IR	18-3	Correlation	21.8182	31.9192	5373.695	1054
Hue/Sat	21-15	Correlation	20.6061	33.3333	5373.92	1055
Hue/Grey	24-18	Intersection	21.2121	32.5253	5380.184	1056
VGS/Thermal IR	3-3	Earth Mover's Distance	34.9495	19.1919	5380.758	1057
Hue/Grey	6-21	Intersection	22.0202	31.5152	5385.509	1058
Hue/Grey	21-18	Intersection	21.4141	32.1212	5391.638	1059
Hue/Sat	24-21	Correlation	20.202	33.5354	5392.632	1060
Hue/Sat	21-6	Bhattacharyya	18.1818	35.9596	5397.695	1061
Hue/Sat	18-15	Correlation	19.798	33.9394	5398.182	1062
VGS/Thermal IR	3-3	Correlation	31.5152	21.8182	5401.281	1063
Saturation/Grey	12-24	Chi Squared	27.2727	25.6566	5408.101	1064
Hue/Sat	18-6	Bhattacharyya	18.1818	35.7576	5410.652	1065
Saturation/Thermal IR	21-3	Correlation	21.6162	31.5152	5417.094	1066
VGS/Thermal IR	15-3	Earth Mover's Distance	33.1313	20.202	5419.572	1067
Hue/Sat	18-12	Correlation	20	33.3333	5422.224	1068
Saturation/Grey	24-24	Chi Squared	26.8687	25.8586	5422.567	1069
Saturation/Grey	9-24	Chi Squared	27.2727	25.4545	5423.146	1070
Saturation/Grey	15-24	Chi Squared	27.2727	25.4545	5423.146	1071
Hue/Sat	21-12	Chi Squared	17.9798	35.7576	5427.2	1072
Hue/Sat	24-9	Correlation	19.3939	33.9394	5430.673	1073
Hue/Grey	6-15	Bhattacharyya	20.202	32.9293	5433.1	1074
Hue/Grey	9-18	Intersection	21.2121	31.7172	5435.037	1075
Hue/Grey	12-18	Intersection	21.2121	31.7172	5435.037	1076
Saturation/Thermal IR	6-3	Earth Mover's Distance	26.4646	26.0606	5437.245	1077
Saturation/Grey	15-12	Chi Squared	25.4545	27.0707	5437.857	1078
Hue/Sat	18-6	Chi Squared	17.3737	36.3636	5438.348	1079
Hue/Grey	15-18	Intersection	20.404	32.5253	5444.179	1080
Hue/Grey	3-12	Bhattacharyya	21.4141	31.3131	5446.817	1081
Hue/Sat	18-9	Correlation	19.1919	33.9394	5446.976	1082
Hue/Sat	21-12	Bhattacharyya	17.5758	35.9596	5447.461	1083
Hue/Grey	6-6	Bhattacharyya	20	32.9293	5449.239	1084
Saturation/Thermal IR	12-3	Correlation	21.0101	31.7172	5450.973	1085
Saturation/Grey	9-12	Bhattacharyya	25.6566	26.6667	5452.357	1086
Saturation/Grey	12-12	Bhattacharyya	25.6566	26.6667	5452.357	1087
Saturation/Grey	21-21	Chi Squared	26.8687	25.4545	5452.609	1088

Saturation/Grey	21-24	Chi Squared	26.8687	25.4545	5452.609	1089
Saturation/Grey	24-21	Chi Squared	26.8687	25.4545	5452.609	1090
Hue/Sat	21-21	Correlation	20.8081	31.9192	5453.176	1091
VGS/Thermal IR	9-3	Earth Mover's Distance	30.303	22.2222	5453.529	1092
Hue/Thermal IR	12-3	Earth Mover's Distance	24.6465	27.6768	5454.398	1093
Hue/Sat	18-18	Correlation	19.596	33.3333	5454.626	1094
Hue/Sat	21-24	Correlation	20.6061	32.1212	5455.461	1095
Hue/Sat	24-6	Chi Squared	16.9697	36.5657	5458.971	1096
Hue/Grey	6-6	Chi Squared	20.202	32.5253	5460.278	1097
Hue/Grey	3-12	Chi Squared	21.4141	31.1111	5460.712	1098
Hue/Sat	24-6	Correlation	18.1818	34.9495	5462.893	1099
Saturation/Grey	12-21	Chi Squared	26.4646	25.6566	5467.198	1100
Saturation/Grey	18-24	Chi Squared	26.6667	25.4545	5467.402	1101
Saturation/Grey	21-12	Chi Squared	25.2525	26.8687	5467.688	1102
Hue/Sat	24-24	Correlation	19.596	33.1313	5468.113	1103
Hue/Sat	24-3	Chi Squared	17.7778	35.3535	5469.83	1104
Hue/Grey	9-15	Intersection	21.8182	30.5051	5470.967	1105
Hue/Grey	18-15	Intersection	21.6162	30.7071	5472.763	1106
Hue/Sat	21-9	Bhattacharyya	17.5758	35.5556	5473.415	1107
Hue/Sat	21-24	Chi Squared	17.5758	35.5556	5473.415	1108
Hue/Sat	24-3	Bhattacharyya	17.5758	35.5556	5473.415	1109
Hue/Grey	18-24	Correlation	23.2323	28.8889	5475.034	1110
Hue/Sat	18-18	Chi Squared	17.3737	35.7576	5477.096	1111
Hue/Sat	24-9	Chi Squared	17.3737	35.7576	5477.096	1112
Hue/Grey	3-24	Bhattacharyya	21.0101	31.3131	5478.647	1113
Hue/Sat	12-9	Chi Squared	17.1717	35.9596	5480.85	1114
Hue/Sat	18-12	Chi Squared	17.1717	35.9596	5480.85	1115
Saturation/Grey	15-21	Chi Squared	26.2626	25.6566	5482.073	1116
Hue/Sat	9-6	Bhattacharyya	17.7778	35.1515	5482.909	1117
Hue/Sat	18-21	Correlation	19.3939	33.1313	5484.383	1118
Hue/Sat	12-6	Chi Squared	17.5758	35.3535	5486.459	1119
Hue/Sat	18-9	Bhattacharyya	17.5758	35.3535	5486.459	1120
Hue/Grey	15-15	Intersection	21.4141	30.7071	5488.625	1121
Hue/Sat	18-9	Chi Squared	17.3737	35.5556	5490.093	1122
Saturation/Thermal IR	24-3	Correlation	21.0101	31.1111	5492.542	1123
Hue/Sat	15-24	Correlation	19.798	32.5253	5492.598	1124
Hue/Sat	15-9	Bhattacharyya	17.1717	35.7576	5493.807	1125
Saturation/Thermal IR	15-3	Correlation	20.8081	31.3131	5494.624	1126
Hue/Grey	3-18	Chi Squared	20.8081	31.3131	5494.624	1127
Hue/Sat	18-24	Correlation	19.596	32.7273	5495.21	1128
Hue/Sat	9-6	Chi Squared	17.7778	34.9495	5496.029	1129
Hue/Sat	21-15	Intersection	17.7778	34.9495	5496.029	1130
Saturation/Grey	6-24	Bhattacharyya	25.8586	25.8586	5496.947	1131
Hue/Sat	15-6	Chi Squared	16.9697	35.9596	5497.602	1132
Hue/Sat	24-9	Bhattacharyya	16.9697	35.9596	5497.602	1133
Hue/Sat	21-18	Correlation	19.3939	32.9293	5497.911	1134
VGS/Thermal IR	15-3	Correlation	26.8687	24.8485	5497.967	1135
Hue/Sat	9-3	Chi Squared	18.3838	34.1414	5499.28	1136
Hue/Sat	18-6	Correlation	18.3838	34.1414	5499.28	1137
Hue/Sat	21-24	Bhattacharyya	17.5758	35.1515	5499.538	1138
Hue/Sat	15-9	Chi Squared	16.7677	36.1616	5501.479	1139
Hue/Sat	21-3	Chi Squared	17.3737	35.3535	5503.138	1140
Hue/Sat	24-24	Chi Squared	17.1717	35.5556	5506.804	1141

Saturation/Grey	6-24	Chi Squared	26.0606	25.4545	5512.033	1142
Saturation/Grey	18-21	Chi Squared	26.0606	25.4545	5512.033	1143
Hue/Grey	18-21	Correlation	23.4343	28.0808	5517.339	1144
Hue/Sat	21-15	Chi Squared	16.5657	36.1616	5518.312	1145
Hue/Sat	21-3	Bhattacharyya	17.5758	34.7475	5525.819	1146
Hue/Grey	3-24	Chi Squared	20.404	31.3131	5526.707	1147
Saturation/Grey	12-24	Bhattacharyya	25.6566	25.6566	5526.941	1148
Saturation/Grey	12-12	Chi Squared	25.0505	26.2626	5527.316	1149
Hue/Sat	21-18	Chi Squared	16.7677	35.7576	5527.351	1150
Hue/Sat	24-9	Intersection	16.7677	35.7576	5527.351	1151
VGS/Thermal IR	24-3	Correlation	21.8182	29.697	5527.453	1152
Saturation/Grey	24-12	Chi Squared	24.8485	26.4646	5527.602	1153
Hue/Grey	3-21	Chi Squared	20.202	31.5152	5528.944	1154
Hue/Sat	21-12	Intersection	17.3737	34.9495	5529.337	1155
Hue/Sat	24-6	Bhattacharyya	16.5657	35.9596	5531.228	1156
Hue/Sat	24-12	Chi Squared	16.5657	35.9596	5531.228	1157
Hue/Sat	21-9	Intersection	17.1717	35.1515	5532.928	1158
Hue/Grey	18-18	Intersection	19.798	31.9192	5533.678	1159
VGS/Thermal IR	9-3	Correlation	22.6263	28.6869	5536.124	1160
VGS/Thermal IR	6-3	Correlation	32.1212	19.596	5536.167	1161
Hue/Grey	24-15	Intersection	20.8081	30.7071	5536.432	1162
Hue/Sat	12-3	Bhattacharyya	16.9697	35.3535	5536.6	1163
Hue/Sat	12-12	Chi Squared	16.7677	35.5556	5540.348	1164
Hue/Sat	18-9	Intersection	16.7677	35.5556	5540.348	1165
Hue/Sat	15-21	Correlation	19.1919	32.5253	5541.392	1166
Saturation/Grey	6-21	Bhattacharyya	24.8485	26.2626	5542.476	1167
Saturation/Grey	15-12	Bhattacharyya	24.8485	26.2626	5542.476	1168
Saturation/Grey	18-12	Chi Squared	24.4444	26.6667	5543.211	1169
Hue/Sat	18-15	Chi Squared	16.5657	35.7576	5544.184	1170
Hue/Sat	24-15	Bhattacharyya	16.5657	35.7576	5544.184	1171
Hue/Sat	24-18	Chi Squared	16.5657	35.7576	5544.184	1172
Hue/Sat	9-3	Bhattacharyya	17.9798	33.9394	5545.658	1173
Hue/Sat	15-3	Bhattacharyya	17.1717	34.9495	5546.047	1174
Hue/Grey	15-24	Correlation	22.8283	28.2828	5549.414	1175
Hue/Sat	12-3	Correlation	18.5859	33.1313	5549.839	1176
Hue/Grey	21-15	Intersection	20.8081	30.5051	5550.449	1177
Hue/Grey	24-24	Correlation	22.6263	28.4848	5550.557	1178
Hue/Grey	3-18	Bhattacharyya	20.6061	30.7071	5552.449	1179
Hue/Sat	12-3	Chi Squared	16.7677	35.3535	5553.393	1180
Hue/Sat	21-21	Chi Squared	16.7677	35.3535	5553.393	1181
Saturation/Grey	6-21	Chi Squared	25.4545	25.4545	5557.032	1182
Hue/Sat	15-6	Bhattacharyya	16.5657	35.5556	5557.182	1183
Hue/Sat	18-21	Chi Squared	16.5657	35.5556	5557.182	1184
Saturation/Thermal IR	9-3	Earth Mover's Distance	25.8586	25.0505	5557.187	1185
Saturation/Grey	6-12	Chi Squared	24.6465	26.2626	5557.677	1186
Hue/Sat	12-15	Correlation	18.9899	32.5253	5557.736	1187
Hue/Sat	15-15	Correlation	18.9899	32.5253	5557.736	1188
Saturation/Grey	9-12	Chi Squared	24.4444	26.4646	5558.052	1189
Hue/Grey	9-24	Correlation	23.6364	27.2727	5560.33	1190
Hue/Grey	21-21	Correlation	23.4343	27.4747	5561.113	1191
Hue/Sat	9-9	Chi Squared	16.9697	34.9495	5562.799	1192
Hue/Sat	15-3	Chi Squared	16.9697	34.9495	5562.799	1193
Hue/Sat	12-18	Correlation	18.5859	32.9293	5563.367	1194

Hue/Grey	21-24	Correlation	22.6263	28.2828	5565.023	1195
Hue/Sat	12-6	Bhattacharyya	16.7677	35.1515	5566.472	1196
Hue/Sat	18-3	Chi Squared	16.7677	35.1515	5566.472	1197
Hue/Sat	18-24	Bhattacharyya	16.7677	35.1515	5566.472	1198
Hue/Sat	12-9	Correlation	19.1919	32.1212	5568.74	1199
Hue/Grey	3-24	Intersection	21.6162	29.2929	5571.757	1200
Saturation/Grey	6-12	Bhattacharyya	25.2525	25.4545	5572.11	1201
Saturation/Grey	9-21	Chi Squared	25.2525	25.4545	5572.11	1202
Hue/Thermal IR	18-3	Earth Mover's Distance	25.6566	25.0505	5572.184	1203
Saturation/Grey	9-21	Bhattacharyya	24.8485	25.8586	5572.348	1204
Hue/Sat	24-3	Intersection	17.1717	34.5455	5572.409	1205
Hue/Sat	18-12	Bhattacharyya	16.3636	35.5556	5574.064	1206
Hue/Sat	18-24	Chi Squared	16.3636	35.5556	5574.064	1207
Hue/Sat	24-6	Intersection	16.3636	35.5556	5574.064	1208
Hue/Sat	24-24	Bhattacharyya	16.3636	35.5556	5574.064	1209
Hue/Sat	12-12	Bhattacharyya	16.1616	35.7576	5577.982	1210
Hue/Sat	12-21	Intersection	17.5758	33.9394	5578.876	1211
Hue/Grey	12-24	Correlation	22.2222	28.4848	5581.905	1212
Hue/Grey	3-21	Intersection	22.0202	28.6869	5583.204	1213
Hue/Sat	12-9	Bhattacharyya	16.5657	35.1515	5583.305	1214
Hue/Sat	12-18	Chi Squared	16.5657	35.1515	5583.305	1215
Hue/Sat	15-18	Bhattacharyya	16.5657	35.1515	5583.305	1216
Hue/Sat	15-21	Chi Squared	16.5657	35.1515	5583.305	1217
Hue/Sat	18-12	Intersection	16.5657	35.1515	5583.305	1218
Hue/Sat	18-15	Intersection	16.5657	35.1515	5583.305	1219
Hue/Sat	24-15	Intersection	16.5657	35.1515	5583.305	1220
Hue/Sat	12-12	Correlation	18.9899	32.1212	5585.084	1221
Hue/Sat	15-3	Correlation	18.9899	32.1212	5585.084	1222
Hue/Grey	12-15	Intersection	20	30.9091	5586.776	1223
Hue/Sat	18-15	Bhattacharyya	16.3636	35.3535	5587.109	1224
Hue/Sat	18-18	Bhattacharyya	16.1616	35.5556	5590.979	1225
Hue/Sat	21-18	Bhattacharyya	16.1616	35.5556	5590.979	1226
Hue/Sat	24-15	Chi Squared	16.1616	35.5556	5590.979	1227
Hue/Grey	6-9	Chi Squared	19.1919	31.7172	5596.245	1228
Hue/Sat	9-12	Bhattacharyya	16.5657	34.9495	5596.425	1229
Hue/Sat	9-15	Chi Squared	16.5657	34.9495	5596.425	1230
Hue/Sat	18-18	Intersection	16.5657	34.9495	5596.425	1231
Hue/Grey	18-12	Correlation	22.0202	28.4848	5597.637	1232
Hue/Sat	9-18	Chi Squared	17.1717	34.1414	5598.941	1233
Hue/Sat	15-12	Chi Squared	15.7576	35.9596	5598.977	1234
Hue/Sat	12-15	Chi Squared	16.3636	35.1515	5600.188	1235
Hue/Sat	12-21	Bhattacharyya	16.3636	35.1515	5600.188	1236
Hue/Sat	15-18	Chi Squared	16.3636	35.1515	5600.188	1237
Hue/Sat	21-21	Bhattacharyya	16.3636	35.1515	5600.188	1238
Hue/Sat	15-18	Correlation	18.7879	32.1212	5601.468	1239
Saturation/Grey	12-21	Bhattacharyya	24.8485	25.4545	5602.39	1240
Saturation/Grey	9-24	Bhattacharyya	24.6465	25.6566	5602.546	1241
Hue/Thermal IR	15-3	Earth Mover's Distance	24.4444	25.8586	5602.798	1242
Hue/Sat	15-9	Intersection	16.1616	35.3535	5604.024	1243
Hue/Sat	15-24	Chi Squared	16.1616	35.3535	5604.024	1244
Hue/Sat	24-18	Intersection	16.1616	35.3535	5604.024	1245
Hue/Sat	12-21	Correlation	18.5859	32.3232	5604.202	1246
Hue/Sat	21-3	Intersection	17.5758	33.5354	5605.646	1247

Hue/Sat	9-9	Bhattacharyya	16.7677	34.5455	5605.954	1248
Hue/Sat	15-12	Correlation	18.3838	32.5253	5607.02	1249
Hue/Grey	6-9	Bhattacharyya	19.3939	31.3131	5607.617	1250
Hue/Sat	24-21	Bhattacharyya	15.9596	35.5556	5607.935	1251
Hue/Sat	12-18	Bhattacharyya	16.5657	34.7475	5609.586	1252
Hue/Sat	24-21	Intersection	16.5657	34.7475	5609.586	1253
Hue/Sat	21-15	Bhattacharyya	15.7576	35.7576	5611.934	1254
Hue/Sat	12-24	Correlation	18.9899	31.7172	5612.589	1255
Hue/Sat	18-3	Bhattacharyya	16.3636	34.9495	5613.307	1256
Saturation/Grey	18-12	Bhattacharyya	24.0404	26.0606	5618.448	1257
Saturation/Grey	21-12	Bhattacharyya	24.0404	26.0606	5618.448	1258
Saturation/Grey	24-12	Bhattacharyya	24.0404	26.0606	5618.448	1259
Hue/Grey	3-21	Bhattacharyya	19.596	30.9091	5619.178	1260
Hue/Sat	15-15	Intersection	16.7677	34.3434	5619.202	1261
Saturation/Thermal IR	12-3	Earth Mover's Distance	26.6667	23.4343	5620.04	1262
Hue/Sat	24-18	Bhattacharyya	15.9596	35.3535	5620.979	1263
Hue/Sat	15-18	Intersection	16.5657	34.5455	5622.787	1264
Hue/Grey	9-12	Correlation	22.4242	27.6768	5624.325	1265
Hue/Sat	24-12	Intersection	15.7576	35.5556	5624.931	1266
Hue/Sat	24-12	Bhattacharyya	15.7576	35.5556	5624.931	1267
Hue/Sat	24-21	Chi Squared	15.7576	35.5556	5624.931	1268
Hue/Sat	12-15	Intersection	17.1717	33.7374	5625.63	1269
Hue/Sat	15-12	Intersection	16.1616	34.9495	5630.222	1270
Hue/Sat	12-24	Intersection	16.7677	34.1414	5632.485	1271
Hue/Grey	6-18	Intersection	19.596	30.7071	5633.155	1272
Hue/Sat	12-15	Bhattacharyya	15.9596	35.1515	5634.058	1273
Hue/Sat	21-6	Intersection	16.3636	34.5455	5639.669	1274
Hue/Sat	21-24	Intersection	16.3636	34.5455	5639.669	1275
Hue/Sat	15-6	Correlation	16.9697	33.7374	5642.381	1276
Hue/Sat	9-12	Chi Squared	16.1616	34.7475	5643.383	1277
Hue/Sat	18-21	Intersection	16.1616	34.7475	5643.383	1278
Hue/Sat	15-15	Chi Squared	15.3535	35.7576	5646.058	1279
Hue/Grey	3-15	Bhattacharyya	19.596	30.5051	5647.172	1280
Hue/Sat	12-21	Chi Squared	15.9596	34.9495	5647.178	1281
Hue/Sat	18-21	Bhattacharyya	15.9596	34.9495	5647.178	1282
Hue/Sat	18-3	Intersection	17.3737	33.1313	5649.264	1283
Hue/Sat	12-9	Intersection	16.5657	34.1414	5649.319	1284
Hue/Sat	12-18	Intersection	16.5657	34.1414	5649.319	1285
Hue/Sat	12-24	Chi Squared	15.7576	35.1515	5651.055	1286
Hue/Grey	9-21	Correlation	22.4242	27.2727	5653.632	1287
VGS/Thermal IR	18-3	Earth Mover's Distance	31.1111	18.9899	5654.158	1288
Hue/Grey	24-12	Correlation	22.0202	27.6768	5655.747	1289
Hue/Grey	24-21	Correlation	22.0202	27.6768	5655.747	1290
Hue/Sat	9-21	Chi Squared	16.1616	34.5455	5656.584	1291
Hue/Sat	12-12	Intersection	16.1616	34.5455	5656.584	1292
Hue/Sat	15-21	Intersection	16.1616	34.5455	5656.584	1293
Hue/Sat	9-18	Intersection	17.5758	32.7273	5659.682	1294
Saturation/Grey	15-21	Bhattacharyya	24.6465	24.8485	5662.949	1295
Hue/Sat	9-15	Bhattacharyya	15.7576	34.9495	5664.175	1296
Hue/Sat	15-24	Bhattacharyya	15.7576	34.9495	5664.175	1297
Saturation/Grey	6-18	Bhattacharyya	23.4343	26.0606	5664.671	1298
VGS/Thermal IR	18-3	Correlation	20.404	29.2929	5667.509	1299
Hue/Sat	15-15	Bhattacharyya	15.5556	35.1515	5668.092	1300

Hue/Sat	15-12	Bhattacharyya	15.3535	35.3535	5672.1	1301
Hue/Sat	15-9	Correlation	17.5758	32.5253	5673.292	1302
Hue/Sat	21-21	Intersection	15.7576	34.7475	5677.335	1303
Hue/Grey	3-6	Bhattacharyya	19.3939	30.303	5677.508	1304
Saturation/Grey	18-21	Bhattacharyya	24.2424	25.0505	5678.321	1305
Saturation/Grey	15-24	Bhattacharyya	24.0404	25.2525	5678.525	1306
Hue/Sat	15-21	Bhattacharyya	15.5556	34.9495	5681.212	1307
Hue/Sat	21-18	Intersection	16.1616	34.1414	5683.116	1308
Hue/Grey	21-9	Correlation	20	29.4949	5685.485	1309
Hue/Sat	9-24	Chi Squared	15.9596	34.3434	5686.789	1310
Saturation/Grey	9-15	Chi Squared	24.2424	24.8485	5693.481	1311
Hue/Grey	3-15	Chi Squared	19.1919	30.303	5693.81	1312
Saturation/Grey	18-24	Bhattacharyya	23.8384	25.2525	5693.889	1313
Saturation/Grey	21-24	Bhattacharyya	23.8384	25.2525	5693.889	1314
Saturation/Grey	24-24	Bhattacharyya	23.8384	25.2525	5693.889	1315
Hue/Sat	9-21	Correlation	18.9899	30.5051	5696.089	1316
VGS/Thermal IR	21-3	Correlation	20.404	28.8889	5696.156	1317
Hue/Sat	18-6	Intersection	16.1616	33.9394	5696.44	1318
Hue/Grey	12-21	Correlation	21.0101	28.0808	5705.888	1319
Hue/Sat	24-24	Intersection	15.5556	34.5455	5707.574	1320
Hue/Grey	24-9	Correlation	19.1919	30.101	5707.91	1321
Saturation/Grey	15-15	Chi Squared	24.0404	24.8485	5708.804	1322
Saturation/Grey	21-15	Chi Squared	24.0404	24.8485	5708.804	1323
Saturation/Grey	12-15	Chi Squared	23.8384	25.0505	5709.008	1324
Saturation/Grey	24-15	Chi Squared	23.8384	25.0505	5709.008	1325
Saturation/Grey	9-18	Chi Squared	23.4343	25.4545	5709.669	1326
Hue/Grey	6-15	Intersection	20.202	28.8889	5712.255	1327
Saturation/Thermal IR	15-3	Earth Mover's Distance	26.4646	22.4242	5712.73	1328
Hue/Grey	6-24	Correlation	22.2222	26.6667	5713.58	1329
Hue/Grey	21-12	Correlation	22.0202	26.8687	5714.518	1330
Hue/Sat	15-6	Intersection	15.7576	34.1414	5717.069	1331
Hue/Grey	15-12	Correlation	21.2121	27.6768	5719.089	1332
Hue/Sat	9-18	Bhattacharyya	15.5556	34.3434	5720.823	1333
Hue/Grey	3-12	Intersection	20.8081	28.0808	5721.864	1334
Hue/Grey	3-6	Chi Squared	19.1919	29.899	5722.05	1335
Hue/Sat	12-6	Correlation	17.9798	31.3131	5722.602	1336
Saturation/Grey	24-21	Bhattacharyya	24.0404	24.6465	5724.005	1337
Saturation/Grey	15-15	Bhattacharyya	23.6364	25.0505	5724.413	1338
Saturation/Grey	18-15	Chi Squared	23.6364	25.0505	5724.413	1339
Hue/Sat	9-21	Bhattacharyya	15.3535	34.5455	5724.661	1340
Saturation/Grey	6-15	Bhattacharyya	23.4343	25.2525	5724.748	1341
Saturation/Grey	15-18	Chi Squared	23.4343	25.2525	5724.748	1342
Saturation/Grey	9-18	Bhattacharyya	23.0303	25.6566	5725.638	1343
Hue/Sat	9-15	Intersection	16.7677	32.7273	5726.616	1344
Hue/Sat	9-24	Intersection	16.7677	32.7273	5726.616	1345
Hue/Sat	9-15	Correlation	18.5859	30.5051	5728.898	1346
Hue/Grey	18-9	Correlation	19.798	29.0909	5730.231	1347
Saturation/Thermal IR	18-3	Earth Mover's Distance	26.8687	21.8182	5730.29	1348
Hue/Thermal IR	21-3	Earth Mover's Distance	24.4444	24.0404	5739.255	1349
Saturation/Grey	21-18	Chi Squared	23.4343	25.0505	5739.867	1350
Hue/Sat	9-21	Intersection	16.7677	32.5253	5740.225	1351
Hue/Sat	9-18	Correlation	18.7879	30.101	5740.638	1352
Saturation/Grey	12-18	Chi Squared	23.0303	25.4545	5740.683	1353

Hue/Grey	15-21	Correlation	21.0101	27.4747	5749.662	1354
Hue/Grey	12-12	Correlation	20.8081	27.6768	5751.001	1355
Hue/Sat	15-3	Intersection	16.7677	32.3232	5753.883	1356
Saturation/Grey	21-21	Bhattacharyya	23.6364	24.6465	5754.775	1357
Saturation/Grey	9-15	Bhattacharyya	23.4343	24.8485	5755.027	1358
Saturation/Grey	18-15	Bhattacharyya	23.0303	25.2525	5755.762	1359
Saturation/Grey	18-18	Chi Squared	23.0303	25.2525	5755.762	1360
Saturation/Grey	18-18	Bhattacharyya	23.0303	25.2525	5755.762	1361
Saturation/Grey	6-18	Chi Squared	22.8283	25.4545	5756.251	1362
Hue/Sat	12-24	Bhattacharyya	14.9495	34.5455	5758.94	1363
Hue/Sat	18-24	Intersection	15.1515	34.1414	5768.312	1364
Saturation/Grey	6-15	Chi Squared	23.8384	24.2424	5769.902	1365
Saturation/Grey	24-18	Chi Squared	23.0303	25.0505	5770.881	1366
Saturation/Grey	15-18	Bhattacharyya	22.8283	25.2525	5771.33	1367
Hue/Grey	18-9	Intersection	17.3737	31.3131	5772.498	1368
Hue/Sat	12-3	Intersection	16.7677	31.9192	5781.306	1369
Hue/Grey	9-9	Correlation	18.7879	29.4949	5783.187	1370
Hue/Sat	9-12	Intersection	16.5657	32.1212	5784.407	1371
Saturation/Grey	24-24	Intersection	23.4343	24.4444	5785.478	1372
Saturation/Grey	21-15	Bhattacharyya	23.0303	24.8485	5786.041	1373
Saturation/Grey	24-18	Bhattacharyya	22.8283	25.0505	5786.449	1374
Saturation/Grey	12-18	Bhattacharyya	22.4242	25.4545	5787.518	1375
Hue/Sat	6-24	Intersection	15.9596	32.7273	5794.202	1376
Hue/Grey	21-9	Intersection	16.7677	31.7172	5795.078	1377
Saturation/Grey	21-24	Intersection	23.0303	24.6465	5801.242	1378
Saturation/Grey	12-15	Bhattacharyya	22.8283	24.8485	5801.61	1379
Saturation/Grey	15-24	Intersection	22.8283	24.8485	5801.61	1380
Saturation/Grey	21-18	Bhattacharyya	22.8283	24.8485	5801.61	1381
Hue/Grey	21-18	Correlation	19.798	28.0808	5802.366	1382
Hue/Grey	9-9	Intersection	17.1717	31.1111	5803.104	1383
Hue/Sat	9-24	Bhattacharyya	15.3535	33.3333	5804.739	1384
Hue/Grey	18-18	Correlation	19.1919	28.6869	5807.754	1385
Saturation/Thermal IR	3-3	Correlation	21.0101	26.6667	5808.589	1386
Hue/Grey	15-9	Correlation	18.5859	29.2929	5813.875	1387
Saturation/Grey	3-24	Chi Squared	23.4343	24.0404	5816.084	1388
Hue/Thermal IR	24-3	Earth Mover's Distance	24.2424	23.2323	5816.247	1389
Saturation/Grey	24-21	Intersection	23.2323	24.2424	5816.247	1390
Hue/Sat	6-21	Chi Squared	15.1515	33.3333	5821.858	1391
Hue/Grey	24-9	Intersection	16.7677	31.3131	5822.753	1392
Hue/Sat	12-6	Intersection	15.7576	32.5253	5824.809	1393
Hue/Sat	9-9	Correlation	17.5758	30.303	5825.71	1394
Hue/Sat	9-12	Correlation	17.5758	30.303	5825.71	1395
Saturation/Grey	24-12	Intersection	23.6364	23.6364	5831.399	1396
Saturation/Grey	12-12	Intersection	23.4343	23.8384	5831.448	1397
Saturation/Grey	24-15	Bhattacharyya	22.8283	24.4444	5832.06	1398
Hue/Sat	6-24	Chi Squared	14.9495	33.3333	5839.018	1399
Hue/Sat	15-24	Intersection	14.5455	33.7374	5846.602	1400
Saturation/Grey	18-12	Intersection	23.6364	23.4343	5846.853	1401
Saturation/Grey	3-24	Bhattacharyya	23.2323	23.8384	5846.935	1402
Saturation/Grey	12-21	Intersection	23.2323	23.8384	5846.935	1403
Saturation/Grey	12-24	Intersection	22.4242	24.6465	5848.077	1404
Hue/Sat	6-24	Bhattacharyya	15.1515	32.9293	5848.873	1405
Hue/Sat	6-15	Intersection	15.9596	31.9192	5848.892	1406

Hue/Grey	12-9	Intersection	16.5657	31.1111	5853.481	1407
Hue/Sat	9-24	Correlation	17.5758	29.899	5853.949	1408
Hue/Grey	15-9	Intersection	16.3636	31.3131	5856.469	1409
VGS/Thermal IR	24-3	Earth Mover's Distance	29.0909	18.1818	5861.159	1410
Saturation/Grey	21-12	Intersection	23.4343	23.4343	5862.306	1411
Saturation/Grey	21-18	Intersection	23.4343	23.4343	5862.306	1412
Saturation/Grey	6-21	Intersection	23.2323	23.6364	5862.34	1413
Saturation/Grey	15-12	Intersection	23.6364	23.2323	5862.34	1414
Saturation/Grey	3-21	Chi Squared	23.0303	23.8384	5862.462	1415
Hue/Sat	6-18	Chi Squared	14.3434	33.7374	5863.893	1416
Hue/Sat	6-12	Intersection	15.7576	31.9192	5865.889	1417
Hue/Sat	6-6	Bhattacharyya	14.9495	32.9293	5866.033	1418
Saturation/Thermal IR	21-3	Earth Mover's Distance	26.2626	20.6061	5870.298	1419
Hue/Sat	6-18	Intersection	16.1616	31.3131	5873.384	1420
Hue/Sat	9-9	Intersection	15.1515	32.5253	5876.052	1421
Saturation/Grey	9-12	Intersection	23.4343	23.2323	5877.793	1422
Saturation/Grey	18-6	Bhattacharyya	22.6263	24.0404	5878.275	1423
Saturation/Grey	24-6	Chi Squared	22.4242	24.2424	5878.609	1424
Saturation/Grey	21-6	Chi Squared	22.0202	24.6465	5879.5	1425
Hue/Sat	6-21	Bhattacharyya	14.9495	32.7273	5879.602	1426
Hue/Grey	15-18	Correlation	19.1919	27.6768	5880.297	1427
Hue/Sat	6-18	Bhattacharyya	14.1414	33.7374	5881.216	1428
Hue/Sat	6-12	Chi Squared	13.9394	33.9394	5885.215	1429
Hue/Sat	6-6	Chi Squared	14.5455	33.1313	5886.947	1430
Saturation/Thermal IR	24-3	Earth Mover's Distance	26.6667	20	5888.886	1431
VGS/Thermal IR	21-3	Earth Mover's Distance	28.8889	17.9798	5892.051	1432
Saturation/Grey	3-12	Chi Squared	23.0303	23.4343	5893.321	1433
Saturation/Grey	21-6	Bhattacharyya	23.0303	23.4343	5893.321	1434
Saturation/Grey	15-6	Bhattacharyya	22.6263	23.8384	5893.639	1435
Saturation/Grey	9-24	Intersection	22.4242	24.0404	5893.933	1436
Saturation/Grey	18-21	Intersection	22.4242	24.0404	5893.933	1437
Saturation/Grey	21-21	Intersection	22.4242	24.0404	5893.933	1438
Saturation/Grey	18-24	Intersection	22.2222	24.2424	5894.3	1439
Saturation/Grey	15-6	Chi Squared	22.0202	24.4444	5894.749	1440
Saturation/Grey	21-15	Intersection	24.6465	21.8182	5895.272	1441
Saturation/Grey	18-15	Intersection	24.8485	21.6162	5895.884	1442
Hue/Sat	6-9	Bhattacharyya	13.9394	33.7374	5898.58	1443
Hue/Grey	9-6	Intersection	18.3838	28.2828	5902.28	1444
Hue/Grey	24-18	Correlation	18.3838	28.2828	5902.28	1445
Hue/Sat	6-9	Chi Squared	13.7374	33.9394	5902.62	1446
Saturation/Grey	6-12	Intersection	23.4343	22.8283	5908.889	1447
Saturation/Grey	6-6	Bhattacharyya	22.6263	23.6364	5909.044	1448
Saturation/Grey	15-21	Intersection	22.4242	23.8384	5909.297	1449
Saturation/Grey	12-6	Bhattacharyya	22.2222	24.0404	5909.624	1450
Hue/Grey	12-6	Intersection	17.5758	29.0909	5910.925	1451
Hue/Grey	24-6	Intersection	17.3737	29.2929	5913.3	1452
Hue/Sat	6-12	Bhattacharyya	13.7374	33.7374	5915.984	1453
Saturation/Grey	9-21	Intersection	23.0303	23.0303	5924.335	1454
Saturation/Grey	24-6	Bhattacharyya	22.8283	23.2323	5924.376	1455
Saturation/Grey	15-18	Intersection	22.6263	23.4343	5924.498	1456
Saturation/Grey	24-18	Intersection	22.4242	23.6364	5924.702	1457
Saturation/Grey	6-24	Intersection	22.2222	23.8384	5924.988	1458
Saturation/Grey	9-6	Bhattacharyya	22.2222	23.8384	5924.988	1459

Saturation/Grey	3-18	Chi Squared	21.4141	24.6465	5926.947	1460
Hue/Grey	12-9	Correlation	17.3737	29.0909	5927.603	1461
Hue/Grey	15-6	Intersection	17.3737	29.0909	5927.603	1462
Hue/Grey	21-6	Intersection	17.1717	29.2929	5930.011	1463
Saturation/Grey	12-18	Intersection	22.6263	23.2323	5939.985	1464
Hue/Grey	6-9	Correlation	18.9899	27.0707	5940.66	1465
Hue/Sat	6-21	Intersection	15.3535	31.3131	5941.46	1466
Saturation/Grey	3-18	Bhattacharyya	21.6162	24.2424	5941.617	1467
Saturation/Grey	21-9	Chi Squared	21.6162	24.2424	5941.617	1468
Saturation/Grey	24-9	Chi Squared	21.4141	24.4444	5942.196	1469
Hue/Grey	6-21	Correlation	18.7879	27.2727	5942.333	1470
Hue/Grey	21-6	Correlation	20.6061	25.2525	5945.29	1471
Hue/Sat	3-9	Chi Squared	15.7576	30.7071	5949.144	1472
Hue/Sat	6-15	Bhattacharyya	13.3333	33.7374	5950.925	1473
Hue/Grey	3-9	Chi Squared	16.3636	29.899	5954.599	1474
Hue/Sat	6-9	Intersection	15.3535	31.1111	5955.355	1475
Saturation/Grey	3-12	Bhattacharyya	22.2222	23.4343	5955.846	1476
Saturation/Grey	15-9	Bhattacharyya	21.2121	24.4444	5958.091	1477
Hue/Grey	18-6	Intersection	16.9697	29.0909	5961.066	1478
Hue/Grey	6-12	Correlation	20.202	25.4545	5962.376	1479
Hue/Grey	9-18	Correlation	17.7778	28.0808	5966.431	1480
Hue/Sat	9-6	Intersection	15.3535	30.9091	5969.291	1481
Saturation/Grey	6-18	Intersection	22.4242	23.0303	5971.17	1482
Saturation/Grey	18-18	Intersection	22.0202	23.4343	5971.578	1483
Saturation/Grey	15-9	Chi Squared	21.2121	24.2424	5973.374	1484
Saturation/Grey	24-15	Intersection	24.2424	21.2121	5973.374	1485
Hue/Sat	6-15	Chi Squared	13.5354	33.1313	5973.775	1486
Hue/Sat	6-3	Chi Squared	15.9596	30.101	5974.33	1487
Saturation/Grey	18-6	Chi Squared	20.8081	24.6465	5974.753	1488
Hue/Sat	9-3	Correlation	16.9697	28.8889	5975.41	1489
Hue/Grey	12-18	Correlation	18.1818	27.4747	5977.068	1490
Hue/Grey	3-9	Bhattacharyya	16.3636	29.4949	5983.008	1491
Hue/Grey	24-6	Correlation	19.1919	26.2626	5983.577	1492
Saturation/Grey	9-18	Intersection	22.0202	23.2323	5987.064	1493
Saturation/Grey	3-21	Bhattacharyya	21.6162	23.6364	5987.71	1494
Saturation/Grey	12-15	Intersection	24.2424	21.0101	5989.309	1495
Saturation/Grey	15-15	Intersection	24.4444	20.8081	5990.003	1496
Saturation/Grey	18-9	Chi Squared	20.8081	24.4444	5990.003	1497
Hue/Sat	6-3	Bhattacharyya	15.7576	30.101	5991.326	1498
Hue/Grey	18-6	Correlation	19.1919	26.0606	5998.492	1499
Saturation/Grey	6-6	Chi Squared	22.0202	23.0303	6002.592	1500
Saturation/Grey	12-6	Chi Squared	21.6162	23.4343	6003.163	1501
Saturation/Grey	21-9	Bhattacharyya	21.4141	23.6364	6003.572	1502
Hue/Sat	9-6	Correlation	16.9697	28.4848	6004.227	1503
Saturation/Grey	12-9	Chi Squared	20.8081	24.2424	6005.285	1504
Hue/Sat	6-6	Intersection	15.7576	29.899	6005.466	1505
Saturation/Grey	9-15	Intersection	24.4444	20.6061	6006.02	1506
Saturation/Grey	9-9	Chi Squared	20.404	24.6465	6006.837	1507
Hue/Sat	3-18	Chi Squared	14.5455	31.3131	6010.181	1508
Hue/Sat	3-9	Bhattacharyya	15.1515	30.5051	6014.405	1509
Saturation/Grey	24-9	Bhattacharyya	21.4141	23.4343	6019.025	1510
Saturation/Grey	18-9	Bhattacharyya	21.0101	23.8384	6019.997	1511
Saturation/Grey	9-9	Bhattacharyya	20.6061	24.2424	6021.303	1512

Hue/Grey	6-9	Intersection	15.5556	29.899	6022.503	1513
Hue/Sat	9-3	Intersection	15.3535	30.101	6025.45	1514
Hue/Grey	21-3	Bhattacharyya	16.9697	28.0808	6033.201	1515
Hue/Grey	3-24	Correlation	18.1818	26.6667	6035.995	1516
Saturation/Grey	12-9	Bhattacharyya	20.6061	24.0404	6036.626	1517
Hue/Grey	21-3	Chi Squared	16.3636	28.6869	6040.303	1518
Saturation/Grey	6-9	Bhattacharyya	21.0101	23.4343	6050.855	1519
Saturation/Grey	9-6	Chi Squared	21.0101	23.4343	6050.855	1520
Saturation/Grey	6-9	Chi Squared	20.8081	23.6364	6051.378	1521
Hue/Grey	3-21	Correlation	17.7778	26.8687	6054.339	1522
Hue/Sat	3-6	Bhattacharyya	14.9495	30.101	6059.729	1523
Hue/Grey	6-18	Correlation	17.7778	26.6667	6069.132	1524
Hue/Sat	3-24	Bhattacharyya	14.1414	30.9091	6072.626	1525
Hue/Sat	3-6	Chi Squared	14.7475	30.101	6076.929	1526
Hue/Sat	3-15	Chi Squared	14.3434	30.5051	6083.297	1527
Hue/Sat	6-15	Correlation	16.3636	28.0808	6083.709	1528
Hue/Grey	15-3	Bhattacharyya	15.9596	28.4848	6088.606	1529
Hue/Sat	3-18	Bhattacharyya	13.9394	30.9091	6089.99	1530
Hue/Sat	3-15	Bhattacharyya	14.1414	30.5051	6100.62	1531
Hue/Grey	3-12	Correlation	18.9899	24.8485	6105.192	1532
Hue/Sat	3-9	Correlation	15.7576	28.4848	6105.603	1533
Hue/Sat	3-12	Bhattacharyya	13.7374	30.9091	6107.394	1534
Hue/Sat	3-21	Chi Squared	13.7374	30.9091	6107.394	1535
Saturation/Grey	3-15	Bhattacharyya	21.8182	21.8182	6112.394	1536
Saturation/Grey	3-15	Chi Squared	22.4242	21.2121	6112.769	1537
Hue/Grey	24-3	Chi Squared	15.1515	29.0909	6113.684	1538
Hue/Grey	24-3	Bhattacharyya	16.1616	27.8788	6115.172	1539
Saturation/Grey	21-6	Intersection	23.8384	19.798	6116.475	1540
Hue/Sat	3-24	Chi Squared	13.9394	30.5051	6117.984	1541
Hue/Grey	9-3	Bhattacharyya	17.1717	26.6667	6119.15	1542
Hue/Grey	9-6	Correlation	18.9899	24.6465	6120.393	1543
Hue/Sat	3-21	Bhattacharyya	13.5354	30.9091	6124.84	1544
Hue/Grey	3-15	Intersection	16.3636	27.4747	6127.483	1545
Hue/Grey	18-3	Bhattacharyya	16.3636	27.4747	6127.483	1546
Saturation/Grey	3-24	Intersection	22.4242	21.0101	6128.705	1547
Saturation/Grey	6-15	Intersection	23.4343	20	6131.153	1548
Hue/Sat	6-24	Correlation	14.7475	29.2929	6133.741	1549
Hue/Grey	9-15	Correlation	18.7879	24.6465	6136.778	1550
Hue/Sat	3-15	Correlation	15.3535	28.4848	6139.727	1551
Hue/Sat	3-18	Correlation	14.3434	29.697	6139.782	1552
Hue/Sat	3-18	Intersection	14.1414	29.899	6142.925	1553
Saturation/Grey	3-21	Intersection	21.8182	21.4141	6144.069	1554
Hue/Sat	6-18	Correlation	14.9495	28.8889	6145.188	1555
Saturation/Grey	15-6	Intersection	23.2323	20	6146.64	1556
Hue/Grey	3-18	Intersection	15.9596	27.6768	6146.717	1557
Hue/Sat	3-6	Intersection	14.7475	29.0909	6148.045	1558
Hue/Sat	3-24	Correlation	14.7475	29.0909	6148.045	1559
Hue/Grey	12-6	Correlation	17.1717	26.2626	6148.866	1560
Hue/Grey	3-18	Correlation	15.7576	27.8788	6149.125	1561
Hue/Sat	3-9	Intersection	14.5455	29.2929	6150.983	1562
Hue/Sat	3-12	Chi Squared	13.5354	30.5051	6152.834	1563
Hue/Sat	3-15	Intersection	13.9394	29.899	6160.289	1564
Saturation/Grey	24-6	Intersection	22.8283	20.202	6161.596	1565

Hue/Sat	6-21	Correlation	14.7475	28.8889	6162.389	1566
Hue/Grey	18-3	Chi Squared	14.7475	28.8889	6162.389	1567
Hue/Sat	6-12	Correlation	15.5556	27.8788	6166.162	1568
Hue/Grey	12-3	Bhattacharyya	15.3535	28.0808	6168.701	1569
Saturation/Grey	18-6	Intersection	23.0303	19.798	6178.348	1570
Hue/Grey	18-15	Correlation	18.1818	24.6465	6186.184	1571
Hue/Grey	15-3	Chi Squared	14.9495	28.2828	6188.472	1572
Hue/Grey	24-15	Correlation	17.9798	24.6465	6202.732	1573
Hue/Grey	15-6	Correlation	16.9697	25.6566	6210.486	1574
Hue/Sat	3-21	Intersection	13.1313	30.101	6216.021	1575
Hue/Sat	3-12	Intersection	13.9394	29.0909	6217.264	1576
Hue/Sat	3-24	Intersection	13.1313	29.899	6230.161	1577
Hue/Grey	15-15	Correlation	17.7778	24.4444	6234.569	1578
Hue/Grey	21-15	Correlation	17.7778	24.4444	6234.569	1579
Hue/Grey	3-9	Intersection	14.5455	28.0808	6237.421	1580
Saturation/Grey	3-12	Intersection	21.8182	20.202	6240.057	1581
Hue/Sat	6-6	Correlation	14.7475	27.6768	6249.317	1582
Hue/Sat	6-9	Correlation	14.7475	27.6768	6249.317	1583
Hue/Sat	3-3	Bhattacharyya	15.7576	26.4646	6252.119	1584
Hue/Sat	3-12	Correlation	13.3333	29.2929	6255.305	1585
Hue/Sat	3-3	Chi Squared	15.7576	26.2626	6266.993	1586
Hue/Grey	12-15	Correlation	17.1717	24.6465	6269.339	1587
Saturation/Grey	12-6	Intersection	22.0202	19.596	6272.826	1588
Hue/Grey	12-3	Chi Squared	13.7374	28.4848	6277.83	1589
Hue/Grey	9-3	Chi Squared	14.7475	27.2727	6278.624	1590
Hue/Sat	3-21	Correlation	13.3333	28.8889	6283.953	1591
Saturation/Grey	3-18	Intersection	20.8081	20.6061	6287.374	1592
Saturation/Grey	12-21	Correlation	19.3939	22.0202	6289.096	1593
Saturation/Grey	9-6	Intersection	21.8182	19.1919	6321.171	1594
Saturation/Grey	3-15	Intersection	22.8283	18.1818	6324.845	1595
Saturation/Grey	24-21	Correlation	19.1919	21.6162	6336.985	1596
Saturation/Grey	9-12	Earth Mover's Distance	22.6263	18.1818	6340.454	1597
Saturation/Grey	12-24	Correlation	20.6061	20	6351.696	1598
Hue/Grey	6-12	Earth Mover's Distance	19.798	20.8081	6351.859	1599
Saturation/Grey	21-18	Correlation	19.3939	21.2121	6352.438	1600
Saturation/Grey	3-9	Chi Squared	18.7879	21.8182	6353.9	1601
Saturation/Grey	6-21	Correlation	18.7879	21.8182	6353.9	1602
Saturation/Grey	15-21	Correlation	18.7879	21.8182	6353.9	1603
Saturation/Grey	9-21	Correlation	18.5859	22.0202	6354.552	1604
Hue/Grey	3-9	Correlation	15.7576	25.0505	6357.105	1605
Hue/Grey	6-6	Intersection	14.3434	26.6667	6357.413	1606
Saturation/Grey	12-12	Correlation	19.798	20.6061	6367.876	1607
Saturation/Grey	9-18	Correlation	19.596	20.8081	6368.08	1608
Saturation/Grey	15-9	Intersection	19.596	20.8081	6368.08	1609
Saturation/Grey	9-12	Correlation	19.3939	21.0101	6368.374	1610
Hue/Sat	6-3	Intersection	13.9394	26.8687	6377.307	1611
Saturation/Grey	9-24	Correlation	20.404	19.798	6383.942	1612
Saturation/Grey	12-9	Intersection	19.3939	20.8081	6384.35	1613
Saturation/Grey	12-12	Earth Mover's Distance	21.6162	18.5859	6386.138	1614
Saturation/Grey	6-6	Intersection	21.8182	18.3838	6386.799	1615
Saturation/Grey	15-6	Correlation	22.0202	18.1818	6387.534	1616
Saturation/Grey	6-12	Earth Mover's Distance	23.2323	16.9697	6393.655	1617
Saturation/Grey	24-24	Correlation	20.404	19.596	6400.163	1618

Saturation/Grey	18-9	Intersection	19.3939	20.6061	6400.367	1619
Saturation/Grey	18-24	Correlation	20.6061	19.3939	6400.367	1620
Saturation/Grey	9-9	Intersection	19.1919	20.8081	6400.653	1621
Saturation/Grey	15-9	Correlation	18.9899	21.0101	6401.02	1622
Saturation/Grey	6-9	Intersection	18.7879	21.2121	6401.469	1623
Saturation/Grey	18-9	Correlation	18.5859	21.4141	6402	1624
Saturation/Grey	21-21	Correlation	18.3838	21.6162	6402.612	1625
Saturation/Grey	18-21	Correlation	18.1818	21.8182	6403.306	1626
Saturation/Grey	21-24	Correlation	20.404	19.3939	6416.433	1627
Saturation/Grey	15-12	Correlation	19.1919	20.6061	6416.67	1628
Saturation/Grey	21-9	Intersection	18.7879	21.0101	6417.405	1629
Saturation/Grey	24-9	Intersection	18.7879	21.0101	6417.405	1630
Saturation/Grey	15-24	Earth Mover's Distance	22.0202	17.7778	6420.67	1631
Saturation/Grey	6-18	Correlation	19.1919	20.404	6432.736	1632
Saturation/Grey	15-24	Correlation	20.6061	18.9899	6433.014	1633
Saturation/Grey	15-18	Correlation	18.7879	20.8081	6433.381	1634
Saturation/Grey	18-18	Correlation	18.7879	20.8081	6433.381	1635
Saturation/Grey	12-18	Correlation	18.5859	21.0101	6433.83	1636
Saturation/Grey	3-6	Bhattacharyya	21.2121	18.3838	6434.369	1637
Saturation/Grey	3-9	Bhattacharyya	18.3838	21.2121	6434.369	1638
Saturation/Grey	21-9	Correlation	18.3838	21.2121	6434.369	1639
Saturation/Grey	21-24	Earth Mover's Distance	21.2121	18.3838	6434.369	1640
Saturation/Grey	18-24	Earth Mover's Distance	21.4141	18.1818	6434.981	1641
Hue/Sat	15-15	Earth Mover's Distance	17.3737	22.2222	6438.246	1642
Hue/Grey	9-12	Earth Mover's Distance	17.1717	22.4242	6439.266	1643
Saturation/Grey	12-24	Earth Mover's Distance	22.4242	17.1717	6439.266	1644
Hue/Sat	9-24	Earth Mover's Distance	16.7677	22.8283	6441.544	1645
Saturation/Grey	3-18	Correlation	20	19.3939	6448.672	1646
Saturation/Grey	24-18	Correlation	18.7879	20.6061	6449.398	1647
Saturation/Grey	24-9	Correlation	18.1818	21.2121	6450.876	1648
Hue/Sat	18-21	Earth Mover's Distance	16.5657	22.8283	6458.377	1649
Hue/Grey	6-15	Correlation	16.5657	22.8283	6458.377	1650
Saturation/Grey	6-24	Correlation	19.798	19.3939	6464.852	1651
Saturation/Grey	3-24	Correlation	20.404	18.7879	6465.464	1652
Saturation/Grey	6-9	Correlation	18.3838	20.8081	6466.281	1653
Saturation/Grey	3-6	Chi Squared	21.0101	18.1818	6466.811	1654
Saturation/Grey	12-9	Correlation	18.1818	21.0101	6466.811	1655
Saturation/Grey	18-21	Earth Mover's Distance	21.2121	17.9798	6467.423	1656
Saturation/Grey	21-6	Correlation	21.2121	17.9798	6467.423	1657
Saturation/Grey	24-6	Correlation	21.4141	17.7778	6468.117	1658
Hue/Sat	12-15	Earth Mover's Distance	16.7677	22.4242	6472.81	1659
Hue/Sat	18-18	Earth Mover's Distance	16.7677	22.4242	6472.81	1660
Hue/Sat	24-24	Earth Mover's Distance	16.7677	22.4242	6472.81	1661
Hue/Sat	6-18	Earth Mover's Distance	16.5657	22.6263	6473.986	1662
Hue/Sat	21-21	Earth Mover's Distance	16.5657	22.6263	6473.986	1663
Saturation/Grey	9-24	Earth Mover's Distance	22.8283	16.3636	6475.259	1664
Saturation/Grey	18-12	Correlation	18.9899	20	6481.318	1665
Saturation/Grey	9-6	Correlation	20.202	18.7879	6481.563	1666
Saturation/Grey	24-12	Correlation	18.5859	20.404	6481.889	1667
Saturation/Grey	9-9	Correlation	18.3838	20.6061	6482.298	1668
Saturation/Grey	12-6	Correlation	20.8081	18.1818	6482.787	1669
Saturation/Grey	18-6	Correlation	20.8081	18.1818	6482.787	1670
Saturation/Grey	12-21	Earth Mover's Distance	21.8182	17.1717	6486.461	1671

Hue/Grey	12-12	Earth Mover's Distance	16.5657	22.4242	6489.644	1672
Hue/Sat	3-6	Correlation	13.1313	26.2626	6491.688	1673
Hue/Grey	21-3	Correlation	13.1313	26.2626	6491.688	1674
Saturation/Grey	24-24	Earth Mover's Distance	20.202	18.5859	6497.988	1675
Hue/Sat	6-15	Earth Mover's Distance	16.3636	22.4242	6506.526	1676
Hue/Sat	15-18	Earth Mover's Distance	16.3636	22.4242	6506.526	1677
Hue/Grey	24-21	Earth Mover's Distance	15.9596	22.8283	6509.13	1678
Hue/Grey	3-6	Intersection	13.9394	25.0505	6511.927	1679
Saturation/Grey	21-12	Correlation	18.7879	19.798	6513.883	1680
Saturation/Grey	18-15	Correlation	20.6061	17.9798	6515.352	1681
Saturation/Grey	21-21	Earth Mover's Distance	20.6061	17.9798	6515.352	1682
Saturation/Grey	6-6	Correlation	21.0101	17.5758	6516.577	1683
Hue/Sat	6-21	Earth Mover's Distance	16.9697	21.6162	6519.025	1684
Saturation/Grey	15-21	Earth Mover's Distance	21.6162	16.9697	6519.025	1685
Saturation/Grey	9-21	Earth Mover's Distance	21.8182	16.7677	6520.005	1686
Hue/Sat	9-9	Earth Mover's Distance	16.5657	22.0202	6521.066	1687
Hue/Sat	12-12	Earth Mover's Distance	16.5657	22.0202	6521.066	1688
Hue/Sat	18-15	Earth Mover's Distance	16.3636	22.2222	6522.217	1689
Hue/Grey	12-21	Earth Mover's Distance	16.3636	22.2222	6522.217	1690
Hue/Sat	9-21	Earth Mover's Distance	16.1616	22.4242	6523.441	1691
Hue/Grey	21-21	Earth Mover's Distance	16.1616	22.4242	6523.441	1692
Hue/Sat	12-21	Earth Mover's Distance	15.9596	22.6263	6524.739	1693
Saturation/Grey	6-12	Correlation	18.9899	19.3939	6529.99	1694
Saturation/Grey	3-21	Correlation	18.3838	20	6530.602	1695
Saturation/Grey	9-15	Correlation	20	18.3838	6530.602	1696
Hue/Grey	9-21	Earth Mover's Distance	18.1818	20.202	6530.969	1697
Hue/Sat	21-24	Earth Mover's Distance	15.9596	22.4242	6540.397	1698
Hue/Sat	12-24	Earth Mover's Distance	15.7576	22.6263	6541.736	1699
Saturation/Grey	3-9	Correlation	19.798	18.3838	6546.782	1700
Hue/Sat	3-3	Intersection	14.9495	23.4343	6547.947	1701
Hue/Sat	6-24	Earth Mover's Distance	17.5758	20.6061	6548.57	1702
Saturation/Grey	3-12	Earth Mover's Distance	23.8384	14.5455	6551.53	1703
Hue/Grey	15-21	Earth Mover's Distance	15.7576	22.4242	6557.393	1704
Saturation/Grey	15-12	Earth Mover's Distance	19.798	18.1818	6563.289	1705
Hue/Sat	6-6	Earth Mover's Distance	16.1616	21.8182	6570.636	1706
Hue/Sat	15-24	Earth Mover's Distance	16.1616	21.8182	6570.636	1707
Hue/Sat	12-18	Earth Mover's Distance	15.9596	22.0202	6571.819	1708
Hue/Sat	9-12	Earth Mover's Distance	15.7576	22.2222	6573.084	1709
Hue/Grey	18-21	Earth Mover's Distance	15.7576	22.2222	6573.084	1710
Hue/Sat	9-18	Earth Mover's Distance	15.5556	22.4242	6574.431	1711
Saturation/Grey	15-18	Earth Mover's Distance	19.1919	18.5859	6579.102	1712
Saturation/Grey	15-15	Correlation	19.798	17.9798	6579.837	1713
Saturation/Grey	21-15	Correlation	19.798	17.9798	6579.837	1714
Saturation/Grey	3-9	Intersection	17.5758	20.202	6580.735	1715
Hue/Sat	3-9	Earth Mover's Distance	16.7677	21.0101	6583.51	1716
Hue/Grey	18-3	Correlation	12.9293	25.2525	6584.248	1717
Hue/Sat	6-9	Earth Mover's Distance	15.9596	21.8182	6587.591	1718
Saturation/Grey	12-15	Correlation	19.3939	18.1818	6595.781	1719
Saturation/Grey	24-21	Earth Mover's Distance	19.596	17.9798	6596.058	1720
Hue/Grey	15-12	Earth Mover's Distance	14.5455	23.2323	6597.876	1721
Hue/Sat	21-18	Earth Mover's Distance	16.1616	21.4141	6602.31	1722
Hue/Sat	9-15	Earth Mover's Distance	15.7576	21.8182	6604.588	1723
Hue/Sat	15-12	Earth Mover's Distance	15.7576	21.8182	6604.588	1724

Hue/Grey	6-3	Bhattacharyya	13.7374	24.0404	6605.548	1725
Hue/Grey	24-24	Earth Mover's Distance	15.3535	22.2222	6607.208	1726
Saturation/Grey	6-21	Earth Mover's Distance	22.8283	14.7475	6611.73	1727
Saturation/Grey	6-15	Correlation	19.3939	17.9798	6612.328	1728
Hue/Grey	15-3	Correlation	11.9192	26.0606	6612.631	1729
Hue/Sat	6-3	Correlation	15.7576	21.6162	6620.401	1730
Hue/Sat	18-24	Earth Mover's Distance	15.5556	21.8182	6621.625	1731
Hue/Grey	21-24	Earth Mover's Distance	15.1515	22.2222	6624.327	1732
Hue/Grey	21-18	Earth Mover's Distance	14.5455	22.8283	6628.971	1733
Saturation/Grey	9-18	Earth Mover's Distance	20	17.1717	6630.264	1734
Hue/Grey	3-15	Correlation	13.9394	23.4343	6634.367	1735
Hue/Sat	24-21	Earth Mover's Distance	15.7576	21.4141	6636.263	1736
Hue/Sat	15-21	Earth Mover's Distance	15.5556	21.6162	6637.438	1737
Hue/Sat	21-15	Earth Mover's Distance	15.5556	21.6162	6637.438	1738
Hue/Grey	24-3	Correlation	12.1212	25.4545	6639.858	1739
Hue/Sat	6-12	Earth Mover's Distance	15.1515	22.0202	6640.059	1740
Hue/Grey	15-24	Earth Mover's Distance	15.1515	22.0202	6640.059	1741
Saturation/Grey	24-15	Correlation	18.7879	18.1818	6644.812	1742
Hue/Grey	9-3	Correlation	12.3232	25.0505	6652.324	1743
Hue/Sat	9-6	Earth Mover's Distance	15.1515	21.8182	6655.831	1744
Hue/Grey	15-18	Earth Mover's Distance	14.7475	22.2222	6658.687	1745
Saturation/Grey	12-18	Earth Mover's Distance	18.7879	17.9798	6661.359	1746
Hue/Grey	9-9	Earth Mover's Distance	14.3434	22.6263	6661.871	1747
Saturation/Grey	12-15	Earth Mover's Distance	19.596	17.1717	6662.665	1748
Hue/Grey	18-24	Earth Mover's Distance	14.7475	22.0202	6674.419	1749
Hue/Sat	15-9	Earth Mover's Distance	15.1515	21.4141	6687.506	1750
Hue/Sat	24-18	Earth Mover's Distance	14.9495	21.6162	6688.804	1751
Saturation/Grey	18-18	Earth Mover's Distance	17.9798	18.3838	6694.259	1752
Hue/Grey	18-12	Earth Mover's Distance	14.1414	22.4242	6694.852	1753
Saturation/Grey	15-15	Earth Mover's Distance	18.9899	17.3737	6694.871	1754
Hue/Sat	24-15	Earth Mover's Distance	14.9495	21.4141	6704.666	1755
Hue/Sat	3-6	Earth Mover's Distance	14.7475	21.6162	6706.004	1756
Hue/Sat	12-9	Earth Mover's Distance	14.7475	21.6162	6706.004	1757
Hue/Grey	6-6	Correlation	14.3434	22.0202	6708.951	1758
Hue/Grey	12-18	Earth Mover's Distance	14.1414	22.2222	6710.543	1759
Hue/Grey	6-21	Earth Mover's Distance	17.1717	18.9899	6711.582	1760
Hue/Grey	18-15	Earth Mover's Distance	13.9394	22.4242	6712.216	1761
Hue/Grey	12-9	Earth Mover's Distance	13.7374	22.6263	6713.963	1762
Hue/Grey	9-24	Earth Mover's Distance	16.1616	20	6714.439	1763
Hue/Sat	21-12	Earth Mover's Distance	14.7475	21.4141	6721.866	1764
Hue/Grey	6-6	Earth Mover's Distance	14.7475	21.4141	6721.866	1765
Hue/Sat	18-12	Earth Mover's Distance	14.5455	21.6162	6723.246	1766
Saturation/Grey	21-12	Earth Mover's Distance	18.5859	17.3737	6727.681	1767
Hue/Grey	3-6	Correlation	13.9394	22.2222	6727.907	1768
Saturation/Grey	24-3	Chi Squared	18.9899	16.9697	6728.334	1769
Hue/Grey	9-15	Earth Mover's Distance	13.7374	22.4242	6729.62	1770
Hue/Sat	3-15	Earth Mover's Distance	16.1616	19.798	6730.619	1771
Hue/Grey	3-12	Earth Mover's Distance	17.5758	18.1818	6743.983	1772
Saturation/Grey	15-3	Chi Squared	18.5859	17.1717	6744.391	1773
Hue/Grey	12-15	Earth Mover's Distance	13.7374	22.2222	6745.311	1774
Hue/Grey	18-18	Earth Mover's Distance	13.7374	22.2222	6745.311	1775
Saturation/Grey	9-3	Bhattacharyya	19.3939	16.3636	6746.195	1776
Saturation/Grey	12-3	Bhattacharyya	19.3939	16.3636	6746.195	1777

Saturation/Grey	21-18	Earth Mover's Distance	17.7778	17.7778	6760.49	1778
Saturation/Grey	18-12	Earth Mover's Distance	17.5758	17.9798	6760.531	1779
Saturation/Grey	18-3	Bhattacharyya	19.3939	16.1616	6763.11	1780
Hue/Grey	12-24	Earth Mover's Distance	15.7576	19.798	6764.571	1781
Hue/Grey	24-18	Earth Mover's Distance	12.9293	22.8283	6768.389	1782
Hue/Grey	21-12	Earth Mover's Distance	14.3434	21.2121	6772.293	1783
Hue/Grey	9-6	Earth Mover's Distance	14.1414	21.4141	6773.721	1784
Hue/Grey	6-9	Earth Mover's Distance	13.9394	21.6162	6775.223	1785
Saturation/Grey	6-9	Earth Mover's Distance	18.9899	16.3636	6778.842	1786
Saturation/Grey	21-3	Chi Squared	18.9899	16.3636	6778.842	1787
Hue/Sat	3-12	Earth Mover's Distance	15.9596	19.3939	6780.066	1788
Saturation/Grey	9-15	Earth Mover's Distance	19.3939	15.9596	6780.066	1789
Saturation/Grey	6-15	Earth Mover's Distance	19.798	15.5556	6781.609	1790
Saturation/Grey	6-24	Earth Mover's Distance	21.0101	14.3434	6788.229	1791
Saturation/Grey	24-18	Earth Mover's Distance	17.5758	17.5758	6793.749	1792
Saturation/Grey	18-3	Chi Squared	17.9798	17.1717	6793.92	1793
Saturation/Grey	21-15	Earth Mover's Distance	17.9798	17.1717	6793.92	1794
Saturation/Grey	9-3	Chi Squared	18.1818	16.9697	6794.124	1795
Hue/Grey	15-15	Earth Mover's Distance	13.5354	21.8182	6794.26	1796
Saturation/Grey	9-9	Earth Mover's Distance	18.3838	16.7677	6794.41	1797
Saturation/Grey	12-3	Chi Squared	18.3838	16.7677	6794.41	1798
Saturation/Grey	15-3	Bhattacharyya	19.3939	15.7576	6797.063	1799
Saturation/Grey	3-6	Intersection	20	15.1515	6799.634	1800
Hue/Grey	18-3	Intersection	10.303	25.4545	6801.292	1801
Hue/Grey	21-3	Intersection	10.303	25.4545	6801.292	1802
Saturation/Grey	3-12	Correlation	17.1717	17.7778	6810.509	1803
Saturation/Grey	24-12	Earth Mover's Distance	17.1717	17.7778	6810.509	1804
Saturation/Grey	15-9	Earth Mover's Distance	17.9798	16.9697	6810.672	1805
Saturation/Grey	6-3	Bhattacharyya	18.7879	16.1616	6812.141	1806
Hue/Grey	12-3	Correlation	9.49495	26.2626	6814.184	1807
Hue/Grey	21-15	Earth Mover's Distance	12.9293	22.2222	6815.346	1808
Saturation/Grey	24-15	Earth Mover's Distance	17.7778	16.9697	6827.26	1809
Saturation/Grey	6-3	Chi Squared	18.1818	16.5657	6827.75	1810
Saturation/Grey	6-6	Earth Mover's Distance	18.3838	16.3636	6828.126	1811
Saturation/Grey	24-3	Bhattacharyya	18.7879	15.9596	6829.097	1812
Hue/Grey	24-3	Intersection	9.49495	26.0606	6829.099	1813
Hue/Grey	15-9	Earth Mover's Distance	12.7273	22.2222	6832.955	1814
Hue/Grey	9-18	Earth Mover's Distance	14.1414	20.6061	6837.545	1815
Hue/Sat	12-6	Earth Mover's Distance	13.7374	21.0101	6840.32	1816
Saturation/Grey	21-9	Earth Mover's Distance	17.1717	17.3737	6843.816	1817
Saturation/Grey	12-9	Earth Mover's Distance	17.9798	16.5657	6844.298	1818
Saturation/Grey	21-3	Bhattacharyya	18.7879	15.7576	6846.094	1819
Saturation/Grey	6-18	Earth Mover's Distance	19.3939	15.1515	6848.306	1820
Hue/Grey	6-15	Earth Mover's Distance	14.3434	20.202	6852.387	1821
Hue/Sat	18-9	Earth Mover's Distance	13.5354	21.0101	6857.766	1822
Hue/Sat	24-12	Earth Mover's Distance	13.5354	21.0101	6857.766	1823
Hue/Grey	6-3	Chi Squared	11.7172	23.0303	6859.094	1824
Saturation/Grey	18-9	Earth Mover's Distance	17.3737	16.9697	6860.568	1825
Saturation/Grey	3-15	Correlation	18.9899	15.3535	6863.833	1826
Hue/Grey	24-15	Earth Mover's Distance	12.5253	22.0202	6866.336	1827
Hue/Grey	3-6	Earth Mover's Distance	14.3434	20	6868.527	1828
Hue/Grey	15-3	Intersection	9.69697	25.2525	6870.913	1829
Hue/Grey	24-12	Earth Mover's Distance	13.3333	21.0101	6875.261	1830

Saturation/Grey	9-6	Earth Mover's Distance	16.9697	17.1717	6877.279	1831
Hue/Grey	6-24	Earth Mover's Distance	15.7576	18.3838	6878.993	1832
Hue/Sat	3-21	Earth Mover's Distance	15.1515	18.9899	6880.952	1833
Hue/Grey	24-9	Earth Mover's Distance	12.5253	21.8182	6882.108	1834
Saturation/Grey	3-21	Earth Mover's Distance	20.8081	13.3333	6891.237	1835
Saturation/Grey	18-15	Earth Mover's Distance	16.9697	16.9697	6894.031	1836
Hue/Sat	3-18	Earth Mover's Distance	15.5556	18.3838	6896.03	1837
Saturation/Grey	3-6	Correlation	18.3838	15.5556	6896.03	1838
Hue/Grey	18-9	Earth Mover's Distance	12.5253	21.6162	6897.922	1839
Hue/Grey	9-3	Intersection	10.5051	23.8384	6904.963	1840
Saturation/Grey	24-9	Earth Mover's Distance	16.9697	16.5657	6927.657	1841
Hue/Grey	21-9	Earth Mover's Distance	11.9192	21.8182	6935.311	1842
Hue/Sat	9-3	Earth Mover's Distance	13.9394	19.596	6935.615	1843
Hue/Sat	21-9	Earth Mover's Distance	13.3333	20.202	6939.419	1844
Hue/Sat	15-6	Earth Mover's Distance	12.7273	20.8081	6943.941	1845
Hue/Sat	3-24	Earth Mover's Distance	15.3535	17.9798	6946.172	1846
Hue/Sat	24-9	Earth Mover's Distance	13.3333	20	6955.558	1847
Hue/Grey	6-18	Earth Mover's Distance	13.5354	19.596	6970.465	1848
Saturation/Grey	12-6	Earth Mover's Distance	16.5657	16.3636	6978.165	1849
Hue/Grey	12-6	Earth Mover's Distance	12.1212	21.0101	6981.044	1850
Saturation/Grey	21-3	Intersection	17.3737	15.3535	6996.068	1851
Hue/Sat	3-3	Earth Mover's Distance	13.9394	18.7879	7000.916	1852
Hue/Sat	21-6	Earth Mover's Distance	12.9293	19.798	7006.834	1853
Hue/Grey	3-3	Bhattacharyya	12.9293	19.798	7006.834	1854
Saturation/Grey	15-6	Earth Mover's Distance	16.1616	16.3636	7011.962	1855
Hue/Grey	3-21	Earth Mover's Distance	17.1717	15.3535	7012.779	1856
Saturation/Grey	3-6	Earth Mover's Distance	18.9899	13.5354	7019.382	1857
Hue/Sat	12-3	Earth Mover's Distance	13.3333	19.1919	7020.533	1858
Hue/Sat	3-3	Correlation	14.7475	17.5758	7030.869	1859
Hue/Sat	18-6	Earth Mover's Distance	12.7273	19.596	7040.664	1860
Hue/Grey	3-3	Chi Squared	12.7273	19.596	7040.664	1861
Saturation/Grey	3-24	Earth Mover's Distance	20	12.3232	7043.611	1862
Hue/Sat	6-3	Earth Mover's Distance	13.3333	18.7879	7053.261	1863
Hue/Grey	12-3	Intersection	8.48485	24.2424	7057.118	1864
Hue/Sat	24-6	Earth Mover's Distance	12.1212	20	7061.342	1865
Hue/Grey	15-6	Earth Mover's Distance	11.7172	20.404	7064.688	1866
Hue/Grey	6-3	Correlation	10.5051	21.6162	7076.679	1867
Saturation/Grey	3-9	Earth Mover's Distance	16.3636	15.3535	7080.039	1868
Saturation/Grey	15-3	Intersection	16.3636	15.3535	7080.039	1869
Saturation/Grey	24-3	Intersection	16.7677	14.9495	7080.602	1870
Saturation/Grey	3-18	Earth Mover's Distance	17.9798	13.7374	7084.275	1871
Saturation/Grey	9-3	Intersection	15.5556	15.9596	7096.823	1872
Hue/Grey	3-24	Earth Mover's Distance	16.7677	14.7475	7097.802	1873
Hue/Grey	3-9	Earth Mover's Distance	13.5354	17.9798	7101.72	1874
Saturation/Grey	12-3	Intersection	15.5556	15.5556	7130.857	1875
Saturation/Grey	18-6	Earth Mover's Distance	15.1515	15.9596	7131.028	1876
Saturation/Grey	6-3	Intersection	15.9596	14.9495	7148.188	1877
Saturation/Grey	3-15	Earth Mover's Distance	18.3838	12.5253	7156.514	1878
Hue/Grey	21-6	Earth Mover's Distance	11.5152	19.3939	7163.452	1879
Hue/Grey	3-18	Earth Mover's Distance	14.5455	16.1616	7165.674	1880
Saturation/Grey	3-3	Chi Squared	16.1616	14.5455	7165.674	1881
Hue/Sat	15-3	Earth Mover's Distance	12.1212	18.5859	7175.47	1882
Saturation/Grey	18-3	Intersection	15.1515	15.3535	7182.149	1883

Hue/Grey	3-15	Earth Mover's Distance	14.5455	15.9596	7182.63	1884
Saturation/Grey	21-6	Earth Mover's Distance	14.3434	15.9596	7199.921	1885
Hue/Grey	18-6	Earth Mover's Distance	10.7071	19.798	7202.791	1886
Saturation/Grey	3-3	Bhattacharyya	15.9596	14.1414	7217.244	1887
Saturation/Grey	24-6	Earth Mover's Distance	14.1414	15.9596	7217.244	1888
Hue/Grey	24-6	Earth Mover's Distance	10.9091	19.3939	7217.266	1889
Hue/Grey	6-3	Intersection	9.09091	21.0101	7251.933	1890
Saturation/Grey	6-3	Earth Mover's Distance	15.9596	13.7374	7252.012	1891
Hue/Grey	3-3	Intersection	11.9192	17.7778	7259.359	1892
Hue/Sat	18-3	Earth Mover's Distance	11.9192	17.3737	7292.666	1893
Hue/Sat	21-3	Earth Mover's Distance	11.7172	17.3737	7310.479	1894
Hue/Grey	9-3	Earth Mover's Distance	10.303	18.5859	7336.904	1895
Saturation/Grey	9-3	Earth Mover's Distance	14.9495	13.7374	7337.412	1896
Saturation/Grey	21-3	Correlation	14.1414	14.3434	7354.376	1897
Saturation/Grey	18-3	Correlation	13.7374	14.7475	7354.612	1898
Saturation/Grey	18-3	Earth Mover's Distance	14.3434	13.9394	7371.74	1899
Hue/Sat	24-3	Earth Mover's Distance	10.9091	17.3737	7382.147	1900
Hue/Grey	6-3	Earth Mover's Distance	9.89899	18.3838	7389.698	1901
Saturation/Grey	12-3	Correlation	12.9293	14.9495	7407.447	1902
Saturation/Grey	15-3	Correlation	12.9293	14.9495	7407.447	1903
Hue/Grey	3-3	Earth Mover's Distance	11.5152	16.3636	7412.304	1904
Hue/Grey	3-3	Correlation	10.303	17.5758	7419.65	1905
Saturation/Grey	15-3	Earth Mover's Distance	13.9394	13.7374	7423.832	1906
Saturation/Grey	12-3	Earth Mover's Distance	14.1414	13.5354	7423.913	1907
Saturation/Grey	21-3	Earth Mover's Distance	13.7374	13.5354	7458.682	1908
Saturation/Grey	6-3	Correlation	13.3333	13.9394	7458.772	1909
Saturation/Grey	24-3	Earth Mover's Distance	13.9394	13.3333	7458.772	1910
Saturation/Grey	9-3	Correlation	12.7273	14.5455	7459.498	1911
Hue/Grey	12-3	Earth Mover's Distance	8.68687	18.7879	7466.746	1912
Saturation/Grey	24-3	Correlation	13.9394	13.1313	7476.299	1913
Hue/Grey	15-3	Earth Mover's Distance	8.88889	17.9798	7514.274	1914
Hue/Grey	18-3	Earth Mover's Distance	8.88889	17.9798	7514.274	1915
Hue/Grey	21-3	Earth Mover's Distance	8.88889	17.9798	7514.274	1916
Hue/Grey	24-3	Earth Mover's Distance	8.48485	17.9798	7551.168	1917
Saturation/Grey	3-3	Earth Mover's Distance	13.1313	10.303	7795.861	1918
Saturation/Grey	3-3	Intersection	11.9192	10.5051	7883.782	1919
Saturation/Grey	3-3	Correlation	10.303	10.303	8045.552	1920